6-6-2020

Copper and Ruthenium Pyridyltriazole Complexes and Their Reactivity Toward Carbon Dioxide and Water

Fatemeh Khamespanah
Louisiana State University and Agricultural and Mechanical College

COPPER AND RUTHENIUM PYRIDYLTRIAZOLE COMPLEXES AND THEIR REACTIVITY TOWARD CARBON DIOXIDE AND WATER

A Dissertation

Submitted to the Graduate Faculty of the
Louisiana State University and
Agricultural and Mechanical College
in partial fulfillment of the
requirements for the degree of
Doctor of Philosophy

in

The Department of Chemistry

by
Fatemeh Khamespanah
B.Sc., Sharif University of Technology, 2014
August 2020

Acknowledgements

First and foremost, I give thanks to God, without whose constant blessings nothing would have been possible. I would like to appreciate the constant love and support from my family, my parents, Fadahossein Khamespanah and Seddighe Hasani; my sister, Somayyeh; and my brothers, Ehsan and Erfan. Their wisdom and strength have enabled me to run at big goals and overcome every challenge that I have encountered. Thank you all from the bottom of my heart; I would not be here without you.

I am forever indebted to my doctoral advisor, Dr. Andrew W. Maverick, for accepting me into his group and always giving me advice, support, and encouragement throughout these past few years. Receiving his feedback has always been invaluable for me and has made me more confident when presenting our research in front of the scientific community. I am also grateful for the many opportunities he has provided me outside our lab environment to attend chemistry workshops and conferences.

I am very grateful to Dr. Frank R. Fronczek for his one-on-one teaching on how to solve and refine X-ray structures. His expertise alongside his sense of humor has made learning this challenging topic very enjoyable for me.

It has been a rewarding experience to work with different facilities here in the chemistry department at LSU. I would like to give my sincere gratitude to Dr. Thomas K. Weldeghiorghis, Dr. David Vinyard, Dr. George G. Stanley, and Dr. Connie M. David for their invaluable assistance and discussions on NMR, EPR and IR spectroscopic and mass spectrometric studies.

There are many people who have influenced my creativity, self-confidence, and knowledge throughout my life to this point. For this, I am grateful to all of my committee members, and my past and present mentors and teachers: Many thanks to Dr. Evgueni E. Nesterov, Dr. Graça

Vicente, Dr. Mojtaba Bagherzadeh, Dr. Justin R. Ragains, Dr. Rendy G. Kartika, Dr. William E. Crowe, and Dr. Matthew Chambers.

Last but not least, I would like to thank my dear friends for their support, liveliness, and kindness. They have given me the extra strength and motivation to get things done. As my surrogate family, you have been a constant comfort every time that I need your companionship.

Table of Contents

List of Abbreviations

ADP……...……adenosine diphosphate

ATP……...adenosine triphosphate

b.p……..boiling point

BMPO (Boc-MPO)……...5-tert-butoxycarbonyl-5-methyl-1-pyrroline-*N*-oxide

bpt……benzylpyridyltriazole

bpy……..2,2′-bipyridine

CAN……ceric ammonium nitrate

CV……...cyclic voltammetry

dabco……..1,4-diazabicyclo[2.2.2]octane

DBU……..1,8-diazabicyclo[5.4.0]undec-7-ene

DHA……dehydroascorbic acid

DKG……..2,3-diketo-L-gulonic acid

DMAP ……...4-dimethylaminopyridine

DMPO……..5,5-dimethyl-1-pyrroline-*N*-oxide

DMSO ……dimethyl sulfoxide

EDTA……ethylenediaminetetraacetate

EPR……electron paramagnetic resonance

ESI-MS……...electrospray ionization-mass spectrometry

fac……..facial

FT-IR……Fourier transform infrared

HER……..hydrogen evolution reaction

I2M……..interaction of two M–O units

m-xpt……..……..……..…….*meta*-xylylenebis(pyridyltriazole)

m.p……melting point

mer……meridional

MLCT……metal to ligand charge transfer

$NADP^+$……..……nicotinamide adenine dinucleotide phosphate

NADPH…….dihydronicotinamide adenine dinucleotide phosphate

NMR……..nuclear magnetic resonance

OEC……..oxygen evolving complex

OTf……..triflate

PSI……...photosystem I

PSII……photosystem II

rotavap……rotatory evaporator

TBAO……...tetrabutylammonium oxalate

THF……...tetrahydrofuran

TMS……..trimethylsilyl

TOF…….turnover frequency

tpy……2,2′:6′,2″-terpyridine

UV/vis……...ultraviolet/visible

WNA……..water nucleophilic attack

WOC……water oxidation catalyst

XRD……X-ray diffraction

Abstract

A variety of pyridyltriazole ligands are readily available via click type cycloaddition of alkynylpyridines and azides. We made functionalized tetradentate *m*-xylylenebis(pyridyltriazole) (*m*-xpt) ligands with NH_2 and NMe_2 electron-donating and NO_2 electron-withdrawing substituents on the pyridine moieties. Complexation of these ligands with Cu(II) gives dimeric macrocycles with square pyramidal geometry at Cu centers. Previous work in our lab with the unsubstituted $[Cu_2(m\text{-xpt})_2(NO_3)_2]^{2+}$ complex showed reduction to Cu(I) by using ascorbate as reducing agent. Oxidation of the Cu(I) solution in air results in formation of an oxalate-bridged dimer, $[Cu_2(m\text{-xpt})_2(\mu_2\text{-}C_2O_4)]^{2+}$. Formation of the oxalate was attributed to reductive coupling of CO_2 molecules. However, in this study we report results indicating that this claim is incorrect and the copper(I) complex does not react with CO_2. Instead, the oxalate was formed from ascorbate (or dehydroascorbic acid) by reaction with O_2. In addition, in the absence of ascorbate and/or its oxidation products the copper(I) complex oxidizes to Cu(II), and with transformation of CO_2 to carbonate a trimer, $[Cu_3(m\text{-xpt})_3(\mu_3\text{-}CO_3)]^{4+}$, forms. Similar results were obtained with the new functionalized complexes.

In another study, we made different ruthenium complexes with pyridyltriazole ligands. Most of the complexes were isolated as crystals and analyzed by X-ray crystallography. High-valent ruthenium complexes made by oxidation of Ru(II) or Ru(III) precursors have been employed as catalyst for oxidation of water to O_2. We tested the two isomers of $[Ru(tpy)(bpt)(H_2O)]^{2+}$ (bpt = benzylpyridyltriazole) for water oxidation; formation of oxygen bubbles was observed from an acidic solution of one of the isomers when excess of ceric ammonium nitrate oxidant was employed.

Chapter 1. Introduction

1.1. Sustainable energy

Providing energy from sustainable sources is one of the most important scientific challenges of the 21st century. Societies always need energy to develop, and today the major part of the global energy needs is provided by fossil fuels. The high rate of fossil fuel consumption to fulfill the world's growing energy demand has created severe environmental issues that alerts the need for development of economical strategies to replace fossil fuels with renewable and clean energy supplies. The Sun provides our planet 164 Watts per square meter, averaged over a 24 hour period,[1] which makes conversion of solar energy to electricity a promising and direct strategy to a sustainable energy future. The intermittency of solar energy demands improved batteries to store the excess electricity produced in the peak production times. Moreover, the solar energy could be used for production of fuels, for example, it can potentially be used for reduction of water to hydrogen which can liberate a large amount of energy when combusted.

Plants over millions of years evolved photosynthetic machinery that harnesses energy from the Sun and produces carbohydrates and O_2. The conversion of solar energy is catalyzed by four multi-subunit membrane protein complexes. The solar energy storage by water oxidation happens in photosystem II (PSII) that pumps electrons to photosystem I (PSI) for reducing $NADP^+$ to NADPH. The electron and proton transfer from PSII to PSI is mediated by another protein complex known as cytochrome b6f. These transformations create a proton gradient that is used by the fourth complex, ATP synthase, to convert ADP to ATP. The NADPH and ATP are then required for the reduction of CO_2 to carbohydrates.

Water oxidation in PSII is catalyzed by the oxygen evolving complex (OEC). The OEC contains a cubane cluster consisting of three manganese and one calcium ions bound via bridging oxygen; a fourth manganese hangs from the cube via a μ-oxo group; see Figure 1.1.[2] The mechanism by which OEC oxidizes H_2O has been extensively studied.[3] The general opinion is that the OEC undergoes four oxidation processes and in the $S_4 \rightarrow S_0$ reaction an O_2 molecule is liberated with regeneration of the OEC. This is called the Kok cycle; see Figure 1.1.

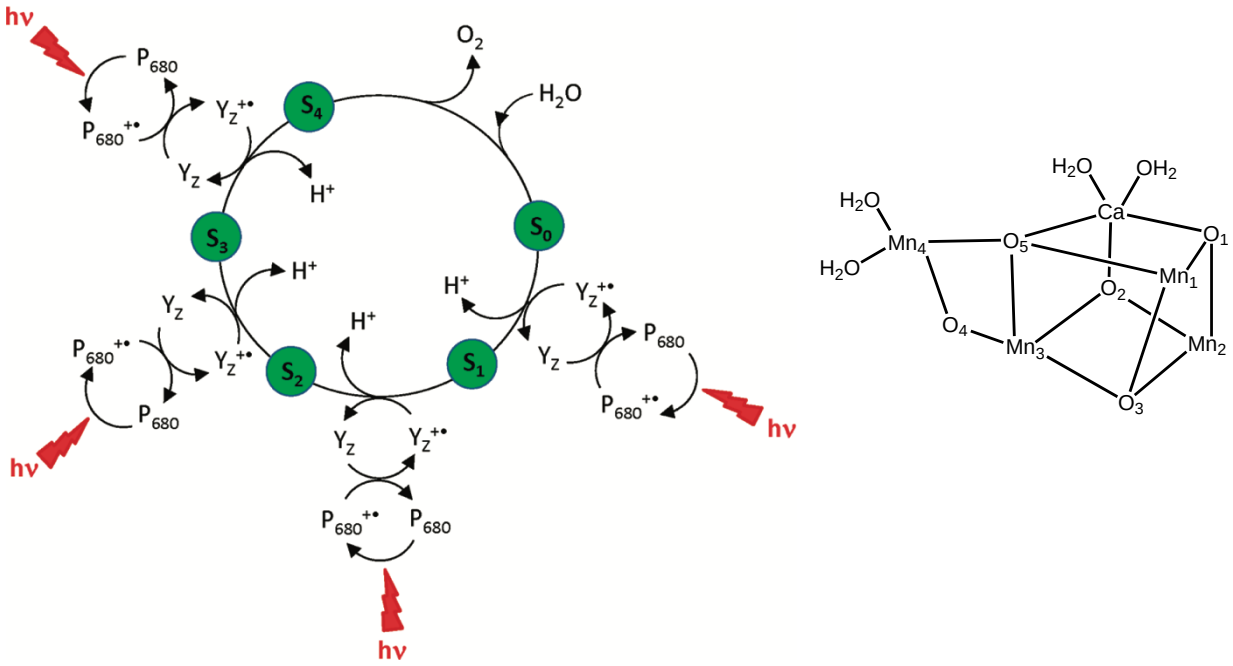

Figure 1.1. (Left) Kok cycle of photosynthetic oxygen evolution. Reprinted with permission from *Accounts of Chemical Research* **2012**, *45* (5), 767-776. (Right) Schematic representation of the OEC active site.[2]

In PSII, a dimeric chlorophyll, P680, gets excited by absorbing light; this creates a hole and an electron. The electron goes to a bound plastoquinone and transfers to PSI through some redox active cofactors. The $P680^{\bullet+}$ is a strong oxidant (E ($P680^{\bullet+}$/ P680) = 1.2 V vs. NHE) and recovers an electron from the Mn_4Ca-cluster in the OEC. Transfer of an electron from OEC to $P680^{\bullet+}$ is mediated by a tyrosine residue (Y_Z) which is a phenol compound that can undergo

reversible proton coupled electron transfer ($Y_Z \rightarrow Y_Z^{\bullet} + H^+ + e^-$) and is hydrogen bonded to a calcium-bound water molecule in the OEC. After 4 electron transfers, the holes combined in the OEC enable formation of O–O bond and formation of O_2, which regenerates the reduced state of the OEC (S_0).

The production of oxygen and electron in photoinitiated water oxidation process generates reactive (reduced) oxygen species also, such as superoxide, hydrogen peroxide, and hydroxyl radical, which can damage PSII constituents. The D1 protein, which provides most of the ligands to the OEC environment, is very susceptible to photoinhibition. Photosynthetic organisms have evolved repair mechanisms to remove photodamaged parts of PSII and insert newly synthesized sites. For example, D1 protein exhibits a high regeneration rate with reinsertion as frequently as every 30 min. With removal of D1, the OEC disassembles, and upon reinsertion of D1, the OEC reassembles.[4] Thus, according to Nocera it seems "nature invests its efforts in continually repairing an unstable catalyst rather than preparing a stable catalyst".[5]

The electrons and protons released in PSII move to other part of the photosystem. The electrons move through cytochrome b6/f to PSI and allow reduction of ferredoxin which can reduce $NADP^+$ to NADPH. The protons contribute in production of a proton gradient which drives production of ATP from ADP by ATP synthase. Combination of ATP, as a phosphate and energy source, NADPH, as a reductant, ribulose-1,5-bisphosphate as five carbon substrate and ribulose-1,5-bisphosphate carboxylase/oxygenase as an enzyme, fixes atmospheric CO_2 molecule to a three-carbon product, glyceraldehyde-3-phosphate (G3P), in a cycle known as the Calvin-Benson cycle. G3P undergoes more reactions with ATP and finally creates different sugars such as glucose.

Nature's approach in storing solar energy and hydrogens in chemical bonds of carbohydrates (or any fuel) has inspired scientists from different disciplines to develop artificial systems to mimic different components of natural photosynthesis, such as technologies to reduce CO_2 to value-added chemicals, for instance fuels (methane, methanol, etc.), and oxidation of H_2O to molecular O_2 for production of protons and electrons.[6]

Both CO_2 reduction and water oxidation are difficult reactions which require multiple electron and proton transfers to produce a stable product. Therefore, using a catalyst to decrease activation free energy is necessary. In the following, we will introduce some pioneer concepts and catalysts in CO_2 reduction and we will narrow our focus on reduction of CO_2 to oxalate. Then we will discuss the development of ruthenium water oxidation catalysts since 1982, when Meyer's group introduced the first ruthenium complex capable of oxidation of water to O_2, followed by recent examples of water oxidation catalysts with earth-abundant metals such as copper-amido and cobalt-oxo catalysts.

1.2. CO_2 reduction

An essential part of artificial photosynthesis is the reduction component, to be coupled with water oxidation to close the catalytic cycle. The electrons created by absorbing light could be used for reduction of protons or for reducing dissolved CO_2 in the solution to useful chemicals and fuels. This process is difficult because of the thermodynamic stability of CO_2 molecule: for instance, direct single electron reduction of CO_2 to $CO_2^{\bullet-}$ occurs at $E° = -1.9$ V vs. NHE.[7] As more efficient technologies for harvesting and converting solar energy to electricity have been developed, many efforts have also been taken to develop catalysts to activate CO_2 with lower kinetic barriers. In contrast to direct electron reduction, proton-coupled multielectron steps are

more feasible due to formation of more stable molecules; see table 1. For instance, reduction of CO_2 to CO or formic acid occurs at E° = –0.53 and –0.61 V vs. NHE. By comparing reduction potentials in table 1, one may think that conversion of CO_2 to for example methanol should be more feasible than to CO or HCOOH. It is noteworthy that the reaction is thermodynamically more favorable to produce methanol, however, storing 6 protons and 6 electrons for this process is a great kinetic challenge. One strategy for production of methanol is addition of hydrosilane's H–Si bond to CO_2 as reported by Parkin et al.[8] The major progress in CO_2 reduction has been achieved in $2e^-$ reduction to carbon monoxide and formate/formic acid. As an industrial solution, a mixture of CO and H_2, also known as synthetic gas, could be converted to liquid hydrocarbon fuels (C_nH_{2n+2}) with n > 1 via the well-developed Fischer-Tropsch process. Alternative to this approach, formic acid could be reduced to formaldehyde and furthermore to methanol which has higher hydrogen to carbon ratio. It is desirable to find an electrocatalyst that facilitates all of the sequences to alcohol or a group of catalysts that could work in parallel to catalyze each step toward formation of alcohols.[7]

Table 1.1. Possible products of CO_2 reduction, and proton reduction to H_2. The potentials are reported at pH 7 in aqueous solution versus NHE, 25 °C, 1 atmosphere gas pressure, and 1 M for the other solutes.[7]

$CO_2 + 2H^+ + 2e^- \longrightarrow CO + H_2O$	E° = –0.53 V
$CO_2 + 2H^+ + 2e^- \longrightarrow HCO_2H$	E° = –0.61 V
$CO_2 + 4H^+ + 4e^- \longrightarrow HCHO + H_2O$	E° = –0.48 V
$CO_2 + 6H^+ + 6e^- \longrightarrow CH_3OH + H_2O$	E° = –0.38 V
$CO_2 + 8H^+ + 8e^- \longrightarrow CH_4 + 2H_2O$	E° = –0.24 V
$CO_2 + e^- \longrightarrow CO_2^{\bullet -}$	E° = –1.9 V
$2H^+ + 2e^- \longrightarrow H_2$	E° = –0.41 V

Nature has separated the reaction centers for CO_2 reduction and water oxidation. A possible reason is that proton reduction to H_2 ($2H^+ + 2e^- \rightarrow H_2$ known as HER: hydrogen evolution reaction) is kinetically and more facile than multielectron and proton reduction of CO_2 to carbohydrates. Therefore, an ideal artificial CO_2 reduction catalyst is expected to operate selectively for reducing CO_2 in aqueous solution and circumvent competing hydrogen evolution with minimal energy loss, i.e. low overpotential.

Examples of metal complexes that mediate reduction of CO_2 to CO are common in the literature, and in general they could be categorized in three main types, with (1) macrocyclic ligands, (2) bipyridine ligands, and (3) phosphine ligands.[7] One example, $Re(bpy)(CO)_3Cl$, reported by Lehn et al. in 1984, showed reasonable stability and activity during reduction of CO_2. Functionalizing the bpy ligand with *tert*-butyl electron donors improved the catalyst activity, with a second order rate constant of 1000 M^{-1} s^{-1} and a Faradaic efficiency of about 99%.[9]

Controlling electrochemical and photochemical reduction of CO_2 over H^+ in aqueous solution is challenging, and metal hydrides can react with protons instead of CO_2 and evolve H_2. Photosynthesis overcomes this challenge by reduction of CO_2 with H_2 equivalents (such as NADPH) instead of using H_2O. Hydrogen is a clean fuel and currently it is being produced in industrial scale by reforming methane (emitting CO_2 as a byproduct), but it could potentially be manufactured by electrolysis of water using renewable solar energy power without releasing CO_2. An alternative to electro/photochemical reduction of CO_2 is catalytic hydrogenation of CO_2 to mostly C_1 products such as formic acid, methanol and methane.[10] One of the complexes facilitates homogeneous hydrogenation of CO_2 is water soluble $[Cp^*Ir^{III}(6DHBP)(OH_2)]^{2+}$ (6DHBP = 6,6′-dihydroxy-2,2′-bipyridine) which shows good activity (initial TOF = 27 h^{-1} at ambient condition)

via pendant base-aided heterolysis of H_2; see Figure 1.2. The initial Ir(III) complex reacts with H_2 and form an Ir(III)-hydride complex with one protonated pendant ligand. At basic condition, the pendant is deprotonated and the negative charge helps coordination of CO_2 to the metal center and reaction with the hydride to form formate.[11]

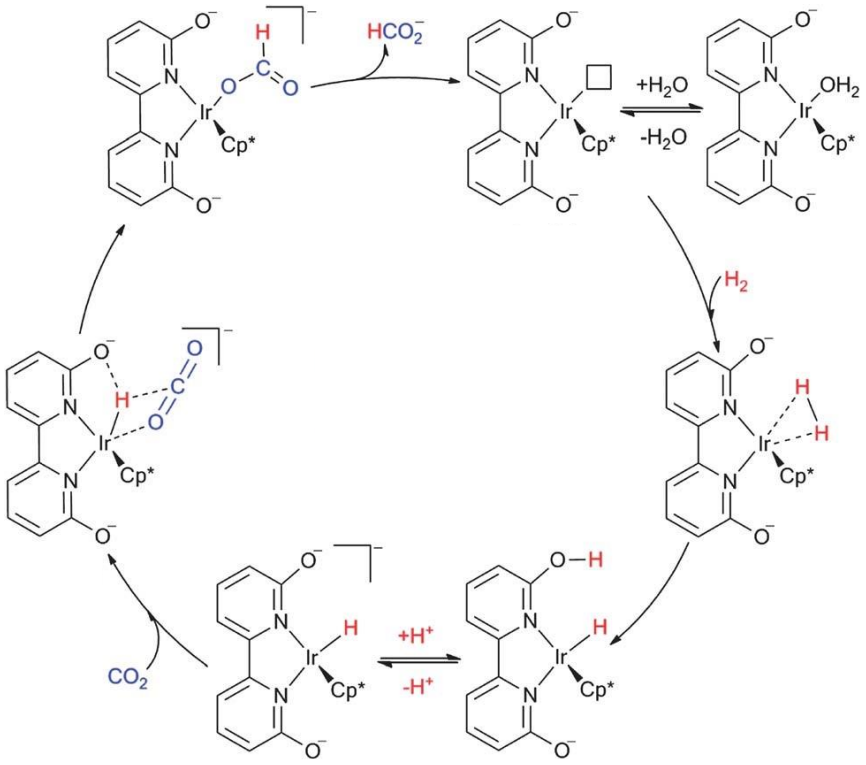

Figure 1.2. Proposed mechanism for the hydrogenation of CO_2 by an Ir(III)-hydride complex. Reprinted with permission from *Energy & Environmental Science* **2012,** *5* (7), 7923-7926. Copyright 2012, Royal Society of Chemistry.

Another potentially desirable transformation of CO_2 is reduction to oxalate ($C_2O_4^{2-}$). Oxalates were traditionally made by oxidation of carbohydrates (e.g. glucose + HNO_3) and can be used as feedstock in petrochemical companies for production of ethylene glycol. This C_2 diol is produced at a rate of more than 20 million tons a year and has application as an antifreeze and as a precursor for manufacturing of polyester fibers and resins. The traditional way of production of ethylene glycol is through oxidation of ethylene to ethylene oxide followed by hydration. Relative

to CO and formate, there are many fewer reports on CO_2 reduction to oxalate in the literature. Formation of oxalate from CO_2 is often modeled as arising from coupling of $CO_2^{\bullet-}$, although direct one electron reduction of CO_2 is very difficult to achieve (judged by the very negative electrode potential in table 1.1).

In chapters 2 and 3 of this dissertation we will show formation of oxalate anion from oxidative degradation of ascorbic acid (or ascorbate), which was previously attributed to CO_2 reduction.[12] Based on results from our lab and survey of the literature, we would like to notify the reader that even in the cases that reactions were performed under nearly pure CO_2 atmosphere, contamination with small quantities of dioxygen and subsequent oxidation of carbon-containing materials in solution to oxalate is probable and should be considered. Therefore, it is critical to provide experimental evidence that the source of the carbon atoms in oxalate is CO_2; for instance, by using labeled $^{13}CO_2$ and examining products by spectroscopic characterization techniques. In spite of the importance of the isotopic labeling experiment for careful investigation of the carbon source, only a few studies characterized ^{13}C-oxalate products. In the following we will discuss all metal assisted reduction of CO_2 to oxalate reported in the literature so far to the best of our knowledge. We will also highlight those studies that investigated the source of carbon in oxalate by labeling experiment.

One example is a diketiminato Ni(I) complex $K_2[LNi^{I}(N_2^{2-})Ni^{I}L]$, L= $[HC(C(^{t}Bu)NC_6H_3(^{i}Pr)_2)_2]^-$, introduced by Limberg's group which upon N_2 elimination forms a Ni(0) complex. This complex reduces CO_2 to form CO and CO_3^{2-} complexes. The authors also found that reaction of the similar Ni(I) precursor, $LNi^{I}(N_2)Ni^{I}L$, with CO_2 forms an oxalate bridged

Ni(II) complex, $LNi^{II}(\mu\text{-}\eta^2\text{:}\eta^2\text{-}C_2O_4)Ni^{II}L$; see Figure 1.3. No experiment with $^{13}CO_2$ was performed to verify the source of carbons in oxalate are CO_2.[13]

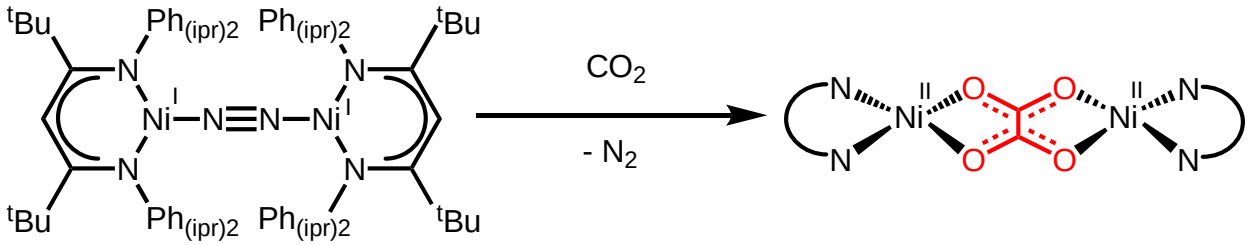

Figure 1.3. Proposed reaction of the $Ni^I(N_2)Ni^I$ complex with CO_2, and formation of $Ni^{II}(C_2O_4)Ni^{II}$ complex reported by Limberg et al.[13] The ligands in product are shown schematically for simplicity.

In another study, an iron(I) complex with tris(phosphino)borate ligand $[PhB(CH_2P(CH_2Cy)_2)_3]^-$ capable of mediating both two electron reduction cleavage of CO_2 to CO and O^{2-} (major product), and coupling of CO_2 to $C_2O_4^{2-}$ (minor product) is described by the Peters lab;[14] see Figure 1.4. FT-IR spectrum of the oxalate dimer shows an intense peak at 1647 cm^{-1} that shifts to 1598 cm^{-1} upon isotopic labeling with $^{13}CO_2$. The authors were motivated to understand the key factors that dictate the product distribution in their system. They showed exposure of methylcyclohexane solution of the complex to CO_2 generates $[LFe]_2(\mu\text{-}O)(\mu\text{-}CO)$ complex and the reaction in benzene or THF (coordinating solvents) favors production of oxalate bridging species, $[LFe]_2(\mu\text{-}\kappa OO'\text{:}\kappa OO'\text{-oxalato})$.[15] Interestingly, similar to Peters' report, Holland et al. found reduction of CO_2 with an $^{tBu}LFe(II)\text{-}N_2^{2-}\text{-}Fe(II)L^{tBu}$ complex, L^{tBu}: an imine ligand, but formation of an oxalate complex was not observed in this study.[16] The authors think formation of CO and CO_3^{2-} went through a similar mechanism that Peters reported. The complex behaves as a source of Fe(I) which reacts with CO_2 to produce a bridging carbonatodiiron complex ($^{tBu}LFe(II)(\mu\text{-}OCO_2)Fe(II)L^{tBu}$) and a dicarbonyl iron(I) complex ($^{tBu}LFe(II)(CO)_2$). They believe reductive

cleavage of C=O bond generates the CO complex and an $[^{tBu}LFe(I)]_2O$ complex as an intermediate that upon reaction with a molecule of CO_2 generates the carbonate dimer.

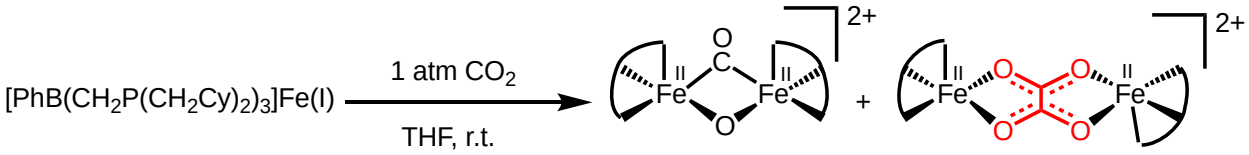

Figure 1.4. Fe(I) mediated CO_2 reductive cleavage and coupling of CO_2 reported by Peters et al.[14] The ligands in products are shown schematically for simplicity.

Among attempts in developing first-row transition metal catalyst for CO_2 reductions, it is noteworthy to mention a report of electrocatalytic reduction of CO_2 selectively to oxalate with a tetranuclear Cu(I)-sulfide complex at a high potential (at –0.03 V vs. NHE in acetonitrile). For comparison, reduction of CO_2 to CO occurs at E° = –0.12 V vs. $Fc^{+/0}$ (ca. 0.51 V vs. NHE) in acetonitrile;[17, 18] see Figure 1.5. The authors claimed that outer sphere reduction of the Cu(II) precursor generates a Cu(I) complex that is selectively oxidized by atmospheric CO_2 in the presence of O_2 and forms an oxalate-bound tetranuclear Cu(II) complex. The oxalate complex was characterized by mass spectrometry and XRD. However, the experimental mass spectra for some species don't match the calculated (simulated) mass spectra. In addition to this inconsistency, when they performed the reaction with $^{13}CO_2$, mass spectrometry did not confirm formation of a fully ^{13}C-labeled oxalate product, which overall makes a reader cautious about the conclusions drawn in this paper.[19] In addition, independent investigation of this system by Stack et al. showed no evidence of formation of oxalate.[20]

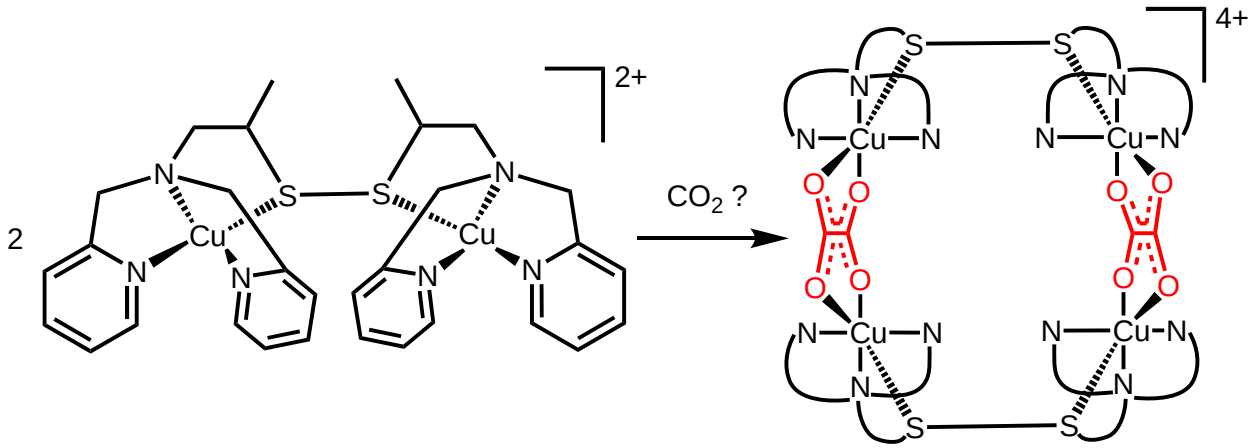

Figure 1.5. Representation of the proposed reaction of the Cu(I) dimer by Bouwman et al., and formation of a doubly oxalate-bridged Cu(II) tetramer.[19] The ligands in the product are shown schematically for simplicity.

Recently, Murray's group reported CO_2 reduction to oxalate by $[Cu_3SL]^-$ and $[Cu_3SeL]^-$ (L= tris(β-diketiminate)cyclophane) trimers and they also investigated the effect of countercation and solvent on the reaction. For example, $[CoCp^*_2][Cu_3SL]$ shows no reactivity toward CO_2 in contrast to the $[K(18\text{-crown-6})]^+$ and $[K(THF)_3]^+$ congeners in which formation of $K_2C_2O_4$ precipitate was proposed. Formation of the oxalate product was based on observing an intense peak in the range of 1615-1680 cm^{-1} and absorption shift in IR spectra from the reaction with $^{13}CO_2$. In addition, a single peak at ca 160 ppm in ^{13}C NMR spectroscopy was assigned to carbon of oxalate. However, the chemical shift reported in IR spectroscopy is not based on performing the reaction with CO_2 or $^{13}CO_2$ in exactly the same condition. Also, the two ^{13}C NMR reported for reaction of $[K(18\text{-crown-6})][Cu_3SL]$ with CO_2 or $^{13}CO_2$ are slightly different with about 5 ppm shift. The ^{13}C NMR was recorded in two different deuterated solvents, but addition of genuine $K_2C_2O_4$ in both solvents could have verified whether the solid is $K_2C_2O_4$ as was claimed.[21]

Other electrocatalysts for reduction of CO_2 have also been investigated. For instance, Savéant et al. employed electrochemically generated anion radical of small molecules such as

nitrile and esters as an electron donor mediator to CO_2 molecule. They found some substituted benzonitriles and substituted and unsubstituted benzoates catalyze the electrochemical reduction of CO_2 in DMF and exclusively transform it to oxalate.[22, 23]

In 1985, Beckers' group showed electrochemical reduction of CO_2 to oxalic acid catalyzed by silver and palladium-porphyrin complexes in anhydrous CH_2Cl_2. Formation of oxalic acid was detected by GC analysis and its diester derivative was detected by esterification with diazomethane. Beside the protons required for formation of oxalic acid, they detected H_2 in the gas phase, but the source of protons for H_2 production is not obvious.[24]

Tanaka et al. reported a series of $(M_3S_2)^{2+}$ clusters with Co, Rh and Ir that could catalyze electrochemical reduction of CO_2 selectively to oxalate. The $(M_3S_2)^{2+}$ complexes upon reduction to $(M_3S_2)^0$ by controlled potential electrolysis produce oxalate under CO_2 atmosphere in CH_3CN solution. For example, the controlled potential electrolysis of acetonitrile solution of $[Rh_3S_2](BPh_4)_2$ at −1.5 V (vs SCE) with glassy carbon electrode in the presence of $LiBF_4$ generates oxalate. In a similar reaction, when Bu_4NBF_4 is present instead of $LiBF_4$, selective formation of formate was detected. The authors were able to detect NBu_3 and 1-butene in the crude mixture, so they assumed probably Bu_4NBF_4 functions as a proton source in two electron reduction of CO_2 to formate. In this series, they highlighted the $(Co_2S_3)^0$ complex which could catalyze CO_2 reduction to oxalate at a relatively accessible potential (–0.7 V vs Ag/AgCl) while knowing that the standard redox potential for $H_2C_2O_4$ ($2CO_2 + 2H^+ + 2e^- \rightarrow H_2C_2O_4$) at pH = 0 at 25 °C is –0.432 V vs NHE.[25-27]

Jaeger et al. reported a neutral Ni(II) macrocycle with $[N_4]^{2-}$ coordinated ligand capable of reduction of CO_2 to oxalate. They showed an important role of substitution on the ligand; while

complexes with COOEt or COMe (in R_2 position; please see ref 25 for structure of the complex) are able to activate CO_2 molecule, the complexes without these substitutions undergo a fast deactivation process in the Ni(I) oxidation state. They performed detailed CV studies and found the symmetrical macrocycle with COOEt substitution is the most active catalyst for oxalate formation reported till then with an electron transfer rate constant of ca. 10^5 M^{-1} s^{-1}. [28]

Potenza's group obtained crystals of a copper dimer with bridging oxalate ligand serendipitously while making a tris(N-benzylpyrazole)Cu(I) complex.[29] Peacock's group also isolated crystals of a copper oxalate dimer originally by chance by aerial oxidation of a Cu(I) complex with triazacyclononane.[30] Although both groups claimed that the oxalate formed from reductive coupling of CO_2 molecules, no evidence was provided to support their claim.

Most of the CO_2 reduction studies mentioned above involve d-block complexes. Ziller's group, instead, examined the chemistry of $(C_5Me_5)_2Sm$ complexes with CO_2 and COS molecules. The divalent Samarium complex enables one electron reduction of CO_2 to oxalate in THF with >90% yield in 6 minutes. In order to identify oxalate-carbons, the same reaction was performed but this time with $^{13}CO_2$. IR spectroscopy studies showed C=O stretching band of the oxalate complex formed under $^{13}CO_2$ atmosphere is shifted by -40 cm^{-1} relative to the unlabeled oxalate complex. This clearly indicates that the origin of carbons is CO_2. Applying the same condition to COS substrate generates a dithiocarbonate (S_2CO^{2-}) through 2 electron reduction process.[31]

1.3. Water oxidation

Nature stores solar energy by converting CO_2 and H_2O to carbohydrates and O_2. A crucial part of this system is a water oxidation catalyst (WOC) that enables conversion of water to protons

and electrons used for reduction of CO_2. The first report of O_2 evolution in the laboratory from an aqueous solution was in 1903, when Cohen and Glaser were measuring the $Co^{II/III}$ potential, and they observed deposition of CoO_x on the surface of electrode with a catalytic current that was attributed to catalytic H_2O oxidation to O_2.

Many years later, when coordination chemistry was better understood, Meyer et al. reported a ruthenium(III) oxo-bridged dimer with bpy ligands, known as the "blue dimer", *cis*-$[(H_2O)Ru(bpy)_2(\mu\text{-}O)Ru(bpy)_2(OH)_2]^{4+}$(**1**). This complex catalyzes the oxidation of H_2O by Ce(IV) oxidant (see Figure 1.6 for structure of complex **1** and other Ru complexes mentioned below). It was initially believed the oxo bridge is necessary for water oxidation and because of synthetic difficulties in preparing such dimers, only the blue dimer and its derivatives were recognized as WOCs for about 20 years. In 2004, Llobet et al. reported the first Ru dimer without oxo bridge capable of oxidation of H_2O to O_2.[32] Many other Ru dimers, especially with N-donating organic bridging ligands, were developed after that to improve reaction rate and efficiency of water oxidation. In order to create efficient WOCs, understanding the mechanism of water oxidation is important. Two major mechanistic pathways are proposed which differ based on how critical O–O bond is formed: (1) water nucleophilic attack (WNA) and (2) interaction of two M–O units (I2M) are both shown in Figure 1.7. In WNA mechanism, water as nucleophile attacks high-valent ruthenium-oxo ($[Ru^{V}=O]^{3+}$) bond. This results in cleavage of M=O π-bond, two electron reduction of the Ru center and formation of ruthenium hydroperoxide ($[Ru^{III}–O–OH]^{2+}$). This species can undergo further oxidation to $[Ru^{IV}–OO^{-}]^{2+}$ to liberate oxygen. In I2M mechanism, the O–O bond forms by radical coupling of two $[Ru^{III}–O^{\bullet}]^{2+}$ species and formation of ruthenium-peroxide dimer that can undergo oxidation and release an oxygen molecule.

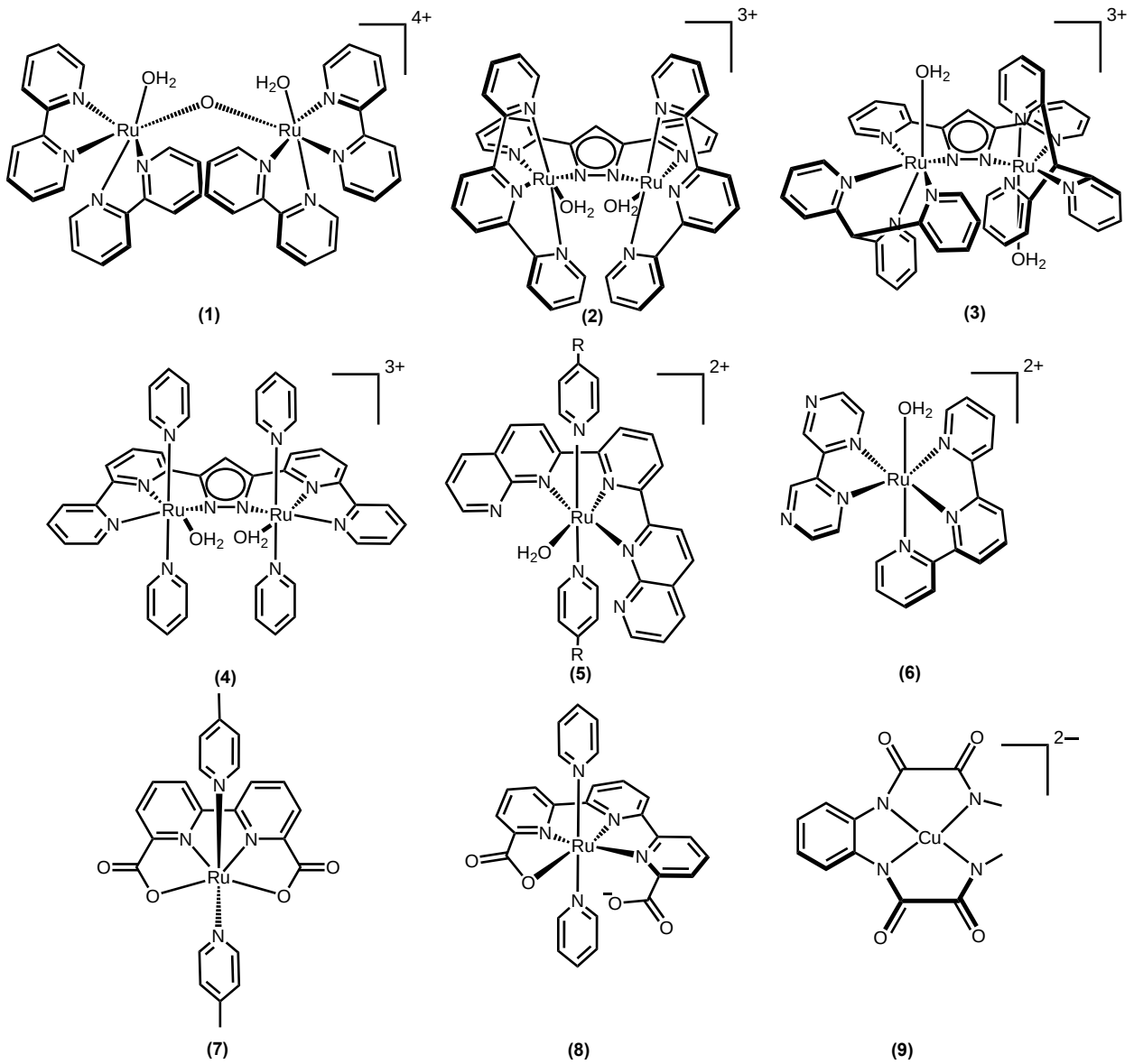

Figure 1.6. Examples of ruthenium and copper complexes capable of H_2O oxidation.[33]

In cases that Ru centers are in close proximity such as $[(H_2O)Ru(tpy)(\mu\text{-}bpp)Ru(tpy)(OH_2)]^{3+}$ (**2**) formation of a Ru–O–O–Ru bond is proposed before O_2 liberation via I2M pathway. For a similar complex, $[(H_2O)Ru(tpm)(\mu\text{-}bpp)Ru(tpm)(OH_2)]^{3+}$ (**3**) in which the H_2O molecules are fixed in trans position an I2M mechanism is also proposed but through formation of O–O bond by intermolecular combination of oxo radicals. The WNA pathway is

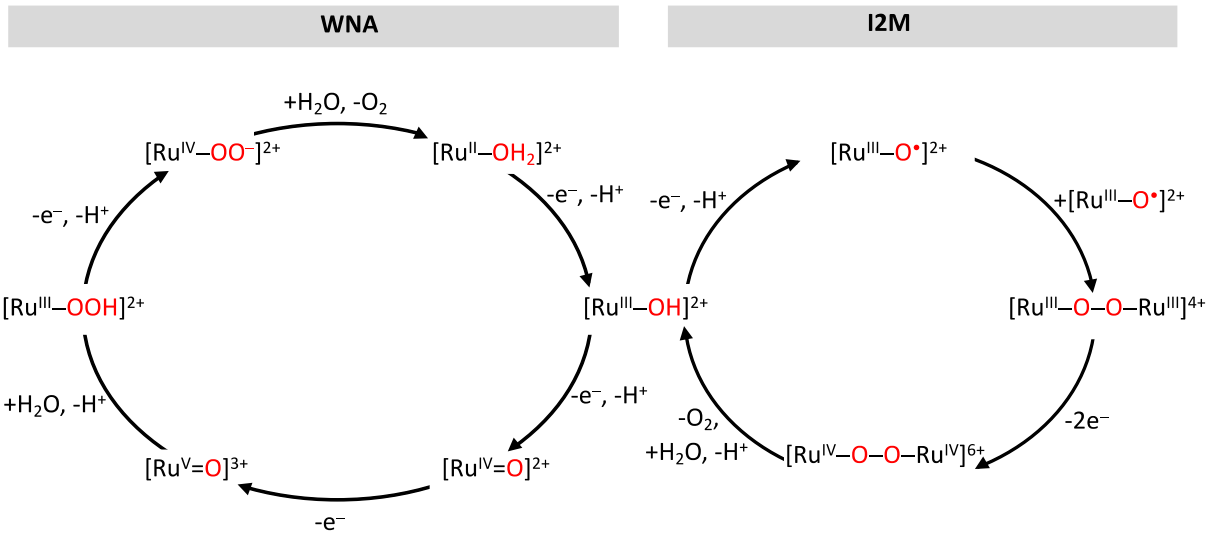

Figure 1.7. Schematic representation of WNA and I2M mechanisms explain two proposed pathways for production of O–O bond in the way of O_2 evolution catalyzed by ruthenium complexes. Based on data in references 5 and 34.

reported for instance in $[(H_2O)Ru(py)_2(\mu\text{-bbp})Ru(py)_2(OH_2)]^{3+}$ (**4**) that bond angles dictated by ligand are separating the two Ru–OH_2 sites.[32]

Although the ability of employing bridging ligands opened the way for synthesizing more diverse catalysts, making dinuclear Ru complexes is a harder task than preparing a distinct mononuclear complex. A breakthrough came with detection of O_2 evolution from monomeric complexes of ruthenium coordinated to the 2,6-di(1,8-naphthyridin-2-yl)pyridine ligand (**5**). The authors didn't performed mechanistic study to verify unimolecular nature of catalysis,[34] but in 2008 Meyer showed one Ru site is enough for H_2O oxidation catalysis by UV/vis spectroscopy studies and providing a Pourbaix diagram of $[(tpy)(bpm)Ru^{II}(OH_2)]^{2+}$ (bpm = 2,2′-bipyrimidine) (**6**).[35] They proposed that Ru monomers lose three electrons and two protons to form a $[Ru^{V}=O]^{3+}$ species, which undergoes nucleophilic attack by an H_2O molecule to form $[Ru^{III}–OOH]^{2+}$. Further oxidation forms a new intermediate which is tentatively assigned as a peroxide $[Ru^{IV}–OO]^{2+}$ and this complex finally liberates O_2 and forms the initial $[Ru–H_2O]^{2+}$ catalyst.

Ruthenium WOCs with neutral ligands usually have high reduction potential. As a consequence, in most cases, strong chemical oxidants such as Ce^{IV} ($E° Ce^{IV/III}$ = 1.61 V vs NHE in 1 M HNO_3), periodate, or peroxomonosulfate are required to activate the catalyst for water oxidation. Using such chemical oxidants is not viable for practical applications in making sustainable fuel cells. An alternative oxidant to the chemical oxidants mentioned above is $Ru(bpy)_3^{3+}$ and its derivatives with reduction potential range of 1.1-1.54 V. $Ru(bpy)_3^{3+}$ is not stable at pH>4, but it can be generated in situ by photo-driven excitation of $Ru(bpy)_3^{2+}$ to $Ru(bpy)_3^{2+}$* and then oxidation by $S_2O_8^{2-}$ as 2 e^- oxidant. The $Ru(bpy)_3^{3+}$ can also be prepared by outer sphere electron transfer on the surface of electrodes. A rational solution to decrease potential of a WOC is to use strongly donating ligands with no electron-accepting ability, which is accomplished by incorporating anionic ligands for the first time in Sun's group. Their Ru catalyst contains a bipyridyldicarboxylate (bda) ligand and two 4-picolines (picoline = 4-methylpyridine), Ru(bda-κ-N^2,O^2)$(pic)_2$ (**7**). Because of the negative charge of ligand, Ru at high oxidation state is stabilized, which results in achieving WOC activity at much lower potential ($E_{1/2}$ Ru(II/III) = –0.06 V vs. $Fc^{+/0}$) than WOC with neutral ligands. The Ru-OH_2 adduct could easily be prepared in situ by dissolving the complex in water accompanied by decoordination of one of the carboxylates. They were also able to represent X-ray structure of the seven-coordinate Ru(IV) dimer. Its bridging OH–H–OH group leads to an overall pseudo-pentagonal-bipyramidal geometry.[36] The same research group reported replacing the picoline ligands with isoquinoline facilitates formation of the peroxo dimer (Ru–O–O–Ru) by π-stacking interaction between the isoquinoline ligands. This catalyst shows TOF of ~300 s^{-1}.[37] The best WOC known so far, judged by TOF, is the carboxylate-based Ru complex **8** shown in Figure 1.6. Complex **8** at basic condition accepts an OH ligand, and forms an efficient WOC which shows TOF of 8000 s^{-1} at pH = 7 and 50000 s^{-1} at pH = 10.[38]

Ru(II) and Ru(III) complexes with typically low spin $4d^6$ and $4d^5$ electronic structure are kinetically inert, which means the ligands are less susceptible to decoordination and displacement with H_2O in aqueous solution. This feature has simplified mechanistic study of reactions in labile Ru-OH_2 sites, but Ru might be expensive for practical applications. Therefore, efforts to employ the lessons learned from Ru complexes in earth-abundant transition metals have led to the discovery and development of Mn, Fe, Co, Ni and Cu WOCs.[39] These complexes are more labile to corrosion to metal oxides and precipitate from the solution or adsorb on electrode surface. The metal oxides could potentially catalyze water oxidation. Therefore, it is essential to check the catalytic current of electrode in the fresh solution of electrolyte without the homogenous catalyst to make sure the current is not from the metal oxide adsorbed on the electrode surface.

One effort in employing first row transition metals is $[Cu^{II}(mox)]^{2-}$ (mox^{4-} = N^1,$N^{1'}$-(1,2-phenylene)bis(N^2-methyloxalamide)) (**9**), reported by Llobet et al. in 2015. Four consecutive oxidations from the metal, tetraanionic and hydroxo ligands at pH = 11.5 enable oxidation of water at potentials > 1.2 V vs. NHE with TOF of 3.6 s^{-1}. For this complex a new mechanism called SET-WNA is proposed which is based on ligand oxidation and stepwise two electron oxidation before O–O bond formation, which is different from traditional WNA that undergoes concerted two electron oxidation at the metal center. Incorporation of electron-donating ligands such as OMe group has decreased the overpotential, but resulted in one order of magnitude lower rate constant. This observation probably indicates the more electron rich complex opens ways for oxidation of ligand besides the water oxidation pathway.[40]

The Nocera group reported that cobalt-phosphate (Co-Pi) films, made by electrodeposition from phosphate buffer solutions of Co(II) salts, promote water oxidation at an onset potential of

1.23 V vs. NHE (lower limit of TOF = ~ 2×10^{-3} s^{-1}) under benign conditions. Studies based on XAS (X-ray absorption spectroscopy), extended X-ray absorption fine structure (EXAFS) and EPR proposed that the Co-Pi film is made of cobalt with oxo in octahedral geometry, and phosphates are coordinated to the outer parts of the cobalt-oxo network. The Co-Pi catalyst resembles the cubane-type structure (M_4O_4) of OEC in PSII; see Figure 1.8.

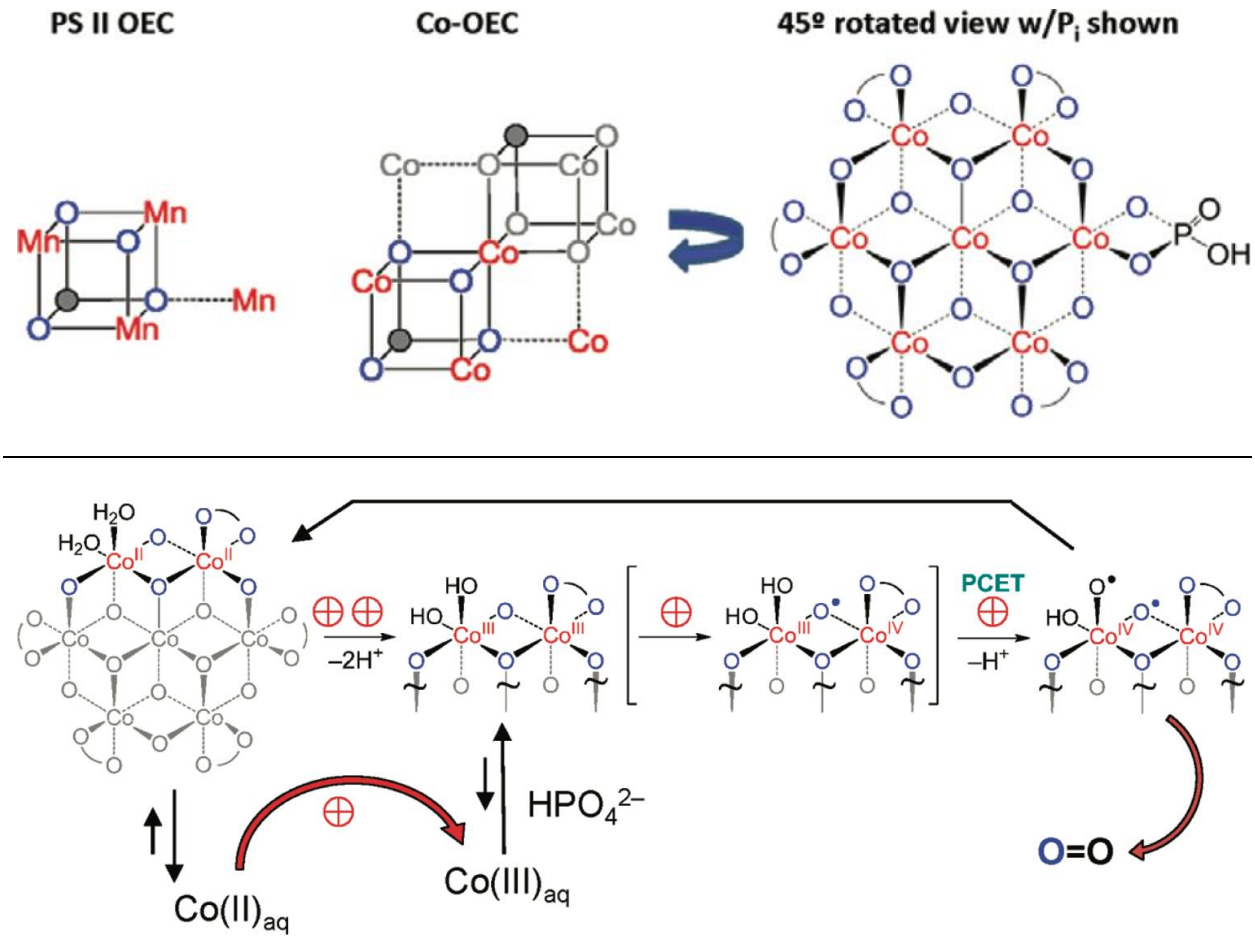

Figure 1.8. Top: (left) Schematic of cubane structure of PSII-OEC. (middle) Structure of the Co-OEC as determined from EXAFS (Pi not shown). Co-OEC is the head-to-tail dimer of the cubane of PSII-OEC. (right) Co-OEC structure rotated by 45° to more clearly show edge sharing octahedra. Bottom: Proposed pathway for water oxidation by Co-OEC. Reprinted with permission from *Accounts of Chemical Research* **2012**, *45* (5), 767-776. Copyright 2019, American Chemical Society.

For this system having proton accepting electrolyte is important and in unbuffered electrolytes, the Co-Pi catalysts undergo protonation during water oxidation which induces corrosion. Labeling experiments with ^{57}Co(II) and ^{32}P-phosphate showed in the absence of applied potential Co-Pi catalyst leach into solution slowly, but they reabsorb on the electrode by reapplying potential of 1.30 V.[5, 41] This self-healing feature along with low cost earth abundant materials of the film has made this system intriguing. Operation in neutral pH enabled to assemble an artificial leaf for water splitting by coupling the Co-Pi OEC to a NiMoZn alloy capable of proton reduction to H_2.[42] In addition, interfacing of water splitting catalysis to H_2-oxidation microorganisms was accomplished to convert CO_2 to biomass via the growth of *Ralstonia eutropha* bacterium.[43]

In this dissertation we will discuss the reactivity of copper dimers toward reduction of CO_2 and their ability to bind oxalate and carbonate as guests. This will be followed by report on preparation of new ruthenium-aqua complexes and their water oxidation ability.

1.4. References

1. Wikipedia. https://en.wikipedia.org/wiki/Sunlight (accessed Apr 20, 2020).

2. Suga, M.; Akita, F.; Hirata, K.; Ueno, G.; Murakami, H.; Nakajima, Y.; Shimizu, T.; Yamashita, K.; Yamamoto, M.; Ago, H., Native structure of photosystem II at 1.95 Å resolution viewed by femtosecond X-ray pulses. *Nature* **2015,** *517* (7532), 99-103.

3. Renger, G.; Renger, T., Photosystem II: the machinery of photosynthetic water splitting. *Photosynthesis Research* **2008,** *98* (1-3), 53-80.

4. Burnap, R. L., D1 protein processing and Mn cluster assembly in light of the emerging photosystem II structure. *Physical Chemistry Chemical Physics* **2004,** *6* (20), 4803-4809.

5. Nocera, D. G., The artificial leaf. *Accounts of Chemical Research* **2012,** *45* (5), 767-776.

6. Karkas, M. D.; Verho, O.; Johnston, E. V.; Åkermark, B., Artificial photosynthesis: molecular systems for catalytic water oxidation. *Chemical Reviews* **2014,** *114* (24), 11863-12001.

7. Benson, E. E.; Kubiak, C. P.; Sathrum, A. J.; Smieja, J. M., Electrocatalytic and homogeneous approaches to conversion of CO_2 to liquid fuels. *Chemical Society Reviews* **2009,** *38* (1), 89-99.

8. Rauch, M.; Parkin, G., Zinc and magnesium catalysts for the hydrosilylation of carbon dioxide. *Journal of the American Chemical Society* **2017,** *139* (50), 18162-18165.

9. Smieja, J. M.; Kubiak, C. P., $Re(bipy\text{-}tBu)(CO)_3Cl^-$ improved catalytic activity for reduction of carbon dioxide: IR-spectroelectrochemical and mechanistic studies. *Inorganic Chemistry* **2010,** *49* (20), 9283-9289.

10. Wang, W.-H.; Himeda, Y.; Muckerman, J. T.; Manbeck, G. F.; Fujita, E., CO_2 hydrogenation to formate and methanol as an alternative to photo-and electrochemical CO_2 reduction. *Chemical Reviews* **2015,** *115* (23), 12936-12973.

11. Wang, W.-H.; Hull, J. F.; Muckerman, J. T.; Fujita, E.; Himeda, Y., Second-coordination-sphere and electronic effects enhance iridium(III)-catalyzed homogeneous hydrogenation of carbon dioxide in water near ambient temperature and pressure. *Energy & Environmental Science* **2012,** *5* (7), 7923-7926.

12. Pokharel, U. R.; Fronczek, F. R.; Maverick, A. W., Reduction of carbon dioxide to oxalate by a binuclear copper complex. *Nature Communications* **2014,** *5*, 5883.

13. Horn, B.; Limberg, C.; Herwig, C.; Braun, B., Nickel(I)-mediated transformations of carbon dioxide in closed synthetic cycles: reductive cleavage and coupling of CO_2 generating $Ni^{I}CO$, $Ni^{II}CO_3$ and $Ni^{II}C_2O_4Ni^{II}$ entities. *Chemical Communications* **2013,** *49* (93), 10923-10925.

14. Lu, C. C.; Saouma, C. T.; Day, M. W.; Peters, J. C., Fe(I)-mediated reductive cleavage and coupling of CO_2: An $Fe^{II}(\mu\text{-}O, \mu\text{-}CO)Fe^{II}$ core. *Journal of the American Chemical Society* **2007,** *129* (1), 4-5.

15. Saouma, C. T.; Lu, C. C.; Day, M. W.; Peters, J. C., CO_2 reduction by Fe(I): solvent control of C–O cleavage versus C–C coupling. *Chemical Science* **2013,** *4* (10), 4042-4051.

16. Sadique, A. R.; Brennessel, W. W.; Holland, P. L., Reduction of CO_2 to CO using low-coordinate iron: formation of a four-coordinate iron dicarbonyl complex and a bridging carbonate complex. *Inorganic Chemistry* **2008,** *47* (3), 784-786.

17. Pegis, M. L.; Roberts, J. A.; Wasylenko, D. J.; Mader, E. A.; Appel, A. M.; Mayer, J. M., Standard reduction potentials for oxygen and carbon dioxide couples in acetonitrile and N,N-dimethylformamide. *Inorganic Chemistry* **2015,** *54* (24), 11883-11888.

18. Pavlishchuk, V. V.; Addison, A. W., Conversion constants for redox potentials measured versus different reference electrodes in acetonitrile solutions at 25 C. *Inorganica Chimica Acta* **2000,** *298* (1), 97-102.

19. Angamuthu, R.; Byers, P.; Lutz, M.; Spek, A. L.; Bouwman, E., Electrocatalytic CO_2 conversion to oxalate by a copper complex. *Science* **2010,** *327* (5963), 313-315.

20. Thomas, A. M.; Lin, B.-L.; Wasinger, E. C.; Stack, T. D. P., Ligand noninnocence of thiolate/disulfide in dinuclear copper complexes: solvent-dependent redox isomerization and proton-coupled electron transfer. *Journal of the American Chemical Society* **2013,** *135* (50), 18912-18919.

21. Cook, B. J.; Di Francesco, G. N.; Abboud, K. A.; Murray, L. J., Countercations and solvent influence CO_2 reduction to oxalate by chalcogen-bridged tricopper cyclophanates. *Journal of the American Chemical Society* **2018,** *140* (17), 5696-5700.

22. Gennaro, A.; Isse, A. A.; Saveant, J.-M.; Severin, M.-G.; Vianello, E., Homogeneous electron transfer catalysis of the electrochemical reduction of carbon dioxide. Do aromatic anion radicals react in an outer-sphere manner? *Journal of the American Chemical Society* **1996,** *118* (30), 7190-7196.

23. Gennaro, A.; Isse, A. A.; Severin, M.-G.; Vianello, E.; Bhugun, I.; Savéant, J.-M., Mechanism of the electrochemical reduction of carbon dioxide at inert electrodes in media of low proton availability. *Journal of the Chemical Society, Faraday Transactions* **1996,** *92* (20), 3963-3968.

24. Becker, J. Y.; Vainas, B.; Eger, R.; Kaufman, L., Electrocatalytic reduction of CO_2 to oxalate by Ag^{II} and Pd^{II} porphyrins. *Journal of the Chemical Society, Chemical Communications* **1985,** (21), 1471-1472.

25. Kushi, Y.; Nagao, H.; Nishioka, T.; Isobe, K.; Tanaka, K., Oxalate formation in electrochemical CO_2 reduction catalyzed by Rhodium-Sulfur cluster. *Chemistry Letters* **1994,** *23* (11), 2175-2178.

26. Kushi, Y.; Nagao, H.; Nishioka, T.; Isobe, K.; Tanaka, K., Remarkable decrease in overpotential of oxalate formation in electrochemical CO_2 reduction by a metal–sulfide cluster. *Journal of the Chemical Society, Chemical Communications* **1995,** (12), 1223-1224.

27. Bratsch, S. G., Standard electrode potentials and temperature coefficients in water at 298.15 K. *Journal of Physical and Chemical Reference Data* **1989,** *18* (1), 1-21.

28. Rudolph, M.; Dautz, S.; Jäger, E.-G., Macrocyclic $[N_4^{2-}]$ coordinated nickel complexes as catalysts for the formation of oxalate by electrochemical reduction of carbon dioxide. *Journal of the American Chemical Society* **2000,** *122* (44), 10821-10830.

29. Stibrany, R. T.; Schugar, H. J.; Potenza, J. A., A copper(II)–oxalate compound resulting from the fixation of carbon dioxide: μ-oxalato-bis[bis(1-benzyl-1H-pyrazole)(trifluoromethane-sulfonato)copper(II)]. *Acta Crystallographica Section E Structure Reports Online* **2005,** *61* (10), m1904-m1906.

30. Farrugia, L. J.; Lopinski, S.; Lovatt, P. A.; Peacock, R. D., Fixing carbon dioxide with copper: crystal structure of [LCu(mu-C_2O_4)CuL][Ph_4B]$_2$ (L = N,N',N''-triallyl-1,4,7-triazacyclo-nonane). *Inorganic Chemistry* **2001,** *40* (3), 558-559.

31. Evans, W. J.; Seibel, C. A.; Ziller, J. W., Organosamarium-mediated transformations of CO_2 and COS: Monoinsertion and disproportionation reactions and the reductive coupling of CO_2 to [O_2CCO_2]$_2$. *Inorganic Chemistry* **1998,** *37* (4), 770-776.

32. Sens, C.; Romero, I.; Rodríguez, M.; Llobet, A.; Parella, T.; Benet-Buchholz, J., A new Ru complex capable of catalytically oxidizing water to molecular dioxygen. *Journal of the American Chemical Society* **2004,** *126* (25), 7798-7799.

33. Matheu, R.; Garrido-Barros, P.; Gil-Sepulcre, M.; Ertem, M. Z.; Sala, X.; Gimbert-Suriñach, C.; Llobet, A., The development of molecular water oxidation catalysts. *Nature Reviews Chemistry* **2019,** *3* (5), 331-341.

34. Zong, R.; Thummel, R. P., A new family of Ru complexes for water oxidation. *Journal of the American Chemical Society* **2005,** *127* (37), 12802-12803.

35. Concepcion, J. J.; Jurss, J. W.; Templeton, J. L.; Meyer, T. J., One site is enough. Catalytic water oxidation by [Ru(tpy)(bpm)(OH_2)]$^{2+}$ and [Ru(tpy)(bpz)(OH_2)]$^{2+}$. *Journal of the American Chemical Society* **2008,** *130* (49), 16462-16463.

36. Duan, L.; Fischer, A.; Xu, Y.; Sun, L., Isolated seven-coordinate Ru(IV) dimer complex with [HOHOH]$^-$ bridging ligand as an intermediate for catalytic water oxidation. *Journal of the American Chemical Society* **2009,** *131* (30), 10397-10399.

37. Duan, L.; Bozoglian, F.; Mandal, S.; Stewart, B.; Privalov, T.; Llobet, A.; Sun, L., A molecular ruthenium catalyst with water-oxidation activity comparable to that of photosystem II. *Nature Chemistry* **2012,** *4* (5), 418-423.

38. Matheu, R.; Ertem, M. Z.; Benet-Buchholz, J.; Coronado, E.; Batista, V. S.; Sala, X.; Llobet, A., Intramolecular proton transfer boosts water oxidation catalyzed by a Ru complex. *Journal of the American Chemical Society* **2015,** *137* (33), 10786-10795.

39. Wang, J.-W.; Zhong, D.-C.; Lu, T.-B., Artificial photosynthesis: Catalytic water oxidation and CO_2 reduction by dinuclear non-noble-metal molecular catalysts. *Coordination Chemistry Reviews* **2018,** *377*, 225-236.

40. Garrido-Barros, P.; Funes-Ardoiz, I.; Drouet, S.; Benet-Buchholz, J.; Maseras, F.; Llobet, A., Redox non-innocent ligand controls water oxidation overpotential in a new family of mononuclear Cu-based efficient catalysts. *Journal of the American Chemical Society* **2015,** *137* (21), 6758-6761.

41. Surendranath, Y.; Kanan, M. W.; Nocera, D. G., Mechanistic studies of the oxygen evolution reaction by a cobalt-phosphate catalyst at neutral pH. *Journal of the American Chemical Society* **2010,** *132* (46), 16501-16509.

42. Reece, S. Y.; Hamel, J. A.; Sung, K.; Jarvi, T. D.; Esswein, A. J.; Pijpers, J. J.; Nocera, D. G., Wireless solar water splitting using silicon-based semiconductors and earth-abundant catalysts. *Science* **2011,** *334* (6056), 645-648.

43. Dogutan, D. K.; Nocera, D. G., Artificial photosynthesis at efficiencies greatly exceeding that of natural photosynthesis. *Accounts of Chemical Research* **2019,** *52* (11), 3143-3148.

Chapter 2. Reactivity of Functionalized Cu(I)-xpt Complexes with CO_2 and Air

2.1. Introduction and previous work

Metal-organic supramolecular chemistry has attracted attention for many years. The most common way to make predictable metal-organic assemblies is to choose a combination of a metal and a ligand with rigid structure such as linear or planar geometry, instead of flexible chelates. As a result, the geometry of the coordinated ligand transfers to the larger assembly and enables predicting the structure of the final supramolecule. Our lab has studied chemistry of complexes with β-diketonate and ketoenamine planar ligands for several years, and used these planar chelating ligands as components of a variety of metallo-supramolecular cages. These studies showed bond between Cu^{2+} and diketonate are somewhat flexible, which permits assembly of unexpected structures. For example, the angle between β-diketones in *m*-phenylenebis(acetylacetone) (*m*-pbaH_2; see Figure 2.1) is about 120°. On the basis of this geometry, formation of a "molecular hexagon" upon treatment with Cu^{2+} was expected; however only a square tetramer was obtained. Similarly, the reaction of *o*-phenylenebis(acetylacetone) with Cu^{2+} yields a dimer instead of a trimer which was expected from the angle of 60° between the β-diketones.[1]

The recent focus of our group has been on metallo-supramolecular structures of Cu^{2+} with pyridyltriazole ligands. The more rigid N-donating pyridyltriazole ligands are expected to yield supramolecular structures with greater predictability. A former member of our group synthesized bis(pyridyltriazole) coordinating ligands with *m*-xylene or 2,7-dimethylnaphthalene linkers (*m*-xpt and npt respectively). Macrocyclic dimers with rectangular shape were synthesized by treatment of $CuCl_2$ or $Cu(NO_3)_2$ and NH_4PF_6 to *m*-xpt or npt ligands; $[Cu_2(m\text{-xpt})_2Cl_2]Cl_2$ (**1**) and

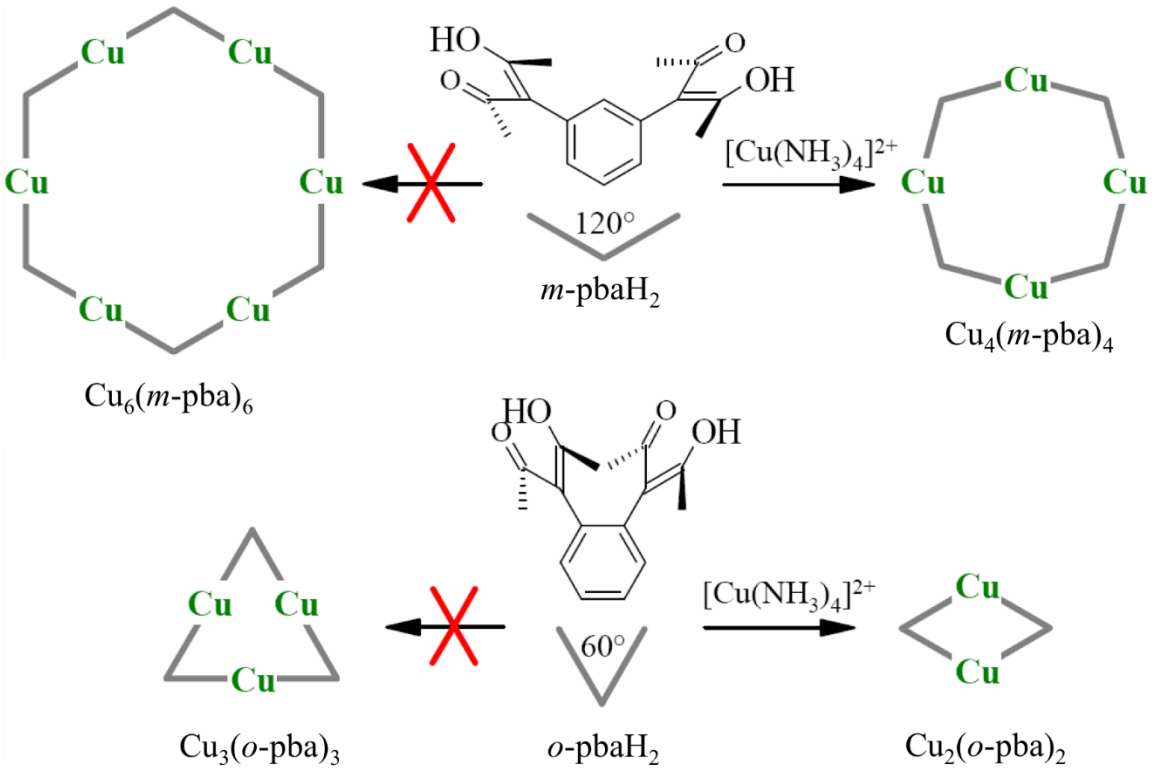

Figure 2.1. Preparation of supramolecular copper complexes from the meta (top) and ortho (bottom) isomers of the bis(β-diketone) $pbaH_2$. Adopted with permission from *Inorganic Chemistry* **2011**, *50* (7), 2748–2753. Copyright 2011, American Chemical Society.

$[Cu_2(npt)_2(DMF)_3(H_2O)](PF_6)_4$ (**2**). The complex with the 2,7-dimethylnaphthalene linker provides a suitable cavity to host 1,4-diazabicyclo[2.2.2]octane (dabco) internally; $[Cu_2(npt)_2(\mu\text{-dabco})](PF_6)_4$ (**3**); see Figure 2.2.[2]

The X-ray crystal structure of **1** and its counterpart $[Cu_2(m\text{-xpt})_2(NO_3)_2](PF_6)_2$ (**4**) showed the distances between copper centers are 7.14 and 6.84 Å respectively, which is theoretically long enough to accommodate a dabco molecule. On the way of exploring the possibility of using those complexes to host dabco molecule, instead of a dabco-bridged dimer similar to **3**, a mixture of carbonate trimer $[Cu_3(m\text{-xpt})_3(\mu_3\text{-}CO_3)](PF_6)_4$ (**5**) and an oxalate dimer $[Cu_2(m\text{-xpt})_2(\mu\text{-}C_2O_4)](PF_6)_2$ (**6**) were isolated unexpectedly; see Figure 2.2. Initially cocrystals of **5** and **6**

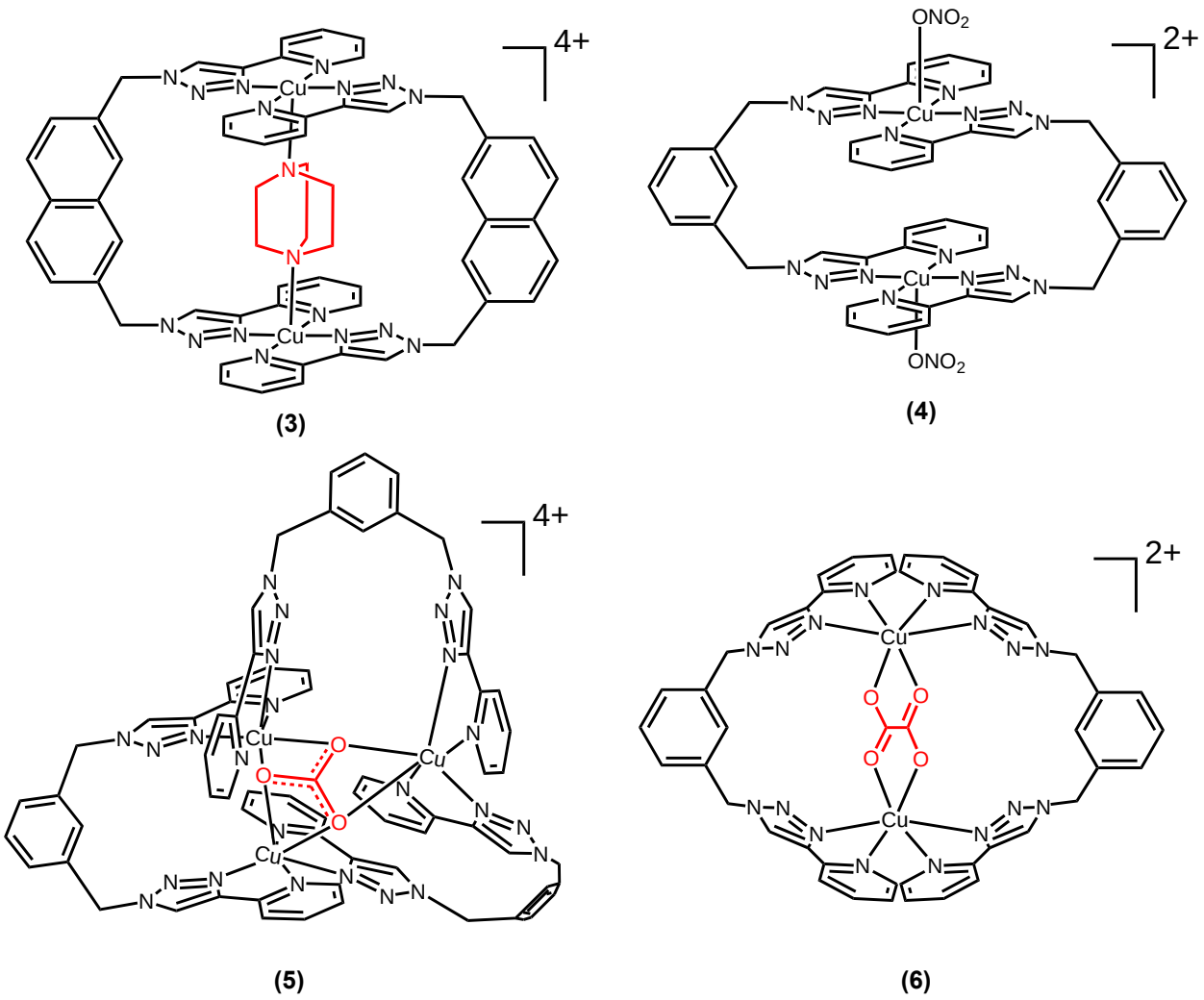

Figure 2.2. Structure of $Cu_2(npt)_2(\mu\text{-dabco})^{4+}$ (**3**), $Cu_2(m\text{-xpt})_2(NO_3)_2^{2+}$ (**4**), $Cu_3(m\text{-xpt})_3(\mu_3\text{-}CO_3)^{4+}$ (**5**) and $Cu_2(m\text{-xpt})_2(\mu\text{-}C_2O_4)^{2+}$ (**6**).

along with discrete crystals of **5** were isolated and characterized by X-ray crystallography. Then, further characterization analysis with IR spectroscopy and elemental analysis confirmed formation of the products.

The source of carbon in formation of carbonate is believed to be the atmospheric CO_2. Carbonate could form in this system if dabco, as a base, enables activation and transformation of CO_2 to CO_3^{2-} via hydration or reaction with hydroxide and deprotonation in DMF solvent, then CO_3^{2-} could work as template in formation of **5**.

Upon addition of dabco to the acetonitrile solution of **4**, the color of solution changed from blue to green and brown under N_2. The color change was interpreted as some of the Cu(II) centers are reduced to Cu(I) by dabco given that solutions of pure Cu(I) complexes are usually yellow. The yellow color of Cu(I) solutions arises from absorption of light with wavelengths roughly shorter than 500 nm due to MLCT bands, and absence of any d-d absorption at longer wavelengths due to having a full d^{10} structure. The ability of tertiary amines such as dabco to release an electron to form a relatively stable radical is shown in the literature. For example, Baran's group recently introduced a strategy in which employing a redox mediator enables oxidation of unactivated methine and methylene carbons at relatively low potentials. In one of their papers a series of N-redox mediators such as dabco, quinuclidine, etc. were tested to identify a viable species for electron transfer. This study showed the redox mediator loses an electron in the anode and forms a stable cationic radical which attacks C–H bond and enables C–H homolytic abstraction and formation of a radical carbon which undergoes aerobic oxidation to form ketone or alcohol; see Figure 2.3.[3] Another example is using tertiary amines such as triethylamine or *N*-ethylmorpholine for reduction of Ru(III) complexes to Ru(II).[4]

Formation of complex **6** was believed to occur through reduction of two CO_2 molecules by Cu(I) centers and formation of a C–C bond according to equation 2.1. It is thermodynamically hard to achieve one electron reduction of CO_2 ($E = -1.9$ V vs NHE).[5] In addition, selective coupling of the highly reactive $CO_2^{\bullet-}$ among many other possible pathways (e.g protonation to $HCO_2^{\bullet}$) sounds challenging too. Therefore, from the chemistry standpoint, studying a possible reductive

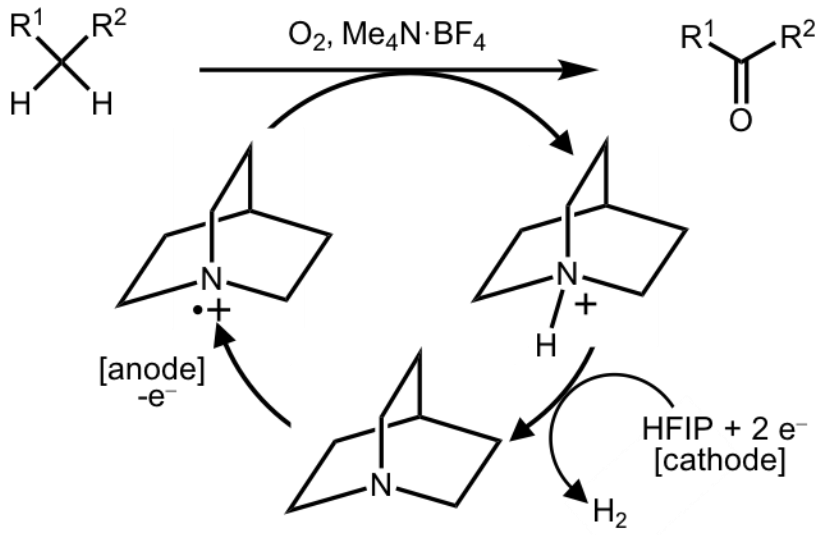

Figure 2.3. Putative mechanism for the quinuclidine-mediated electrochemical C−H oxidation. HFIP:Hexafluoro-2-propanol.[3]

coupling of CO_2 to oxalate is more interesting than hydration of CO_2 to carbonate.

$$2Cu^{+} + 2CO_2 \rightarrow 2Cu^{2+} + C_2O_4^{2-} \qquad (2.1)$$

With the aim of controlling the direction of the reaction toward selective formation of oxalate product, our group tried different solvents and reducing agents. The oxalate dimer **6** was obtained in ca. 96% yield when **4** was reduced to $[Cu_2(m\text{-xpt})_2](PF_6)_2$ (**7**) by ascorbate at room temperature under N_2 atmosphere, and subsequently exposing the solution to air or a balloon of CO_2. Complete conversion of **1** to **7** was detected by monitoring disappearance of Cu(II) d-d absorption at 722 nm and appearance of a new absorption at 364 nm due to Cu(I) to pyridyltriazole charge transfer. Upon exposure of the yellow solution of **7** to a balloon of CO_2 (or air) a new Cu(II) d-d absorption peak at 731 nm appeared. From this crude mixture single crystals of **6** were obtained and analyzed by X-ray crystallography. The FT-IR spectrum of **6** showed a new strong peak at 1670 cm^{-1} which was assigned to oxalate C=O stretching band. Following enhancement of the Cu(II) absorption peak in the course of the reaction with CO_2 showed formation of **6** obeys pseudo-first-order kinetics, with a rate constant of 0.019 h^{-1}.[6]

We envisioned that an *m*-xpt ligand with electron-donating functional groups such as NH_2 or NMe_2 could make the Cu(I) complex a more powerful reductant, leading to faster CO_2 reduction. On the other hand, an electron-withdrawing functional group such as NO_2 was expected to decrease the rate of CO_2 reduction to oxalate. In the following, we will discuss synthesis of three new functionalized xpt ligands and their Cu complexes (see Figure 2.4), and a study of their reactions with CO_2 and air. These results led to revisiting the proposed reductive coupling of CO_2 as the original source of oxalate.

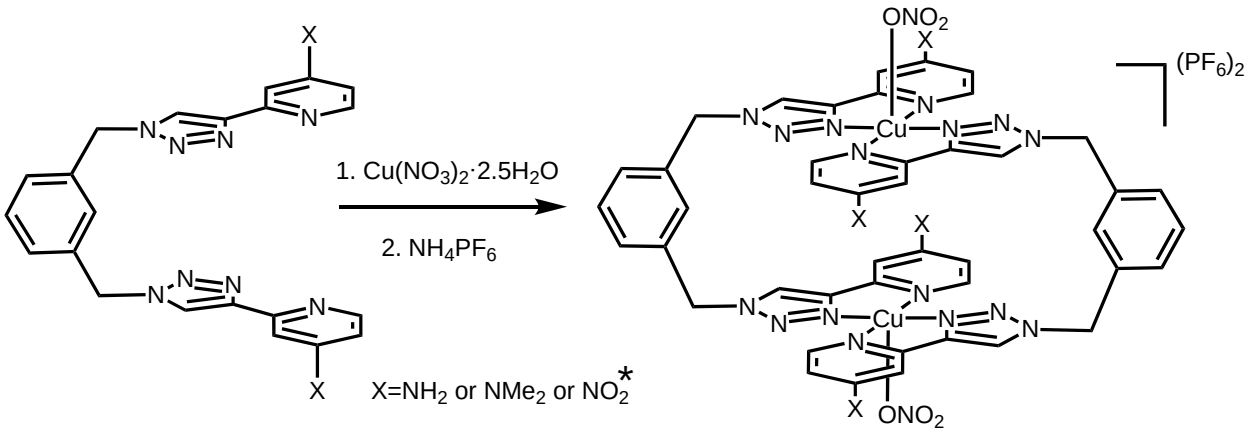

Figure 2.4. Structure of functionalized-xpt ligands and their complexes. * In the case of O_2N-xpt, metathesis with NH_4PF_6 was not performed.

2.2. Results and discussion

The ability of ligands to donate electrons to metal centers could be estimated by comparing their basicity or pK_a. According to Baran's pK_a table,[7] protonated pyridine has pK_a of 5.2. Substituting the 4-position of pyridine with NH_2 or NO_2 changes the pK_a of the conjugate acid to 9.2 or 1.6, respectively. The electronic effect of these substitutions on the redox properties of the metal center is shown for instance in $[(tpm)(4,4'\text{-}(X)_2\text{-bpy})Ru^{II}(H_2O)]^{2+}$ complexes by Llobet.[8] The $Ru^{III/II}$ potential for X = H is 0.40 V and decreases to 0.21 when X = NH_2 and increases to 0.56 V for X = NO_2 at the same condition.

2.2.1. H_2N-xpt

Due to synthetic simplicity, we decided to modify the pyridine part of the *m*-xpt ligand. Synthesis of the H_2N-xpt ligand (**8**) initiated from deprotonating commercially available 2-ethynylpyridine-4-amine·HCl with Na_2CO_3 and following our normal "click" procedure. However, extraction couldn't be used for separation of the H_2N-xpt product because of its low solubility in chloroform. Therefore, after working up the reaction with NH_3/Na_2H_2EDTA solution, chloroform was added only to remove possible impurities. Then the suspension in the aqueous layer was filtered and the solid was washed with fresh water and chloroform and dried in air. This gave light cream solid **8** in good yield. Complexation with $Cu(NO_3)_2$ gave $[Cu_2(H_2N\text{-}xpt)_2(NO_3)_2](NO_3)_2$ (**9**) and after metathesis with NH_4PF_6 $[Cu_2(H_2N\text{-}xpt)_2(NO_3)_2](PF_6)_2$ (**10**) was obtained.

Cyclic voltammetry of **9** and **10** both show an irreversible $Cu^{II/I}$ redox process; see Figure 2.5. This makes it difficult to compare redox potentials of **9** and **10** to that of **4**. However, an estimate can be made by comparing the cathodic peak potentials of the three complexes: **9**, E_{pc} = 0.014 V; **10**, 0.029 V; and **4**, 0.18 V all vs. Ag/AgCl. This estimates reduction of **9** and **10** to be harder than that of **4**. This was expected, since there is more electron density on the Cu centers of **9** and **10** than on those of **4**. In agreement with these electrochemical results, chemical reduction to Cu(I) by ascorbate is also more difficult for **9** and **10**: an excess of ascorbate and stirring for a longer time had to be employed to observe complete reduction.

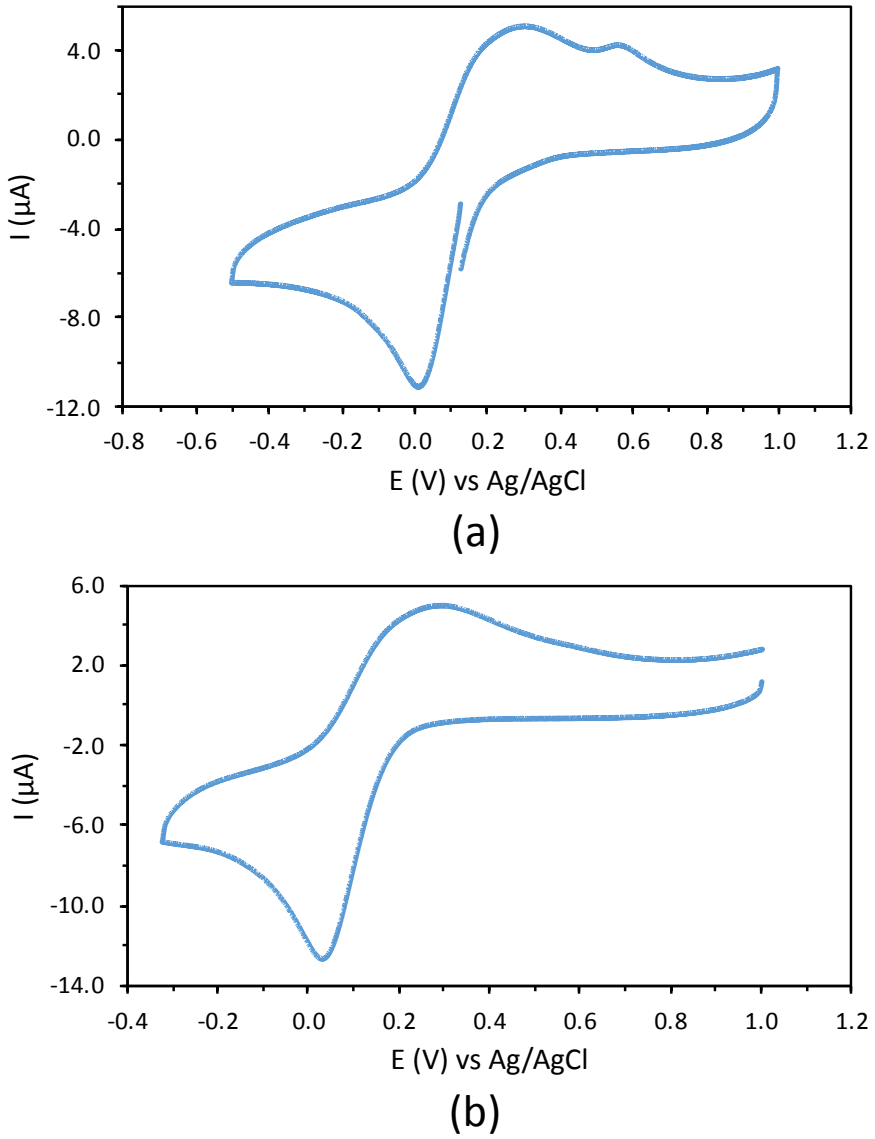

Figure 2.5. CV of (a) $[Cu_2(H_2N\text{-xpt})_2(NO_3)_2](NO_3)_2$ (**9**) and (b) $[Cu_2(H_2N\text{-xpt})_2(NO_3)_2](PF_6)_2$ (**10**). The solutions are in DMF containing 0.1 M Bu_4NPF_6 recorded on a static glassy carbon disc working electrode with a Pt wire auxiliary electrode and Ag/AgCl reference electrode at 25 °C at a scan rate of 100 mV s^{-1}. Addition of ferrocene to solution of **9** showed $E_{1/2}$ $Fc^{+/0}$ = 0.552 V (ΔEp = 0.077 V) and to solution of **10** showed $E_{1/2}$ $Fc^{+/0}$ = 0.559 V (ΔEp = 0.090 V).

I attempted to study the reaction of CO_2 with the new *in situ* generated copper(I) complexes, $Cu_2(H_2N\text{-xpt})_2(NO_3)_2$ (**11**) and $Cu_2(H_2N\text{-xpt})_2(PF_6)_2$ (**12**) made by ascorbate; see Figure 2.6 for UV-vis absorption spectra of yellow solution of $Cu_2(H_2N\text{-xpt})_2(NO_3)_2$, and successive spectra showing development of a green color (λ_{max}=678 nm) due to Cu(II) after

exposure to CO_2. However, crystals grown by ether vapor diffusion into the oxidized mixture were of the $[Cu_3(H_2N\text{-xpt})_3(\mu_3\text{-}CO_3)](NO_3)_4$ trimer (**13**), and not of the oxalate complex $[Cu_2(H_2N\text{-xpt})_2(\mu\text{-}C_2O_4)](NO_3)_2$ (**15**). See the crystal structure of **13** in Figure 2.7 and for the $[Cu_3(H_2N\text{-xpt})_3(\mu_3\text{-}CO_3)](PF_6)_4$ (**14**) in Figure 2.14. In complex **13**, the copper centers are about 4.6 Å apart, and make a triangle void with about 9 $Å^2$ area that fits a carbonate molecule. Although we were able to isolate only crystals of **13** from exposure of **11** to a balloon of CO_2, formation of **15** cannot be ruled out. Conversion of **11** into **13** by reaction with CO_2 only is extremely unlikely. Instead, it is much more likely that some O_2 was introduced into the flask along with the CO_2 (or via a leak). Then, reaction of O_2 with Cu(I) could yield Cu(II), and Cu(II) could react with CO_2 in the presence of a base to produce CO_3^{2-}. In a similar reaction, comparing the FT-IR spectrum of the crude

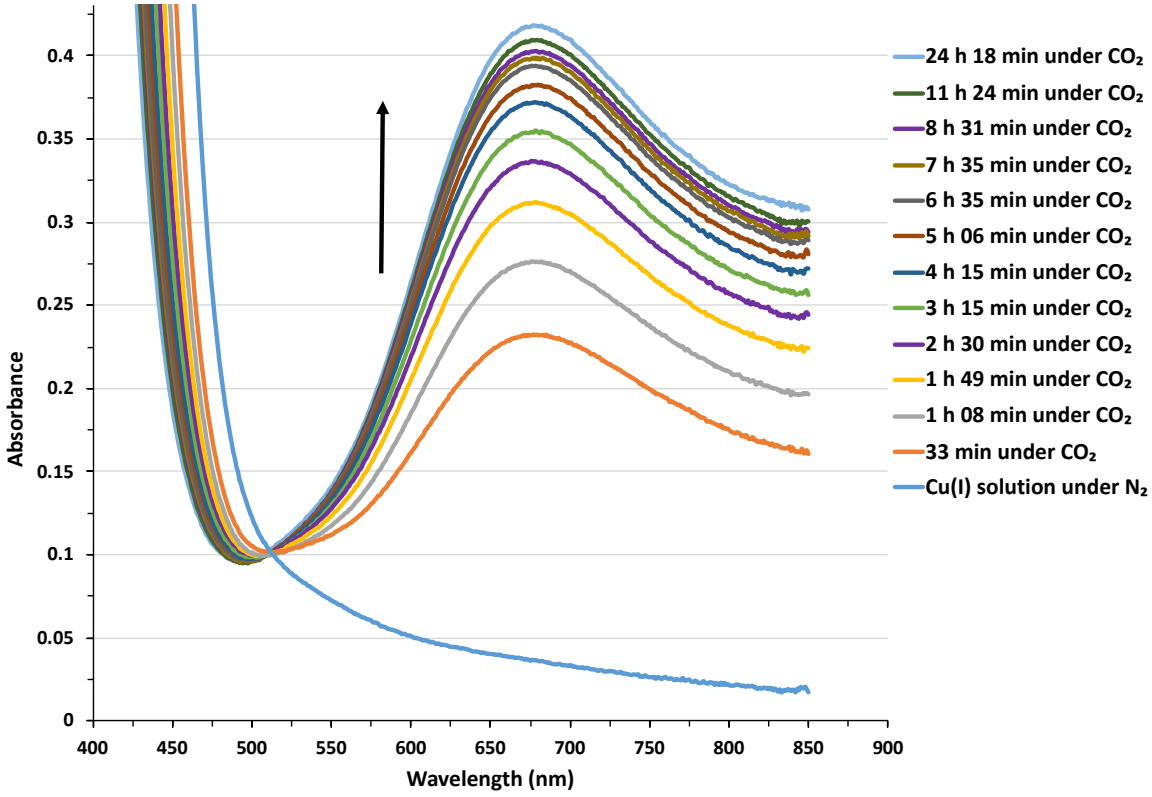

Figure 2.6. UV/vis absorption spectra of DMF solution of $Cu_2(H_2N\text{-xpt})_2(NO_3)_2$ (**11**) (dark blue line) and gradual increase of Cu(II) absorption upon exposure to a balloon of CO_2.

mixture obtained from **12** with the spectrum of authentic samples of **14** and $[Cu_2(H_2N\text{-xpt})_2(\mu\text{-}C_2O_4)](PF_6)_2$ (**16**) made by treatment of **10** to $CsHCO_3$ or tetrabutylammonium oxalate (TBAO) was not helpful to determine whether some **16** is produced; this is due to the similarity of the patterns in the IR fingerprint region of **14** and **16**.

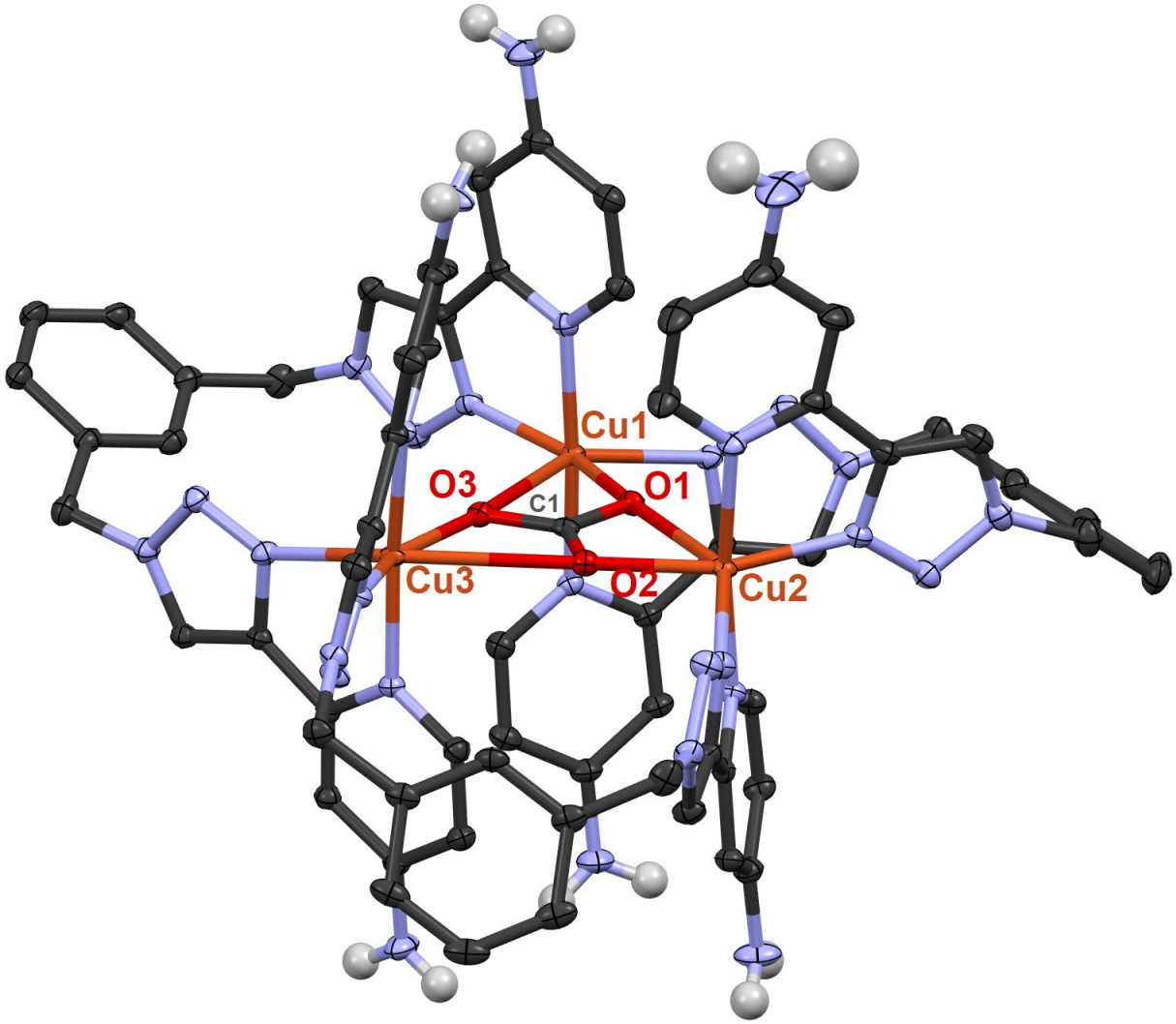

Figure 2.7. X-ray structure of $[Cu_3(H_2N\text{-xpt})_3(\mu_3\text{-}CO_3)](NO_3)_4\cdot 5DMF\cdot 4H_2O$ (**13**$\cdot 5DMF\cdot 4H_2O$). The thermal ellipsoids are at the 50% probability level, and hydrogen atoms (except in NH_2), counter-anions, and solvent molecules are removed for clarity.

2.2.2. Me_2N-xpt

We considered whether to pursue the chemistry of H_2N-xpt further. However, because of the high price of the required 2-ethynylpyridine-4-amine·HCl precursor (ca. $500/1g), we decided to synthesize the Me_2N-xpt (**17**) ligand instead. Me_2N-xpt is expected to have a slightly higher basicity than **8**. At the same time the methyl group promotes solubility in organic solvents. For example, unlike **8**, ligand **13** is soluble in chloroform and could be extracted from NH_3/Na_2H_2EDTA aqueous solution.

The synthetic steps for **17** are shown in Figure 2.8. 4-dimethylamino-2-iodo-pyridine (**18**) was synthesized from dimethylaminopyridine with 50% yield using n-BuLi and iodide. 2-bromo-4-dimethylaminopyridine (**19**) is commercially available with a reasonable price but it could be prepared in good yield by reduction of 2-bromo-4-nitropyridine (**20**) to 4-amino-2-bromopyridine (**21**) then methylation with paraformaldehyde. Sonogashira coupling of trimethylsilylacetylene and **18** (or **19**), produced a mixture of TMS-protected (**22**) and deprotected product (**23**). Treatment of **22** with KF resulted in deprotection to **23**. An unknown byproduct forms during Sonogashira coupling that its production could be reduced by using NEt_3 as both source of base and solvent. Cu-catalyzed click reaction with α,α′-diazido-*m*-xylene (formed *in situ*) produced **17**. Complexation of **17** with $Cu(NO_3)_2$ formed $[Cu_2(Me_2N\text{-xpt})_2(NO_3)_2](NO_3)_2$ (**24**) and metathesis with NH_4PF_6 formed $[Cu_2(Me_2N\text{-xpt})_2(NO_3)_2](PF_6)_2$ (**25**). We also made authentic samples of $[Cu_3(Me_2N\text{-xpt})_3(\mu_3\text{-}CO_3)](PF_6)_4$ (**27**), and $[Cu_2(Me_2N\text{-xpt})_2(\mu\text{-}C_2O_4)](PF_6)_2$ (**28**) by treatment of **25** with $CsHCO_3$ and TBAO respectively (see experimental section for characterization data). Electrochemical measurements of **25** will be carried out as soon as possible.

Using two equivalents of ascorbate and exposing the resulting yellow solution of $[Cu_2(Me_2N\text{-xpt})_2](PF_6)_2$ (**26**) to air formed **27** as major product and adding excess amount of

ascorbate formed more of the **28**. X-ray structures of **27** and **28** are shown in Figure 2.9. In **28** the Cu1···Cu2 distance is 5.244(1) Å which is about 0.2 Å shorter than the distance in **6**. The bond distances in $Cu_1–N_{pyridine}$, $Cu_1–N_{triazole}$, and $Cu_1–O_{oxalate}$ are very similar to those in **6** with 0.1-0.3 Å difference.

Reduction of **4** with one equivalent of ascorbate, followed by oxidation, forms the oxalate product only, while the more electron-rich **10** and **25** systems lead to the carbonate trimer (with stoichiometric ascorbate) or the oxalate dimer (with excess ascorbate). This was puzzling, and it made us reexamine the chemistry of **4** reported previously.[6] We also revisit the proposed reductive coupling of CO_2 to oxalate pathway, which will be discussed in Chapter 3.

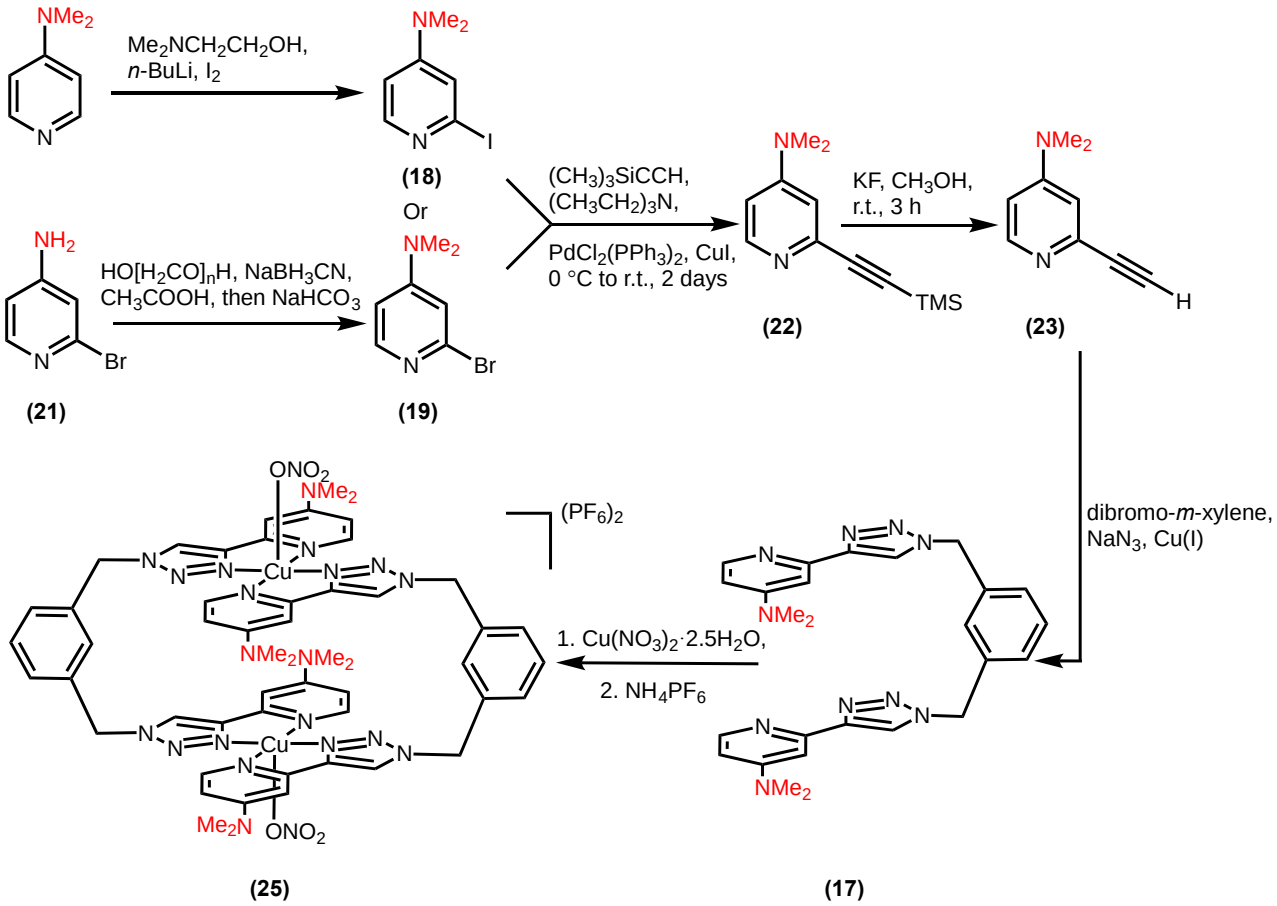

Figure 2.8. Synthetic pathway to preparation of $[Cu_2(Me_2N\text{-xpt})_2(NO_3)_2](PF_6)_2$ (**25**).

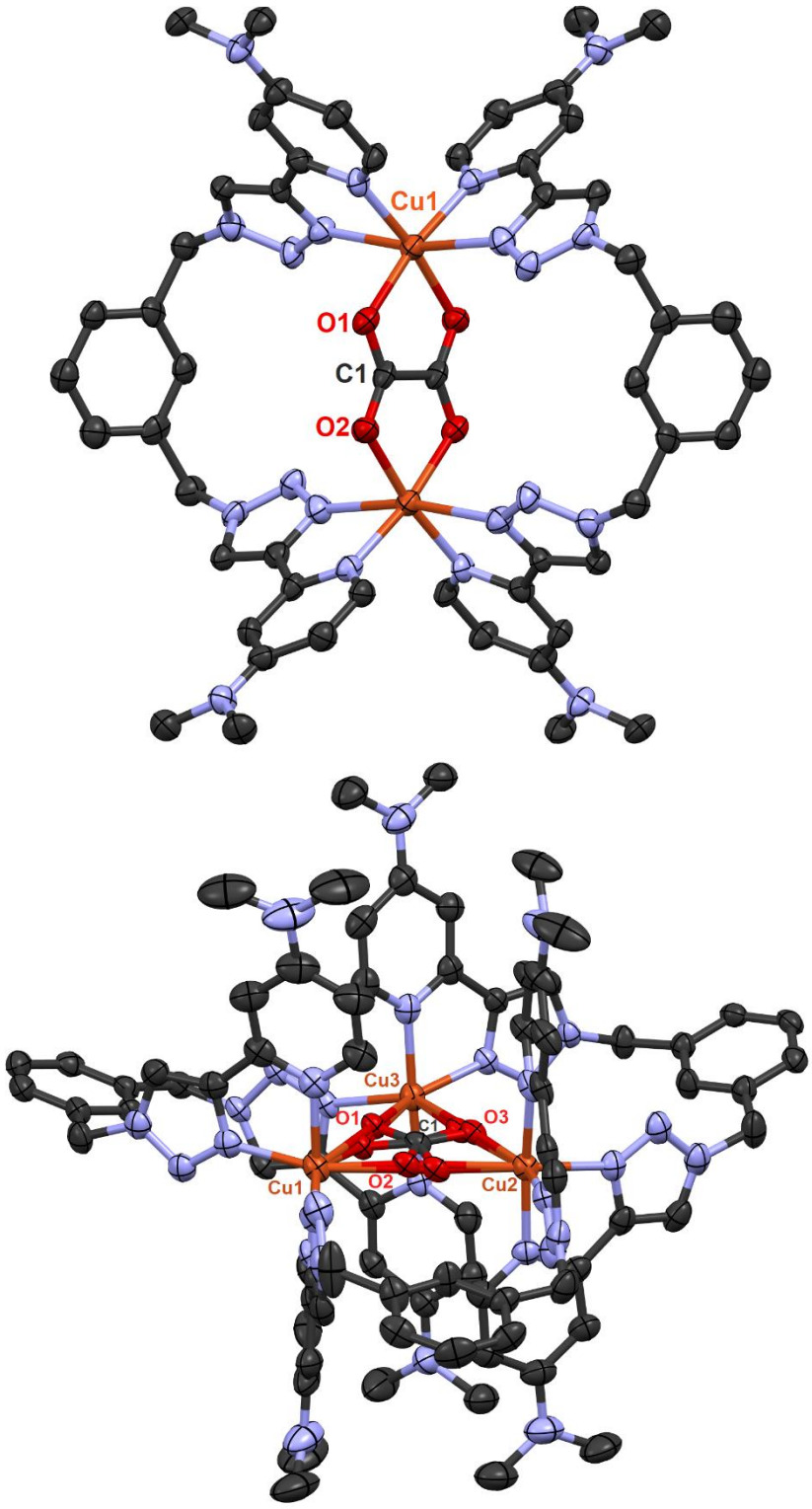

Figure 2.9. X-ray structures of $[Cu_3(Me_2N\text{-}xpt)_3(\mu_3\text{-}CO_3)](PF_6)_4\cdot DMF$ (**27**·DMF) (top) and $[Cu_2(Me_2N\text{-}xpt)_2(\mu\text{-}C_2O_4)](PF_6)_2\cdot 2DMF$ (**28**·2DMF) (bottom). The thermal ellipsoids are at the 50% probability level, and hydrogen atoms, counter-anions, and solvent molecules are removed for clarity. The carbonate is disordered into two orientations.

2.2.3. O_2N-xpt

To see the effect of electron withdrawing groups on chemistry of our Cu(I) complexes we made O_2N-xpt (**29**) ligand. Starting from 2-bromo-4-nitropyridine (**20**) we followed our normal procedure for Sonogashira coupling and this made 4-nitro-2-(trimethylsilylethynyl)pyridine (**30**) in good yield. TMS deprotection with a fluoride solution formed 2-ethynyl-4-nitro-pyridine (**31**), which was used for the "click" reaction to make ligand **29**. The electron deficient complex $[Cu_2(O_2N\text{-xpt})_2(NO_3)_2](NO_3)_2$ (**32**) was prepared from **29** by treatment with $Cu(NO_3)_2{\cdot}2.5H_2O$. This nitrate complex was not soluble in water, ethanol and methanol so it couldn't be converted to a PF_6 salt by metathesis with aqueous solution of NH_4PF_6. Reduction of **32** with ascorbate formed a brown solution which didn't change color upon exposure to air and gradually formed a brown solid; see Figure 2.25. These reactions made it difficult to do a detailed comparison of **32** with the other Cu(II) complexes. Electrochemical measurements of **32** will be carried out as soon as possible.

2.3. Experimental

General

Unless stated otherwise, reactions were conducted under an atmosphere of N_2. Commercially available reagents were purchased from Alfa Aesar, BeanTown Chemicals, Sigma-Aldrich, Combi-Blocks and TCI and were used without further purification. Anhydrous DMF was purchased from MilliporeSigma. NMR spectra were recorded on Bruker 400 MHz (Avance 400) or 500 MHz (Avance 500) spectrometers. FT-IR spectra (ATR, diamond) were recorded on a Tensor 27 or Alpha P FT-IR spectrometer (Bruker). Electrospray ionization mass spectra were measured on an Agilent 6210 instrument. UV/vis spectra were recorded on an Aviv 14DS spectrometer (Aviv Biomedical).

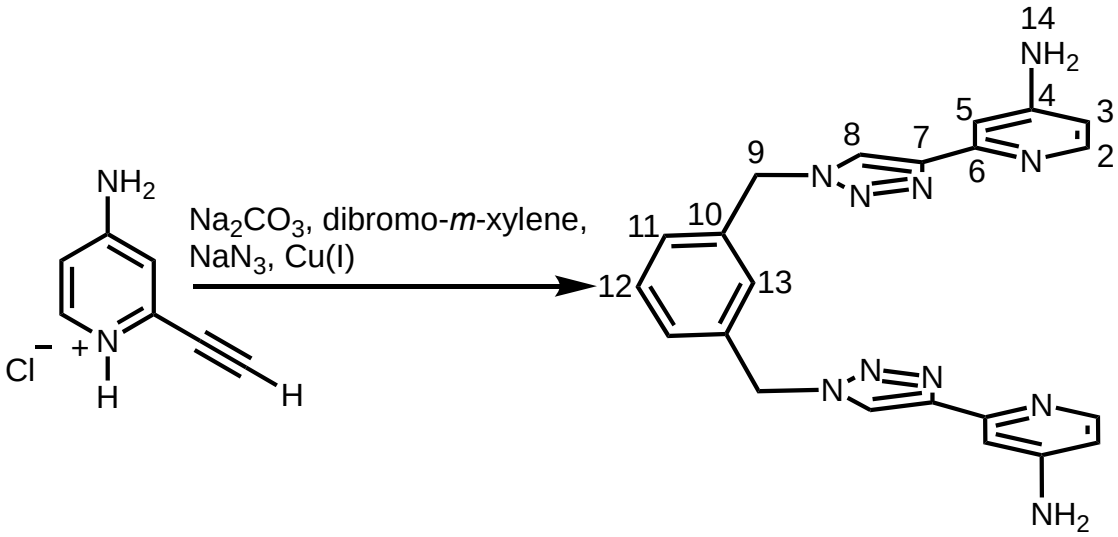

Synthesis of *m*-xylylenebis(4-aminopyridyltriazole), H_2N-xpt (8).

260.4 mg (0.9865 mmol) α,α′-dibromo-*m*-xylene was dissolved in 20 mL of DMF-water (4:1 v/v); then 134.6 mg (2.071 mmol) NaN_3 and 334.6 mg (3.156 mmol) Na_2CO_3 were added. To this colorless mixture, 98.5 mg (0.395 mmol) $CuSO_4.5H_2O$ was added which turned the color of solution immediately to dark brown. Then 156.3 mg (0.7892 mmol) ascorbic acid was added, and

the color of solution turned to colorless/light blue. Then 305.0 mg (1.973 mmol) 2-ethynylpyridine-4-amine·HCl was added, and the mixture was left to stir for 20 hours under nitrogen, during which time the formation of a yellow/orange solid was observed. The reaction mixture was worked up with NH_3/Na_2H_2EDTA solution (2.00 g of $Na_2H_2EDTA{\cdot}2H_2O$ in 5 mL of 28% aqueous NH_3, diluted to 100 mL with H_2O) in a separatory funnel. 2 × 50 mL chloroform was added to extract impurities. Then the aqueous layer was filtered. The collected solid was washed further with water and chloroform, then left to dry in air. This afforded 376.5 mg of **8** as a light cream solid (89%). ^{1}H NMR (400 MHz, $(CD_3)_2CO$) δ 8.29 (s, 2H, H8), 8.01 (d, J = 5.56 Hz, 2H, H2), 7.54 (s, 1H, H13), 7.4 (m, 5H, H11 & H12 & H5), 6.50 (dd, J_1 = 5.6 Hz, J_2 = 2.32 Hz, 2H, H3), 5.69 (s, 4H, H9), 5.57 (s, br, 4H, H14). ESI-MS: m/z $[H_2N\text{-xpt+H}]^+$ 425.1953 (calcd 425.1945), $[H_2N\text{-xpt+Na}]^+$ 447.1774 (calcd 447.1765), $[H_2N\text{-xpt+K}]^+$ 463.1495 (calcd 463.1504).

Synthesis of $[Cu_2(H_2N\text{-xpt})_2(NO_3)_2](NO_3)_2$ (9).

A reaction flask was charged with **8** (352.4 mg, 0.8302 mmol) and 15 mL of chloroform then a solution of $Cu(NO_3)_2{\cdot}2.5H_2O$ (193.1 mg, 0.8302 mmol in 15 mL acetonitrile) was added dropwise. The color of the mixture became green. This was stirred under N_2 for 5 hours and then centrifuged. The supernatant, which was almost colorless, was decanted. A few mL of chloroform was added to the green solid and the mixture centrifuged again. The supernatant was decanted and the green solid was dried in air; yield 456.2 mg (90%). See FT-IR spectrum of the solid in Figure 2.10. ESI-MS: m/z $[Cu(NH_2\text{-xpt})]^+$ 487.11524 (calcd 487.11684), $[Cu_2(NH_2\text{-xpt})_2(NO_3)_3]^+$ 1160.19481 (calcd 1160.19659).

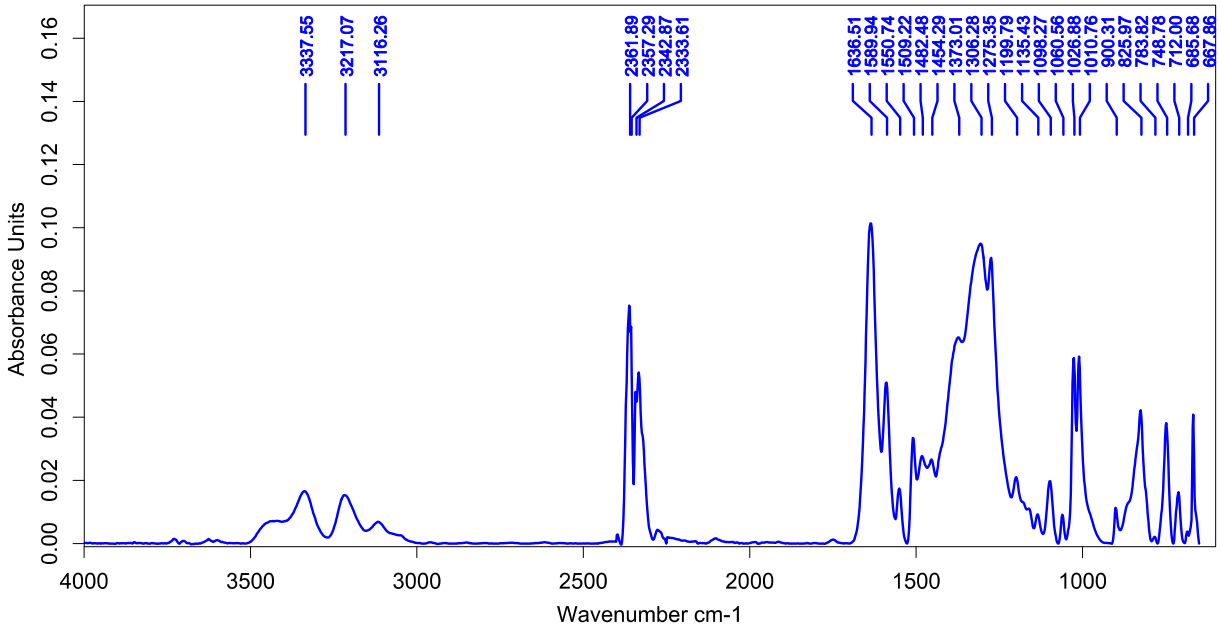

Figure 2.10. FT-IR spectrum of $[Cu_2(H_2N\text{-xpt})_2(NO_3)_2](NO_3)_2$ (**9**).

Synthesis of $[Cu_2(NH_2\text{-xpt})_2(NO_3)_2](PF_6)_2$ (10).

To 307.9 mg (0.2515 mmol) **9** was added 45 mL water, and the suspension was stirred for about 30 minutes in a 50 °C water bath to give a clear solution. A solution of NH_4PF_6 (247.7 mg, 1.520 mmol in 3 mL water) was added. The mixture was left to stir and cool to room temperature, then kept in an ice bath for 15 minutes. The resulting precipitate was collected and washed with ice cold water, then dried in air to give 315.3 mg of **10** as a green powder (90%). See FT-IR spectrum of **10** in Figure 2.11 ESI-MS: m/z $[Cu(NH_2\text{-xpt})]^+$ 487.11536 (calcd 487.11684), $[Cu_2(NH_2\text{-xpt})_2(PF_6)]^+$ 1119.19559 (calcd 1119.19786), $[Cu_2(NH_2\text{-xpt})_2(PF_6)_3]^+$ 1409.12465 (calcd 1409.12622).

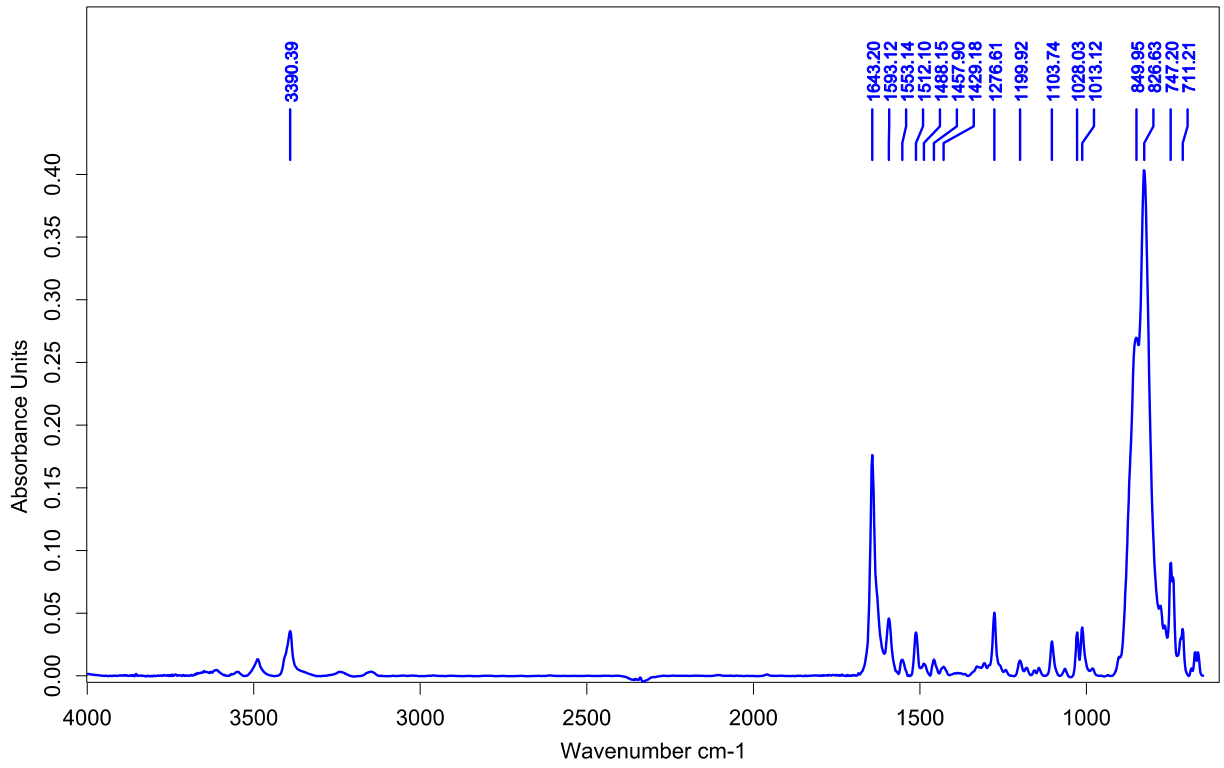

Figure 2.11. FT-IR spectrum of $[Cu_2(NH_2\text{-xpt})_2(NO_3)_2](PF_6)_2$ (**10**).

Reaction of *in situ* generated $[Cu_2(H_2N\text{-xpt})_2](NO_3)_2$ (11) or $[Cu_2(H_2N\text{-xpt})_2](PF_6)_2$ (12) with a balloon of CO_2 and formation of $[Cu_3(H_2N\text{-xpt})_3(\mu_3\text{-}CO_3)](NO_3)_4$ (13) or $[Cu_3(H_2N\text{-xpt})_3(\mu_3\text{-}CO_3)](NO_3)_4$ (14).

A Schlenk flask sealed to a cuvette was charged with **9** (17.7 mg, 0.0145 mmol) and ascorbic acid (3.9 mg, 0.022 mmol) then evacuated for 30 minutes. 5 mL N_2-purged DMF was added to the solids and the solution, stirred under N_2 for 5 hours. The color of the solution changed to yellow during this time, and complete conversion to **11** was observed by UV/vis spectroscopy. At this point the solution was exposed to a balloon of CO_2 and formation of Cu(II) was followed by UV/vis spectroscopy as shown in Figure 2.6. Then half of the resulting solution was poured into a watch glass for evaporation of solvent, and the FT-IR spectrum of the residual solid was recorded; see Figure 2.12. The rest of the solution was used for ether vapor diffusion and formed crystals of **13**; see Figure 2.7. Similar reactions with **10** (21.1 mg, 0.0159 mmol) and ascorbic acid (3.8 mg, 0.022)

formed crystals of **14**. See Figure 2.13 for FT-IR spectrum of the product mixture and Figure 2.14 for X-ray structure of **14**.

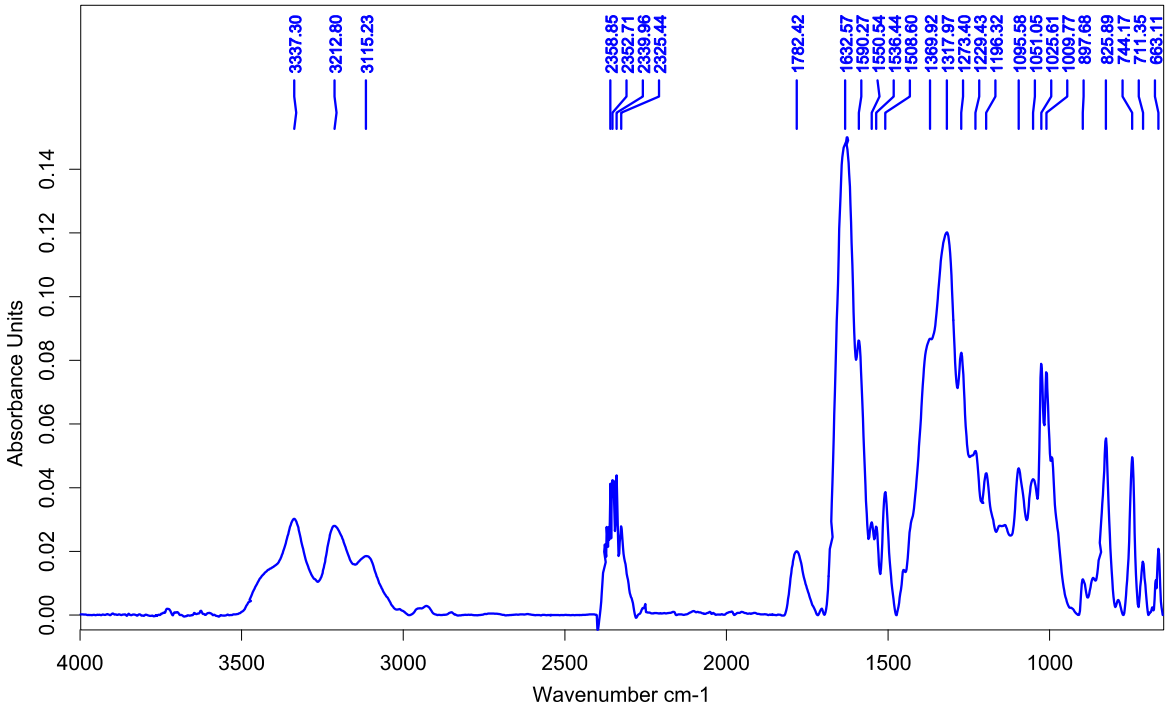

Figure 2.12. FT-IR spectrum of the crude mixture obtained after exposure of $[Cu_2(H_2N\text{-}xpt)_2](NO_3)_2$ (**11**) to a balloon of CO_2.

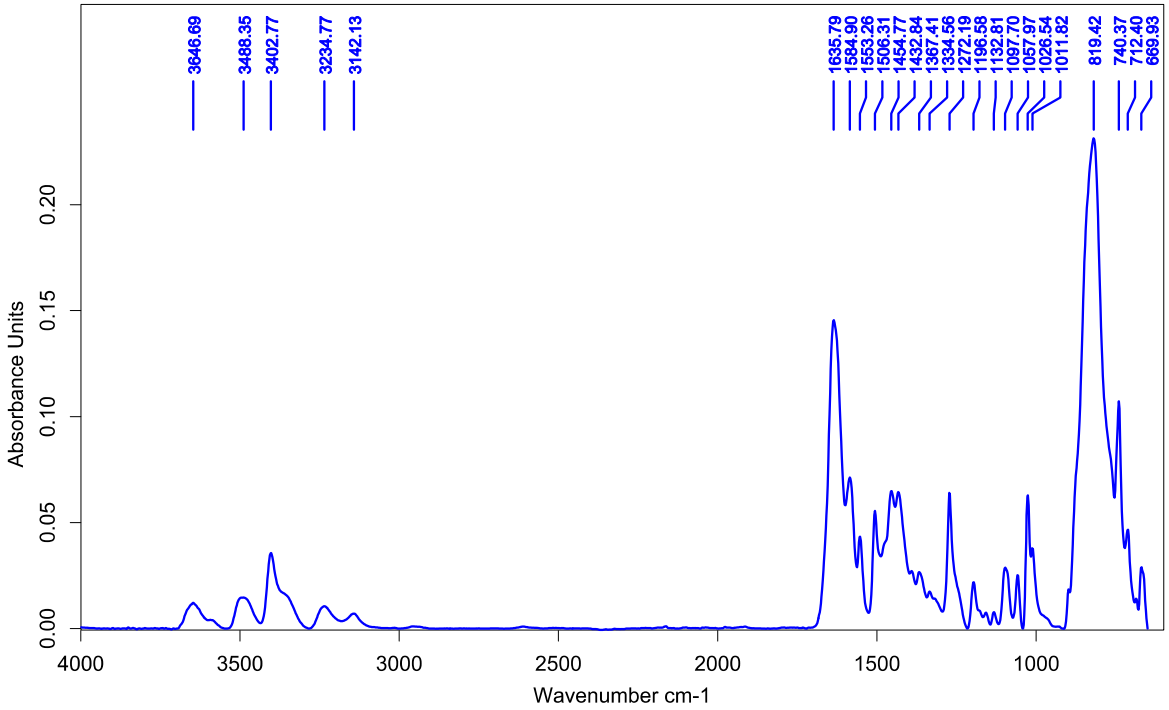

Figure 2.13. FT-IR spectrum of crude mixture obtained after exposure of $[Cu_2(H_2N\text{-xpt})_2](PF_6)_2$ (**12**) to a balloon of CO_2.

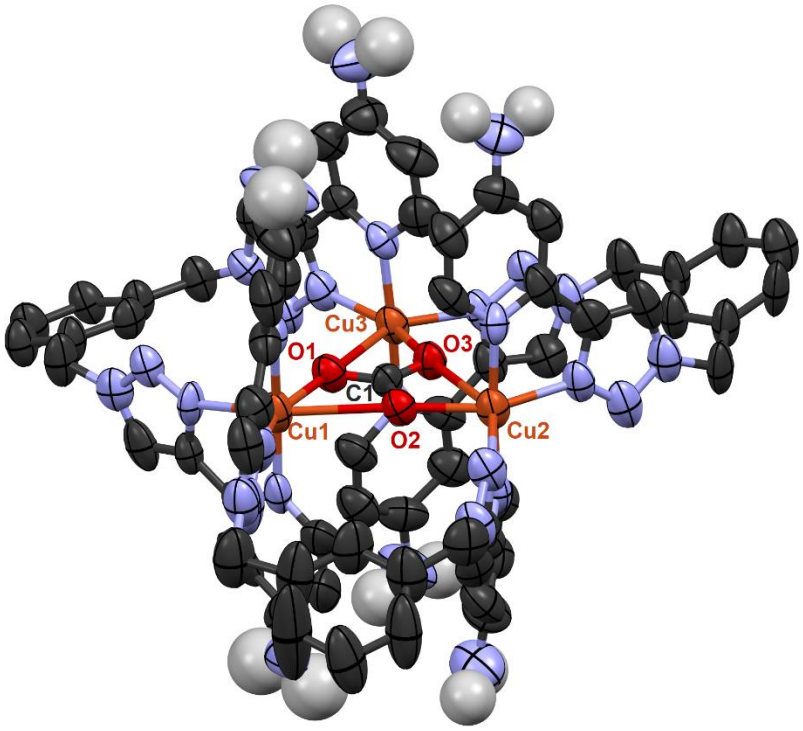

Figure 2.14. X-ray structure of $[Cu_3(H_2N\text{-xpt})_3(\mu_3\text{-}CO_3)](PF_6)_4 \cdot 3DMF$ (**14**·3DMF). There are two $[Cu_3(H_2N\text{-xpt})_3(\mu_3\text{-}CO_3)]^{4+}$ cations in the asymmetric unit; only one of them is shown for clarity. Solvent molecules, PF_6 and hydrogens are omitted (except hydrogens attached to NH_2).

Synthesis of $[Cu_3(H_2N\text{-xpt})_3(\mu_3\text{-}CO_3)](PF_6)_4$ (14) by addition of $CsHCO_3$ to 10.

To a solution of **10** (28.0 mg, 0.0201 mmol in 5 mL DMF) in a reaction flask $CsHCO_3$ (2.7 mg, 0.013 mmol) was added. Solution was stirred under N_2 for 2 days in which the color of solution changed to dark green. A portion of the solution was poured into a watch glass for evaporation of DMF, then FT-IR spectrum of the residual solid was recorded; see Figure 2.15.

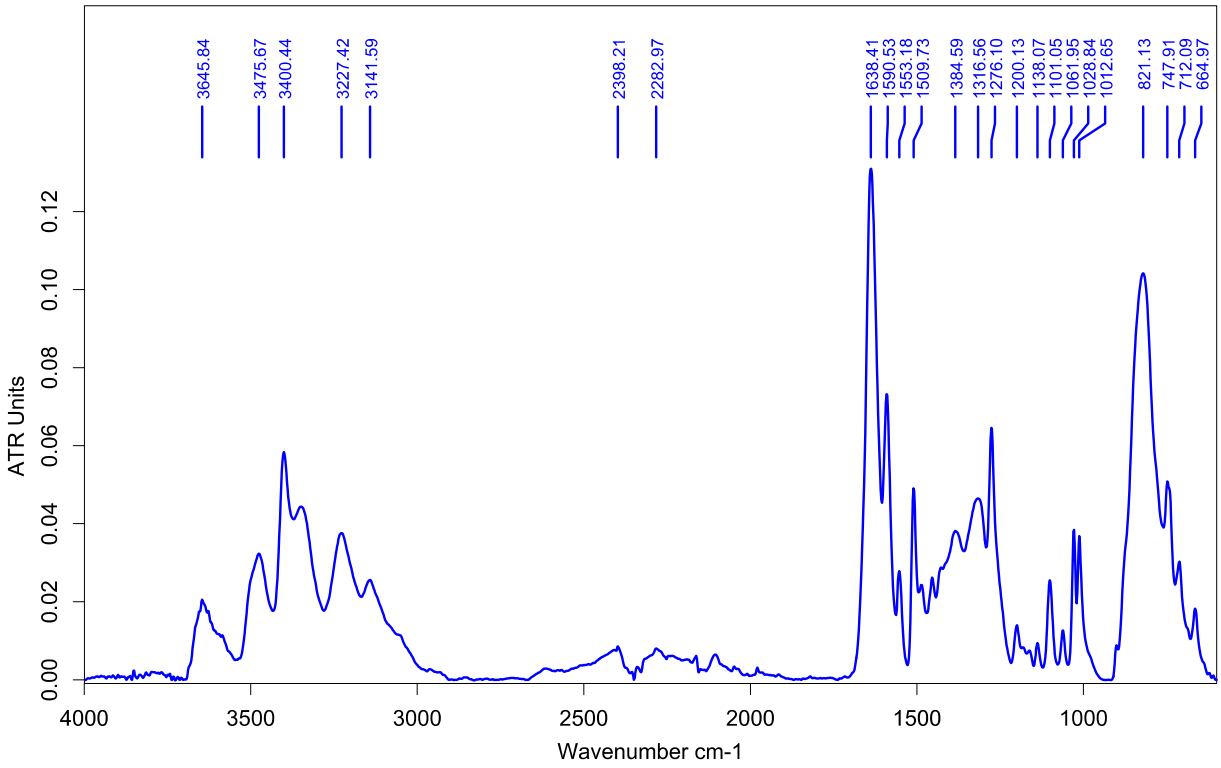

Figure 2.15. FT-IR spectrum of $[Cu_3(H_2N\text{-xpt})_3(\mu_3\text{-}CO_3)](PF_6)_4$ (**14**) made by addition of $CsHCO_3$.

Synthesis of $[Cu_2(H_2N\text{-xpt})_2(\mu\text{-}C_2O_4)](PF_6)_2$ (16) by addition of tetrabutylammonium oxalate (TBAO) to 10.

To a solution of complex **10** (21.7 mg, 0.0156 mmol in 7 mL DMF), TBAO solution (9.7 mg, 0.017 mmol in 2 mL DMF) was added under N_2 dropwise until the first sign of a permanent turbidity was observed. A portion of the solution was poured into a watch glass for evaporation of

DMF, then FT-IR spectrum of the residual solid was recorded; see Figure 2.16. Efforts to crystallize **16** were not successful.

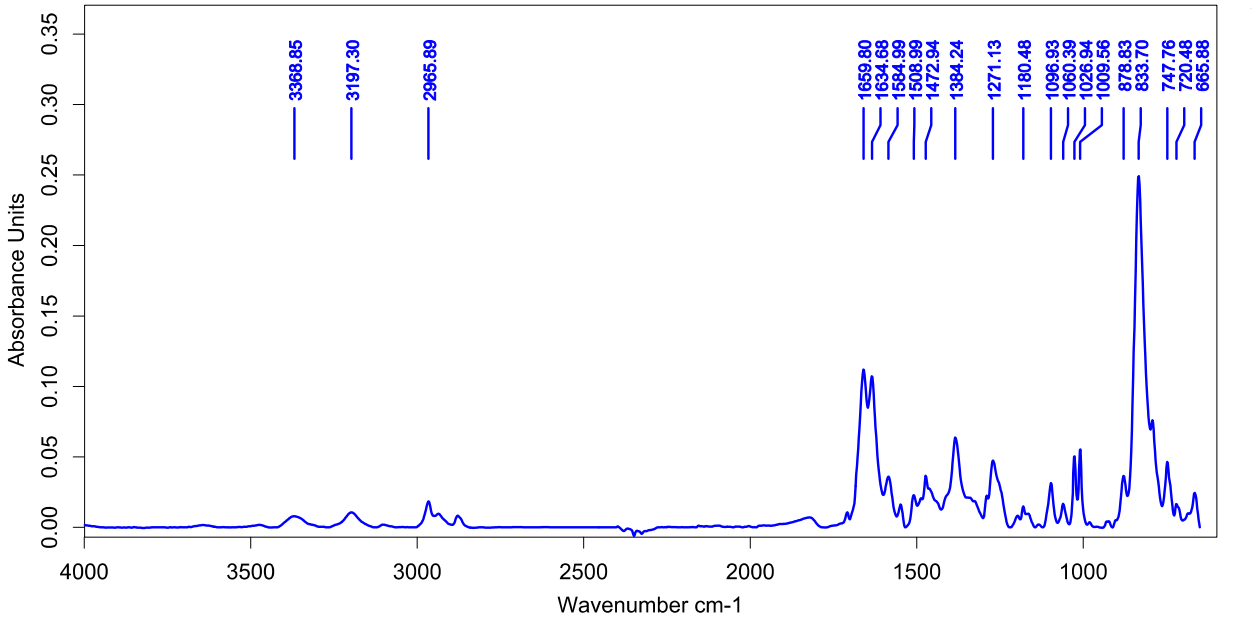

Figure 2.16. FT-IR spectrum of $[Cu_2(H_2N\text{-xpt})_2(\mu\text{-}C_2O_4)](PF_6)_2$ (**16**) made by addition of TBAO.

Exposure of 10 to CO_2; formation of $[Cu_3(NH_2\text{-xpt})_3(\mu_3\text{-}CO_3)](PF_6)_4$ (14).

A Schlenk flask was charged with 21.6 mg of **10** (0.0176 mmol) and evacuated, then 10 mL N_2-purged DMF was added to the solid under N_2. The reaction flask was evacuated and purged with CO_2 three times then sealed under CO_2. After a week the solution was exposed to air and used for crystallization with diffusion of ether. This formed blue crystals of **14**, and its structure was confirmed by X-ray crystallography. A portion of the solution was dried in air and used for FT-IR spectroscopy; see Figure 2.17.

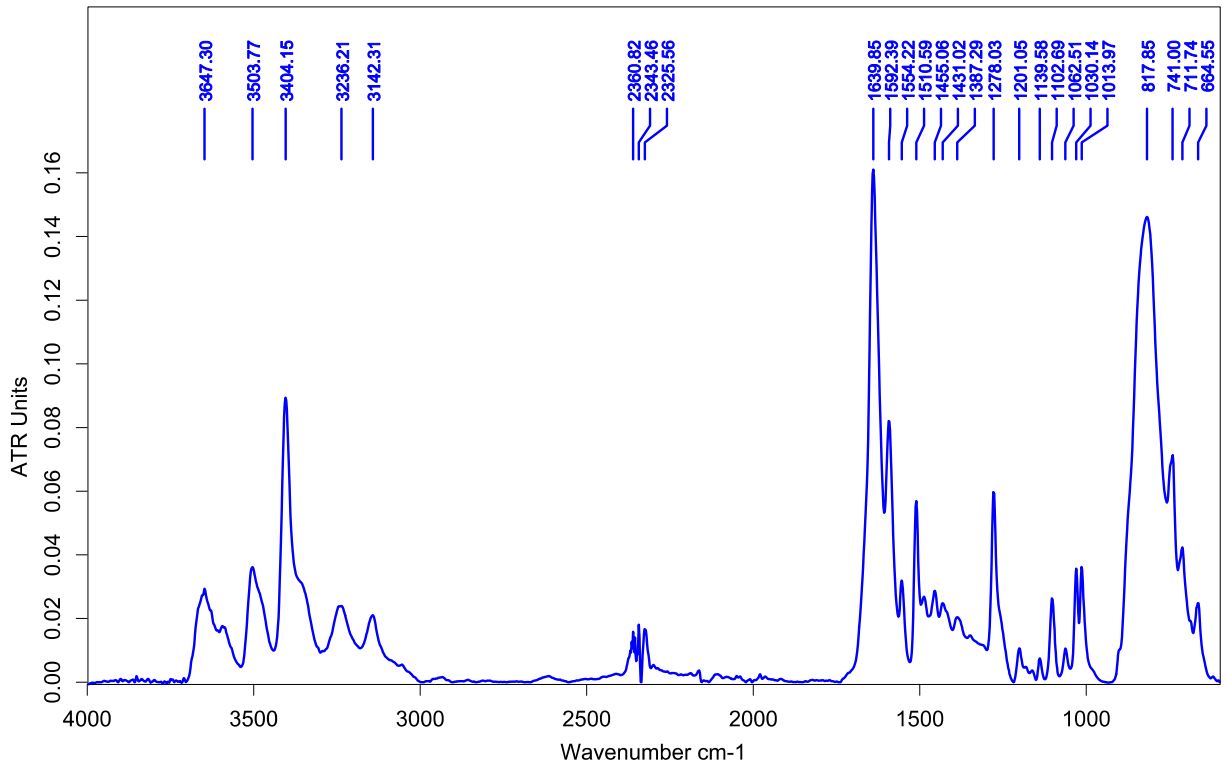

Figure 2.17. FT-IR spectrum of the crude mixture obtained from exposure of $[Cu_2(NH_2\text{-xpt})_2(NO_3)_2](PF_6)_2$ (**10**) to CO_2.

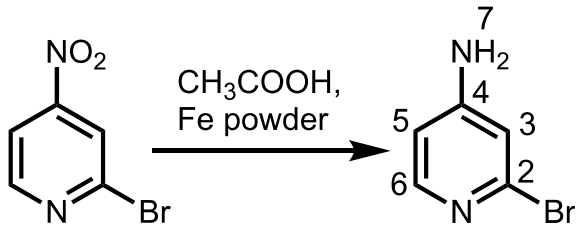

Synthesis of 4-amino-2-bromopyridine (21).

Reduction of the 4-nitro-2-bromopyridine (**20**) group was performed according to a procedure reported by Erdelyi et al. for a similar aminopyridine compound.[9] Compound **20** (1.0018 g, 4.9352 mmol) was dissolved in 30 mL acetic acid, forming a yellow solution. Then 1.38 g (24.7 mmol) Fe powder was added, and the reaction mixture was warmed to 50 °C and stirred under nitrogen for 15 minutes. The color of the solution turned to brown and then white/grey. The mixture was left to cool to room temperature then basified with an ice-cold aqueous solution of NaOH. The

aqueous solution was extracted with DCM then the combined organic layers were dried over $MgSO_4$, filtered and condensed *in vacuo*. This afforded 805.2 mg (94%) of **21**. ^{1}H NMR (400 MHz, $CDCl_3$) δ 7.94 (d, J = 5.64 Hz, 1H, H6), 6.70 (d, J = 2.12 Hz, 1H, H3), 6.46 (dd, J_1 = 5.64, J_2 = 2.16 Hz, 1H, H5), 4.24 (s, br, 2H, H7).

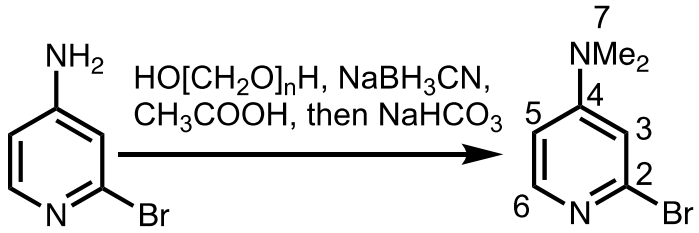

Synthesis of 2-bromo-4-dimethylaminopyridine (19).

2-bromo-4-dimethylaminopyridine (**19**) was made according to a procedure reported by Erdelyi et.al for a similar dimethylaminopyridine compound .[9] In a round bottom flask **21** (201.8 mg, 1.166 mmol) was dissolved in 8 mL glacial acetic acid and formed a yellow solution. Paraformaldehyde (385.3 mg, 12.83 mmol based on the MW. of CH_2O monomer) was added to the above solution. While the suspension was stirring, sodium cyanoborohydride was added (591 mg, 9.40 mmol). The mixture was stirred under N_2 for 48 hours, then basified by addition of an aqueous solution of NaOH. The aqueous solution was extracted with chloroform several times. Combined organic layers were dried over $MgSO_4$, filtered and the solvent was evaporated *in vacuo*. 268.3 mg of crude mixture was collected which shows 90% conversion to the desired product by ^{1}H NMR analysis; 10% unreacted starting material remained. ^{1}H NMR of **19** (400 MHz, $CDCl_3$) δ 7.95 (d, J = 6.04, 1H, H6), 6.71 (d, J = 2.4, 1H, H3), 6.46 (dd, J_1 = 6.04, J_2 = 2.44 Hz, 1H, H5), 2.98 (s, 6H, H7).

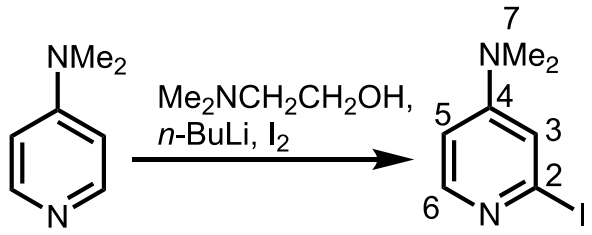

Synthesis of 4-dimethylamino-2-iodo-pyridine (18).

The compound was prepared by using a general procedure reported by Fort et al. with some modifications, since with the original procedure we observed solubility issue and low yield toward the desired product **18**.[10] A two neck round bottom flask was charged with 350 mL dry THF and purged with argon. 2-dimethylaminoethanol was purged with argon for 15 minutes, and 1.77 mL (1.57 g, 0.0176 mmol) of it was added to the THF, then the solution was cooled to –5 °C and stirred for 30 minutes. At this point 22.0 mL n-BuLi (35.2 mmol; 1.6 M in hexane) was added to the solution dropwise over 45 minutes. After addition of half of n-BuLi, the color of solution turned to yellow. This clear solution was stirred at –5 °C for 30 minutes under argon, then 1.077 g (8.812 mmol) 4-dimethylaminopyridine (DMAP) was added in one portion. The resulting orange solution was stirred for 1 hour then cooled to –78 °C. Then, an iodine solution (2.8 g, 22 mmol in dry THF) was added, which changed the color of the reaction mixture to yellow gradually. The mixture was stirred for two hours at –78 °C and for two additional hours at 0 °C. The crude mixture was poured into distilled water and stirred for 10 minutes then the THF layer was separated. The aqueous layer was extracted furthermore with chloroform. The combined organic layers were dried over $MgSO_4$, filtered and evaporated *in vacuo*. ^{1}H NMR of the crude product showed peaks of the desired product (55-65% conversion for different trials) as well as peaks that could be assigned to unreacted DMAP and bis(dimethylamino)bipyridine by-product. The crude mixture was purified by column chromatography using EtOAc as eluent (R_f = 0.8). ^{1}H NMR (400 MHz, $(CD_3)_2CO$) δ

7.86 (d, J = 6.0 Hz, 1H, H6), 6.85 (d, J = 2.52 Hz, 1H, H3), 6.41 (dd, J_1 = 6.0 Hz, J_2 = 2.48 Hz, 1H, H5), 2.93 (s, 6H, H7).

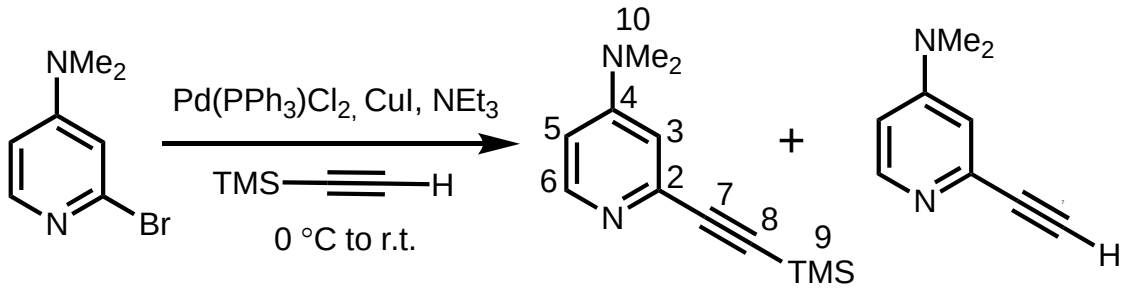

Synthesis of 4-dimethylamino-2-(trimethylsilylethynyl)pyridine (22).

A Schlenk flask was charged with 0.8641 g (4.298 mmol) **19** and evacuated for 30 minutes and then transferred to a glove box, and 245 mg (0.349 mmol) $PdCl_2(PPh_3)_2$ and 90 mg (0.47 mmol) CuI were added. The reaction flask was evacuated for 30 minutes, while in a separate flask triethylamine was purged with nitrogen. Then 40 mL ice-cold NEt_3 was added to the mixture under nitrogen and a yellow suspension was obtained. This was kept in ice bath then ethynyltrimethylsilane (0.6 mL, T ~ 2 °C, d = 0.709 g/mL, ca. 4.3 mmol) was added dropwise over 10 minutes. The mixture was stirred for 2 hours at 0 °C then left to warm to room temperature and stirred for 3 days and the color of solution changed to brown. The crude mixture was filtered and the solid washed with ether. To the filtrate saturated $NH_4Cl_{(aq)}$ was added, and the aqueous layer was extracted with ether. The combined organic layers were washed with the fresh $NH_4Cl_{(aq)}$ solution one more time then the organic layer was dried over $MgSO_4$, filtered and concentrated *in vacuo*. This gave a brown oil. The crude mixture was purified by column chromatography one time with hexane-acetone (3:1 v/v) and second time with EtOAC as eluent. This gave a negligible amount of the TMS-protected product **22** and 0.1695 g (1.159 mmol) of 4-dimethylamino-2-ethynylpyridine (**23**) as a white solid. This white solid was rinsed one time with hexane and dried *in vacuo* (27 %). See the next experiment for characterization of **23**. ^{1}H NMR of **22**: (400 MHz,

$CDCl_3$) δ 8.16 (d, J = 6.0 Hz, 1H, H6), 6.70 (d, J = 2.64, 1H, H3), 6.42 (dd , J_1 = 6.08, J_2 = 2.72 1H, H5), 3.0 (s, 6H, H10), 0.25 (s, 9H, H9).

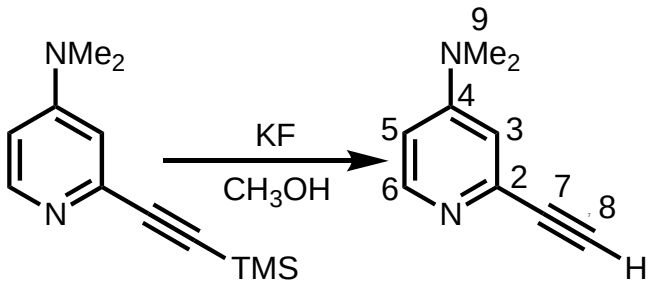

Deprotection of 22 to 4-dimethylamino-2-ethynylpyridine (23).

We did the above Sonogashira coupling in a mixture of THF and NEt_3 also, and isolated a mixture of **22** and **23**. Deprotection of **22** was performed according to a procedure reported by Erdelyi et al. for deprotection of a similar TMS-protected acetyl compound.[9] After Sonogashira coupling of 4.60 g (0.0229 mol) of **19**, a crude mixture of **22** and **23** were obtained. Without any purification, the crude mixture was dissolved in 280 mL methanol and 30 mL THF. A solution of KF (5.2 g, 0.090 mol in 100 mL methanol) was added to the above solution dropwise. The solution was stirred under nitrogen for 2 hours then concentrated *in vacuo*, and the residue re-dissolved in DCM and extracted with water. The aqueous layer was extracted with DCM one more time; then the combined organic layers were dried over $MgSO_4$, filtered and concentrated *in vacuo*. To the residue EtOAc was added and sonicated, then centrifuged and the clear solution was loaded on a column of silica gel for purification. Using EtOAc as eluent (R_f = 0.5) gave 1.29 g (38.6%) of **23** as a white-creamy solid. ^{1}H NMR (400 MHz, $(CD_3)_2CO$) δ 8.08 (d, J = 6.0 Hz, 1H, H6), 6.76 (d, J = 2.8, 1H, H3), 6.58 (dd , J_1 = 6.0, J_2 = 2.8 Hz, 1H, H5), 3.51 (s, 1H, H8), 3.01 (s, 6H, H9). ^{13}C NMR (100 MHz, $(CD_3)_2CO$) δ 155.18 (C4), 150.59 (C6), 143.32 (C2), 111.08 (C3), 107.30 (C5), 85.23 (C7), 76.18 (C8), 39.13 (C9). m.p. = 72 °C.

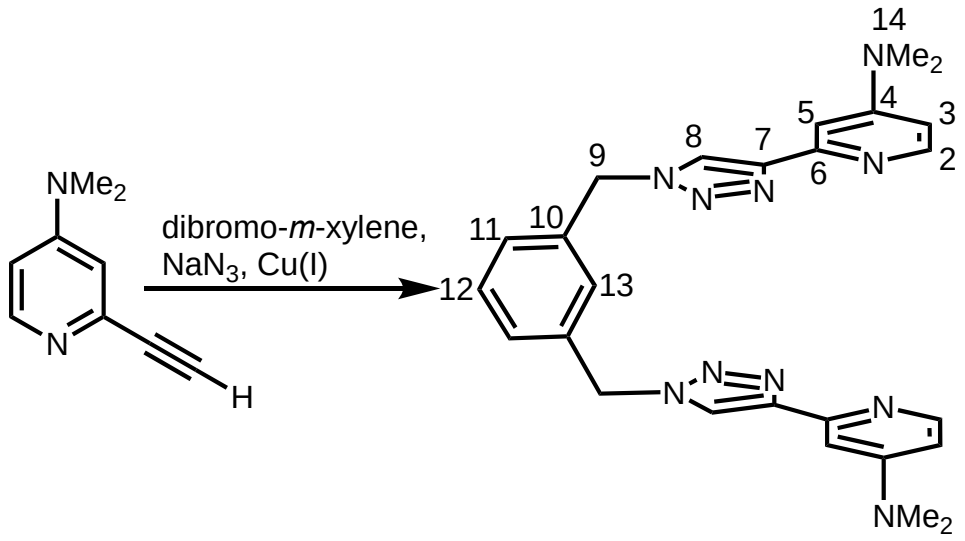

Synthesis of *m*-xylylenebis(4-dimethylaminopyridyltriazole), Me_2N-xpt (17).

1.1332 g (4.4121 mmol) α,α′-dibromo-m-xylene was dissolved in 20 mL of a DMF–water mixture (4:1 v/v), then 602.3 mg (9.265 mmol) NaN_3 and 468 mg (4.42 mmol) Na_2CO_3 were added. To this colorless mixture, 444 mg (1.78 mmol) $CuSO_4 \cdot 5H_2O$ was added, which turned the color of solution immediately to dark brown. Then 622.1 mg (3.532 mmol) ascorbic acid was added, and the color of solution turned to colorless/light blue. To the mixture a solution of **23** was added (1.2900 g, 8.8242 mmol in 10 mL DMF), and left to stir for 20 hours under nitrogen. During this time, formation of a yellow/orange solid was observed. The mixture was worked up with NH_3/Na_2H_2EDTA aqueous solution (2.00 g of $Na_2H_2EDTA \cdot 2H_2O$ in 5 mL of 28% aqueous NH_3, diluted to 100 mL with H_2O) in a separatory funnel. The aqueous layer was extracted with chloroform. The combined organic layers were dried over $MgSO_4$ and concentrated *in vacuo*. The residual DMF was evaporated under a stream of nitrogen. Then the crude mixture was sonicated with ether, and the resulting suspension was filtered. The solid was dried in air, which afforded 1.035 g (48%) of **17** as a white solid. ^{1}H NMR (400 MHz, $CDCl_3$) δ 8.15 (d, J = 6 Hz, 2H, H2), 8.05 (s, 2H, H8), 7.46 (d, J = 2.56, 2H, H5), 7.26-7.38 (m, 4H, H11-H13), 6.43 (dd, J_1 = 5.96 Hz,

J_2 = 2.64 Hz, 2H, H3), 5.55 (s, 4H, H9), 3.08 (s, 12H, H14). ESI-MS: m/z $[Me_2N\text{-}xpt+H]^+$ 481.25668 (calcd: 481.25712), $[Me_2N\text{-}xpt+Na]^+$ 503.23817 (calcd: 503.23906).

Synthesis of $[Cu_2(Me_2N\text{-}xpt)_2(NO_3)_2](PF_6)_2$ (25).

Me_2N-xpt (299.2 mg, 0.6199 mmol) was dissolved in 5 mL chloroform, and added dropwise (over 1 hour) to a solution of $Cu(NO_3)_2{\cdot}2.5H_2O$ (144.4 mg, 0.6208 mmol) in 5 mL acetonitrile under nitrogen. The mixture was stirred for one hour and then filtered, and the solid washed with ether and dried in air. This afforded 380 mg of $[Cu_2(Me_2N\text{-}xpt)_2(NO_3)_2](NO_3)_2$ (**24**) (ca. 90%) as a green solid.

Complex **24** (151.9 mg, 0.1133 mmol) was dissolved in 50 °C water. To the hot solution, an aqueous solution of NH_4PF_6 (110.0 mg, 0.6748 mmol in 5 mL water) was added. The resulting suspension was stirred for 10 minutes at room temperature and then kept in an ice bath for an additional 10 minutes. The resulting green precipitate was collected, washed with water and dried in air. This afforded 146.5 mg of **25** as a green solid (86%). The colors of powders of **24** and **25** are shown in Figure 2.18 and their FT-IR spectra are shown in Figures 2.19 and 2.20. ESI-MS of **25**: m/z $[Cu(Me_2N\text{-}xpt)]^+$ 543.1893 (calcd:543.1794), $[Cu(Me_2N\text{-}xpt)_2(PF_6)]^+$ 1168.38920 (calcd:1168.39346), $[Cu_2(Me_2N\text{-}xpt)_2(PF_6)]^+$ 1231.32333 (calcd:1231.32252), $[Cu_2(Me_2N\text{-}xpt)_2(PF_6)_3]^+$ 1521.2366 (calcd:1521.2514).

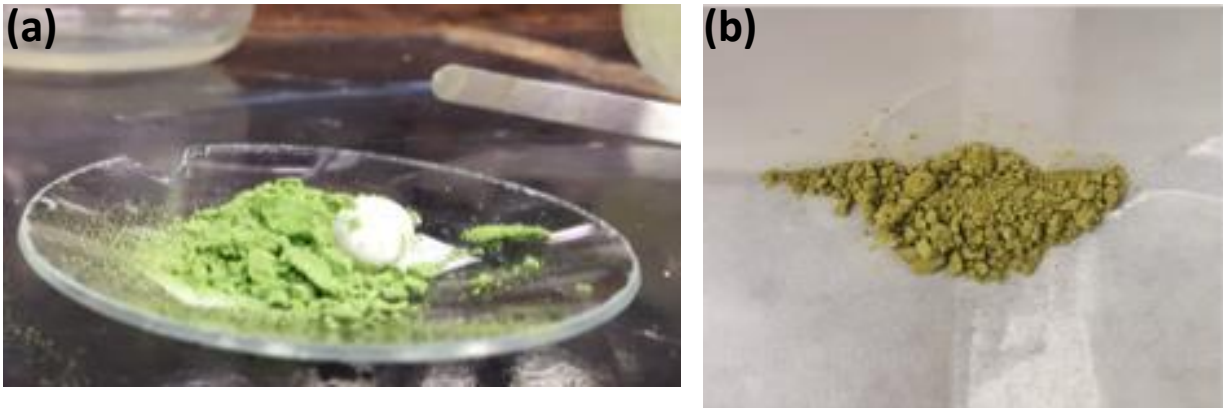

Figure 2.18. (a) $[Cu_2(NMe_2\text{-xpt})_2(NO_3)_2](NO_3)_2$ (**24**) (b) $[Cu_2(NMe_2\text{-xpt})_2(NO_3)_2](PF_6)_2$ (**25**) complex.

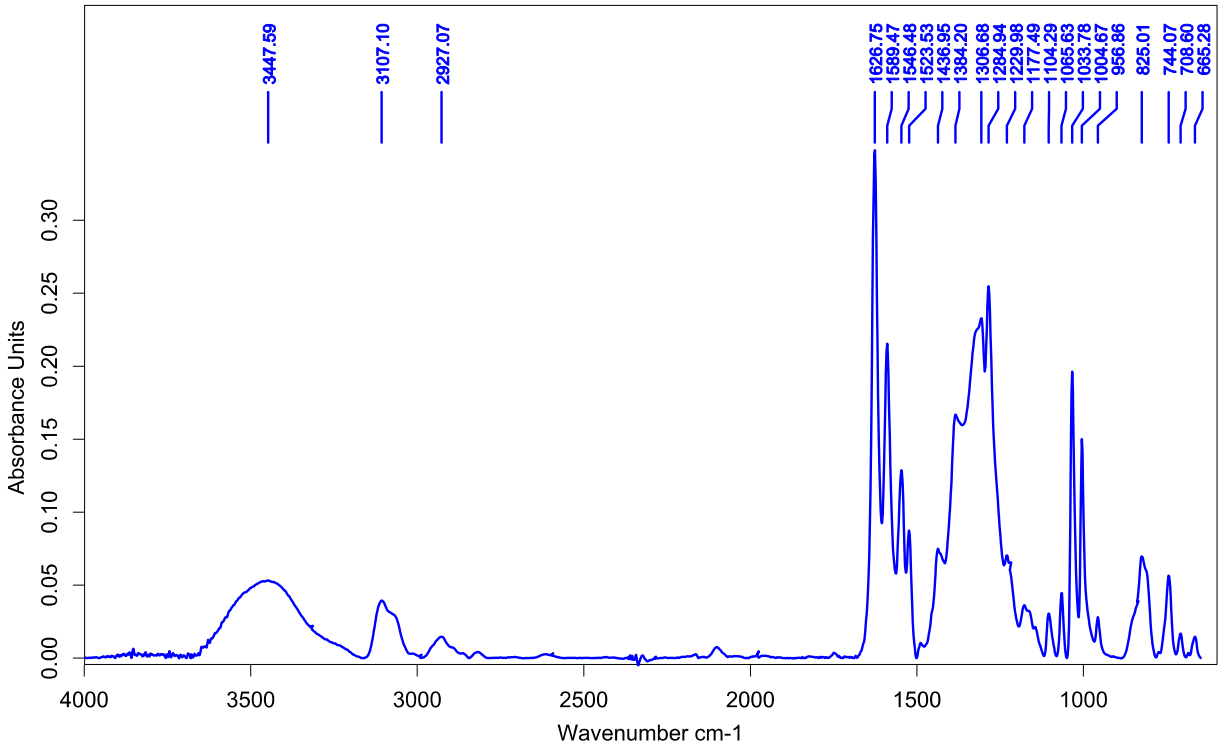

Figure 2.19. FT-IR spectrum of $[Cu_2(NMe_2\text{-xpt})_2(NO_3)_2](NO_3)_2$ (**24**).

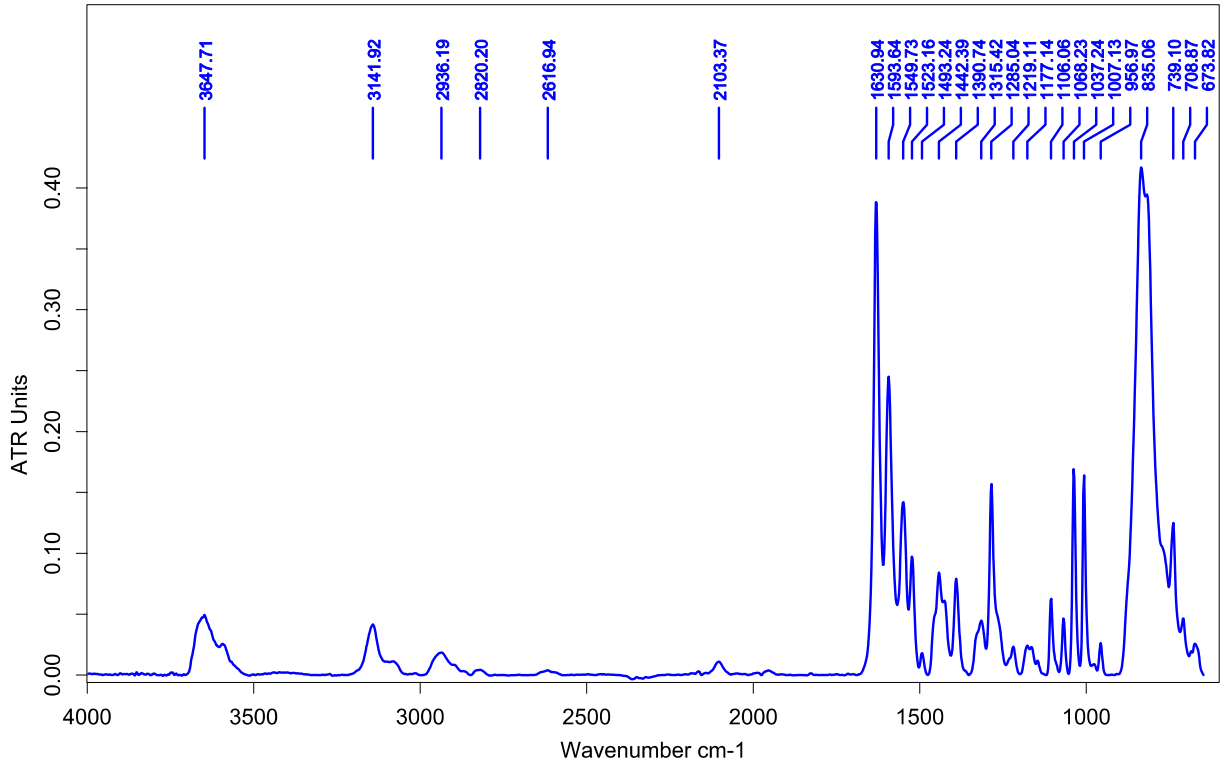

Figure 2.20. FT-IR spectrum of $[Cu_2(NMe_2\text{-xpt})_2(NO_3)_2](PF_6)_2$ (**25**).

Reaction of *in situ* generated $[Cu_2(NMe_2\text{-xpt})_2](PF_6)_2$ (26) with air and formation of a mixture of $[Cu_3(NMe_2\text{-xpt})_3(\mu_3\text{-}CO_3)](PF_6)_4$ (27) and $[Cu_2(NMe_2\text{-xpt})_2(\mu\text{-}C_2O_4)](PF_6)_2$ (28).

A Schlenk flask sealed to a cuvette was charged with complex **25** (23.1 mg, 0.0154 mmol) and sodium ascorbate (6.0 mg, 0.030 mmol), then evacuated for 30 minutes. 4 mL N_2-purged DMF was added to the solids, and the resulting solution was stirred under N_2 for 4 hours. The color of the solution changed to yellow and complete conversion to **26** was observed by UV/vis spectroscopy. The solution was exposed to CO_2 with complete exclusion of O_2. The solution became slightly turbid but no color change was observed by UV/vis spectroscopy over two days; see Figure 2.21. At this point the solution was exposed to air and stirred for ca. 24 h. The solution became green and was used for ether vapor diffusion, which formed mostly blue crystals of **27** and a small amount of green crystals of **28**; see Figure 2.9.

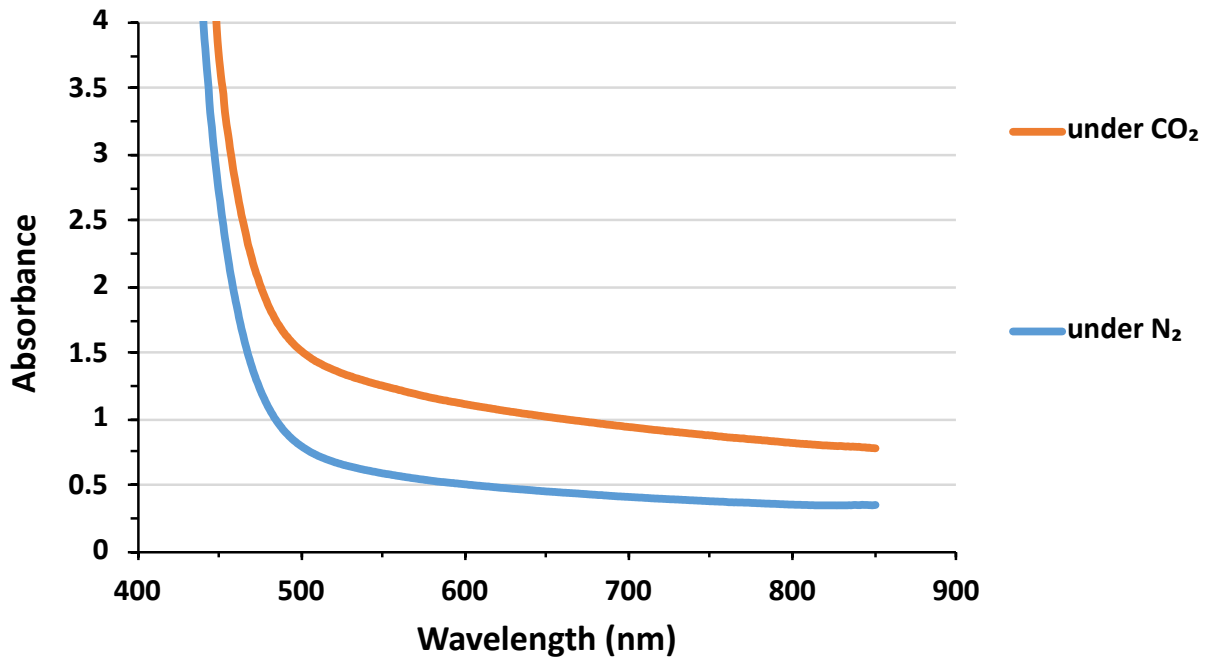

Figure 2.21. UV/vis absorption spectrum of the solution of *in situ* generated $[Cu_2(NMe_2\text{-}xpt)_2](PF_6)_2$ (**26**); Complete reduction of $[Cu_2(NMe_2\text{-}xpt)_2(NO_3)_2](PF_6)_2$ (**25**) with ascorbate under N_2 (blue), and no absorptions attributable to Cu(II) upon treatment with CO_2 (orange) for about two days.

Synthesis of $[Cu_3(Me_2N\text{-}xpt)_3(\mu_3\text{-}CO_3)](PF_6)_4$ (27) by addition of $CsHCO_3$ to 25.

To a solution of **25** (35.0 mg, 0.0232 mmol in 5 mL DMF), $CsHCO_3$ (5.2 mg, 0.027 mmol) was added. The solution was stirred under N_2 for two days, during which time the color of solution changed from green to a more intense green. Ether vapor diffusion to the crude mixture formed crystals of **27**. The crystals were dried in vacuum with a slight heating and used for FT-IR spectroscopy; see Figure 2.22. ESI-MS: m/z $[Cu_3(Me_2N\text{-}xpt)_3(CO_3)(PF_6)_3]^+$ 2124.41193 (calcd: 2124.41506).

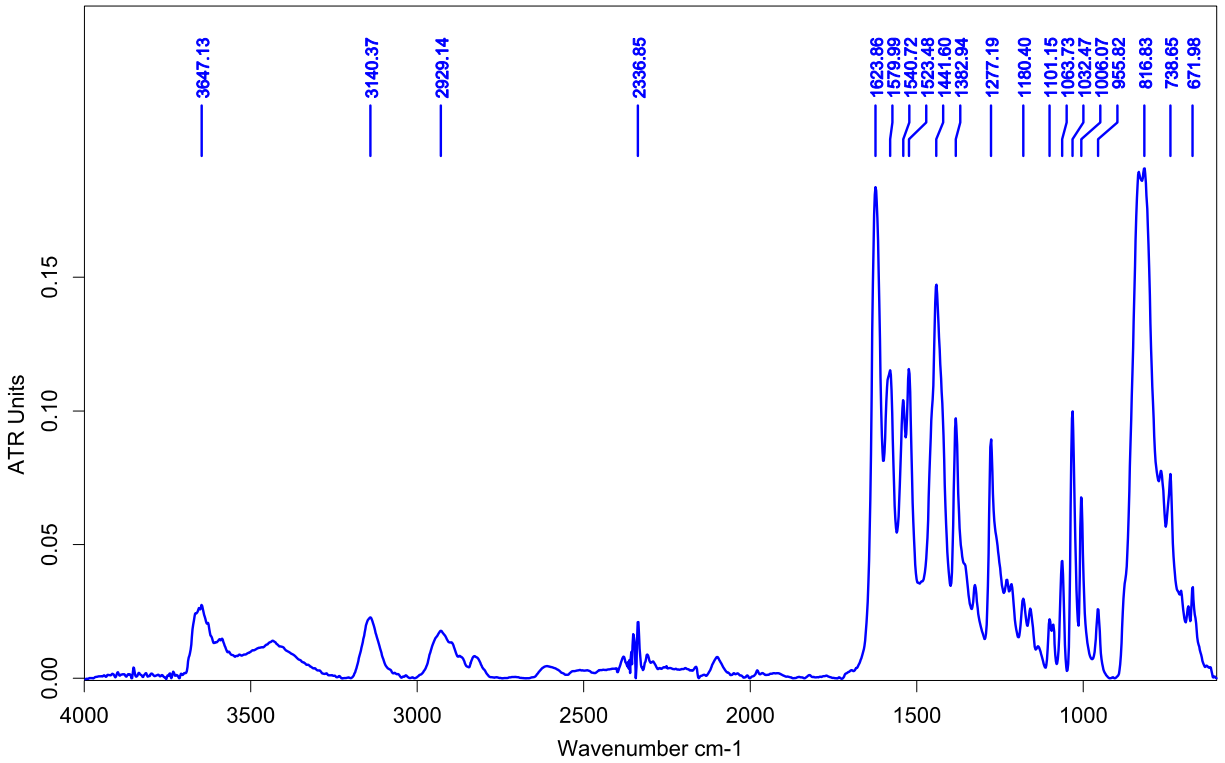

Figure 2.22. FT-IR spectrum of $[Cu_3(Me_2N\text{-}xpt)_3(\mu_3\text{-}CO_3)](PF_6)_4$ (**27**) obtained by addition of $CsHCO_3$.

Synthesis of $[Cu_2(Me_2N\text{-}xpt)_2(\mu\text{-}C_2O_4)](PF_6)_2$ (28) by addition of TBAO to 25.

To a solution of **25** (41.5 mg, 0.0276 mmol in 5 mL DMF), a solution of TBAO (16.8 mg, 29.3 mmol) in 2 mL DMF was added dropwise. Addition was stopped when the first sign of permanent turbidity was observed. The color of solution turned to light green (λ_{max} = 705 nm) and it was stirred for 30 minutes. The solution was used for crystallization with ether vapor diffusion and the resulting crystals of **28** were dried in vacuum with a slight heating and used for FT-IR spectroscopy; see Figure 2.23. ESI-MS: m/z $[Cu_2(Me_2N\text{-}xpt)_2(C_2O_4)(PF_6)]^+$ 1319.30219 (calcd: 1319.30217).

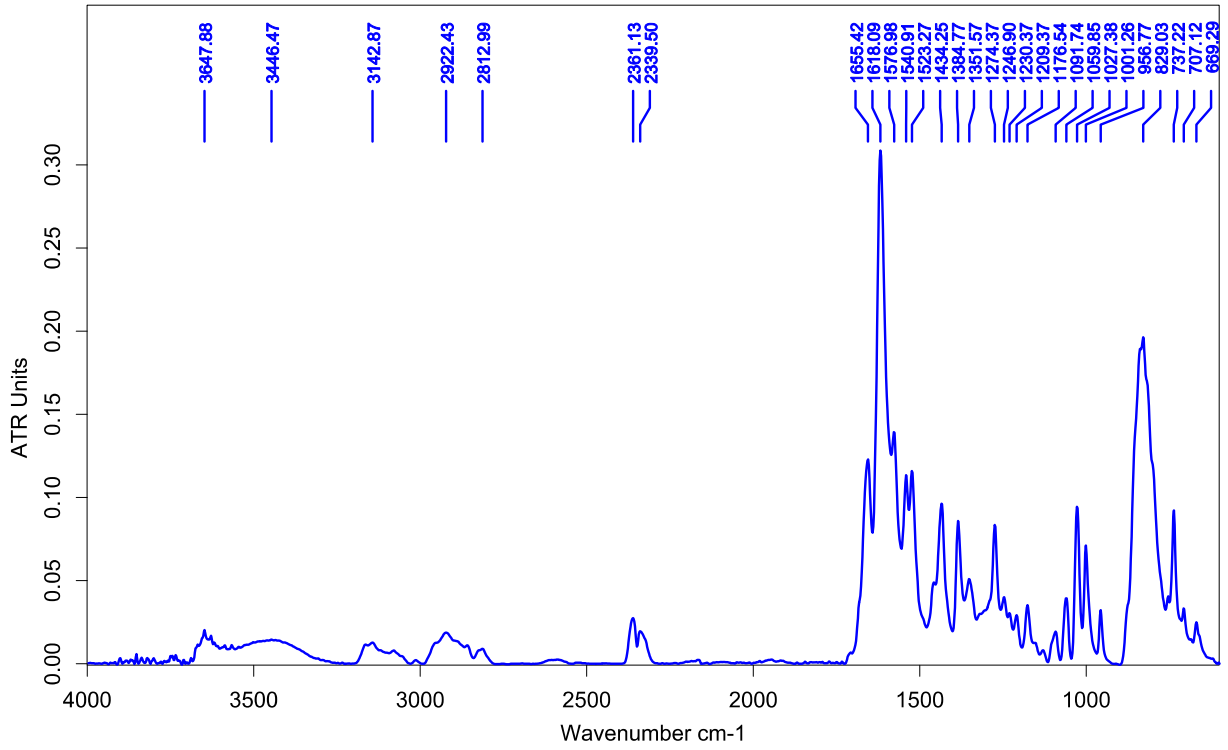

Figure 2.23. FT-IR spectrum of $[Cu_2(Me_2N\text{-}xpt)_2(\mu\text{-}C_2O_4)](PF_6)_2$ (**28**) obtained by addition of TBAO.

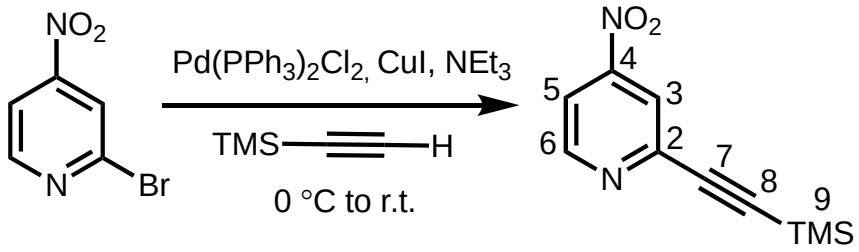

Synthesis of 4-nitro-2-(trimethylsilylethynyl)pyridine (30).

The title compound was prepared according to Elderly's method with some modifications.[9] A Schlenk flask was charged with 867.5 mg (4.274 mmol) 2-bromo-4-nitropyridine (**20**) and evacuated for 25 minutes, then transferred to a glove box and 230 mg (0.328 mmol) $PdCl_2(PPh_3)_2$ and 82 mg (0.43 mmol) CuI were added. The reaction flask was evacuated for 30 minutes. In a separate flask triethylamine was purged with N_2 and cooled to 0 °C for one hour. The reaction flask was filled with N_2 and 30 mL NEt_3 was added. Then 0.6 mL cold ethynyltrimethylsilane (400

mg, 4.33 mmol, T ~ 2 °C, d = 0.709 g/mL) was added dropwise under N_2. With careful exclusion of O_2 in each step the resulting suspension remains yellow. The suspension was stirred at 0 °C for two hours then left to stir at room temperature for two more hours. The suspension was filtered and the solid was washed with ether. To the filtrate 70 mL more of ether was added and washed with 2 × 100 mL saturated $NH_4Cl_{(aq)}$. Then the organic layer was dried over $MgSO_4$, filtered and concentrated *in vacuo*. The crude mixture was purified by column chromatography using DCM-hexane (4:1 v/v) (R_f = 0.5). This afforded 804.8 mg (85.5%) of the desired product as a white/very light cream solid. ^{1}H NMR (400 MHz, $CDCl_3$) δ 8.86 (d, J_1 = 5.2, 1H, H6), 8.14 (d, J_1 = 2.0, 1H, H3), 7.95 (dd, J_1 = 5.2, J_2 = 2.0 Hz, 1H, H5), 0.30 (s, 9H, H9). ^{13}C NMR (125.7 MHz, $CDCl_3$) δ 153.87 (C4), 152.16 (C6), 145.76 (C2), 119.84 (C3), 115.43 (C5), 101.85 (C7 or C8), 99.08 (C7 or C8), -0.37 (C9). m.p. = 98 °C.

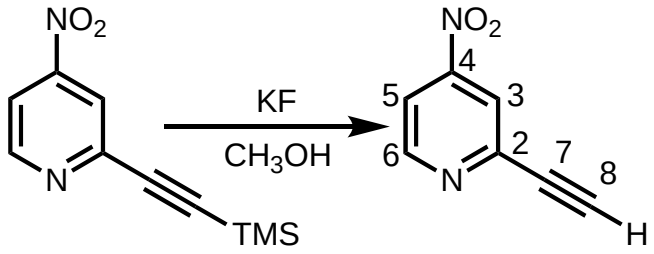

Synthesis of 2-ethynyl-4-nitropyridine (31).

The protected acetylene **30** (804.8 mg, 3.653 mmol) was dissolved in 80 mL methanol, and a solution of KF (642.2 mg, 11.05 mmol) was added dropwise under N_2. The color of the solution changed from light yellow to yellow/orange during the addition. The solution was stirred under N_2 for 4 hours and then evaporated *in vacuo*. The residue was re-dissolved in DCM and poured into saturated NH_4Cl(aq). The aqueous layer was extracted with additional DCM, and then the combined organic layers were dried over $MgSO_4$, filtered and concentrated *in vacuo*. The crude mixture was purified by column chromatography using DCM-hexane (4:1 v/v) as eluent (R_f = 0.4).

This afforded 433 mg of the desired product as a white solid (80%). ^{1}H NMR (500 MHz, $CDCl_3$) δ 8.89 (d, J = 5.5 Hz, 1H, H6), 8.17 (d, J = 2.0 Hz, 1H, H3), 8.00 (d, J_1 = 5.5, J_2 = 2.0 Hz, 1H, H5), 3.35 (s, 1H, H8). ^{13}C NMR (125.7 MHz, $CDCl_3$) δ 153.91 (C4), 152.35 (C6), 145.03 (C2), 120.13 (C3), 116.00 (C5), 81.24 (C7), 80.35 (C8). m.p. = 86 °C.

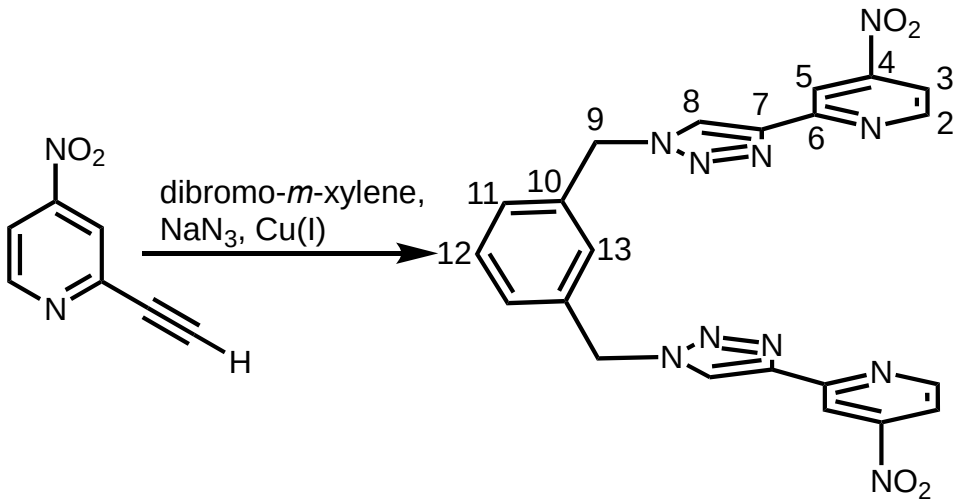

Synthesis of *m*-xylylenebis(4-nitropyridyltriazole), O_2N-xpt (29).

α,α′-dibromo-*m*-xylene (1.170 g, 4.432 mmol) was dissolved in 30 mL of DMF-water (4:1 v/v), then 606.1 mg (9.323 mmol) NaN_3, and 469.7 mg (4.431 mmol) Na_2CO_3 were added. To this colorless mixture, 442.6 mg (1.773 mmol) $CuSO_4 \cdot 5H_2O$ was added which changed the color of solution to dark brown. Then 624.4 mg (3.545 mmol) ascorbic acid was added, and the color of solution turned to colorless/light blue. To the mixture a solution of **31** was added (1.313 g, 8.864 mmol in 10 mL DMF), and left to stir for 20 hours under nitrogen, during which time formation of a brown solid was observed. The reaction mixture was worked up with an aqueous solution of Na_2H_2EDTA (1 g in 100 mL water), then it was extracted with chloroform. The combined organic layers were dried over $MgSO_4$, concentrated *in vacuo* and kept under N_2 stream to evaporate the residual DMF. The solid was triturated with ether and then collected and dried in air. This afforded 1.57 g (72%) of **29** as a white-cream solid. ^{1}H NMR (500 MHz, $CDCl_3$) δ 8.87 (d, J = 2.0 Hz, 2H,

H5), 8.81 (d, J = 5.5 Hz, 2H, H2), 8.14 (s, 2H, H8), 7.92 (d, J_1 = 5.5, J_2 = 2.0 Hz, 2H, H3), 7.33-7.46 (m, 4H, H11-13), 5.62 (s, 4H, H9). ^{13}C NMR (125.7 MHz, $CDCl_3$) δ 154.83 (C4), 153.31 (C6), 151.76 (C2), 147.48 (C7), 135.63 (C10), 130.46 (C12), 128.88 (C13), 127.93 (C11), 123.14 (C8), 115.20 (C3), 113.05 (C5), 54.22 (C9). ESI-MS: m/z $[O_2N\text{-xpt+H}]^+$ 485.14271 (calcd 485.14288), $[O_2N\text{-xpt+Na}]^+$ 507.12519 (calcd 507.12482), $[O_2N\text{-xpt+K}]^+$ 523.09880 (calcd 523.09876). m.p. = >140 °C.

Synthesis of $[Cu_2(O_2N\text{-xpt})_2(NO_3)_2](NO_3)_2$ (32).

To 330.6 mg (0.6824 mmol) **29** in 20 mL chloroform, 159.9 mg (0.6875 mmol) $Cu(NO_3)_2\cdot 2.5H_2O$ in 20 mL acetonitrile was added and the mixture was stirred under nitrogen for 15 hours. Formation of a green precipitate was observed. The suspension was centrifuged and the supernatant was decanted and dried in air. 404.6 mg of **32** (88%) was obtained and it was used for FT-IR spectroscopy; see Figure 2.24. ESI-MS: m/z $[Cu(O_2N\text{-xpt})_2(NO_3)]^+$ 1093.1828 (calcd:1093.1886), $[Cu_2(O_2N\text{-xpt})_2(NO_3)]^+$ 1156.1106 (calcd:1156.1182).

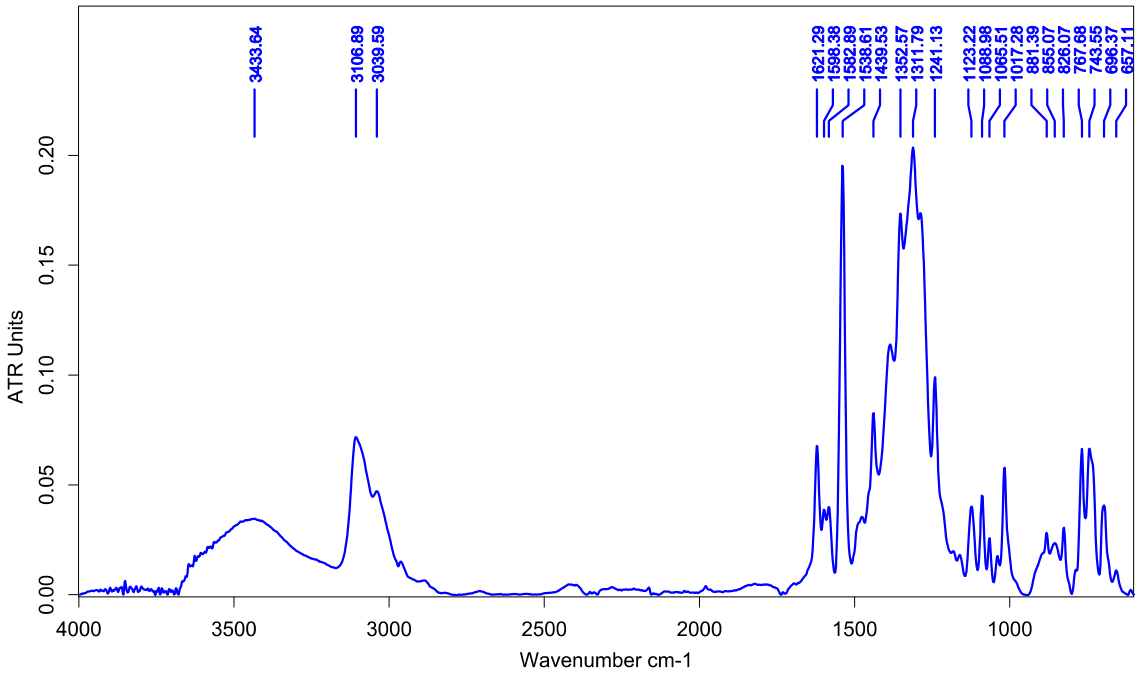

Figure 2.24. FT-IR spectrum of $[Cu_2(O_2N\text{-xpt})_2(NO_3)_2](NO_3)_2$ (**32**).

Reaction of $[Cu_2(O_2N\text{-xpt})_2(NO_3)_2](NO_3)_2$ (32) with ascorbate.

A reaction flask was charged with 32.5 mg (0.0242 mmol) of **32** and 4.9 mg (0.025 mmol) sodium ascorbate then evacuated for 1 hour and 30 minutes. 6 mL N_2-purged anhydrous DMF was added to the solids under nitrogen with stirring. The solution was green at first, and turned to brown and a brown solid formed gradually; see Figure 2.25.

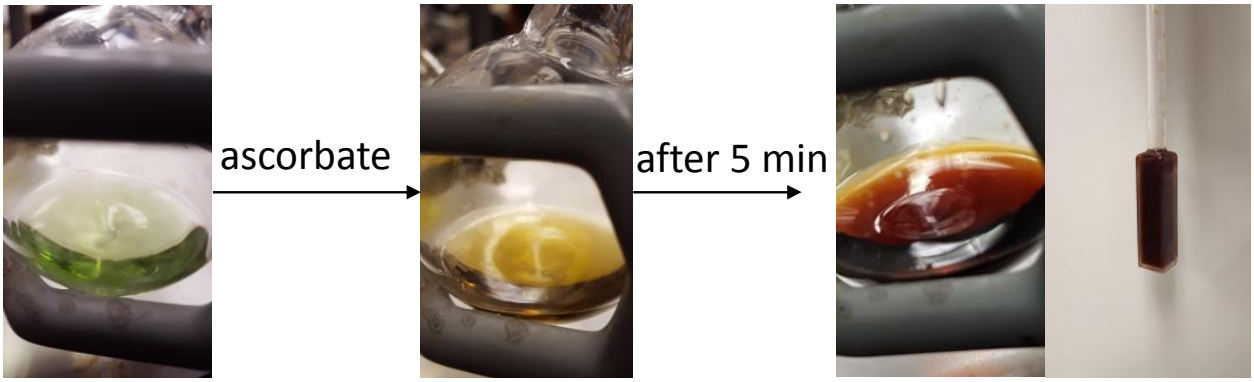

Figure 2.25. Color changes of green solution of $[Cu_2(O_2N\text{-xpt})_2(NO_3)_2](NO_3)_2$ (**32**) after addition of ascorbate.

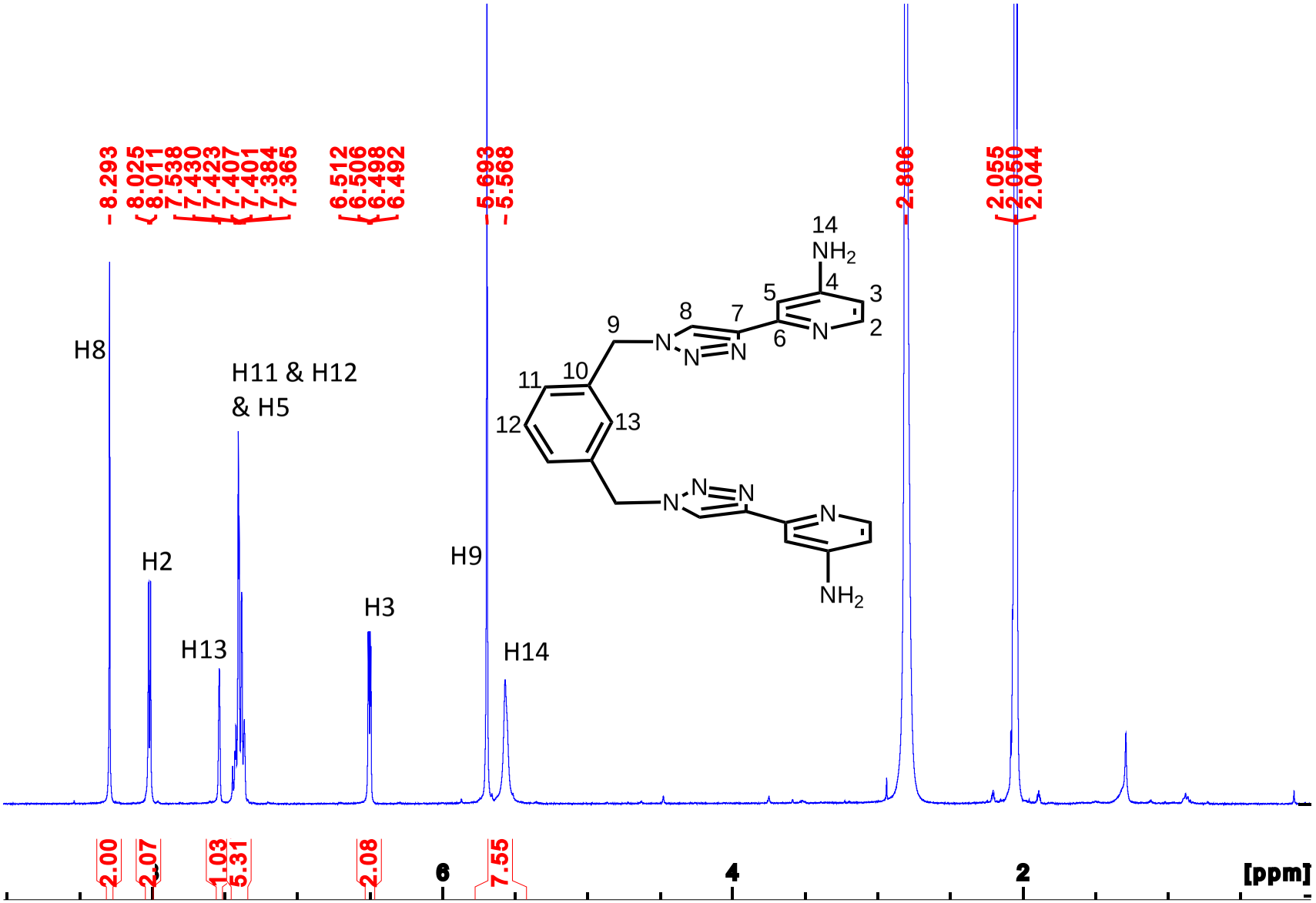

Figure 2.26. ^{1}H NMR of **8** in $(CD_3)_2CO$ at 400 MHz.

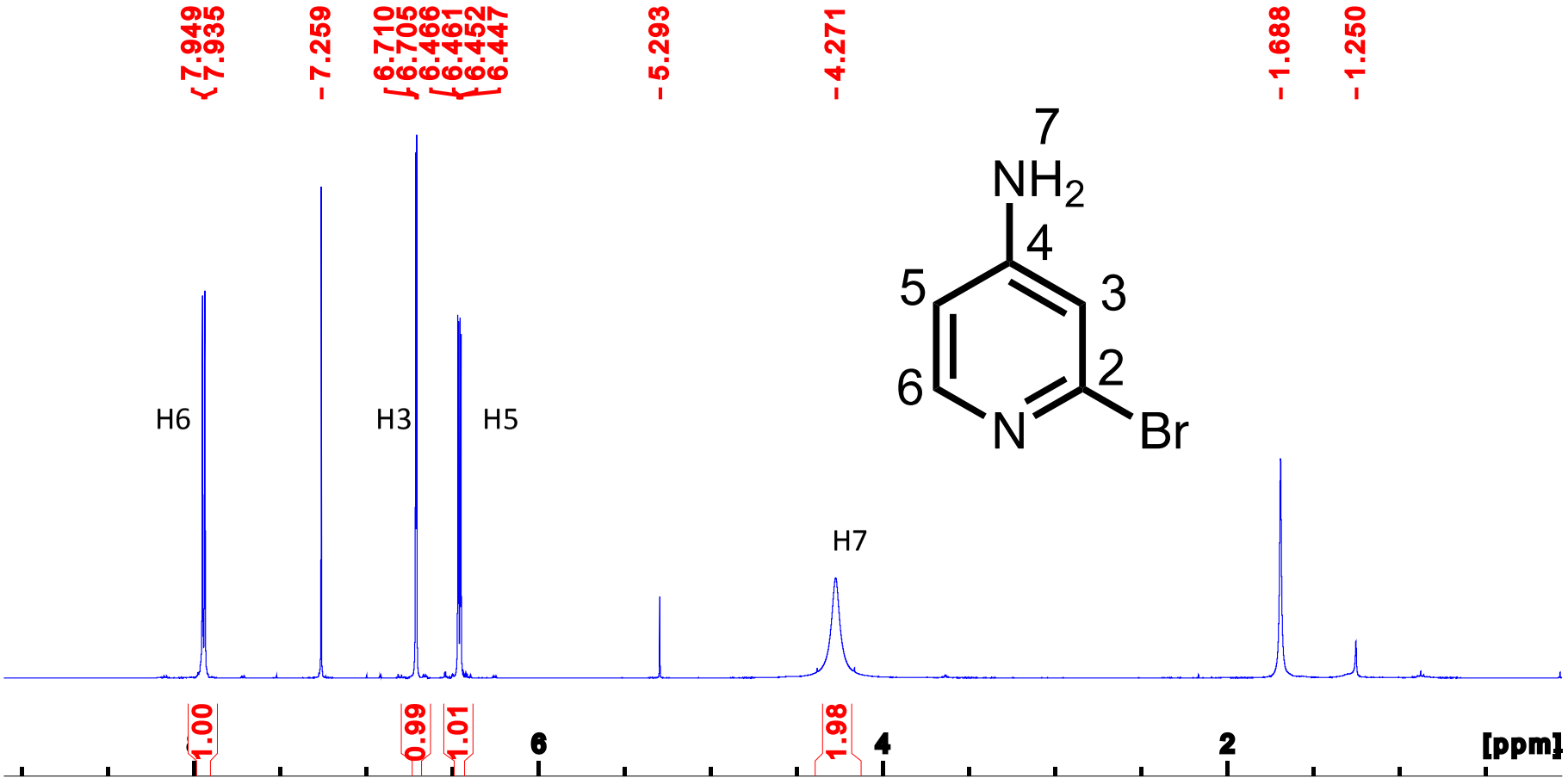

Figure 2.27. ^{1}H NMR of **21** in $CDCl_3$ at 400 MHz.

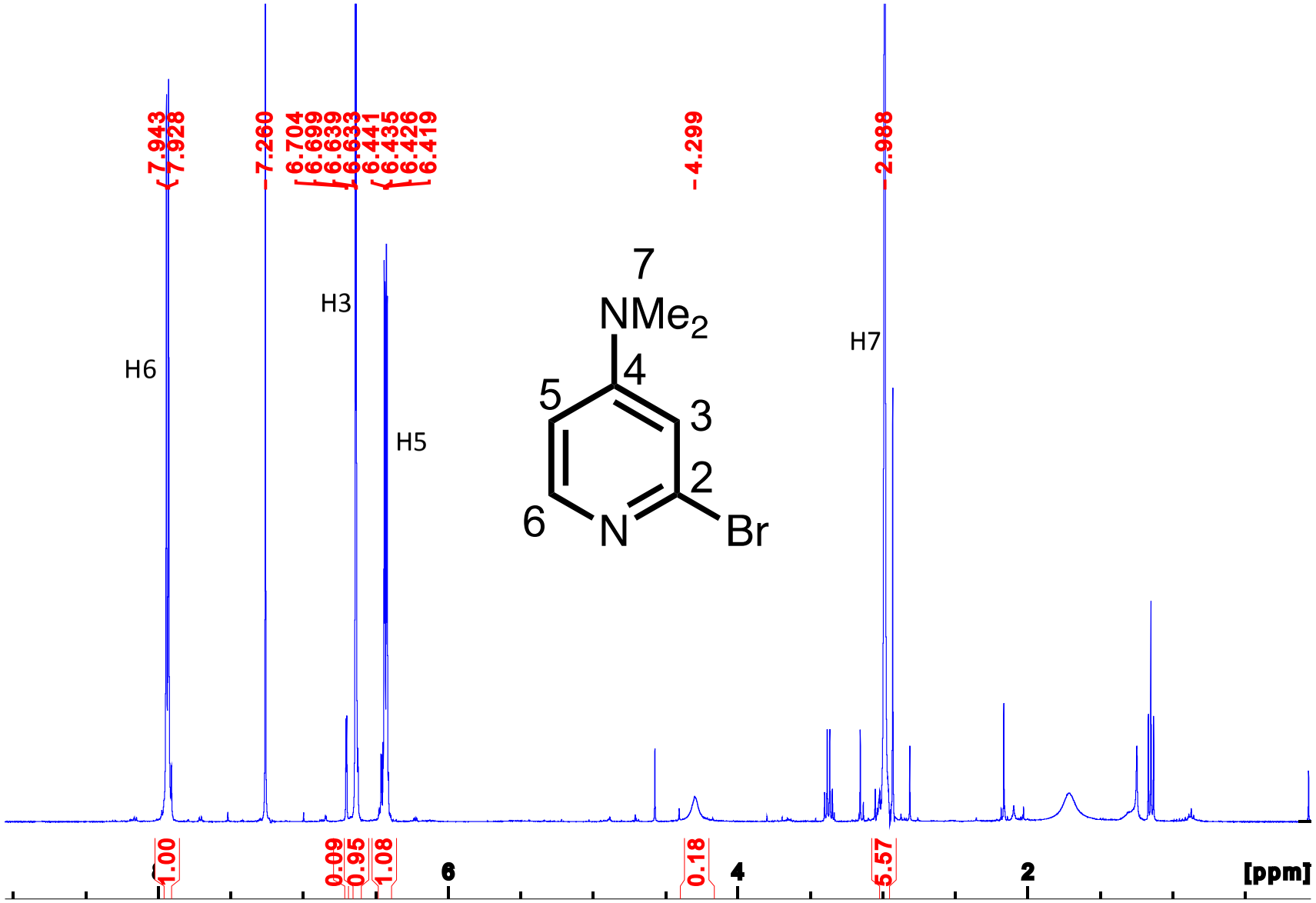

Figure 2.28. ^{1}H NMR spectrum of a mixture of **19** and ca. 9% **21** in $CDCl_3$ at 400 MHz. Only peaks belonged to hydrogens of **19** are labeled.

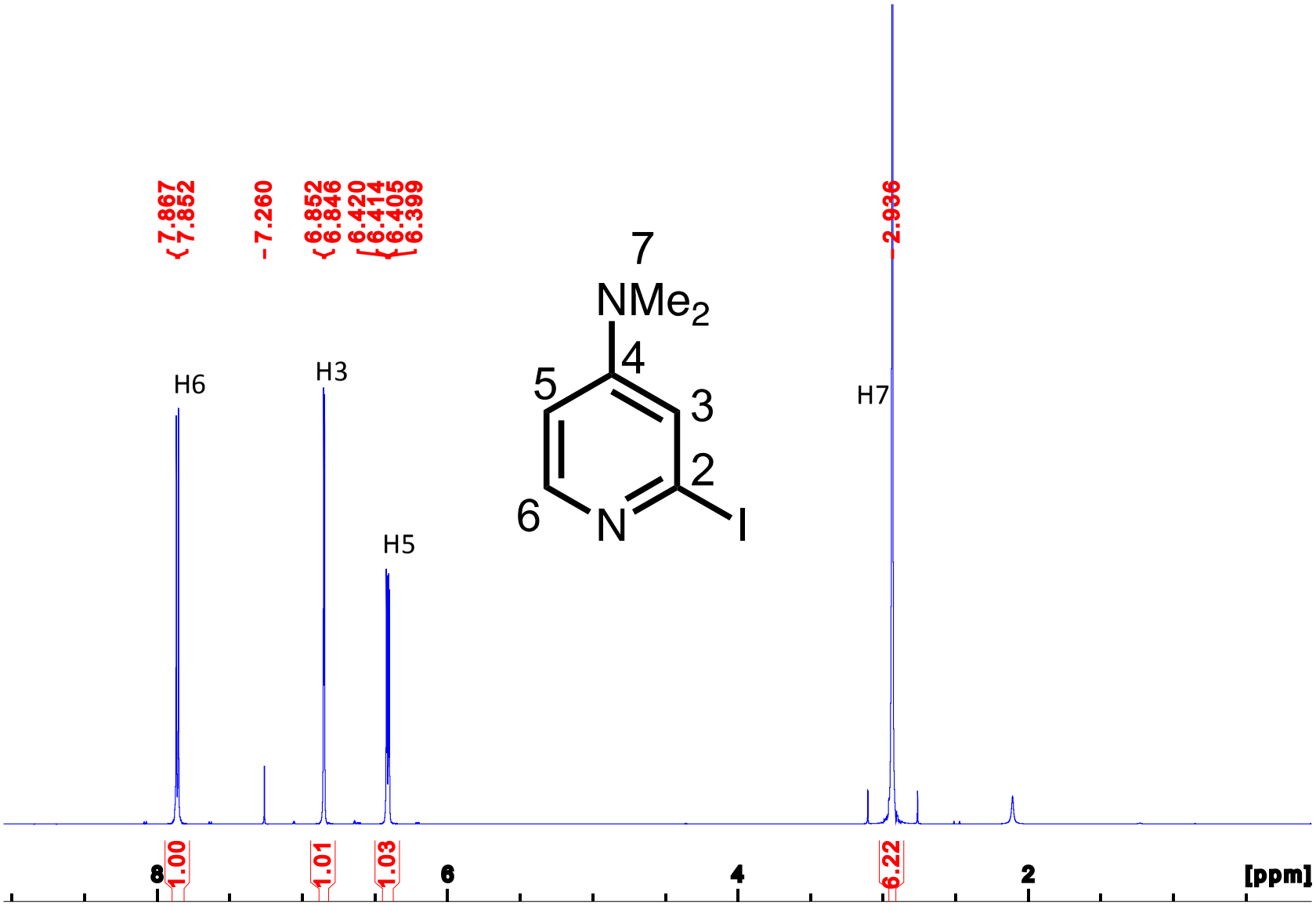

Figure 2.29. ^{1}H NMR of **18** in $CDCl_3$ at 400 MHz.

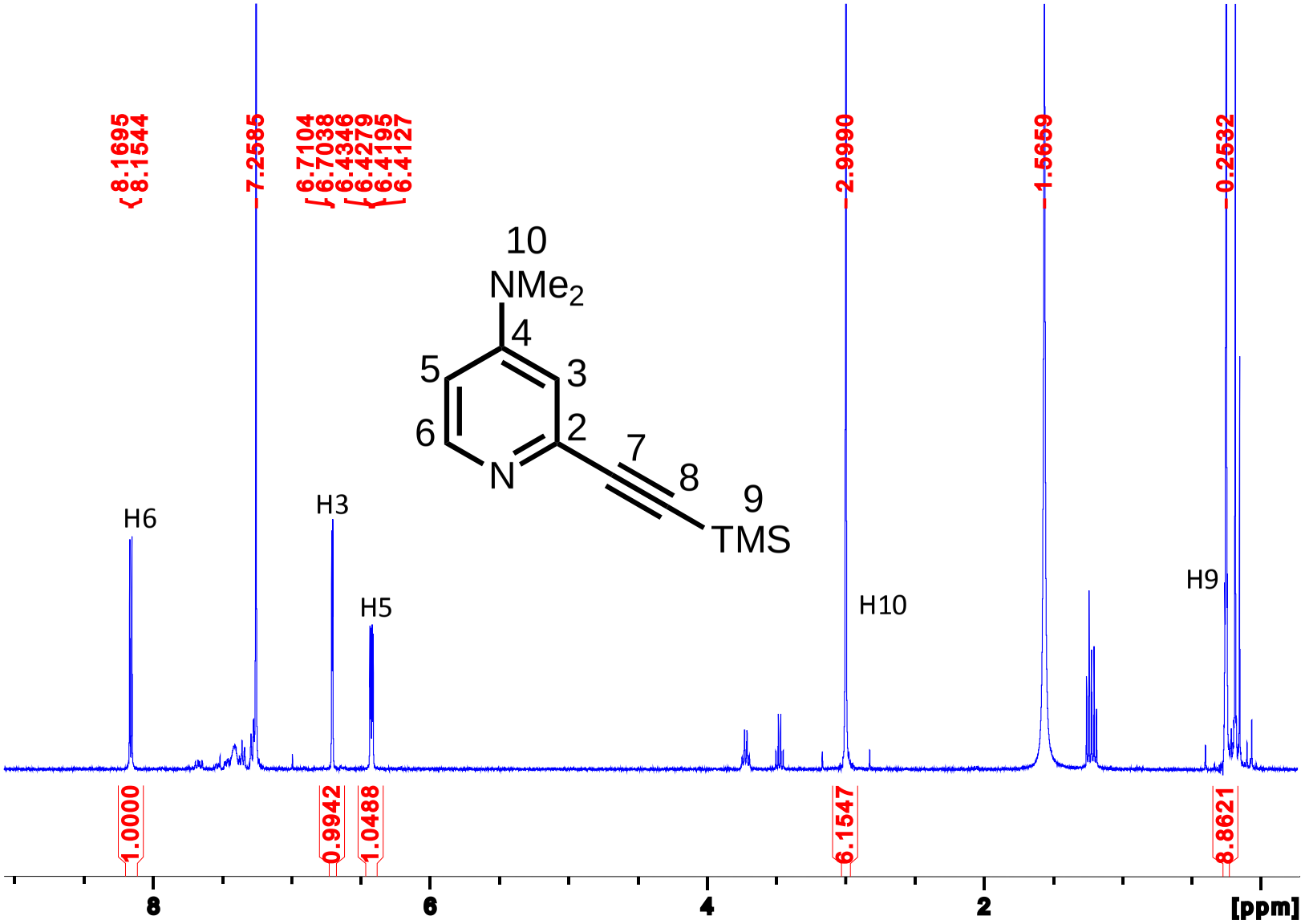

Figure 2.30. ^{1}H NMR of **22** in $CDCl_3$ at 400 MHz.

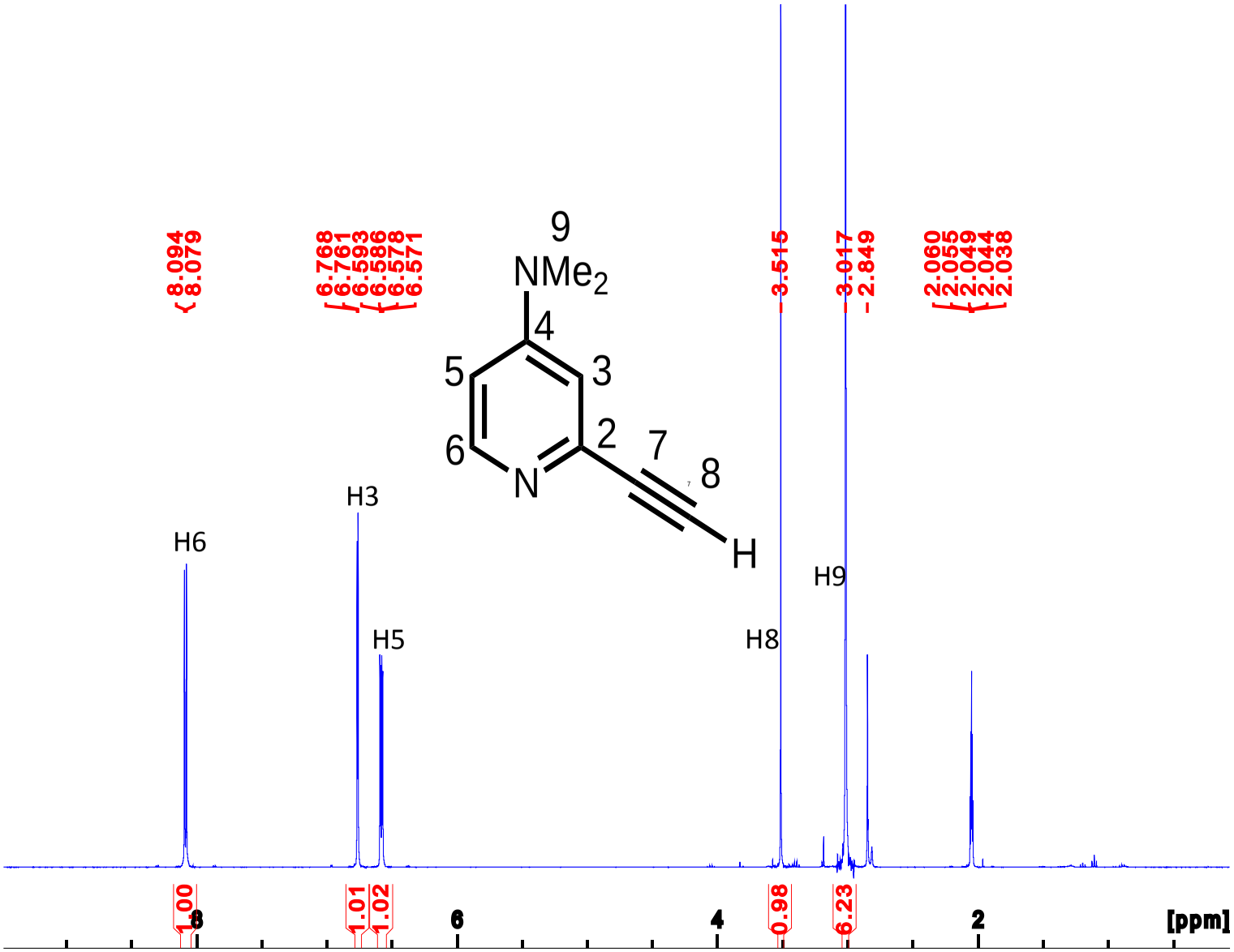

Figure 2.31. ^{1}H NMR of **23** in $(CD_3)_2CO$ at 400 MHz.

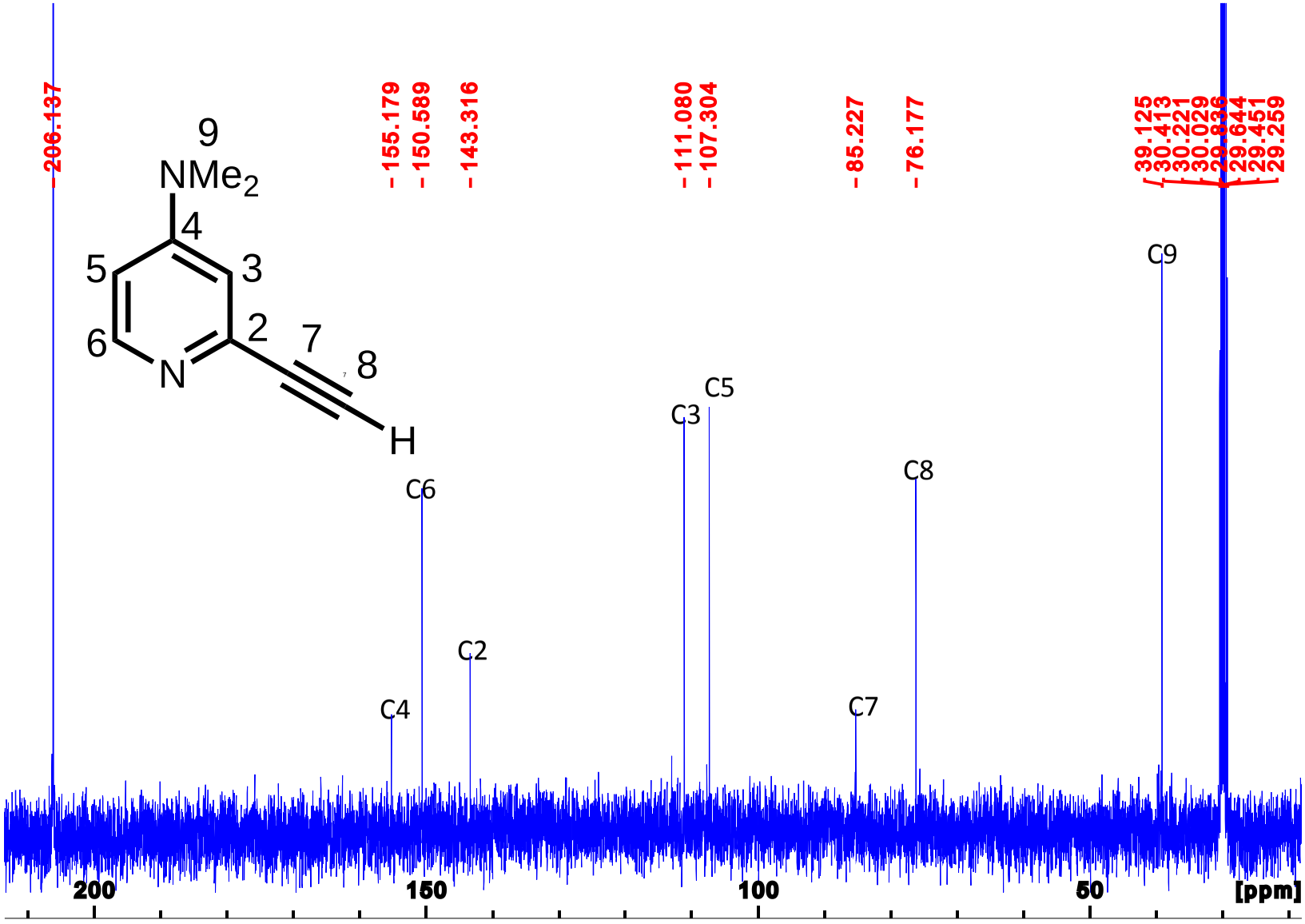

Figure 2.32. ^{13}C NMR of **23** in $(CD_3)_2CO$ at 125.7 MHz.

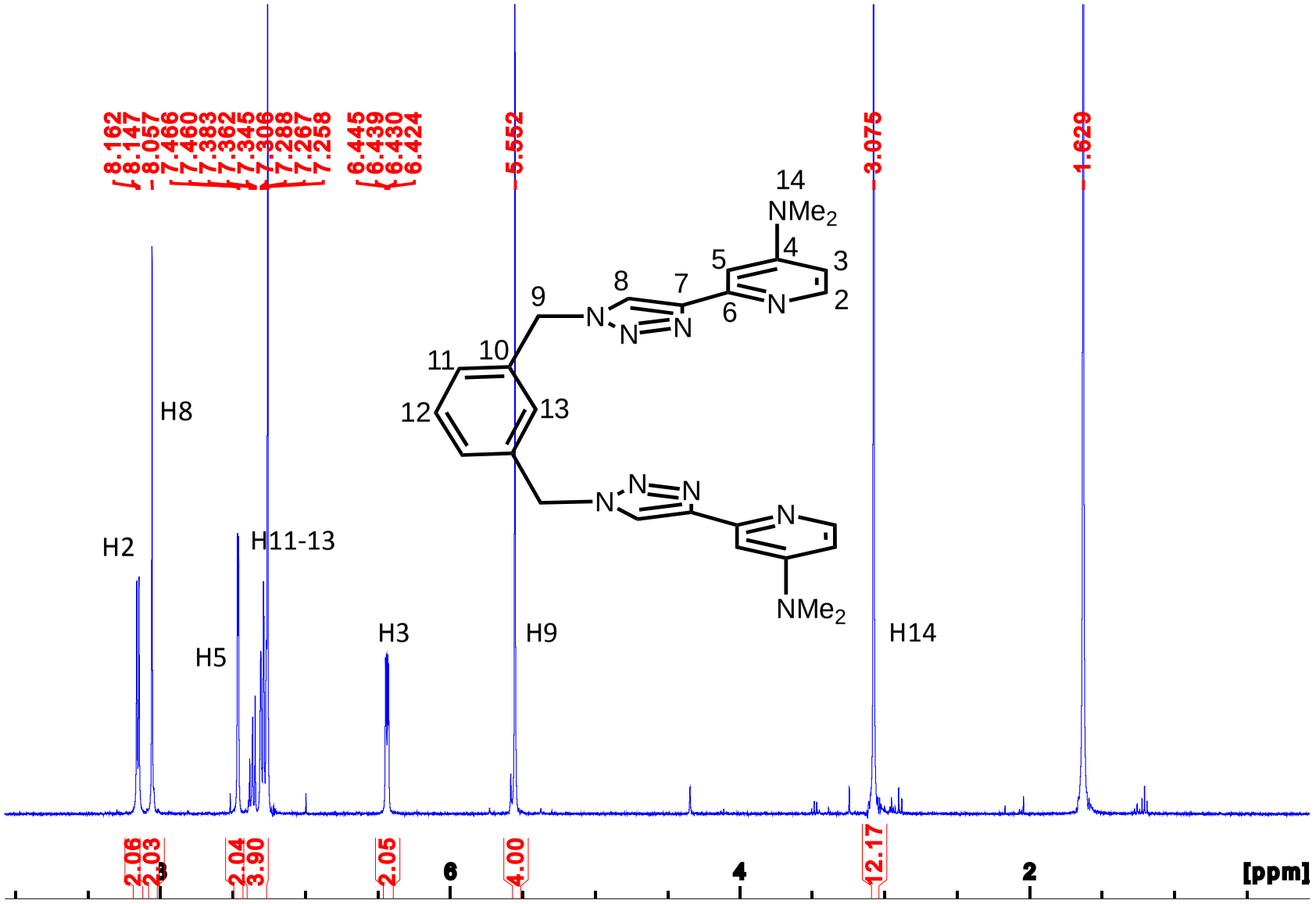

Figure 2.33. ^{1}H NMR of **17** in $CDCl_3$ at 400 MHz.

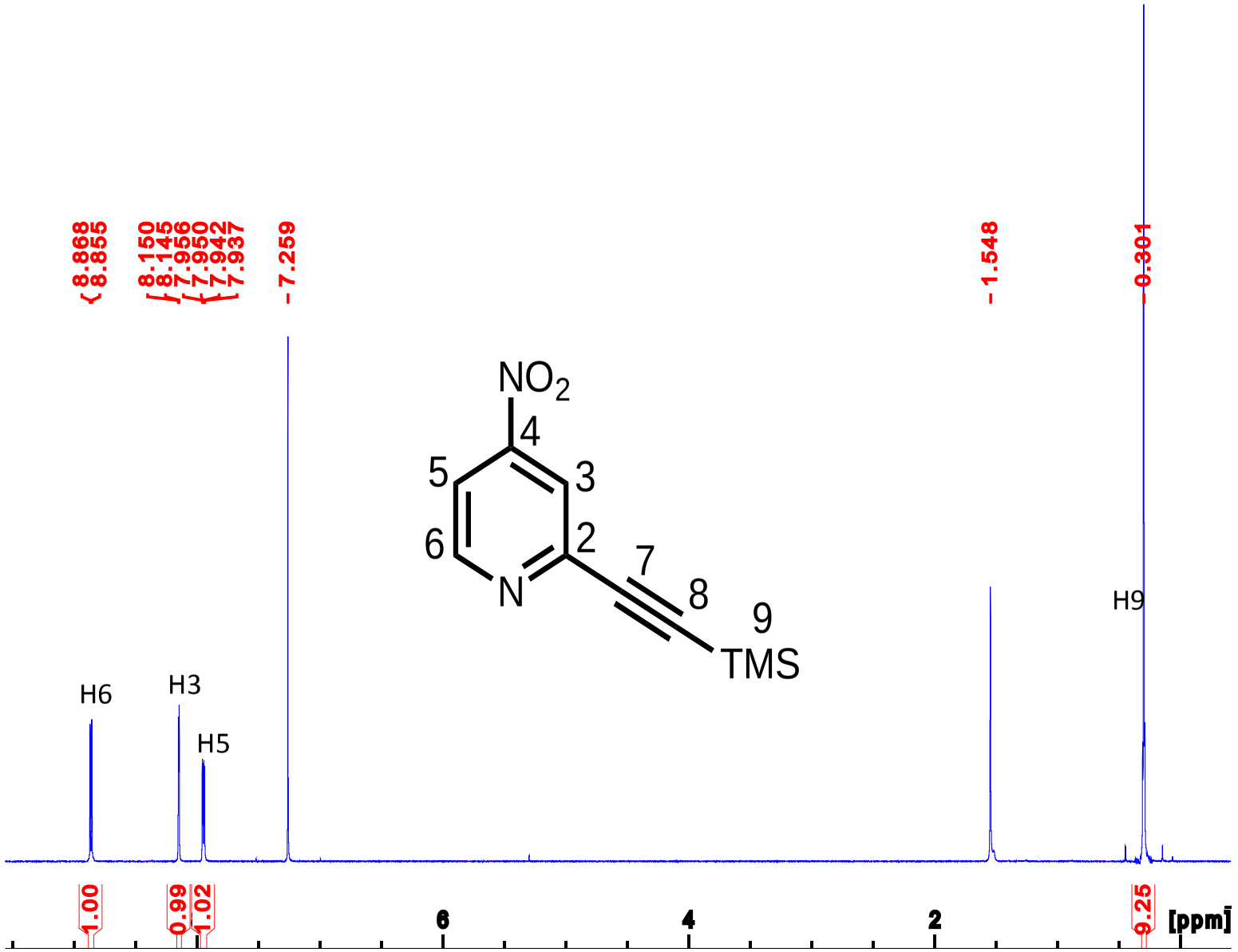

Figure 2.34. ^{1}H NMR of **30** in $CDCl_3$ at 400 MHz.

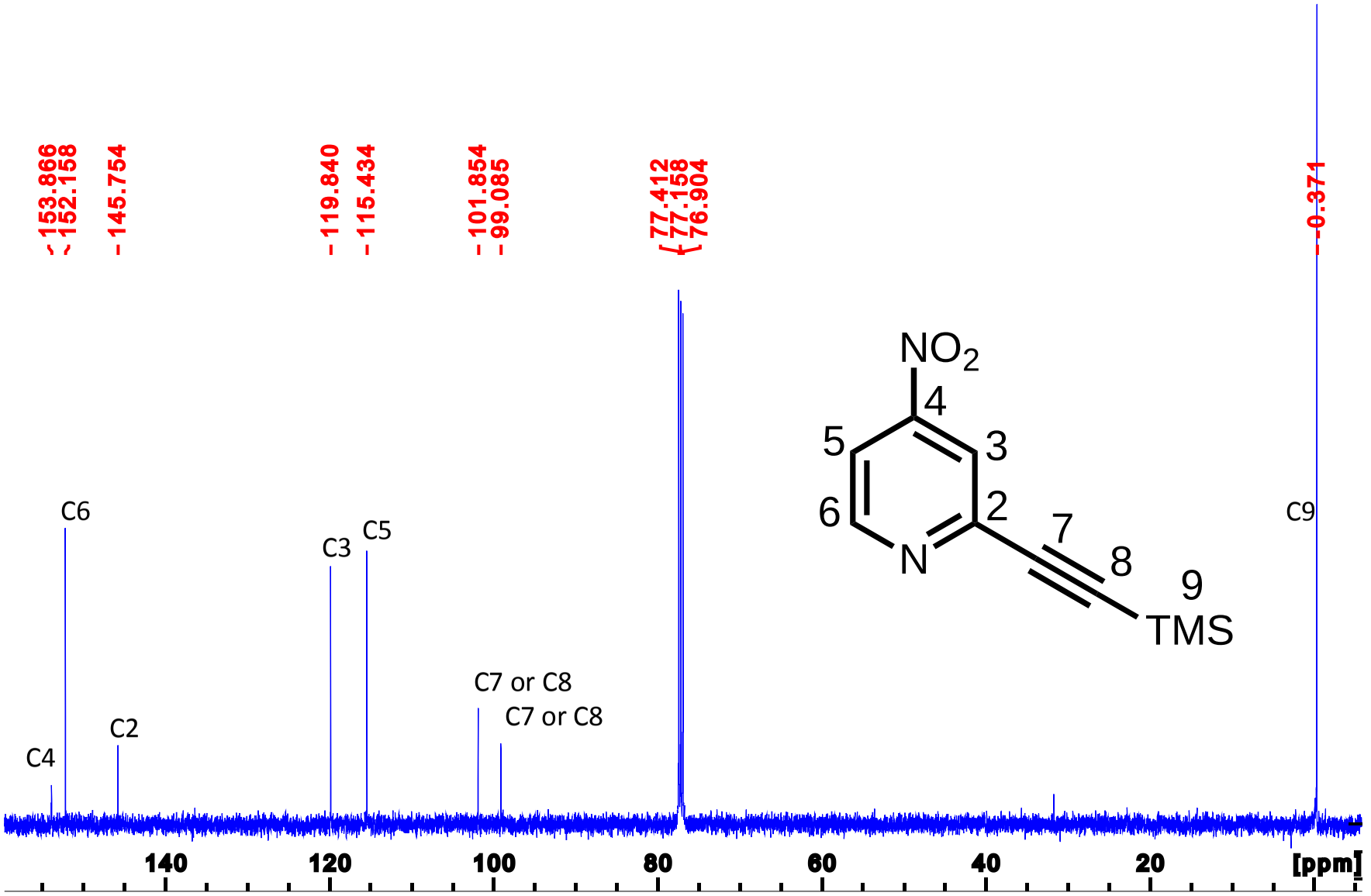

Figure 2.35. ^{13}C NMR of **30** in $CDCl_3$ at 125.7 MHz.

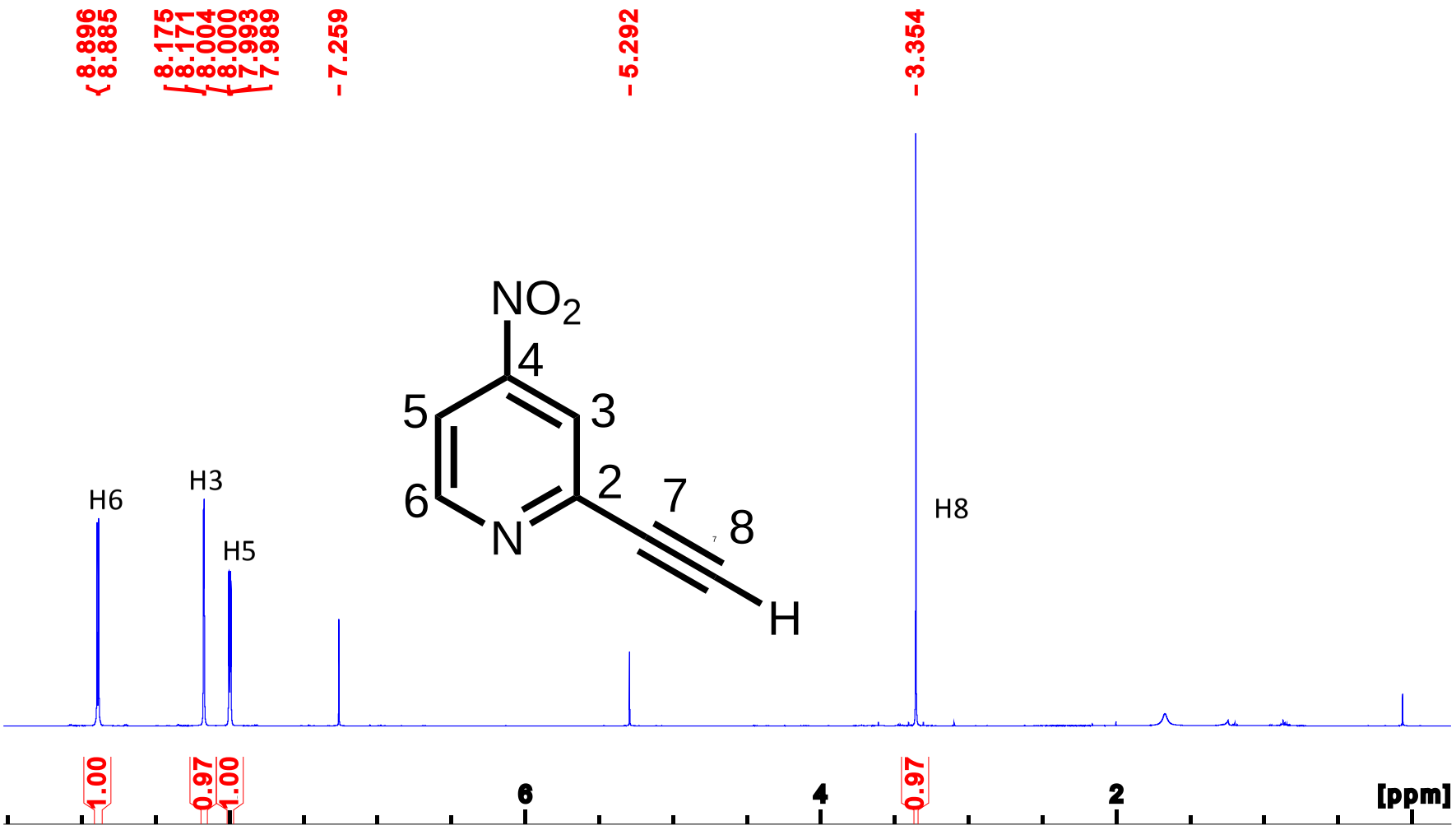

Figure 2.36. ^{1}H NMR of **31** in $CDCl_3$ at 500 MHz.

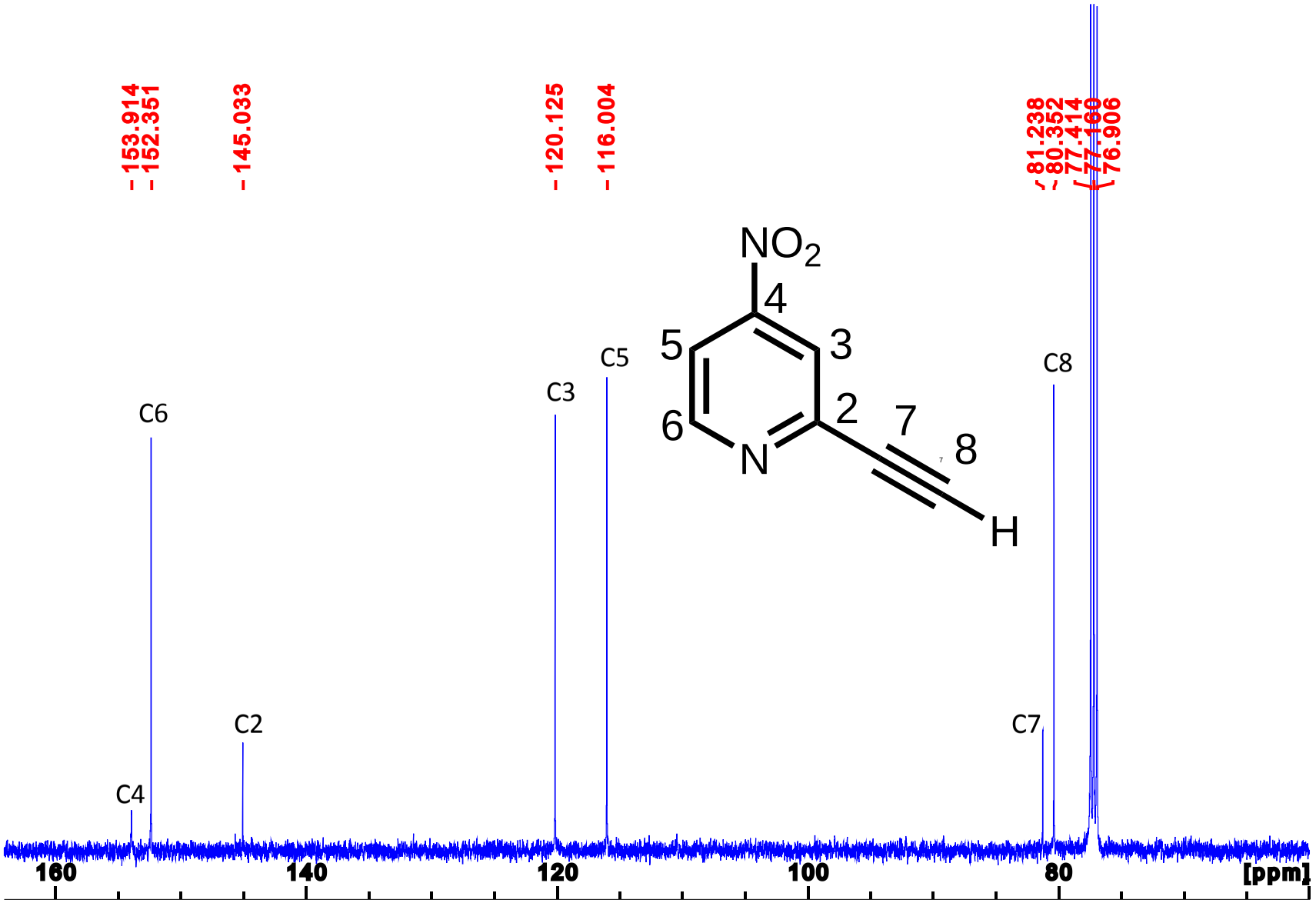

Figure 2.37. ^{13}C NMR of **31** in $CDCl_3$ at 125.7 MHz.

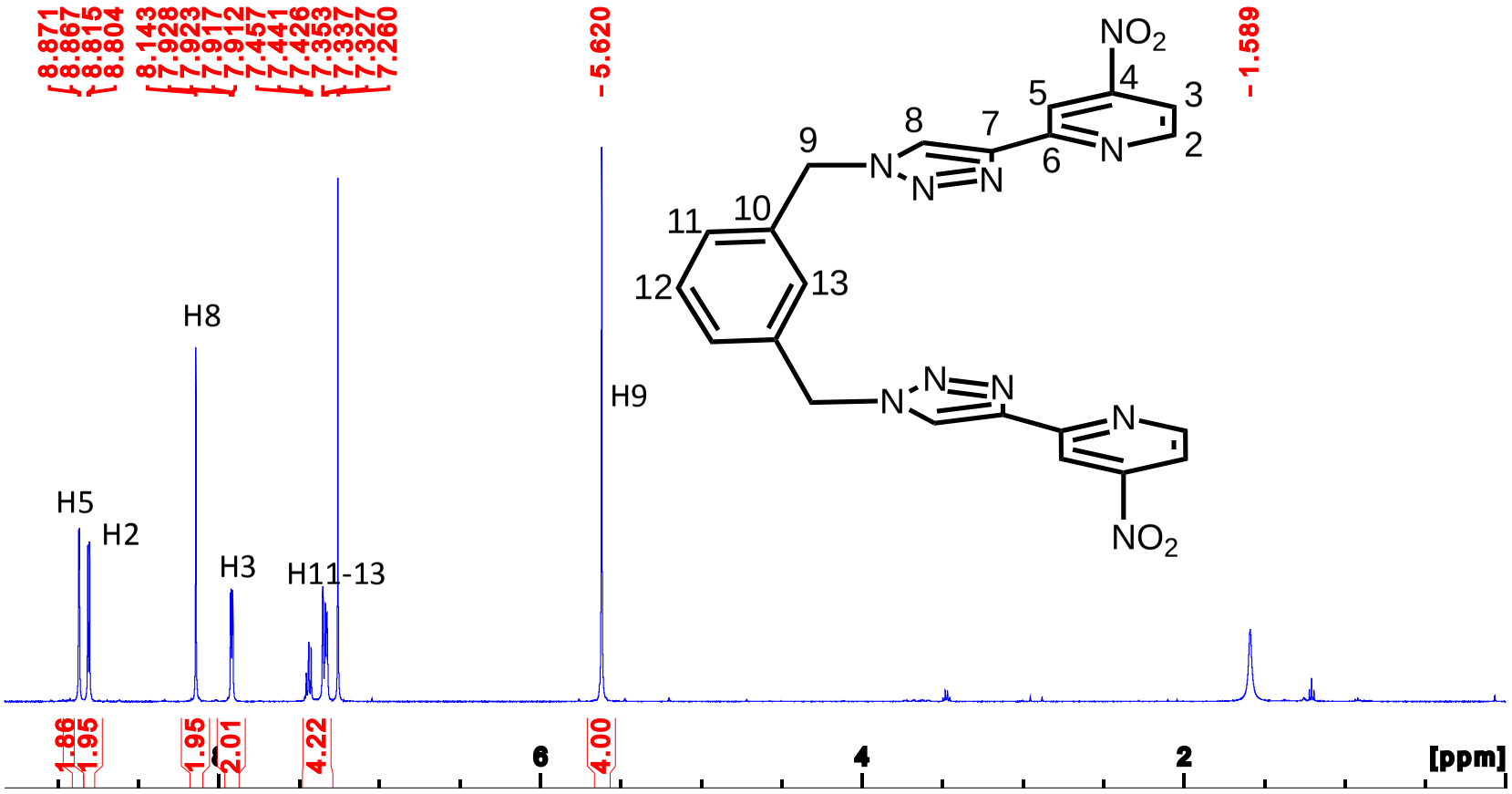

Figure 2.38. ^{1}H NMR of **29** in $CDCl_3$ at 500 MHz.

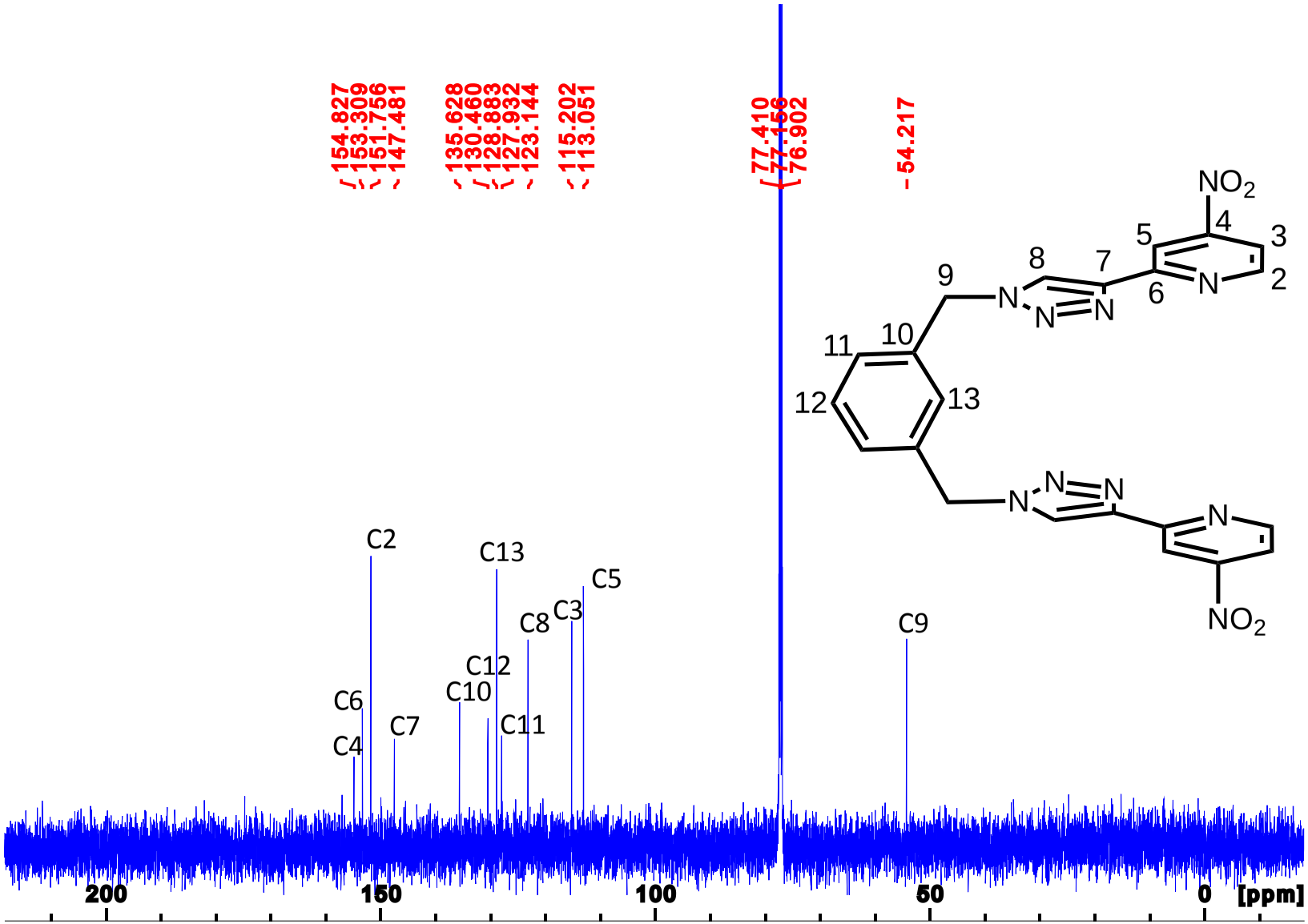

Figure 2.39. ^{13}C NMR of **29** in $CDCl_3$ at 125.7 MHz.

2.4. References

1. Pariya, C.; Fronczek, F. R.; Maverick, A. W., Bis(o-phenylenebis (acetylacetonato)) dicopper(II): A strained copper(II) dimer exhibiting a wide range of colors in the solid state. *Inorganic Chemistry* **2011,** *50* (7), 2748-2753.

2. Pokharel, U. R.; Fronczek, F. R.; Maverick, A. W., Cyclic pyridyltriazole–Cu(II) dimers as supramolecular hosts. *Dalton Transactions* **2013,** *42* (39), 14064-14067.

3. Kawamata, Y.; Yan, M.; Liu, Z.; Bao, D.; Chen, J.; Starr, J. T.; Baran, P. S., Scalable, electrochemical oxidation of unactivated C–H bonds. *Journal of the American Chemical Society* **2017,** *139* (22), 7448-7451.

4. Wasylenko, D. J.; Ganesamoorthy, C.; Koivisto, B. D.; Henderson, M. A.; Berlinguette, C. P., Insight into water oxidation by mononuclear polypyridyl Ru catalysts. *Inorganic Chemistry* **2010,** *49* (5), 2202-2209.

5. Lamy, E.; Nadjo, L.; Saveant, J. M., Standard potential and kinetic parameters of the electrochemical reduction of carbon dioxide in dimethylformamide. *Journal of Electroanalytical Chemistry* **1977,** *78* (2), 403-407.

6. Pokharel, U. R.; Fronczek, F. R.; Maverick, A. W., Reduction of carbon dioxide to oxalate by a binuclear copper complex. *Nature Communications* **2014,** *5*, 5883.

7. Essential of heterocyclic chemistry-I. https://www.scripps.edu/baran/heterocycles (accessed Mar 24, 2020).

8. Llobet, A., Synthesis, spectral and redox properties of a new series of aqua complexes of ruthenium(II). *Inorganica Chimica Acta* **1994,** *221* (1-2), 125-131.

9. Carlsson, A.-C. C.; Mehmeti, K.; Uhrbom, M.; Karim, A.; Bedin, M.; Puttreddy, R.; Kleinmaier, R.; Neverov, A. A.; Nekoueishahraki, B.; Gräfenstein, J.; Rissanen, K.; Erdeĺyi, M., Substituent effects on the $[N–I–N]^+$ halogen bond. *Journal of the American Chemical Society* **2016,** *138* (31), 9853-9863.

10. Cuperly, D.; Gros, P.; Fort, Y., First direct C-2-lithiation of 4-DMAP. Convenient access to reactive functional derivatives and ligands. *The Journal of Organic Chemistry* **2002,** *67* (1), 238-241.

Chapter 3. The Origin of Oxalate: Reduction of Carbon Dioxide vs. Oxidation of Ascorbate

3.1. Introduction

In a previous publication,[1] the oxalate ion in $[Cu_2(m\text{-xpt})_2(\mu\text{-}C_2O_4)](PF_6)_2$ (**6**) was claimed to result from reductive coupling of CO_2; see Figure 3.1. The FT-IR spectrum of **6** showed a band at 1670 cm^{-1}, and FT-IR of a similar complex prepared by use of $^{13}CO_2$ showed a peak at 1651 cm^{-1}. These bands were assigned to the C=O stretching vibrations in **6** and $[Cu_2(m\text{-xpt})_2(\mu\text{-}^{13}C_2O_4)](PF_6)_2$ (**6**-$^{13}C_2$), respectively.

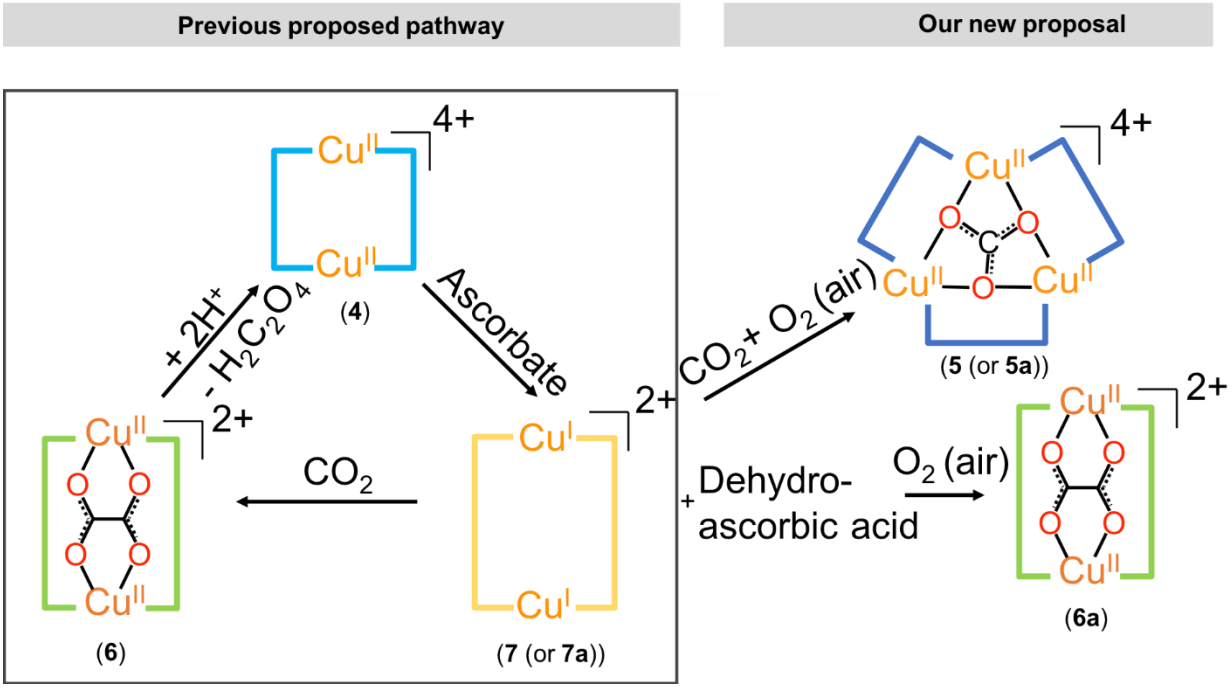

Figure 3.1. The previous proposed reaction cycle based on carbon dioxide reduction is shown in the box on the left. Experiments described in this chapter show that $[Cu_2(m\text{-xpt})_2](PF_6)_2$ (**7**) does not reduce CO_2 to oxalate. Instead, our new discoveries of the chemistry of **7** with CO_2 and O_2 are shown in the right. Each bracket represents one *m*-xpt ligand, and its color represents the observed color of the complex.

After the above work was published, an additional experiment gave results that were not completely consistent with the proposal of reductive coupling of CO_2 to oxalate: Instead of using ascorbate or ascorbic acid as reductant for $[Cu_2(m\text{-xpt})_2(NO_3)_2](PF_6)_2$ (**4**) a Cu(I) solution was prepared directly by treatment of $[Cu^I(CH_3CN)_4]PF_6$ with *m*-xpt ligand, in 1:1 ratio, in DMF or acetonitrile. When these yellow solutions were exposed to air, mostly $[Cu_3(m\text{-xpt})_3(\mu_3\text{-}CO_3)](PF_6)_4$ trimer (**5**) formed with little or none of the oxalate complex **6**. The result of this experiment raised an important concern: If $[Cu_2(m\text{-xpt})_2](PF_6)_2$ (**7**) is the redox mediator of reduction coupling of CO_2 to oxalate, according to Equation 2.1, then oxalate should form whether **7** comes from a mixture of $[Cu^I(CH_3CN)_4]PF_6$ and *m*-xpt or from ascorbate reduction of **4**. Therefore, it seems that formation of the oxalate complex may not be occurring by reaction 2.1.

In this chapter, we are revisiting reactions reported in the original paper[1] in an effort to resolve conflicting results such as those described above. The results of these investigations might also explain the fact that complexes $[Cu_2(NH_2\text{-xpt})_2(NO_3)_2](PF_6)_2$ **10** and $[Cu_2(NMe_2\text{-xpt})_2(NO_3)_2](PF_6)_2$ **25** formed oxalate dimers only in the presence of excess ascorbate.

3.2. Results and discussion

In order to have a better understanding of the role of ascorbate in formation of oxalate we prepared a Cu(I)-xpt complex using an alternative approach that doesn't require ascorbate for reduction of Cu(II) to Cu(I). This was accomplished by comproportionation of $Cu(BF_4)_2$ and Cu metal in the presence of *m*-xpt ligand and anhydrous DMF. Reaction of $Cu(BF_4)_2$ with copper foil in DMF produced mostly Cu(I), but UV/vis spectra of these solutions indicated that some Cu(II) remained. This is not surprising, given that DMF does not stabilize Cu(I) as strongly as some other solvents (such as CH_3CN).[2] However, when a stoichiometric amount of *m*-xpt was added to the

mixture, reaction to produce Cu(I) went essentially to completion. The $[Cu^{I}_2(m\text{-xpt})_2](BF_4)_2$ (**7a**) solution absorbs light exactly at the same wavelength (λ_{max} = 364 nm) that was observed for complex **7** made by ascorbate reduction of **4**. Exposure of **7a** to air formed a dark green Cu(II) solution which formed only green crystals of $[Cu_3(m\text{-xpt})_3(\mu_3\text{-}CO_3)](BF_4)_4$ (**5a**) via ether vapor diffusion (see Figure 3.2) without formation of any $[Cu_2(m\text{-xpt})_2(\mu\text{-}C_2O_4)](BF_4)_2$ (**6a**). This is similar to the product of reaction of $Cu^{I}(CH_3CN)_4PF_6$/*m*-xpt mixture with air.

$$Cu(BF_4)_2 + Cu(0) + 2m\text{-xpt} \rightarrow [Cu^{I}_2(m\text{-xpt})_2](BF_4)_2 \qquad (3.1)$$

$$2CO_2 + 2e^- \rightarrow CO + CO_3^{2-} \qquad (3.2)$$

There are multiple possibilities for formation of carbonate complex. One is reaction of CO_2 with a base to form bicarbonate and further deprotonation to carbonate. The second possibility is 2 electron reduction of CO_2 to CO and CO_3^{2-}; see Equation 3.2. In this system reduction could occur through intermediacy of an O^{2-} species also, and reaction of CO_2 with O^{2-} generates carbonate. To distinguish the two pathways, we decided to analyze reaction headspace gas for CO with FT-IR spectroscopy. We first showed it is possible to detect the peak of 1% v/v of CO in CO_2; see Figure 3.19. Then we made **6a** solution in 0.138 mmol scale according to Equation 3.1. The solution doesn't show a significant color change under CO_2, so it was exposed to a mixture of CO_2 and O_2 gas which could ideally make 0.138 mmol (ca. 3 mL at room temperature) of CO according to Equation 3.2. After giving three days to reaction for completion a sample of headspace gas was injected into an N_2-filled IR gas cell. Only the peak belonging to CO_2 absorption could be observed, and there was no detectable CO. As a result, we assigned formation of **5a** to reaction of CO_2 with a base. We propose that Cu(I) is oxidized to Cu(II) by oxygen. Then reaction of CO_2 with OH^- generates HCO_3^- which is deprotonated to CO_3^{2-}; see Equation 3.3. The coordination of

m-xpt to copper is labile, so the starting dimeric Cu(II) complex can rearrange to form a trimer and host a carbonate molecule; see Equation 3.4.

$$CO_2 + OH^- \rightarrow HCO_3^- \rightarrow CO_3^{2-} + H^+ \qquad (3.3)$$

$$3Cu_2(m\text{-xpt})_2^{4+} + 2CO_3^{2-} \rightarrow 2Cu_3(m\text{-xpt})_3(\mu_3\text{-}CO_3)^{4+} \qquad (3.4)$$

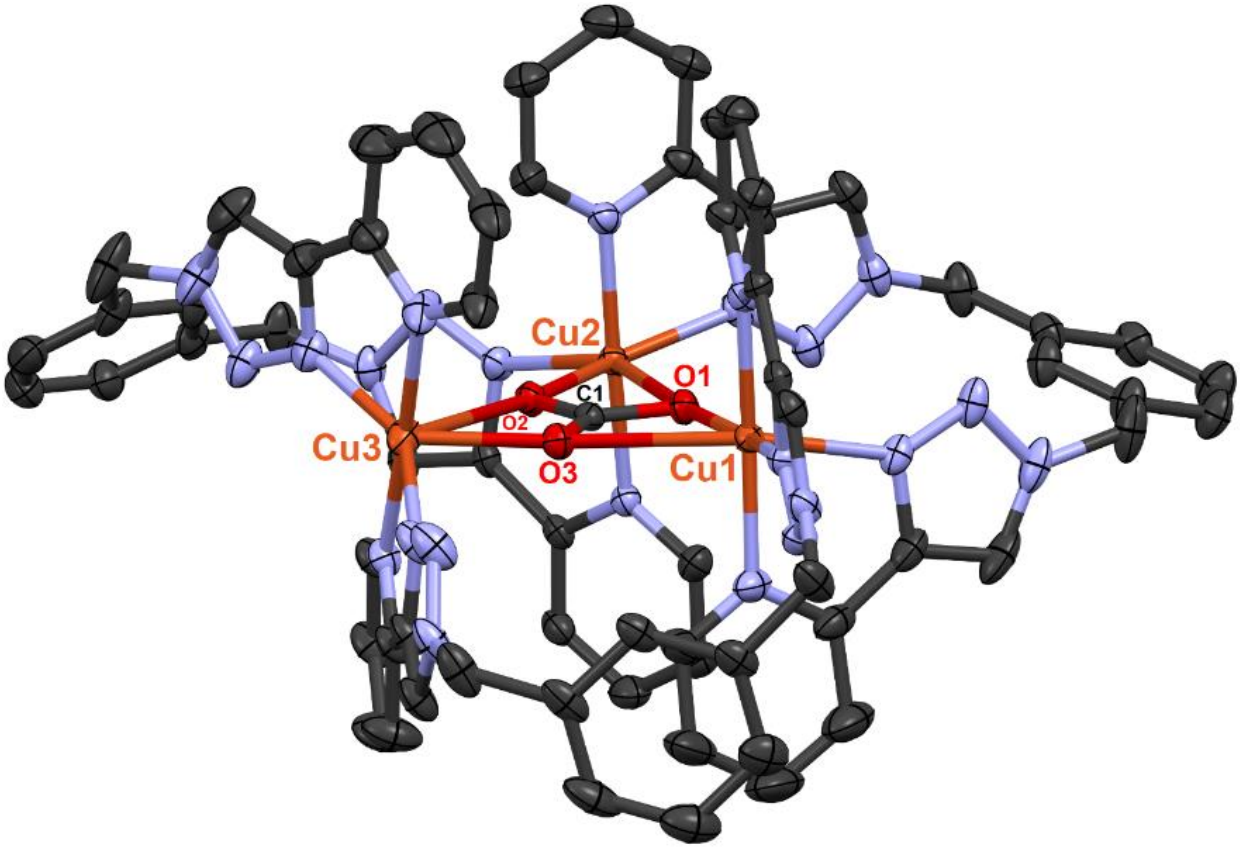

Figure 3.2. X-ray structure of $[Cu_3(m\text{-xpt})_3(\mu_3\text{-}CO_3)](BF_4)_4 \cdot 2.5DMF$ (**5a**·2.5DMF). The thermal ellipsoids are at the 50% probability level. Hydrogen atoms and DMF molecules are removed for clarity.

Since complex **6** was formed as the sole product in the case of reduction of **1** with ascorbate, we looked more closely at ascorbate (or ascorbic acid) chemistry and how it works as a reducing agent. Ascorbic acid (also known as Vitamin C) with a general formula of H_2A is soluble in organic solvents and it is a weak acid that could easily be deprotonated to ascorbate (HA^-); for example with 1 eq of the strong base diazabicycloundecene (DBU) in CH_3CN.[3] An ascorbate ion can be

oxidized to an ascorbyl radical ($HA^{\bullet}$ or $A^{\bullet-}$) and then to dehydroascorbic acid (A, sometimes also abbreviated DHA) by releasing a total of two electrons and one proton in two steps; see Figure 3.6).[4] According to Mayer et al., ascorbate often reacts with concerted transfer of e^- and H^+ and the process of formation of ascorbyl radical is a proton-coupled electron transfer.[3]

Ascorbyl radical in the presence of a proton source rapidly disproportionates to ascorbate and DHA, but in the presence of an oxidant it releases an electron and converts to DHA as mentioned. In our experiments one equivalent of ascorbate as stoichiometric amount (or sometimes slightly more than one equivalent, e.g 1.5) was used to provide two equivalents of electrons required for reduction of two copper centers in **4**. Therefore, after complete reduction of **4**, there is at least one equivalent of DHA in the yellow solution of **7**. We initially considered comproportionation of dehydroascorbate and ascorbate to ascorbyl radical[4], and hypothesized that a radical mediator such as ascorbyl radical cation might be required somehow for the formation of complex **6**. In fact, such a comproportionation has low equilibrium constant (2×10^{-15}). To test our proposal, we added dehydroascorbate and ascorbate mixtures at different ratio directly to the solution of **7a**, and the solution was exposed to air. Although this solution generates the carbonate complex as mentioned above, addition of DHA to the same solution resulted in formation of oxalate bridged complex **6a**; see structure of **6a** in Figure 3.3. As a result, we realized dehydroascorbic acid is an effective intermediate in formation of oxalate product.

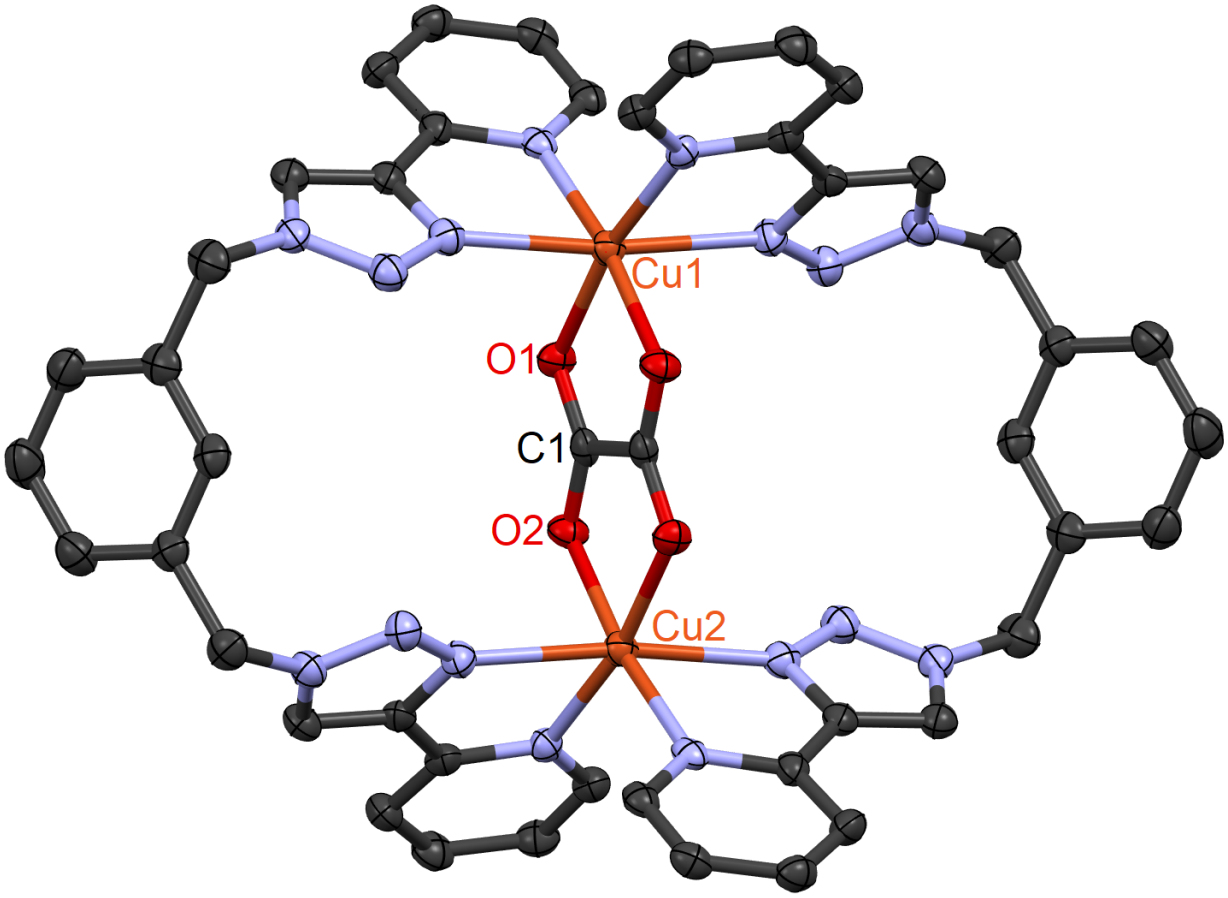

Figure 3.3. X-ray structure of $[Cu_2(m\text{-xpt})_2(\mu\text{-}C_2O_4)](BF_4)_2\cdot 2DMF$ (**6a**·2DMF). The thermal ellipsoids are at the 50% probability level. Hydrogen atoms and DMF molecules are removed for clarity.

To understand whether the source of carbons in oxalate is CO_2 molecule or they come from carbon containing compounds in the solution such as DHA, we did three major control experiments: (a) full exclusion of O_2 during exposure of a solution of **7** to pure CO_2, (b) exposure of **7** to pure O_2, and (c) employing labeled $^{13}CO_2/O_2$, and preparing genuine $[Cu_2(m\text{-xpt})_2(\mu\text{-}^{13}C_2O_4)](PF_6)_2$ (**6**-^{13}C).

3.2.1. Full exclusion of O_2 during exposure of a solution of 7 to pure CO_2

We exposed a DMF solution of **7** made by reaction of **4** with ascorbate to pure CO_2 with rigorous exclusion of O_2, using Schlenk techniques. Figure 3.8 shows UV-vis spectra for this experiment. The first three spectra show no absorption bands between 600-850 nm under CO_2,

indicating that **7** is stable under CO_2, and the small absorption observed after 4 days belongs to production of ca. 12×10^{-5} mmol of $[Cu_2(m\text{-xpt})_2(C_2O_4)](PF_6)_2$ **6** (assuming $\varepsilon = 98\ M^{-1}$). This means <0.5% of **7** has been oxidized to Cu(II). This amount of Cu(II) formation is much less than that observed under air or O_2; we attribute it to leakage of a small amount of air (ca. 6 μL) into the flask. When the same solution was exposed to air or a mixture of CO_2/O_2 (1:1), complex **6** formed as mentioned in the original paper. Therefore, **7** is not reactive with CO_2 and formation of oxalate needs oxygen. This encouraged us to do EPR studies to detect possible reactive oxygen species (ROS) in the solution.

3.2.2. Exposure of 7 to pure O_2

Some Cu(I) complexes with electron rich ligands are able to transfer an electron to oxygen. For instance, in biology, reversible Cu(I)/oxygen interactions occur in hemocyanin proteins, which are blood oxygen carriers in mollusks and arthropods. Copper in oxygenase enzymes catalyzes oxidation of biological substrates by activating oxygen. In cytochrome c oxidase, which is required for aerobic respiration, copper and iron reduce O_2 to H_2O or H_2O_2 while effecting one electron substrate oxidation. Copper is also found in Cu/Zn superoxide dismutase, an enzyme that detoxifies superoxides, by converting it to oxygen and hydrogen peroxide: $2HO_2^{\bullet} \rightarrow H_2O_2 + O_2$. [5,6]

Karlin's and Tolman's groups have elucidated insights into the coordination of O_2 to copper complexes.[6,7] One electron reduction of O_2 generates superoxide radical: $O_2 + e^- \rightarrow O_2^{\bullet-}$. The concentration of superoxide in cells is limited by superoxide dismutases converting $2HO_2^{\bullet}$ to H_2O_2 and O_2. Two electron reduction of O_2 generates hydrogen peroxide also: $O_2 + 2H^+ + 2e^- \rightarrow H_2O_2$. Hydrogen peroxide, in the Fenton reaction, can be reduced by one electron to OH^- and $OH^{\bullet}$.

We exposed a yellow solution of **7** to pure dioxygen at −70 °C (or −40 °C), and we didn't observe any change in the color of solution that could be assigned to oxidation of Cu(I) to Cu(II) and/or formation of copper-oxo species. This suggests that complex **7** is not electron rich enough to reduce dioxygen and stabilize it, in contrast to the Cu(I) species introduced by Dr. Tolman and Dr. Karlin that showed a rapid color change upon exposure to O_2 at −70 °C.[8-10]

Although we didn't see any color change of **7** under O_2 at cryogenic temperature, the solution turned to green at room temperature and formed complex **6**. This critical observation enabled us to realize that CO_2 is not required for formation of oxalate, but presence of O_2 is essential.

One of the best ways of studying radicals is EPR spectroscopy. Direct detection of highly reactive $OH^{\bullet}$ and $O_2^{\bullet-}$ radicals is very difficult by EPR due to their short lifetime in solution. However, oxygen radicals can be studied indirectly through their reaction with nitrones. The most popular spin (radical) trap is dimethylpyrroline *N*-oxide, DMPO, which was first synthesized by Janzen and Liu in 1973.[11] Since then, DMPO was widely used in detection of radicals generated by biological and chemical systems. DMPO is EPR silent, but radicals add to the DMPO double bond to generate nitroxide radicals which are EPR active and have longer lifetimes than $OH^{\bullet}$ and $O_2^{\bullet-}$ radicals. DMPO is redox inert and forms distinguishable EPR spectra with different radicals which enables scientist to realize what type of radical exists in a given reaction. On the other hand, the major disadvantage of DMPO is that it reacts with superoxide slowly and the superoxide adduct of DMPO rapidly decomposes to hydroxyl radical adduct (DMPO/$^{\bullet}$OOH $t_{1/2}$ = 45 s).

In our research we used the BocMPO (BMPO) nitrone as spin trap (see Figure 3.4) which has all of the advantages of DMPO, and in addition, pure BMPO is commercially available and could be stored for a long time in a refrigerator without decomposition. The superoxide adduct of

BMPO is much more stable than its DMPO analogue (BMPO/$^{\bullet}$OOH $t_{1/2}$ = 20 minutes). In our measurements, in order to have an excess of spin trap relative to the radicals, we made a 400 mM BMPO solution in DMF and added 1 microliter of it to 9 microliters of different solutions of sodium ascorbate, Cu(I), Cu(II) complexes and etc. with approximately 4 mM concentration (giving ca. 10 times excess of BMPO).

We first showed that solutions of reactants and solvent don't form reactive radical adducts with BMPO. EPR spectra showed that a solution of **7** doesn't contain radicals. In contrast, the same Cu(I) solution upon stirring in air (reaction with oxygen) at room temperature showed an EPR peak with splitting pattern consistent with the BMPO–hydroxyl radical adduct. EPR of a similar copper solution containing DABCO also showed the presence of hydroxyl radical; see Figure 3.22. Zhang's group also reported generation of H_2O_2 and $OH^{\bullet}$ during oxidation of ascorbic acid by oxygen catalyzed by $CuSO_4$.[12] They proposed that $OH^{\bullet}$ is generated by reaction of Cu(I) with H_2O_2 through the Fenton reaction. To realize whether our complex **4** is able to reduce O_2 to H_2O_2, we compared reduction potentials. Cyclic voltammetry of DMF solution of complex **4** showed $E_{1/2}(Cu^{II}/Cu^{I})$ = –0.27 vs. Fc/Fc^{+}. Figure 3.5 provides reduction potential of different oxygen species in aqueous solution. Specifically, the first reduction which is thermodynamically harder than the other steps has $E_{1/2}$ = –0.33 V vs. NHE. Probably a better comparison can be made by the formal potential of $O_2/O_2^{\bullet-}$ in DMF as –1.23 vs Fc/Fc^{+}, reported by Saha and Ohsaka.[13] Although the condition they used for recording cyclic voltammetry is different from ours, comparing redox potential of complex **4** with –1.23 shows spontaneous outer sphere electron reduction of oxygen with complex **4** is not favorable (E_{rxn} = –0.96 V, ΔG = +22 kCal, $K = 10^{-16}$). Considering the equilibrium constant of reaction in Equation 3.5, [**7**] = 4 mM and solubility of atmospheric O_2 in DMF[14] as 0.005 M (note that 21% of air is O_2), only a very small amount of

superoxide would be formed by outer-sphere reaction of Cu(I) with O_2 (see Equation 3.5), and it might not have been detectable in an EPR measurement. This should be considered as a raw analysis, since consumption of $O_2^{\bullet-}$ for example by reacting with BMPO can push the equilibrium between the Cu(I) and O_2 forward to generate more of the $O_2^{\bullet-}$. In addition, reduction of oxygen can become more favorable through inner-sphere reduction of O_2 and formation of for example $[Cu^{2+}O_2^{\bullet-}]^+$ species. Therefore, ΔG is not necessarily an indication of whether an EPR-detectable amount of superoxide forms with our complex **7**.

$$Cu^+ \text{ (in complex } \mathbf{7}) + O_2 \rightarrow Cu^{2+} + O_2^{\bullet-} \quad E_{rxn} = -0.96 \text{ V}, \quad K = 10^{-16} \qquad (3.5)$$

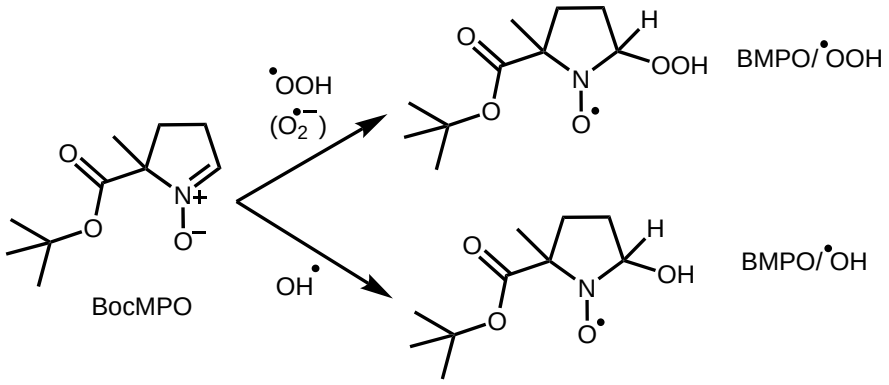

Figure 3.4. Addition of reactive oxygen species to BMPO spin trap and formation of new hydroxyl and superoxide adducts.

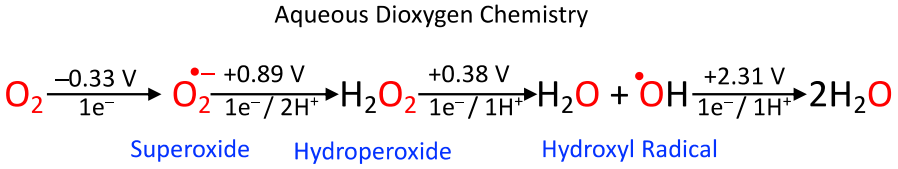

Figure 3.5. Stepwise reduction of dioxygen. Reduction potentials are given in volts vs NHE at 25 °C, 1 bar, pH = 7, in H_2O. Adapted with permission from *Chemical Reviews* **2018**, *118* (22), 10840-11022. Copyright 2018, American Chemical Society.

These results led us to explore whether an oxidation process, such as oxidation of ascorbate or dehydroascorbic acid, could produce oxalate. Dehydroascorbic acid in aqueous solution slowly

hydrolyzes to 2,3–diketo-L-gulonic acid (DKG). In addition, DHA can be oxidized to a range of products such as L-threonic acid and oxalic acid (or their salts, depending on pH); see Figure 3.6. Dewhirst et al. elucidated oxidation products generated by action of various reactive oxygen species (ROS) on DHA and DKG. They employed an electrophoretic system at different pH to resolve what products with which ratio form when ascorbic acid, DHA, and DKG break down.[15] In addition, oxidative degradation of ascorbic acid by (a) inorganic oxidants (sodium periodate,[16] sodium hypoiodite[18]); (b) oxygen;[17,19] and (c) O_2 in the presence of Gd,[20,21] Co,[20] Pd,[22] Pt,[22] Cd,[23] Fe,[24] or Cu[25] compounds is reported to yield oxalate. These results also support our revised proposal of formation of oxalate through oxidation of dehydroascorbic acid rather than reductive coupling of CO_2.

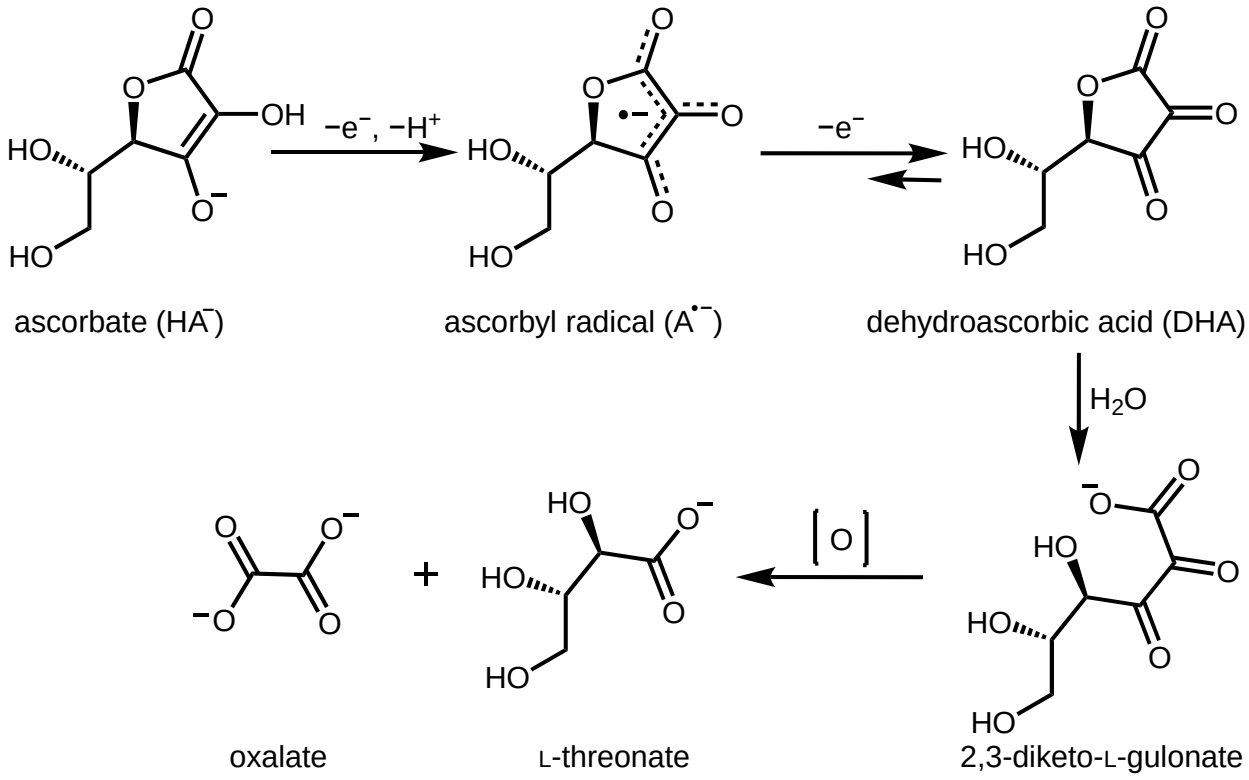

Figure 3.6. Oxidation of ascorbate to dehydroascorbic acid and further hydrolysis and oxidation to oxalate.

3.2.3. Employing labeled $^{13}CO_2$

We synthesized pure crystals of genuine **6**-$^{13}C_2$, $[Cu_2(m\text{-xpt})_2(\mu\text{-}^{13}C_2O_4)](PF_6)_2$, by direct treatment of $(Bu_4N)_2{}^{13}C_2O_4$ with complex **4**. $(Bu_4N)_2{}^{13}C_2O_4$ is soluble in organic solvents, and synthesized by addition of Bu_4NOH to $H_2{}^{13}C_2O_4$ and characterized by ^{13}C NMR and ^{1}H NMR. The FT-IR spectrum of **6**-$^{13}C_2$, as shown in Figure 3.12, contains three characteristic peaks at 1574, 1600, 1668 cm^{-1}. ESI-MS spectrum of **6**-$^{13}C_2$ shows a peak due to $[Cu_2(m\text{-xpt})_2(^{13}C_2O_4)](PF_6)^+$; see Figure 3.13. Having these reference spectra in hand, we exposed a solution of **7** (prepared from **4** and sodium ascorbate) to a mixture of $^{13}CO_2/O_2$. Green crystals of an oxalate complex were isolated from the crude mixture which contains four characteristic peaks at 1574, 1611, 1639, 1669 cm^{-1}; see Figure 3.12. Using ESI-MS, we could detect a peak and isotope pattern that can be assigned to $[Cu_2(m\text{–xpt})_2(C_2O_4)](PF_6)^+$; see Figure 3.13. This result clearly disproves the possibility of $^{13}CO_2$ involvement in the formation of oxalate.

The band at 1668 cm^{-1} in **6** was previously assigned as $\tilde{\nu}_{CO}$ of oxalate **6**.[1] However, comparing the FT-IR in figure 3.12, enabled us to assign this vibration to the peak at 1639 cm^{-1}, because it shifts to lower energy (1600 cm^{-1}) on ^{13}C substitution. This −39 cm^{-1} shift is close to those for polymeric $[(bpy)Cu(\mu\text{-}C_2O_4)]_\infty$ (observed shift, −30 cm^{-1})[27] and for aqueous $Na_2C_2O_4$ (observed shift, −43 cm^{-1}).[27] In addition, since the peak at 1668 cm^{-1} shows negligible shift between **6** and **6**-$^{13}C_2$, we now assign it to co-crystallized solvent DMF.

To summarize the above results, the Cu(I) dimer **7** does not react with pure CO_2, but it is oxidized to Cu(II) by O_2. If only CO_2 and O_2 are present, the product is the carbonate-bridged trimer **5**. If ascorbate or DHA is present, they are also oxidized by O_2, producing oxalate, and the oxalate-bridged dimer **6** is formed. In a separate experiment, we isolated crystals of **6** by stirring

4 and DHA for 7 days. Thus, reduction of Cu(II) to Cu(I) is not required for oxalate to be generated and incorporated into the host complex.

This conclusion is also consistent with the chemistry of complexes $[Cu_2(H_2N\text{-}xpt)_2(NO_3)_2](PF_6)_2$ **10** and $[Cu_2(Me_2N\text{-}xpt)_2(NO_3)_2](PF_6)_2$ **25** explained in chapter 2 of this dissertation. The purpose of making those electron-rich complexes was to make them more powerful reducing agents. This could make them more reactive toward CO_2, but it can make them more reactive toward oxygen too. Therefore, there are two competitive reaction pathways: (a) oxidation of Cu(I) centers to Cu(II) and hydration of CO_2 to carbonate; and (b) oxidation of ascorbate or DHA to oxalate. When stoichiometric amounts of ascorbate were used for reduction of **10** and **25**, there is a minimum amount of DHA in the solution that could oxidize to oxalate, while the reactive Cu(I) centers could readily oxidize to Cu(II) and form carbonate trimer **14** or **27**. However, when excess ascorbate was used, formation of oxalate dimer was observed, due to accessibility of ascorbate in the solution and oxidation to oxalate. Chakravarty et al., similar to us, found formation of an oxalate complex when a solution of $[Cu_2(OH)(OH_2)(OAc)(bpy)_2](ClO_4)_2$ and ascorbic acid was exposed to air.[25]

Some other research groups have also reported instances of *in situ* oxalate formation which they attributed to reductive coupling of CO_2 molecules at first. However, most of the accounts rely on crystallographic observation of oxalate in the solid-state reaction products, without careful testing of the reactions in the presence and absence of O_2. One example is formation of an oxalate coordination polymer from 2,3-pyrazinedicarboxylic acid, H_2pzdc, under hydrothermal conditions; see Figure 3.7. The authors initially assigned formation of oxalate to decarboxylation and reductive coupling of CO_2 molecules,[28] but they eventually reported separately a decomposition pathway of H_2pzdc ligand to oxalate and identified the possible intermediates

involved in formation of oxalate, since the reaction was under acidic and oxidizing conditions. They also provided a list of 59 literature references that reported in situ formation of oxalate during reactions. The authors cautioned readers that in those examples it is possible that oxalate is generated by oxidation or decomposition of organic molecules under a variety of conditions.[29]

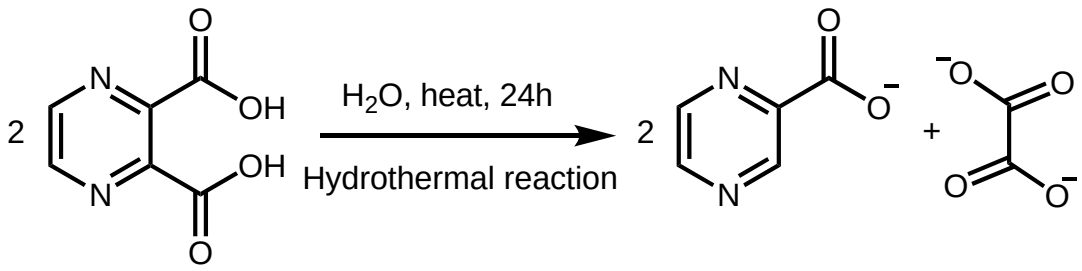

Figure 3.7. Proposed formation of oxalate via decomposition of 2,3-pyrazinedicarboxylic acid, H_2pzdc, as reported by Soares-Santos et al.[30] and Cahill et al.[28]

3.3. Experimental

General

Unless stated otherwise, reactions were conducted under an atmosphere of N_2. Commercially available reagents were purchased from Alfa Aesar, BeanTown Chemicals, ICON Isotopes, Sigma-Aldrich, and TCI and were used without further purification. Anhydrous DMF was purchased from MilliporeSigma. For experiments mentioned below, *m*-xpt, $[Cu_2(m\text{-xpt})_2(NO_3)_2](PF_6)_2$ (**4**) and $[Cu_2(m\text{-xpt})_2](PF_6)_2$ (**7**) were prepared according to literature procedures.[1,31] A stock anhydrous solid of $Cu(BF_4)_2$ was prepared by keeping a regular $Cu(BF_4)_2 \cdot xH_2O$ under flow of N_2 for a week. NMR spectra were recorded on Bruker 400 MHz (Avance 400) spectrometers. FT-IR spectra (ATR, diamond) were recorded on a Tensor 27 or Alpha P FT-IR spectrometer (Bruker). Electrospray ionization mass spectra were measured on an Agilent 6210 instrument. UV/vis spectra were recorded on an Aviv 14DS spectrometer (Aviv Biomedical).

Treatment of *in situ* generated $[Cu_2(m\text{-xpt})_2](PF_6)_2$ (7) with CO_2.

$[Cu_2(m\text{-xpt})_2(NO_3)_2](PF_6)_2$ (**4**) (28.3 mg, 0.0213 mmol) and sodium ascorbate (5.4 mg, 0.027 mmol) were placed in a Schlenk flask connected to a cuvette and the flask was evacuated for 20 minutes. Argon-purged DMF (6 mL) was added to the solids with stirring under N_2. The solution was left to stir under N_2 for about 1 hour. During this time the Cu(II) centers in **4** were reduced to **7** and the color changed to yellow. Then, the N_2 was replaced by CO_2 in three alternating cycles of vacuum and CO_2. The absorption of the solution under N_2 or CO_2 was followed by UV/vis spectroscopy; see Figure 3.8.

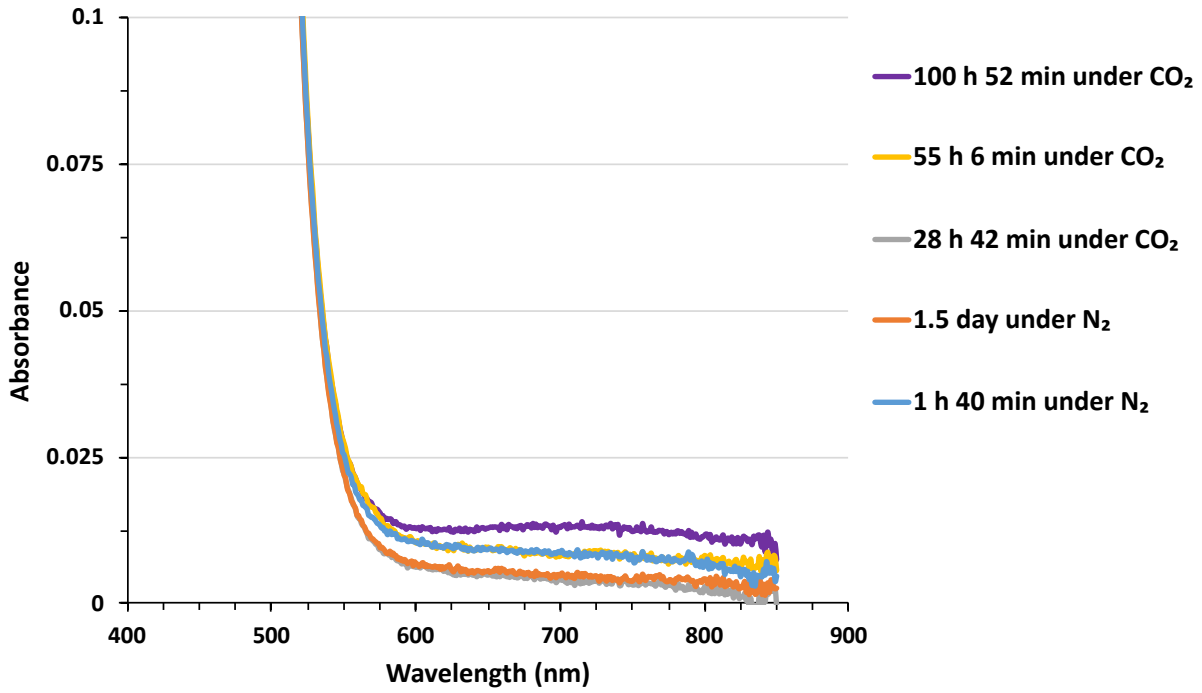

Figure 3.8. UV/vis absorption spectra of $[Cu_2(m\text{-xpt})_2](PF_6)_2$ (**7**) (3.55 mM) under N_2 and CO_2 over ca. 4 days. Gray (29 h) and yellow (55 h) spectra show no absorption due to Cu(II). Purple spectrum (101 h) shows <0.5% of **7** has been oxidized to Cu(II). This amount of Cu(II) formation is much less than that observed under air or O_2; we attribute it to leakage of a small amount of air (ca. 6 μL) into the flask.

Exposure of *in situ* generated $[Cu_2(m\text{-xpt})_2](PF_6)_2$ (7) to a mixture of CO_2 and O_2 at –70 °C and then air.

Complex **4** (26.8 mg, 0.0202 mmol) and sodium ascorbate (4.3 mg, 0.021 mmol) were placed in a Schlenk flask sealed to a cuvette. The reaction flask was evacuated for 20 minutes. N_2-purged DMF (6 mL) was added to the solid under N_2. Then N_2 was bubbled into a flask containing DMF then into the solution for 1 h with stirring (to avoid evaporation of solvent and keeping concentration of solution constant). Complete conversion to **7** occurred in an hour, and then the yellow solution was cooled to –70 °C. At this point N_2 was replaced by a mixture of CO_2 and O_2 (~1:1). After 10 hours no color change was observed, then the solution was exposed to air and was

allowed to warm up to room temperature. Oxidation of **7** to **6** was followed by UV/vis spectroscopy as shown in Figure 3.9.

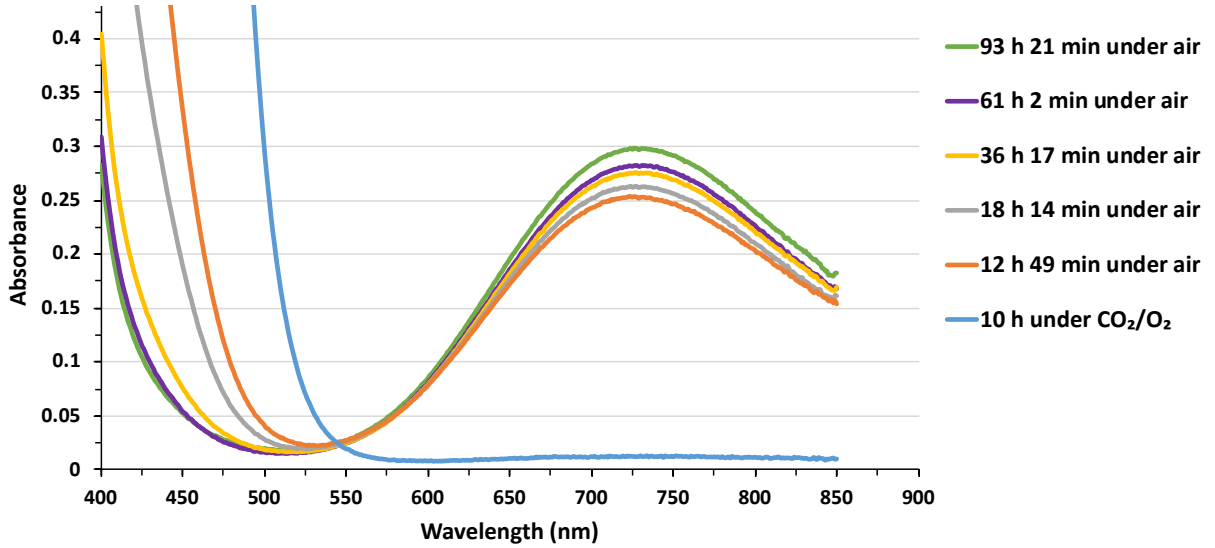

Figure 3.9. UV/vis absorption spectra of $[Cu_2(m\text{-xpt})_2](PF_6)_2$ (**7**) under a mixture of CO_2 and O_2 (~1:1) at –70 °C and after exposure to air at room temperature.

Exposure of *in situ* generated $[Cu_2(m\text{-xpt})_2](PF_6)_2$ (7) to a mixture of CO_2 and O_2 (~1:1) at room temperature.

$[Cu_2(m\text{-xpt})_2(NO_3)_2](PF_6)_2$ (**4**) (20.0 mg, 0.0150 mmol) and sodium ascorbate (4.5 mg, 0.023 mmol) were placed into a cuvette sealed to a stopcock. The reaction flask was evacuated for 20 minutes. N_2-purged DMF (4.6 mL) was added to the solids. N_2 was bubbled into a flask containing DMF then into the solution for 1 h with stirring, and complete conversion to **7** was observed by UV/vis spectroscopy. At this point the N_2 was replaced by a CO_2 and O_2 (~1:1) mixture. The progress of the reaction was followed by UV/vis spectroscopy and upon completion the whole green solution (λ_{max} = 725 nm) was transferred to a test tube and used for ether vapor diffusion. After a week, green crystals of $[Cu_2(m\text{-xpt})_2(C_2O_4)](PF_6)_2$ (**6**) were collected, rinsed with ether and dried in air (6.9 mg, 35%); see FT-IR of the crystals in Figure 3.10. ESI-MS: m/z $[Cu_2(m\text{-xpt})_2(C_2O_4)](PF_6)^+$ 1147.13205 (calcd: 1147.13338).

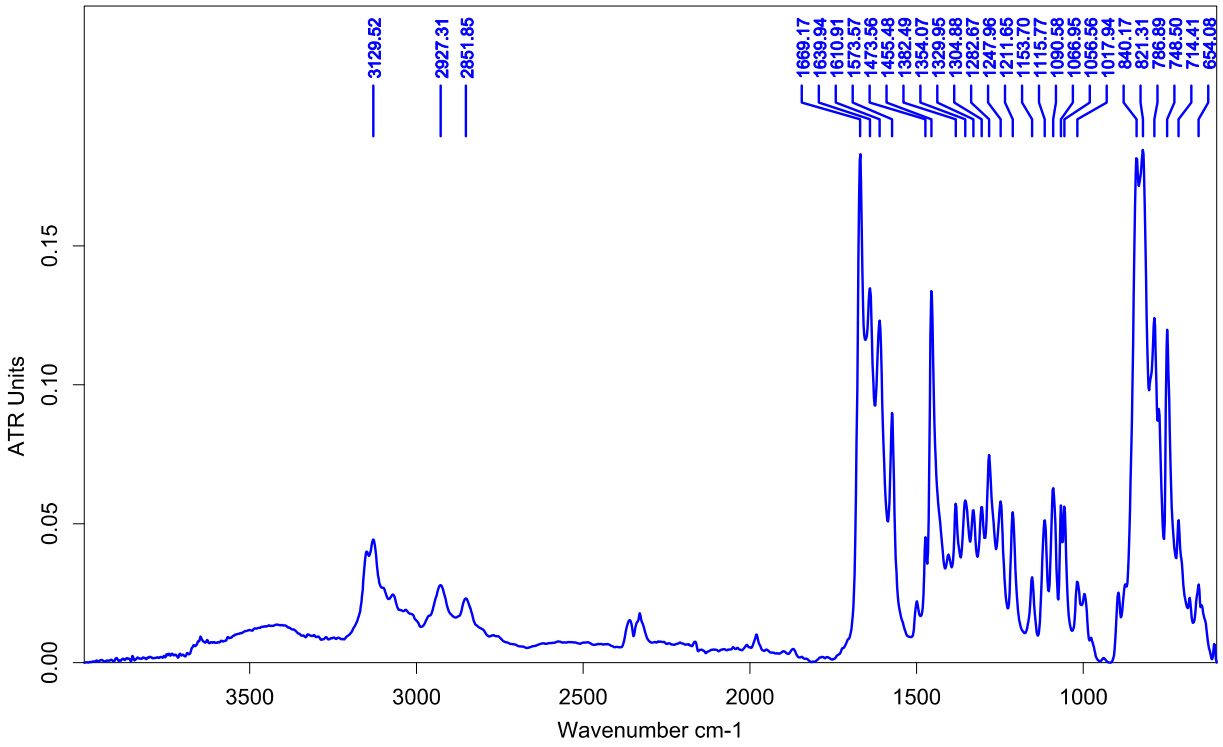

Figure 3.10. FT-IR spectrum of green crystals of $[Cu_2(m\text{-xpt})_2(C_2O_4)](PF_6)_2$ (**6**) obtained by reaction of *in situ* generated $[Cu_2(m\text{-xpt})_2](PF_6)_2$ (**7**) with a mixture of CO_2 and O_2 (~1:1).

Reaction of *in situ* generated $[Cu_2(m\text{-xpt})_2](PF_6)_2$ (7) with O_2.

Complex **4** (20.1 mg, 0.0151 mmol) and sodium ascorbate (4.6 mg, 0.022 mmol) were placed in a flask connected to a cuvette, which was evacuated for 40 minutes. In mean time DMF was purged with argon, then 6 mL of it was transferred to the reaction flask. The mixture was stirred under N_2 for ca. 50 min, during which time the color of solution turned to yellow. At this point the solution was exposed to pure O_2. Progress of the reaction was followed by UV/vis spectroscopy (see Figure 3.11) and upon completion (after about 23 hours), the O_2 was replaced by N_2, the reaction flask was transferred to glove box, and the whole solution used for crystallization by ether vapor diffusion. This resulted in formation of green crystals of **6**, which were analyzed by X-ray crystallography, and uncharacterized blue/green clusters.

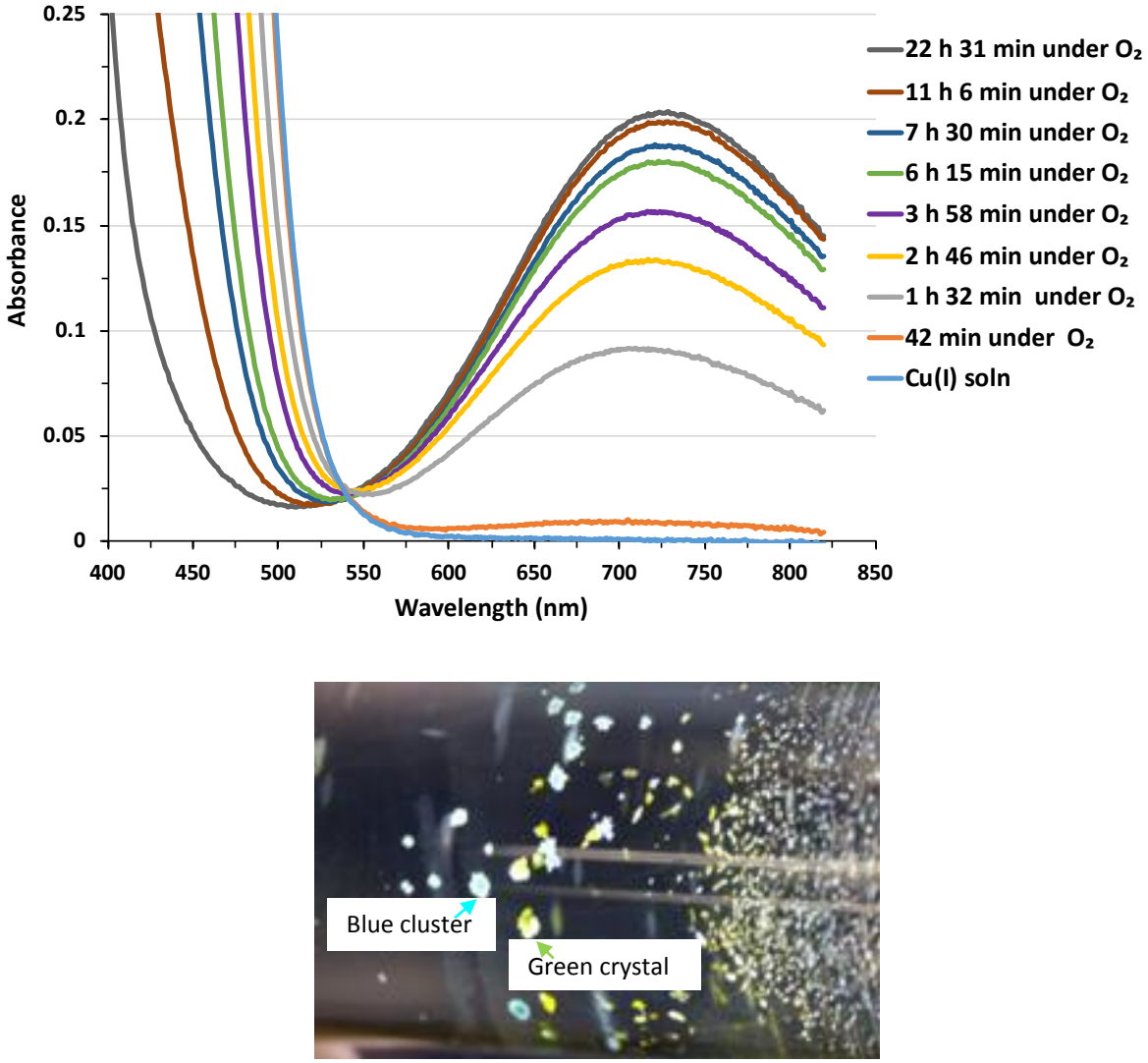

Figure 3.11. Top: UV/vis spectra show changes in the electronic absorption spectrum of a solution of **7** during reaction with O_2. Bottom: green crystals of $[Cu_2(m\text{-xpt})_2(C_2O_4)](PF_6)_2$ (**6**) and blue microcrystalline clusters after vapor diffusion of ether into the crude mixture.

Reaction of *in situ* generated $[Cu_2(m\text{-xpt})_2](PF_6)_2$ (7) with O_2 in the presence of $^{13}CO_2$.

A similar DMF solution of in situ generated **7** was exposed to a mixture of O_2 and $^{13}CO_2$ (~1:1).

This procedure also generated the oxalate complex **6**, which showed no evidence of ^{13}C labeling;

see FT-IR and ESI-MS data in Figures 3.12 and 3.13.

Preparation of authentic $[Cu_2(m\text{-xpt})_2(^{13}C_2O_4)](PF_6)_2$ (6-$^{13}C_2$) via $(Bu_4N)_2{}^{13}C_2O_4$.

$H_2{}^{13}C_2O_4$ (4.8 mg, 0.037 mmol) and Bu_4NOH (62.4 mg of 1 M solution in methanol, density 0.83 g/mL; 0.075 mmol) were mixed in 20 mL methanol under N_2, and the solution was stirred under N_2 for ca. 16 h. The solvent was evaporated to give $(Bu_4N)_2{}^{13}C_2O_4$ as a white solid. ^{1}H and ^{13}C NMR of this solid match those reported in the literature.[32] N_2-purged DMF (2 mL) was added to this solid, and the resulting solution was added dropwise to **4** (49.6 mg, 0.0373 mmol, in 5 mL of N_2-purged DMF), with stirring. The color of the solution gradually changed from blue to green. Addition was stopped when the first sign of permanent turbidity was observed. At this point the solution was stirred for one additional hour under N_2, and then set up for crystallization by ether vapor diffusion. After a week, green crystals of **6**-$^{13}C_2$ were collected, washed with ether, and dried in air (25.7 mg, yield 53%). See FT-IR and ESI-MS data in Figures 3.12 and 3.13.

^{1}H NMR of $(Bu_4N)_2{}^{13}C_2O_4$, (400 MHz, D_2O) δ 3.20 (t, J = 8.6, 2H, H3), 1.66 (m, 2H, H4), 1.37 (m, 2H, H5), 0.95 (t, J = 7.4, 3H, H6). ^{13}C NMR of $(Bu_4N)_2{}^{13}C_2O_4$, (400 MHz, D_2O) δ 173.51, 58.13, 23.13, 19.14, 12.82.

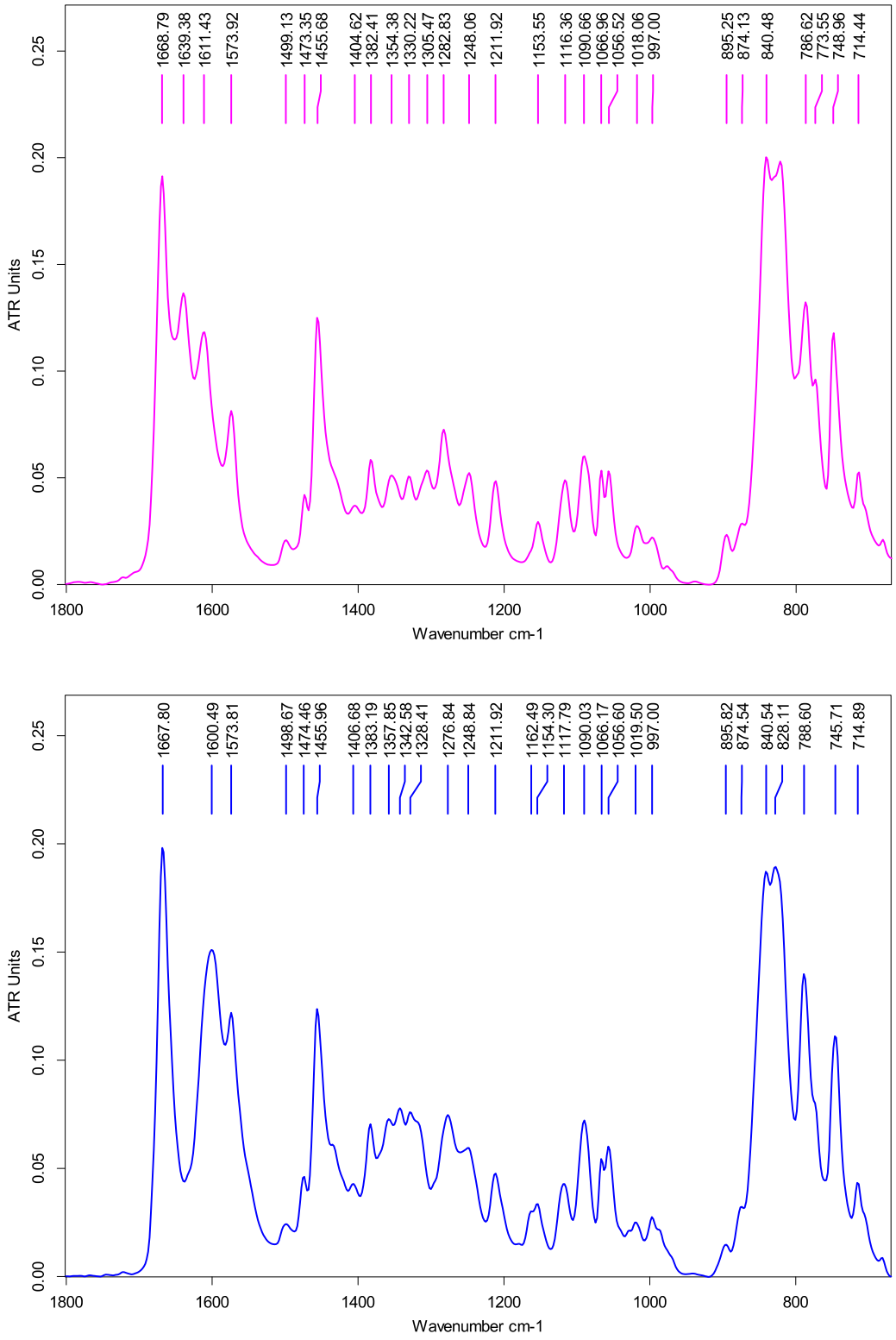

Figure 3.12. FT-IR spectra of **6** and **6**-$^{13}C_2$. Top (magenta), unlabeled, prepared from **4** by ascorbate reduction, followed by exposure to a mixture of $^{13}CO_2$ and O_2. Bottom (blue), ^{13}C-labeled, prepared from **4** by treatment with $(Bu_4N)_2(^{13}C_2O_4)$.

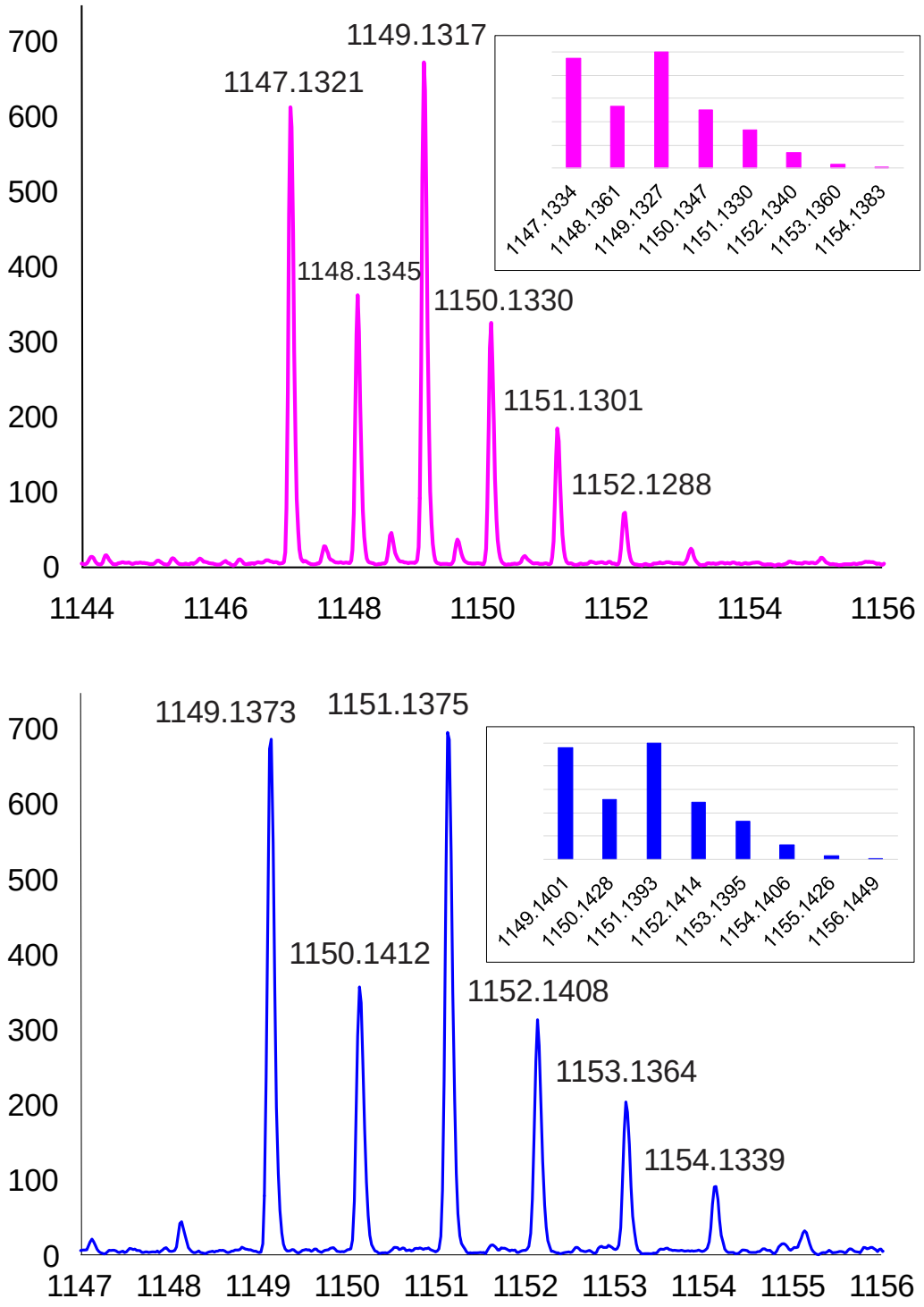

Figure 3.13. ESI mass spectra, $[Cu_2(m\text{-xpt})_2(\mu\text{-}C_2O_4)](PF_6)^+$ peak, from **6** and **6**-$^{13}C_2$. Top (magenta), unlabeled, prepared from **4** by ascorbate reduction, followed by exposure to a mixture of $^{13}CO_2$ and O_2. Bottom (blue), ^{13}C-labeled, prepared from **4** by treatment with $(Bu_4N)_2(^{13}C_2O_4)$. Insets are calculated isotope masses and relative intensities.

Reaction of 4 and dehydroascorbic acid (DHA) with air.

Equimolar amounts of **4** and DHA were dissolved in DMF, and the solution stirred in air for 7 days. A portion of the solution was poured into a watch glass for evaporation of solvent and FT-IR spectrum of the residual solid was recorded; see Figure 3.14. Crystals of **6** were deposited by vapor diffusion of ether into this solution.

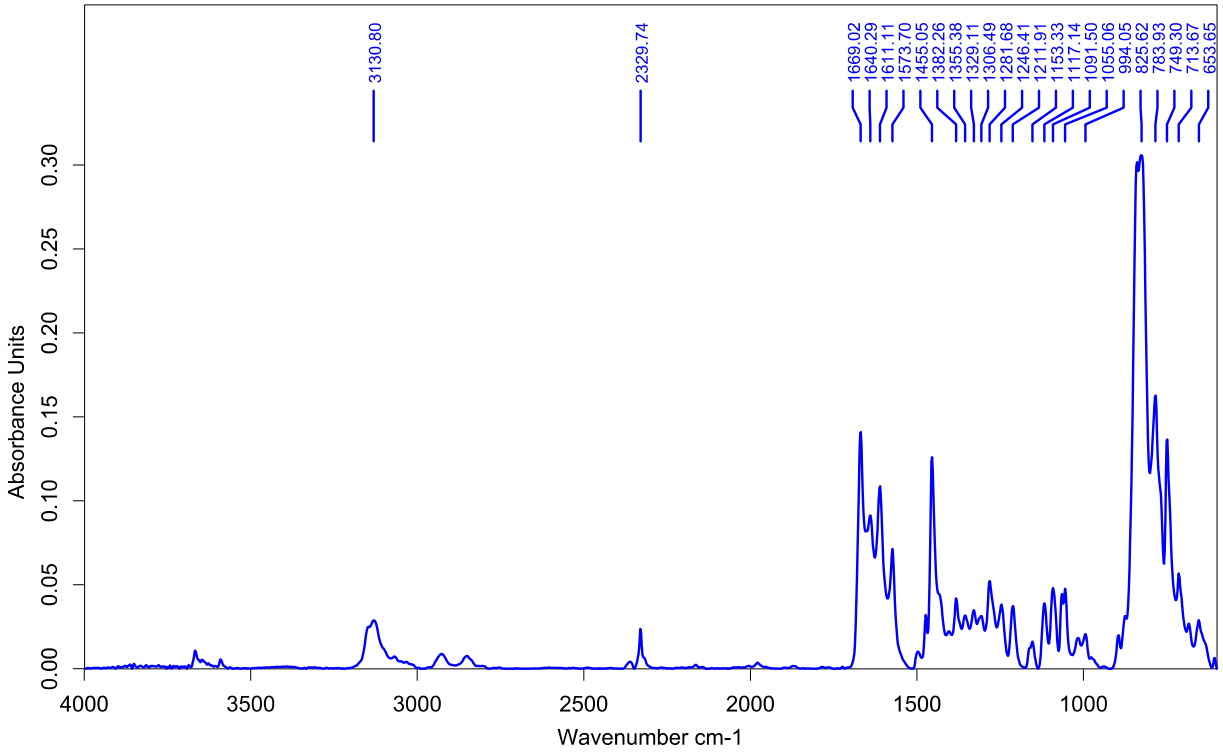

Figure 3.14. FT-IR spectrum of the solid obtained by treatment of **4** with DHA.

Preparation of $[Cu^{I}_2(m\text{-xpt})_2](BF_4)_2$ (7a) in anhydrous DMF solution.

Copper(II) tetrafluoroborate and *m*-xpt (in 2:1) and an excess of copper foil (ca. 0.2 g) were added to a reaction flask sealed to a cuvette. The flask was evacuated for 30 min. Then, N_2-purged anhydrous DMF was added and the mixture was stirred under flowing N_2 for 3 h to achieve complete reduction of Cu(II) to Cu(I). The resulting **7a** solution was transferred to a Schlenk flask via cannula under N_2 for subsequent experiments, to remove it from the unreacted Cu foil.

Reaction of $[Cu^{I}_2(m\text{-xpt})_2](BF_4)_2$ (7a) with air.

A solution of **7a** in DMF was prepared as above, from $Cu(BF_4)_2$ (12.7 mg, 0.0535 mmol), *m*-xpt (42.2 mg, 0.107 mmol), excess copper foil (ca. 0.2 g) and 5 mL N_2-purged anhydrous DMF. This solution was transferred to another Schlenk flask via cannula under N_2 and kept initially under N_2 and then exposed to CO_2. The solution is stable under both gases. At this point the solution was exposed to air and stirred for 3 days, by which time it had turned to green. Then, it was used for crystallization with ether vapor diffusion. Blue plates of $[Cu_3(m\text{-xpt})_3(\mu_3\text{-}CO_3)](BF_4)_4\cdot 2.5DMF$ (**5a**) were collected and analyzed by X-ray crystallography and FT-IR spectroscopy; see Figures 3.2 and 3.15.

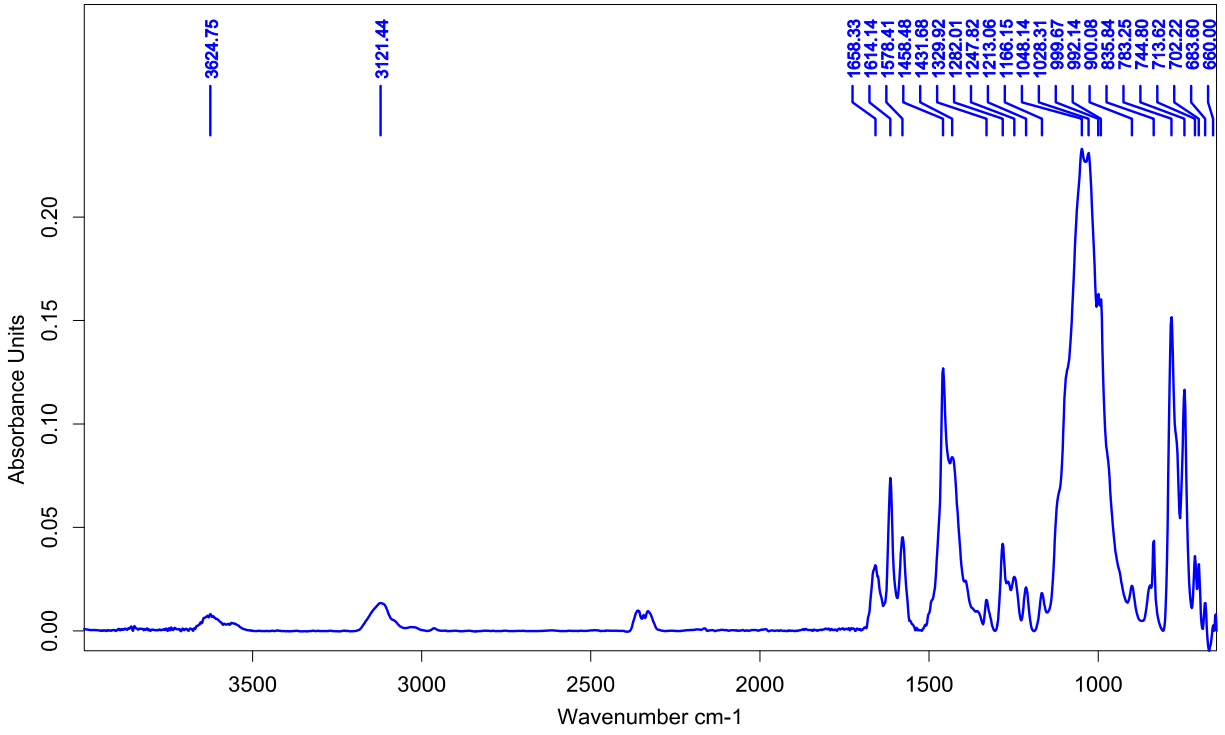

Figure 3.15. FT-IR spectrum of blue crystals of $[Cu_3(m\text{-xpt})_3(\mu_3\text{-}CO_3)](BF_4)_4\cdot 2.5DMF$ (**5a**).

Reaction of $[Cu^{I}_2(m\text{-xpt})_2](BF_4)_2$ (7a) with a mixture of CO_2 and O_2 (~1:1) in the presence of dehydroascorbic acid (DHA).

A solution of **7a** in DMF was prepared as above, from $Cu(BF_4)_2$ (20.7 mg, 0.0873 mmol), *m*-xpt (70.0 mg, 0.177 mmol), excess copper foil (ca. 0.2 g) and 7 mL N_2-purged anhydrous DMF. The yellow solution was transferred to another reaction flask sealed to a cuvette via cannula under N_2 which contained 76.8 mg (0.441 mmol) of DHA. This solution was stable under N_2 and then CO_2. However, it undergoes oxidation upon exposure to a mixture of CO_2 and O_2 (~1:1), turning green over a period of a few days. The resulting solution (λ_{max} = 726 nm) was used for ether vapor diffusion and green crystals of $[Cu_2(m\text{-xpt})_2(\mu\text{-}C_2O_4)](BF_4)_2$ (**6a**) formed. The same result was obtained when a solution of **7a** was exposed to air. Reactions were monitored by UV/vis spectroscopy as shown on Figures 3.16 and 3.17.

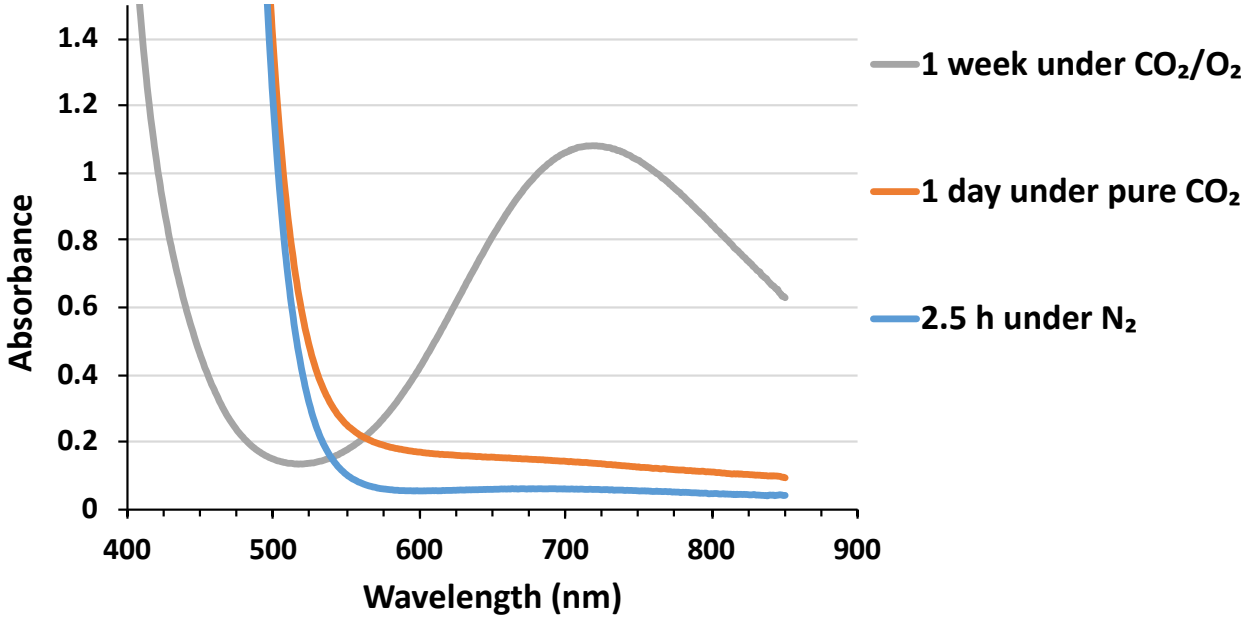

Figure 3.16. UV/vis absorption spectrum of $[Cu_2(m\text{-xpt})_2](BF_4)_2$ (**7a**) under N_2, CO_2 and after stirring for a week under a mixture of CO_2 and O_2.

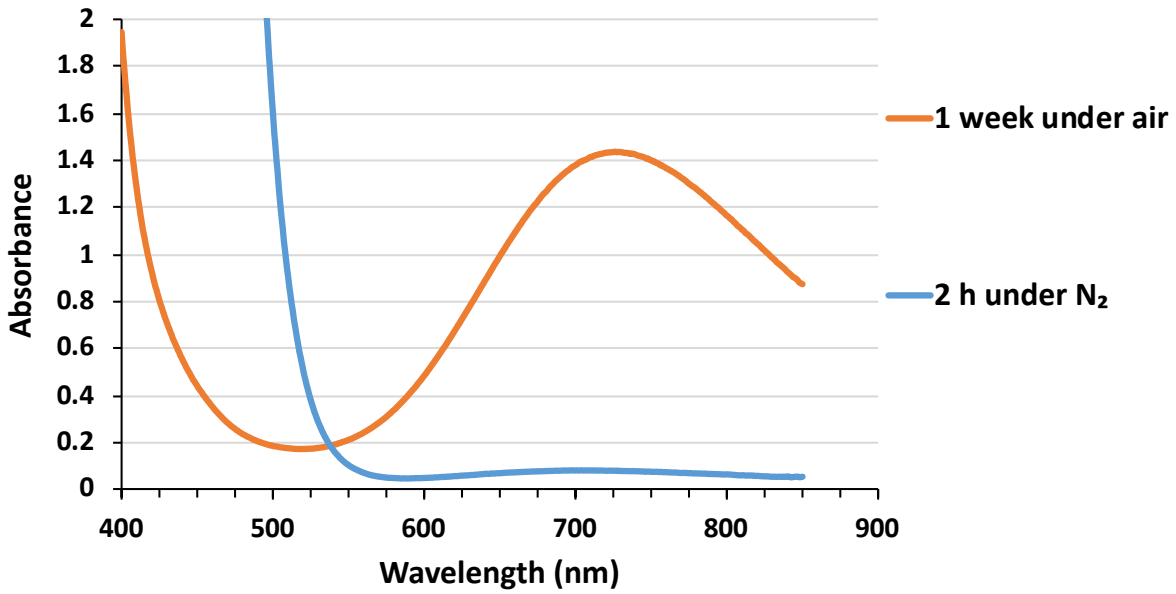

Figure 3.17. UV/vis absorption spectrum of $[Cu_2(m\text{-xpt})_2](BF_4)_2$ (**7a**) in DMF under N_2 and after stirring for a week under air.

CO and CO_2 detection by FT-IR spectroscopy.

The bands belonging to CO and CO_2 were detected by filling an IR gas cell (V = 96 mL) one time with pure CO and then with CO_2 gas; see Figure 3.18. In a separate experiment, the cell was filled with pure CO_2, and 1 mL CO was injected into it; the CO peak could readily be observed; see Figure 3.19). Therefore, it is possible to detect ca. 1% v/v of CO in the CO_2 with this method. In another experiment, a Schlenk flask (V = 85 mL) was charged with a stir bar and 30 mL DMF, then it was evacuated and filled with CO_2. 5 mL of headspace gas was injected into N_2-filled FTIR gas cell. CO_2 peak was observed with no detectable CO peak as expected. The Schlenk flask was evacuated and filled with fresh CO_2 then 0.5 mL CO was injected into the flask then 5 mL of the head space gas was injected into N_2-filled IR gas cell. Concentration of CO in the cell is ca. 0.05% (v/v) and its absorption peak could be detected; see Figure 3.20.

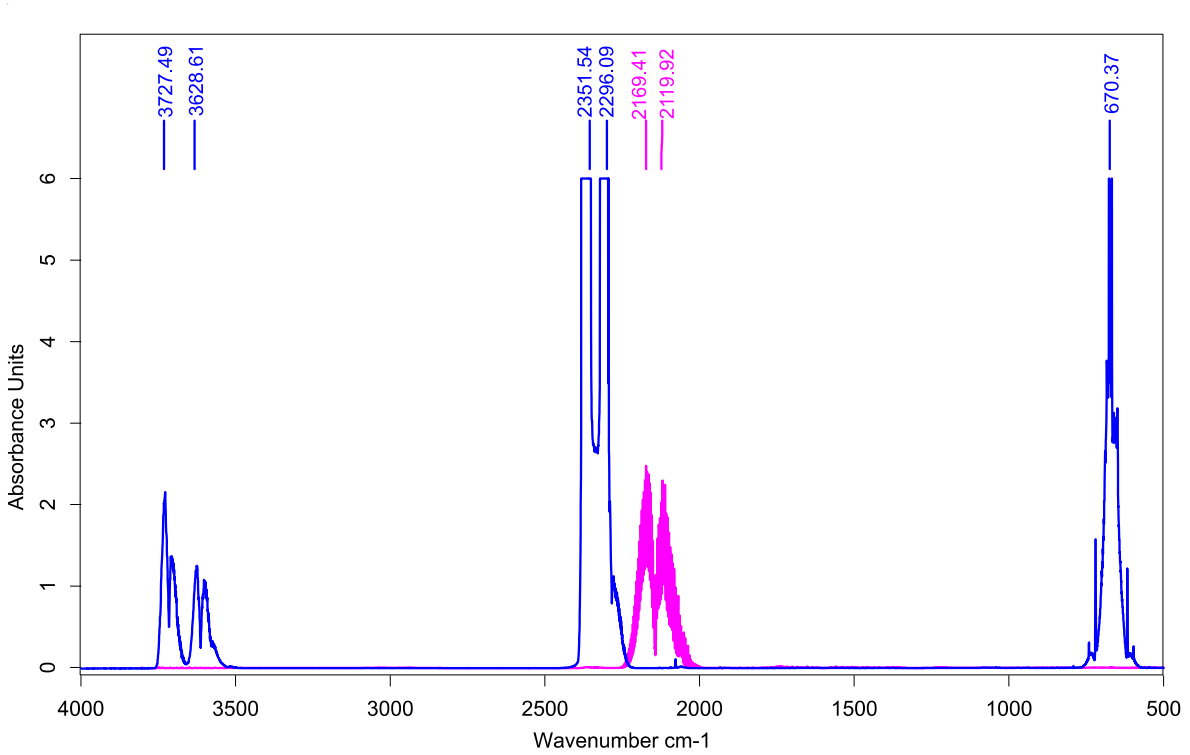

Figure 3.18. FT-IR Spectrum of CO (blue) and CO_2 (magenta).

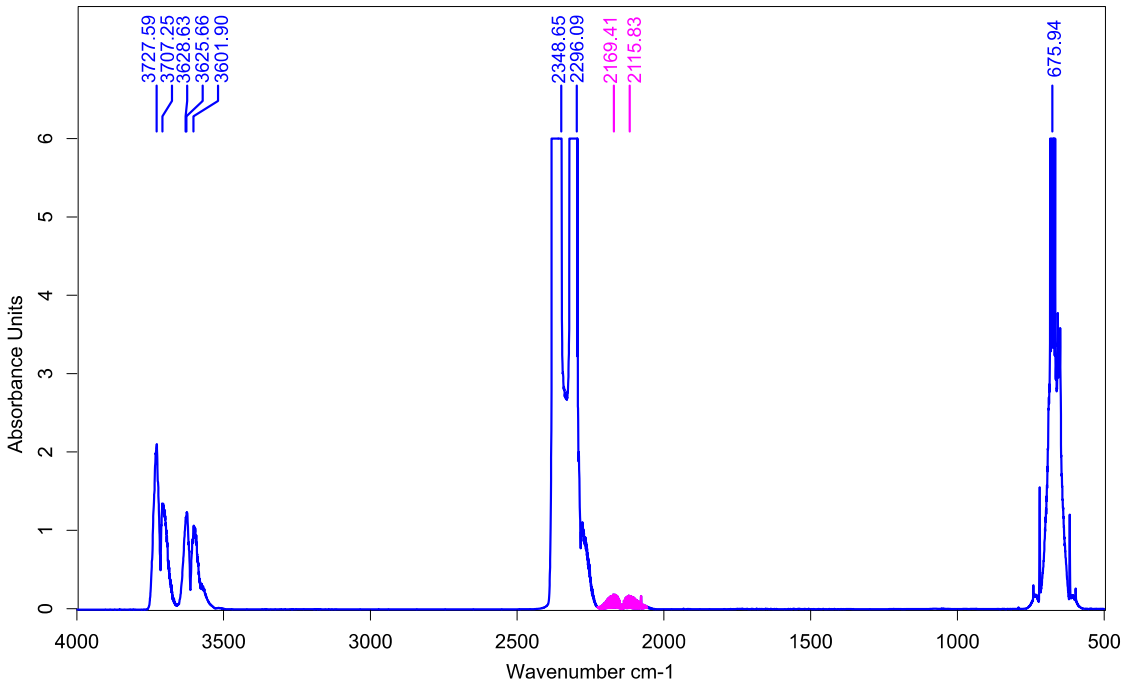

Figure 3.19. 1 mL CO injected into CO_2-filled IR gas cell. Concentration of CO is about 1% (v/v) and in this FT-IR spectrum the CO peak (highlighted in magenta) could be observed.

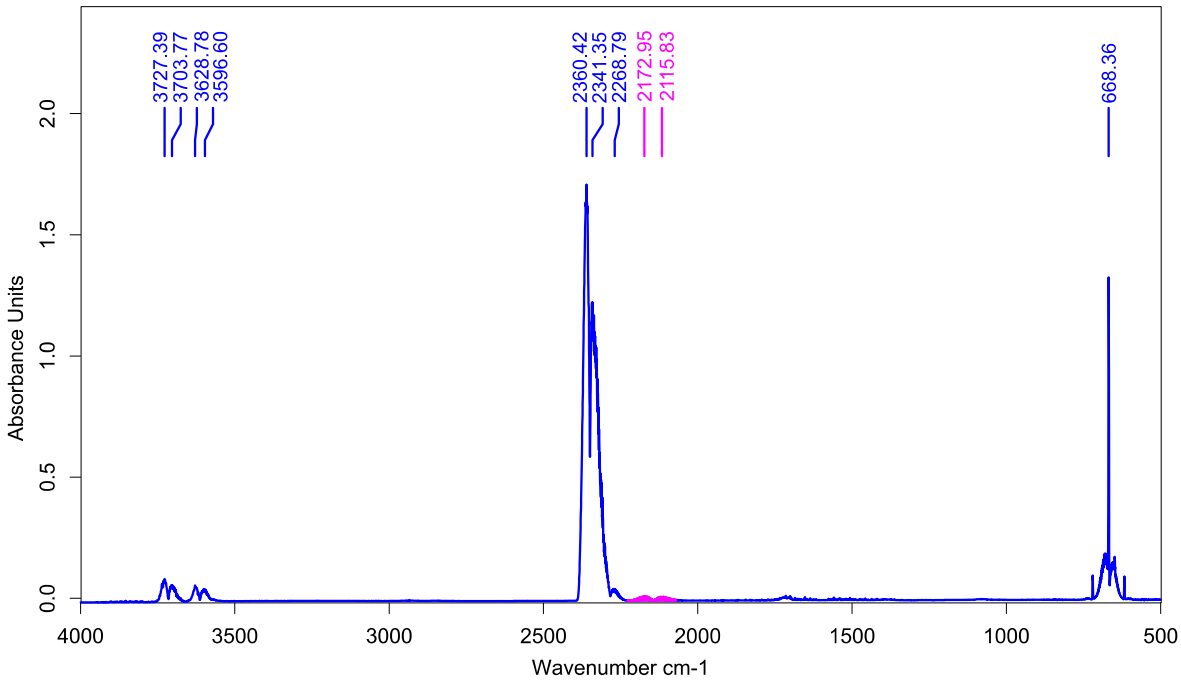

Figure 3.20. 0.5 mL CO was injected into CO_2 filled reaction flask then 5 mL of head space gas was injected into N_2-filled IR gas cell; the concentration of CO is ca. 0.05%. The CO absorption peak (highlighted in magenta) could be detected in this FT-IR spectrum.

Headspace gas analysis of reaction of $[Cu_2(m\text{-xpt})_2](BF_4)_2$ (7a) with a mixture of CO_2 and O_2 (~1:1)

A solution of **7a** in DMF was prepared as above, from $Cu(BF_4)_2$ (65.3 mg, 0.239 mmol), *m*-xpt (217.0 mg, 0.550 mmol), excess copper foil (ca. 0.36 g) and 21 mL N_2-purged anhydrous DMF. Then the yellow solution was transferred to an N_2-filled Schlenk flask and exposed to a mixture of CO_2 and O_2 (~1:1). The headspace volume of flask was 64 mL and this reaction ideally could form 5.7 mL CO according to equation 3.2, and assuming ideal gas condition with 1 mol of ideal gas has 24 L volume at room temperature. The color of solution gradually turned to green and after 3 days 12 mL of headspace gas was injected to the N_2-filled IR gas cell, and no CO absorption peak was observed beside CO_2; see Figure 3.21.

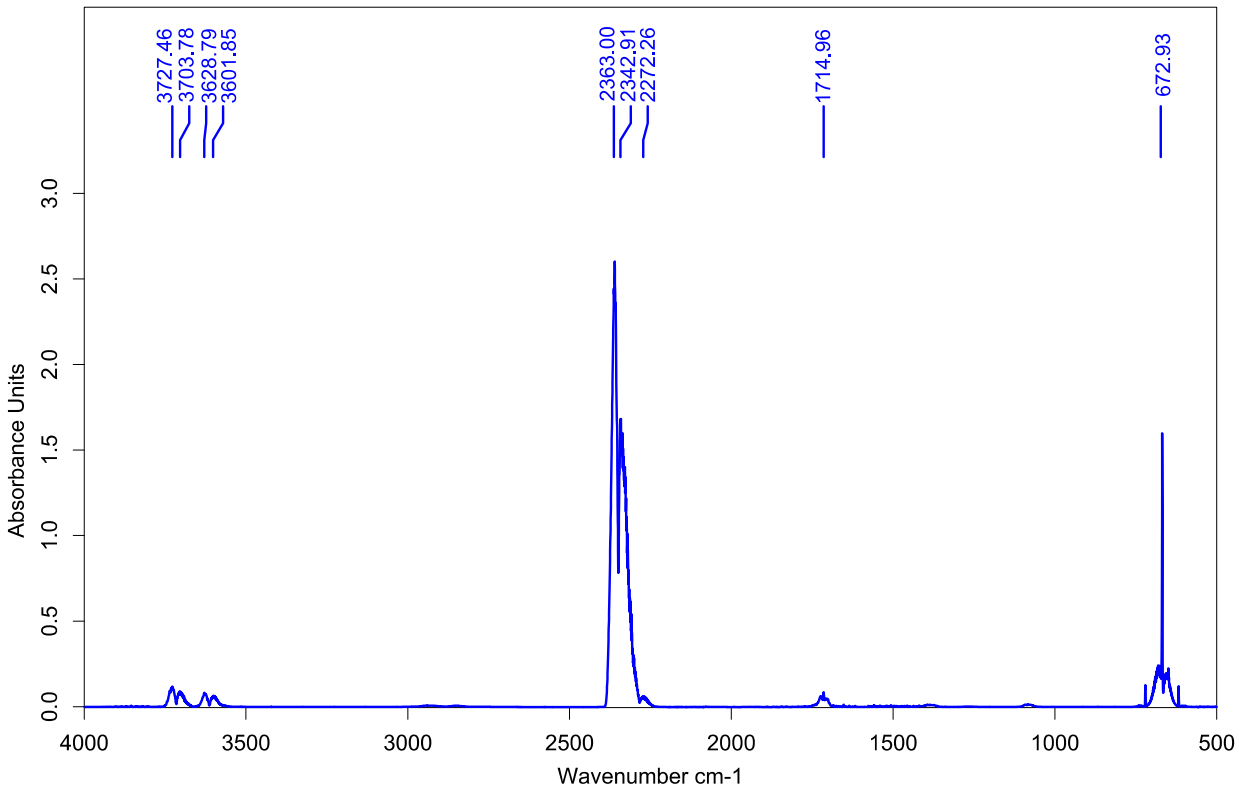

Figure 3.21. FT-IR spectrum of head space gas after completion of the reaction of $[Cu_2(m\text{-xpt})_2](BF_4)_2$ (**7a**) with a mixture of CO_2 and O_2. No CO absorption peak could be detected.

EPR studies of reaction of Cu(I) solutions with air.

Following solutions were prepared:

Solution **A:** 1.2 mg (6.0 μmol) of BocMPO and 14.2 mg (0.0151 mL) DMF were combined and centrifuged to get a consistent solution with concentration of 0.4 M.

Solution **B**: 8.1 mg (0.041 mmol) of pure sodium ascorbate was added to 10 mL DMF. Sodium ascorbate is only slightly soluble in DMF, so the suspension was stirred for a while then left on bench top to precipitate the undissolved solid.

Solution **C**: 7.5 mg (0.043 mmol) of pure ascorbic acid was dissolved in 10 mL of DMF (~ 4 mM solution).

Solutions **D-H** contain ~ 4 mM solution of **4** or **7** were prepared as bellow:

Solution **D**: 32.1 mg (0.0241 mmol) of complex **4** was dissolved in 6 mL of DMF.

Solution **E**: Complex **4** (32.1 mg, 0.0241 mmol) and sodium ascorbate (5.8 mg, 0.029 mmol) were placed into a vial. Then 6 mL DMF was added and the solution was stirred for an hour under N_2.

Solution **F**: This was prepared same as solution **E**, but after stirring under N_2 for an hour, the solution was exposed to air for 1.5 hour with stirring, before using for EPR measurement.

Solution **G**: Complex **4** (32.1 mg, 0.0241 mmol) and ascorbic acid (5.1 mg, 0.029 mmol) were placed into a vial. Then 6 mL DMF was added with stirring under N_2.

Solution **H**: Complex **4** (32.9 mg, 0.0247 mmol) and DABCO (5.0 mg, 0.045 mmol) were placed into a vial and the solution was stirred under N_2.

0.1 μL of solution **A** was added to 0.9 μL of each solution, **B-H**, in air and immediately used for recording the EPR spectrum. See the spectra in Figure 3.22.

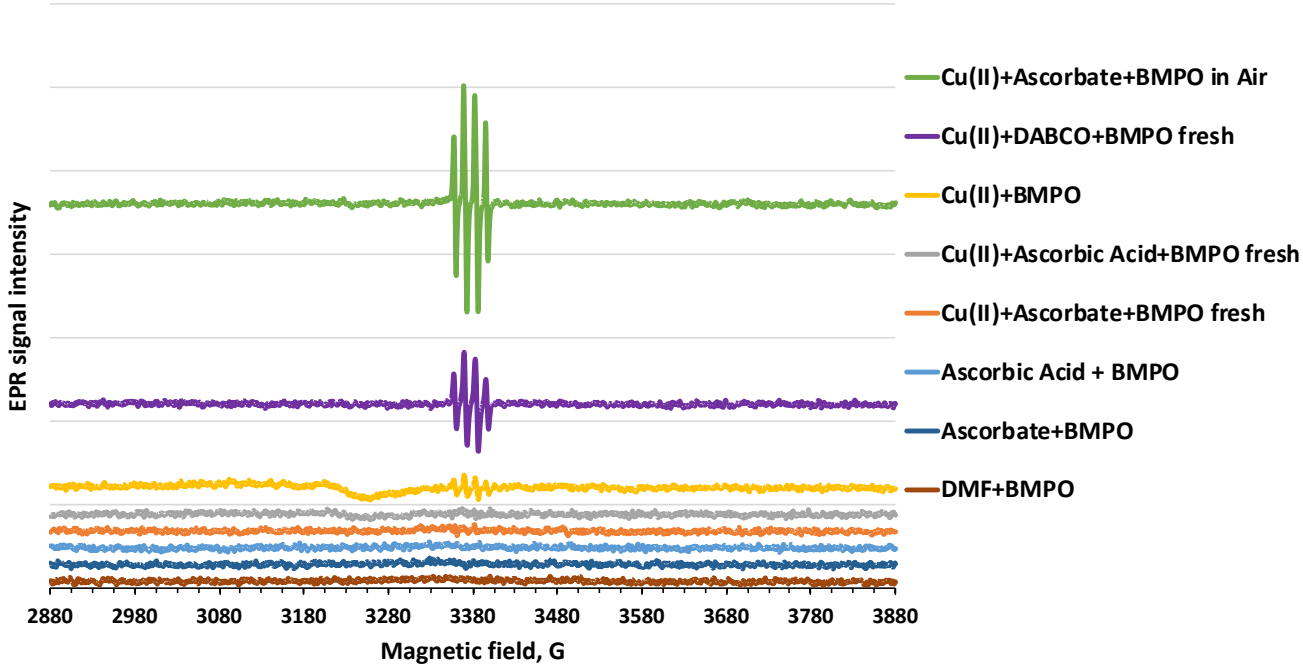

Figure 3.22. EPR spectra of solutions **A** to **H** prepared as mentioned above.

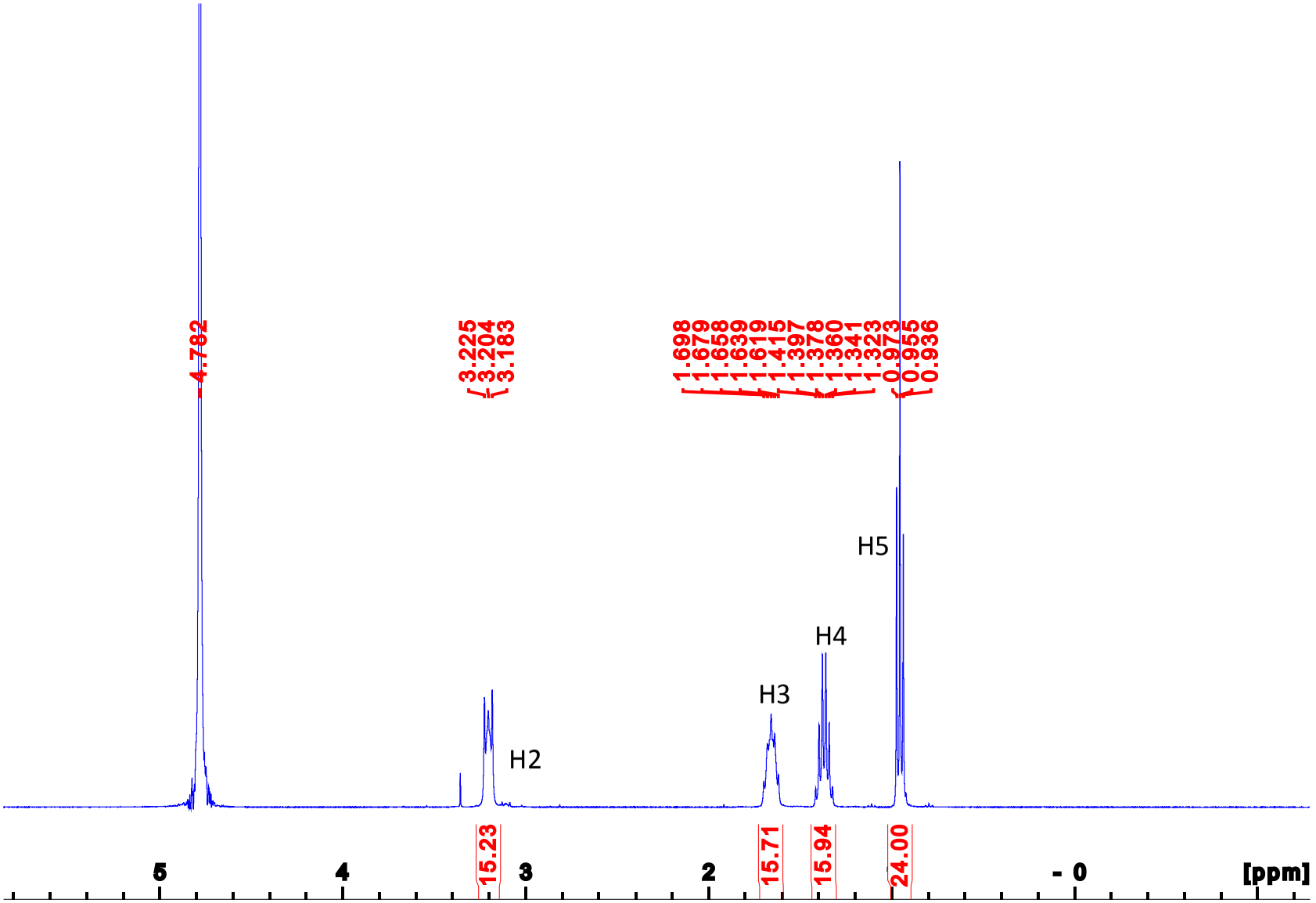

Figure 3.23. ^{1}H NMR of $(Bu_4N)_2{}^{13}C_2O_4$ in D_2O at 400 MHz.

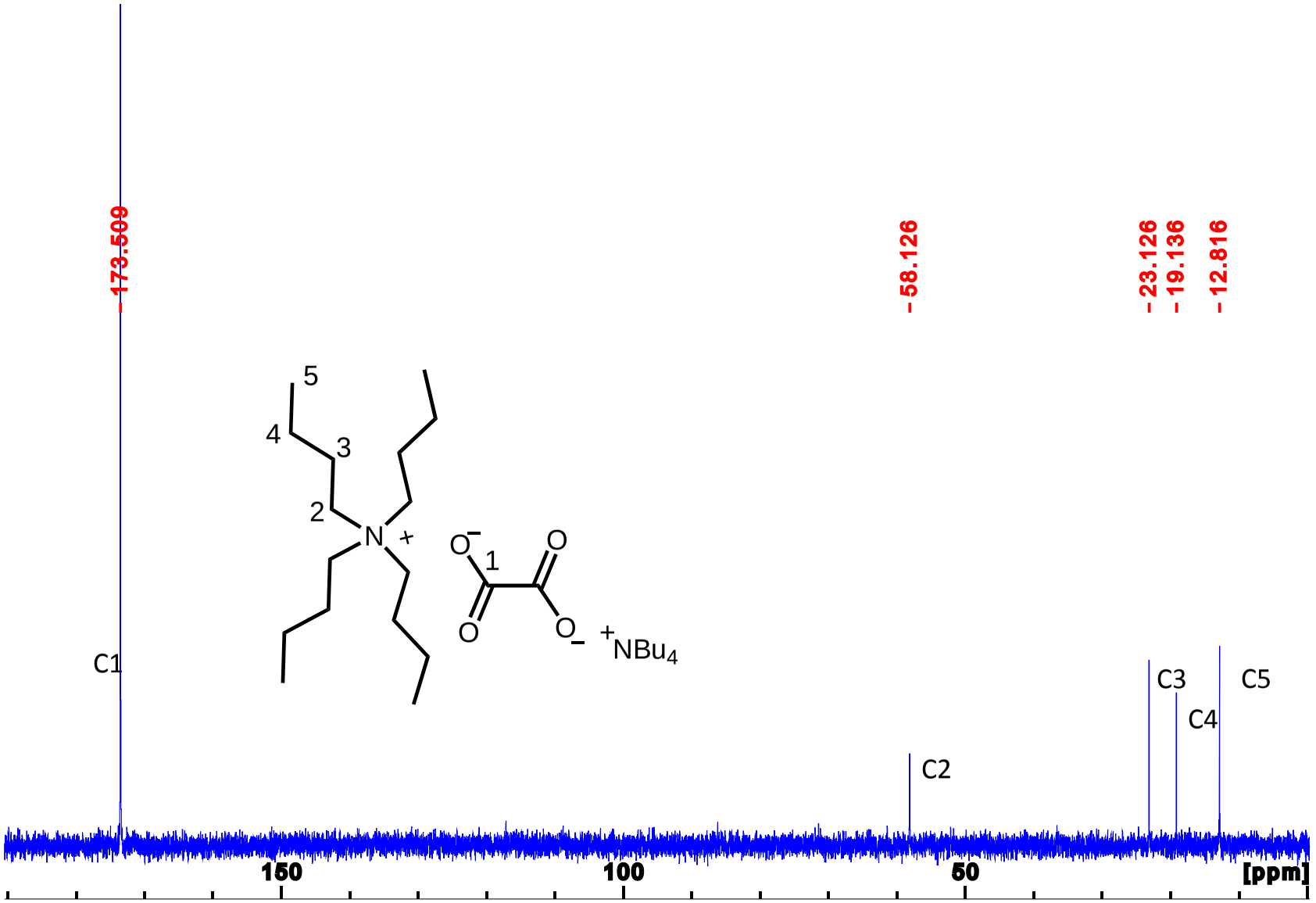

Figure 3.24. ^{13}C NMR of $(Bu_4N)_2{}^{13}C_2O_4$ in D_2O at 400 MHz.

3.4. References

1. Pokharel, U. R.; Fronczek, F. R.; Maverick, A. W., Reduction of carbon dioxide to oxalate by a binuclear copper complex. *Nature Communications* **2014,** *5*, 5883.

2. Nelson, I.; Larson, R.; Iwamoto, R., Polarographic evidence for the stability of copper(I) ion in some non-complexing nonaqueous solvents. *Journal of Inorganic and Nuclear Chemistry* **1961,** *22* (3-4), 279-284.

3. Warren, J. J.; Mayer, J. M., Surprisingly long-lived ascorbyl radicals in acetonitrile: concerted proton-electron transfer reactions and thermochemistry. *Journal of the American Chemical Society* **2008,** *130* (24), 7546-7547.

4. Creutz, C., The complexities of ascorbate as a reducing agent. *Inorganic Chemistry* **1981,** *20* (12), 4452-4453.

5. Osredkar, J.; Sustar, N., Copper and zinc, biological role and significance of copper/zinc imbalance. *Journal of Clinical Toxicology* **2011,** *3* (2161), 0495.

6. Adam, S. M.; Wijeratne, G. B.; Rogler, P. J.; Diaz, D. E.; Quist, D. A.; Liu, J. J.; Karlin, K. D., Synthetic Fe/Cu complexes: toward understanding heme-copper oxidase structure and function. *Chemical Reviews* **2018,** *118* (22), 10840-11022.

7. Lam, B. M.; Halfen, J. A.; Young, V. G.; Hagadorn, J. R.; Holland, P. L.; Lledós, A.; Cucurull-Sánchez, L.; Novoa, J. J.; Alvarez, S.; Tolman, W. B., Ligand macrocycle structural effects on copper−dioxygen reactivity. *Inorganic Chemistry* **2000,** *39* (18), 4059-4072.

8. Garcia-Bosch, I.; Cowley, R. E.; Díaz, D. E.; Siegler, M. A.; Nam, W.; Solomon, E. I.; Karlin, K. D., Dioxygen activation by a macrocyclic copper complex leads to a Cu_2O_2 core with unexpected structure and reactivity. *Chemistry–A European Journal* **2016,** *22* (15), 5133-5137.

9. Park, G. Y.; Qayyum, M. F.; Woertink, J.; Hodgson, K. O.; Hedman, B.; Narducci Sarjeant, A. A.; Solomon, E. I.; Karlin, K. D., Geometric and electronic structure of $[\{Cu(MeAN)\}_2(\mu\text{-}\eta^2\text{:}\eta^2(O_2^{2-}))]^{2+}$ with an unusually long O–O bond: O–O bond weakening vs activation for reductive cleavage. *Journal of the American Chemical Society* **2012,** *134* (20), 8513-8524.

10. Lewis, E. A.; Tolman, W. B., Reactivity of dioxygen−copper systems. *Chemical Reviews* **2004,** *104* (2), 1047-1076.

11. Janzen, E. G.; Julia, I.; Liu, P., Radical addition reactions of 5,5-dimethyl-1-pyrroline-1-oxide. ESR spin trapping with a cyclic nitrone. *Journal of Magnetic Resonance* **1973,** *9* (3), 510-512.

12. Zhou, P.; Zhang, J.; Zhang, Y.; Liu, Y.; Liang, J.; Liu, B.; Zhang, W., Generation of hydrogen peroxide and hydroxyl radical resulting from oxygen-dependent oxidation of L-ascorbic acid via copper redox-catalyzed reactions. *RSC Advances* **2016,** *6* (45), 38541-38547.

13. Saha, M. S.; Ohsaka, T., Electrode kinetics of the O_2/O_2^- redox couple at Hg electrode in the presence of PVC in aprotic media. *Electrochimica Acta* **2005,** *50* (24), 4746-4751.

14. Sato, T.; Hamada, Y.; Sumikawa, M.; Araki, S.; Yamamoto, H., Solubility of oxygen in organic solvents and calculation of the Hansen solubility parameters of oxygen. *Industrial & Engineering Chemistry Research* **2014,** *53* (49), 19331-19337.

15. Dewhirst, R. A.; Fry, S. C., The oxidation of dehydroascorbic acid and 2,3-diketogulonate by distinct reactive oxygen species. *Biochemical Journal* **2018,** *475* (21), 3451-3470.

16. Harkrader, R. J.; Plunkett, L. M.; Tolbert, B. M., Periodate degradation of labeled ascorbic acid. *Analytical Biochemistry* **1976,** *72* (1-2), 310-314.

17. Herbert, R. W.; Hirst, E. L.; Percival, E. G. V.; Reynolds, R. J. W.; Smith, F., The constitution of ascorbic acid. *Journal of the Chemical Society* **1933**, 1270-1290.

18. Shin, D. B.; Feather, M. S., The degradation of L-ascorbic acid in neutral solutions containing oxygen. *Journal of Carbohydrate Chemistry* **1990,** *9* (4), 461-469.

19. Kurata, T.; Miyake, N.; Otsuka, Y., Formation of L-threonolactone and oxalic acid in the autoxidation reaction of L-ascorbic acid: possible involvement of singlet oxygen. *Bioscience, Biotechnology, and Biochemistry* **1996,** *60* (7), 1212-1214.

20. Ünaleroğlu, C.; Zümreoğlu-Karan, B.; Zencir, Y.; Hökelek, T., pH-independent decomposition reactions of L-ascorbic acid in aqueous metal solutions—I. Formation and structures of Co^{II} and Gd^{III} oxalates. *Polyhedron* **1997,** *16* (13), 2155-2161.

21. Magda, D.; Gerasimchuk, N.; Lecane, P.; Miller, R. A.; Biaglow, J. E.; Sessler, J. L., Motexafin gadolinium reacts with ascorbate to produce reactive oxygen species. *Chemical Communications* **2002,** (22), 2730-2731.

22. Arendse, M. J.; Anderson, G. K.; Rath, N. P., Oxidative degradation of the ascorbate anion in the presence of platinum and palladium. Formation and structures of platinum and palladium oxalate complexes. *Polyhedron* **2001,** *20* (19), 2495-2503.

23. Orioli, P.; Bruni, B.; Di Vaira, M.; Messori, L.; Piccioli, F., Decomposition of ascorbic acid in the presence of cadmium ions leads to formation of a polymeric cadmium oxalate species with peculiar structural features. *Inorganic Chemistry* **2002,** *41* (17), 4312-4314.

24. de Ruiter, G.; Costa, J. S.; Lappalainen, K.; Roubeau, O.; Gamez, P.; Reedijk, J., The system iron(II)/mpzbpy mediates the H_2O_2 oxidation of cyclohexane and cyclooctene and the aerobic oxidative cleavage of ascorbic acid to oxalate. *Inorganic Chemistry Communications* **2008,** *11* (7), 787-790.

25. Thomas, A. M.; Mandal, G. C.; Tiwary, S. K.; Rath, R. K.; Chakravarty, A. R., Ascorbate oxidation leading to the formation of a catalytically active oxalato bridged dicopper(II) complex

as a model for dopamine β-hydroxylase. *Journal of the Chemical Society, Dalton Transactions* **2000**, 1395-1396.

26. Csonka, R.; Kaizer, J.; Giorgi, M.; Reglier, M.; Hajba, L.; Mink, J.; Speier, G., Oxidative C-H and C-C bond cleavage by a (2,2'-bipyridine)copper(I) chloride complex. *Inorganic Chemistry* **2008,** *47* (14), 6121-6123.

27. Kuroda, D. G.; Hochstrasser, R. M., Two-dimensional infrared spectral signature and hydration of the oxalate dianion. *The Journal of Chemical Physics* **2011,** *135* (20), 204502.

28. Ziegelgruber, K. L.; Knope, K. E.; Frisch, M.; Cahill, C. L., Hydrothermal chemistry of Th(IV) with aromatic dicarboxylates: New framework compounds and in situ ligand syntheses. *Journal of Solid State Chemistry* **2008,** *181* (2), 373-381.

29. Knope, K. E.; Kimura, H.; Yasaka, Y.; Nakahara, M.; Andrews, M. B.; Cahill, C. L., Investigation of in situ oxalate formation from 2,3-pyrazinedicarboxylate under hydrothermal conditions using nuclear magnetic resonance spectroscopy. *Inorganic Chemistry* **2012,** *51* (6), 3883-3890.

30. Soares-Santos, P. C. R.; Cunha-Silva, L.; Paz, F. A. A.; Ferreira, R. A. S.; Rocha, J.; Carlos, L. D.; Nogueira, H. I. S., Photoluminescent lanthanide-organic bilayer networks with 2, 3-pyrazinedicarboxylate and oxalate. *Inorganic Chemistry* **2010,** *49* (7), 3428-3440.

31. Pokharel, U. R.; Fronczek, F. R.; Maverick, A. W., Cyclic pyridyltriazole–Cu(II) dimers as supramolecular hosts. *Dalton Transactions* **2013,** *42* (39), 14064-14067.

32. Yang, C. T.; Fu, Y.; Huang, Y. B.; Yi, J.; Guo, Q. X.; Liu, L., Room-temperature copper-catalyzed carbon–nitrogen coupling of aryl iodides and bromides promoted by organic ionic bases. *Angewandte Chemie International Edition* **2009,** *48* (40), 7398-7401.

Chapter 4. New Ruthenium-Pyridyltriazole Complexes for Water Oxidation Studies

4.1. Introduction

One of the common oxidants used for water oxidation is ceric ammonium nitrate (CAN) which is a powerful enough oxidant to oxidize water to O_2. This reaction (see Equation 4.1) is ordinarily very slow, which makes it an ideal system for testing the effectiveness of water oxidation catalysts (WOCs). One of the widely used metals for catalyzing oxidation of water is ruthenium. Ru(II) and Ru(III) have low-spin $4d^6$ and $4d^5$ electronic configuration respectively, and they are kinetically stable. Therefore, one can rely on most of the ligands remaining attached to ruthenium. In the Ru water oxidation catalysts introduced in Chapter 1, Ru-OH_2 is the active site. Research with ruthenium systems has explored very active catalysts with TOF even higher than that of the oxygen-evolving complex (OEC) in PSII.[1] The standard redox potential for oxidation of H_2O to O_2 is 1.23 V vs. NHE, and at this potential many organic molecules, including ligands, are also oxidized. Therefore, finding an efficient and stable catalyst which can oxidize water with minimal decomposition is a subject of ongoing research.

$$4Ce^{IV} + 2H_2O \rightarrow O_2 + 4H^+ + 4Ce^{III} \qquad E°_{cell} = 0.38 \text{ V (in 1 M } HNO_3) \qquad (4.1)$$

In this project we decided to synthesize new ruthenium complexes with pyridyltriazole ligands to study their water oxidation activity. Crowley's research on $Ru(bpt)_3^{2+}$ showed $E_{1/2}$ ($Ru^{III/II}$) is 0.89 V vs Fc/Fc^+ and $E_{1/2}$ ($Ru^{III/II}$) for $Ru(bpy)_3^{2+}$ is 0.80 V in DMF vs Fc/Fc^+.[2,3] This means it is harder to oxidize $Ru(bpt)_3^{2+}$ relative to the bpy complex, which is consistent with having three electronegative nitrogens in the triazole. In general, a water oxidation catalyst is expected to undergo sequential oxidations at potentials close to the thermodynamic value of the

water oxidation. To this aim a new generation of ruthenium water oxidation catalysts (WOC) have been developed containing anionic ligands. Those examples could catalyze oxidation of water at lower potential than ruthenium complexes with neutral ligands. In our experiments, we could not use $Ru(bpt)_3^{2+}$ because it has no readily accessible coordination sites where water can bind and react. Thus, I needed to prepare Ru pyridyltriazole complexes that also contain vacant coordination sites for water, so that they may function as WOCs

4.2. Results and discussion

There are a few examples of ruthenium complexes with pyridyltriazole ligands in the literature. One study is from Crowley's lab shows the two diastereomeric *fac* and *mer* isomers of $Ru(bpt)_3(PF_6)_2$ (**1**) with octahedral geometry could be synthesized in good yield by microwave irradiation of an ethylene glycol solution of $RuCl_3$ and bpt ligand.[4]

We were interested to make similar complexes with one or two vacant sites for coordination of aqua ligands, such as $[Ru(bpt)_2(H_2O)_2]^{2+}$, to test their reactivity toward water oxidation. To do this, we first followed a procedure developed in Meyer's group for synthesis of *cis*-$Ru(bpy)_2Cl_2$.[5] The chlorides could be removed by a Ag^+ solution and replaced by aqua ligands. Refluxing $RuCl_3$, two equivalents of bpt and LiCl in DMF didn't yield the desired product, as judged by the ^1H NMR of the product mixture. We then changed the solvent to ethanol which (like DMF) readily reduces Ru(III) to Ru(II). Refluxing $RuCl_3$ and two equivalents of bpt ligand in ethanol and then metathesis with PF_6 anion formed two isomers of *fac*- and *mer*-**1**, identified by comparison of ^1H NMR of crude mixture with the spectra reported in Crowley's paper.[4] Since using even two equivalents of ligand resulted in tris-ligated complex, we thought addition of excess

LiCl may avoid coordination of the third ligand. However similar products were obtained in the presence of excess of LiCl.

Instead of starting with Ru(III), we then turned our attention to a well-known Ru(II) precursor, "$RuCl_2(DMSO)_4$" (which is actually *fac*-[$RuCl_2$(DMSO-*S*)$_3$(DMSO-*O*)]) precursor. We synthesized this precursor according to Wilkinson's procedure by refluxing $RuCl_3$ in DMSO.[6] It is known that three of the DMSO molecules are coordinated through Sulfur (*S*-bonded DMSO) and one DMSO molecule is weakly coordinated to the Ru center by e^- donation from oxygen (*O*-bonded). By refluxing $RuCl_2(DMSO)_4$ and bpt ligand in acetone (or chloroform) for 12 h, complete conversion to (*OC*-6-14)-Ru(bpt)$(DMSO)_2Cl_2$ (**2**), was observed; see Figure 4.1. "*OC*-6-14" in this name is the *configuration number*, which describes the positions of coordinating ligands, according to Chemical Abstracts stereochemical notation.[7,8] Then to replace the remaining DMSO molecules we added one and even excess equivalents of bpt ligand to the mixture and continued refluxing. However, no further substitution occurred. Refluxing at higher temperature in toluene (bp = 110.6 °C) for an extended amount of time also didn't lead to substitution of additional DMSO molecules, but the complex isomerized to the (*OC*-6-32)-Ru(bpt)$(DMSO)_2Cl_2$ (**3**); see Figure 4.1. Therefore, complex **3** is the thermodynamically stable product of the reaction of $RuCl_2(DMSO)_4Cl_2$ with bpt.[9] The lengths of important bonds, the distances of the Ru atoms from the mean planes of the bpt ligands, and the angles between the pyridyltriazole and benzyl mean planes, are reported in Table 4.1. We performed 2D NMR analysis to fully assign the peaks in the ^1H and ^{13}C NMR spectra. In the structure of **2**, the DMSO molecules are bonded through S, with

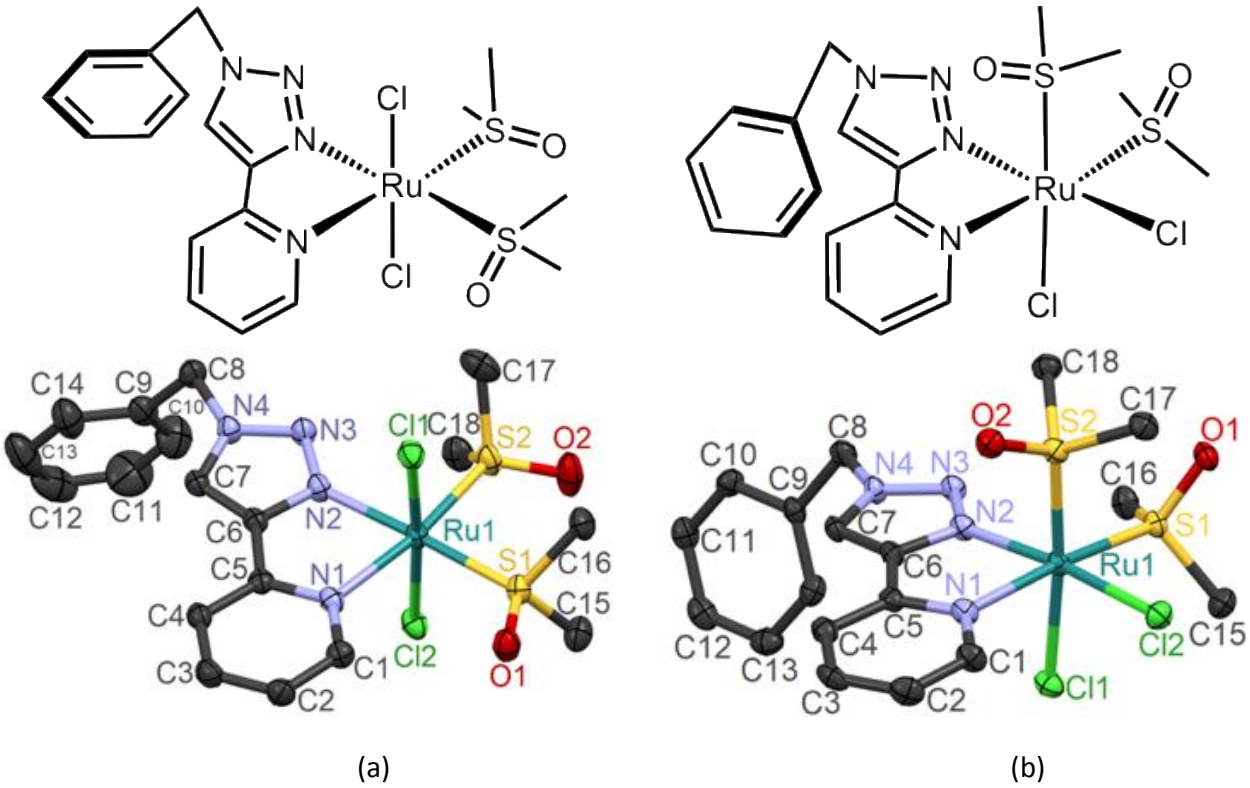

Figure 4.1. X-ray crystal structures of (a) (*OC*-6-14)- and (b) (*OC*-6-32)-Ru(bpt)(DMSO)$_2$Cl$_2$, (**2**) and (**3**), respectively.

S1–Ru1–S2 = 91.27 (2)°, and they are in slightly different environments, in agreement with the NMR data. The ^{1}H NMR resonances for the two DMSO ligands differ by more in **3** (four singlet peaks) than they do in **2**, as expected. Unlike in **2**, the benzylic methylene hydrogens in **3** are inequivalent, and they appear as a multiplet at 5.67 ppm. The packing structure of **2** shows a non-classical hydrogen bond between Cl2 and H7; see Table 4.2. The methine hydrogen (H7) showing a downfield ^{1}H NMR peak at 7.93 ppm. Li & Flood took advantage of this C–H(triazole)· · ·Cl interaction in preparing a neutral, macrocyclic receptor for chloride ions.[10] Hydrogen bonds to triazole H atoms were also used by White & Beer in creating a host system that can strongly bind halides.[11] The packing structure of **3** also shows a close interaction of H7, this time with O1 (see

Table 4.1. Selected bond distances for complexes **2** and **3**, the distance between Ru and the mean plane of the pyridyltriazole (Å), the N1–Ru–N2 angle, and the angle between the pyridyltriazole and benzyl mean planes (°).

	Complex 2	**Complex 3**
Ru1 - N1	2.1714 (18)	2.126 (3)
Ru1 - N2	2.0890 (19)	2.044 (3)
Ru1 - Cl1	2.3835 (6)	2.4175 (9)
Ru1 - Cl2	2.4157 (6)	2.4167 (9)
Ru1 - S1	2.2814 (6)	2.2530 (9)
Ru1 - S2	2.2440 (6)	2.2434 (9)
Ru1· · ·mean plane of pyridyltriazole	0.0728 (2)	0.048 (3)
N1 - Ru - N2	77.10 (7)	78.32 (12)
Pyridyltriazole plane· · ·benzyl plane	77.75 (7)	69.52 (10)

Table 4.2). Two other isomers of the Ru(bpt)$(DMSO)_2Cl_2$, with DMSO ligands trans and Cl ligands cis (the *OC*-6-43 isomer) or with cis DMSO and Cl ligands and pyridyl trans to Cl (*OC*-6-42), are possible. We did not observe any other materials in the NMR spectra or in the isolated products that were attributable to these isomers.

Table 4.2. Hydrogen-bond geometry (Å, °) for **2** and **3**.

	D - H· · ·A	**D - H**	**H· · ·A**	**D· · ·A**	**D - H· · ·A**
Complex **2**	C7 - H7· · ·Cl2^{i}	0.95	2.49	3.438 (2)	172
Complex **3**	C7 - H7· · ·O1^{ii}	0.95	2.11	3.031 (4)	164

Symmetry code: (i) –x+1/2, y-1/2, z (ii) x+1, y, z

In an additional attempt to isolate a bis(bpt)-Ru complex, we tried refluxing $RuCl_2(DMSO)_4$ and excess amount of bpt in ethanol and DMF also, but they didn't result in the

isolation of the desired product. For instance, in the case of ethanol, crystals of *mer*-$Ru(bpt)_3Cl_2$ were obtained.

We did similar reactions with the *m*-xpt ligand, which could potentially make a Ru dimer similar to the $[Cu_2(m\text{-xpt})_2Cl_2]Cl_2$ reported in chapter 2 of this dissertation. From refluxing a chloroform solution of *m*-xpt and $Ru(DMSO)_4Cl_2$ a yellow product was obtained that is assigned to $Cl_2(DMSO)_2Ru$-(xpt)-$Ru(DMSO)_2Cl_2$ (**4**), tentatively, based on our observation with bpt ligand. However, we were unable to isolate this compound in pure form to characterize it better. The only complex that we could isolate and characterize by X-ray analysis from a variety of trials was (*OC*-6-33)-$[Ru(m\text{-xpt})(CH_3CN)_2](NO_3)_2$ (**[5](NO$_3$)$_2$**) (or $[(OC\text{-}6\text{-}33)\text{-}Ru(m\text{-xpt})(CH_3CN)_2](BF_4)_2$ (**6**)) in trace amount, which was characterized by ^{1}H NMR; see X-ray structure of **6** in Figure 4.2. We then conducted removal of the chlorido ligands from **2** by treatment with $AgPF_6$ or AgOTf and then coordination of a bpt ligand. The choice of solvent for removing chlorides was found to be important. For example, formation of AgCl was observed in DCM but NMR of the crude mixture

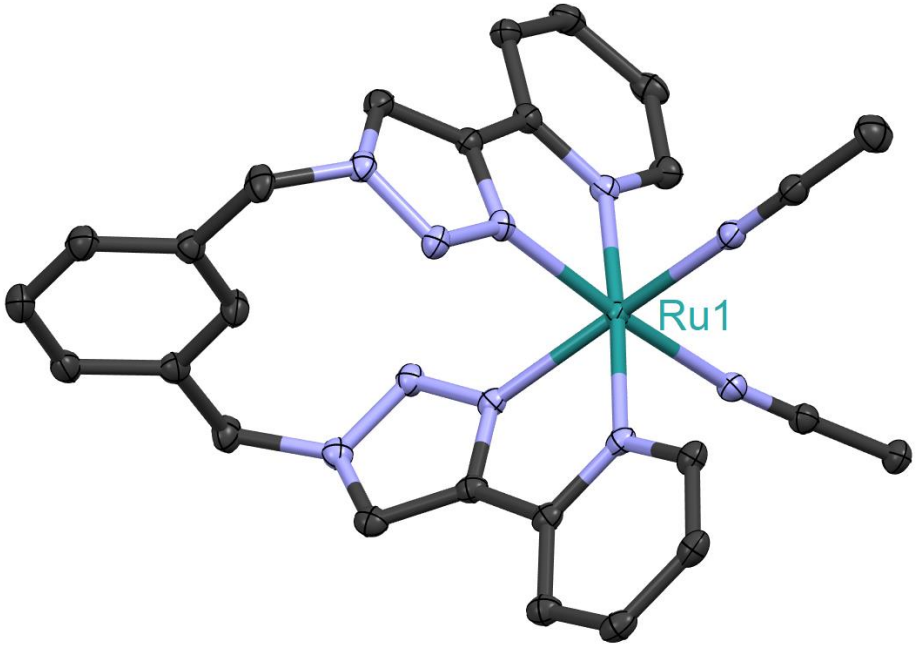

Figure 4.2. X-ray structure of $[Ru(m\text{-xpt})(CH_3CN)_2](BF_4)_2$ (**6**). The thermal ellipsoids are at the 50% probability level. Hydrogen atoms and anions are removed for clarity.

showed broad peaks, perhaps because of oxidation of Ru(II) to Ru(III) during chloride abstraction. In contrast, the reaction in acetonitrile was clean and formed a pure product that was tentatively assigned as $[Ru(bpt)(CH_3CN)_2(DMSO)_2](BF_4)_2$ (**7**). We refluxed this complex with bpt ligand for 5 days in an attempt to displace additional DMSO ligands. Although some new peaks could be observed, the peaks of **7** could still be detected. No new crystal was obtained from this crude mixture, so we think acetonitrile is strongly bound to the ruthenium. After that, acetone was tested as solvent, since it is a coordinating ligand that could stabilize a Ru(II) intermediate (before addition of bpt), and at the same time the metal–acetone coordination bond should be weak enough to allow coordination of the second bpt molecule. The reaction in acetone was successful. The crude mixture couldn't be purified by column chromatography using different solvent systems that we tried, but crystals of (*OC*-6-32)-$[Ru(bpt)_2(DMSO)_2](PF_6)(SiF_6)_{0.5}$ (**8**) could be isolated, albeit with low yield; see Figure 4.3. We used $AgPF_6$ for removing the chlorides; however, the crystal structure of **8** showed both SiF_6^{2-} and PF_6^-. We believe this is because the new batch of $AgPF_6$ that we used for this experiment was contaminated with Ag_2SiF_6. Therefore, we repeated this reaction using AgOTf, and this formed crystals of (*OC*-6-32)-$[Ru(bpt)_2(DMSO)_2](OTf)_2$ (**9**); see Experimental section. Since **8** and **9** still contain two DMSO ligands, we surmised that this will be a difficult approach for making the desired $[Ru(bpt)_2(H_2O)_2]^{2+}$ complex.

Another approach to preparing Ru(II) complexes of heterocyclic ligands was reported by Yi et al.: refluxing $[(COD)RuCl_2]_x$ with 4,4-dimethyl-2-(2-pyridyl)oxazoline in dichloroethane forms (pymox-Me_2)$Ru(COD)Cl_2$ and (pymox-Me_2)$_2RuCl_2$; see Figure 4.4.[12]

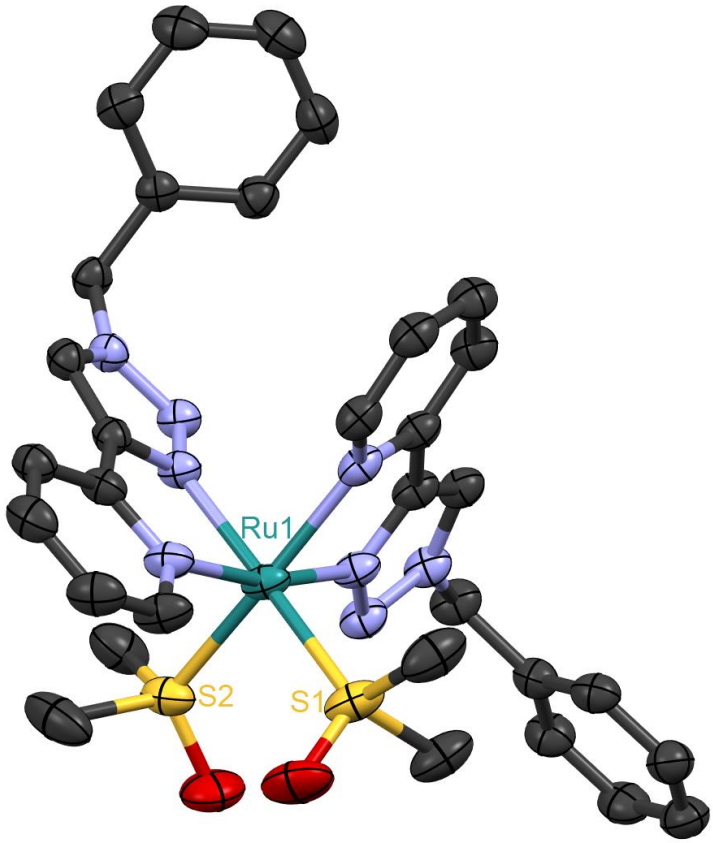

Figure 4.3. X-ray structure of (*OC*-6-32)-[Ru(bpt)$_2$(DMSO)$_2$](PF$_6$)(SiF$_6$)$_{0.5}$ (**8**). The thermal ellipsoids are at the 50% probability level. Hydrogen atoms and anions are removed for clarity.

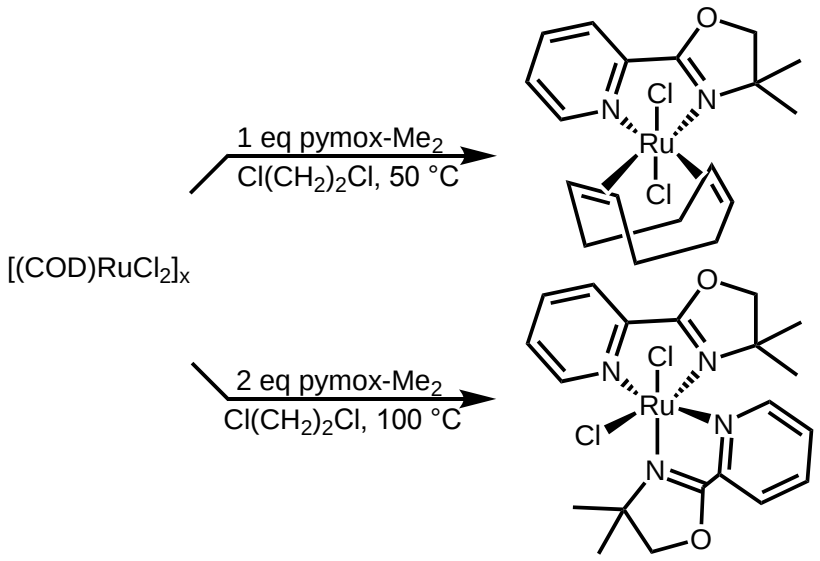

Figure 4.4. Conditions used for synthesis of (pymox-Me$_2$)Ru(COD)Cl$_2$ and (pymox-Me$_2$)$_2$RuCl$_2$ according to Yi et al.[12]

We tried a similar precursor, [Ru(*p*-cymene)Cl_2]$_2$, for our research. Stirring a chloroform solution of [Ru(p-cymene)Cl_2]$_2$ with two equivalents of bpt at room temperature formed [Ru(bpt)(*p*-cymene)Cl]Cl (**10**) readily, which was characterized by ^{1}H NMR. Two more equivalents of the bpt ligand was added to the same solution and refluxed. No considerable change in the major peaks of the ^{1}H NMR spectrum of the crude mixture was observed even after reflux for 3.5 days. At first, we concluded from this observation that bpt couldn't displace the *p*-cymene ligand. However, layering a methanol solution of the crude mixture with ether after a couple of months formed a few orange crystals of (*OC*-6-12)-Ru(bpt)$_2$$Cl_2$ (**11**) which were analyzed by XRD; see Figure 4.5. Thus, in this reaction, bpt had displaced the *p*-cymene ligand, at least in low yield. Building on this observation, we thought using the higher-boiling dichloroethane (b.p. = 83 °C) could help to achieve coordination of the second bpt. However, similar to the experiment in $CHCl_3$, only the mono(bpt)-ligated complex **10** was obtained as the major product in dichloroethane. The mass spectrum of the crude mixture in acetonitrile showed a strong peak of [Ru(bpt)(p-cymene)Cl]$^+$, and beside that three weak peaks belonging to [Ru(bpt)$_2$Cl]$^+$, [Ru(bpt)$_2$(CH_3CN)Cl]$^+$ and [Ru(bpt)$_3$]$^{2+}$ were observed. Then we tested refluxing the reaction mixture in DMF (b.p. = 153 °C). A red/brown solution and brown blackish solid was formed. The solution was dried then redissolved in water/acetone and treated with $AgPF_6$ then NH_4PF_6. A yellow precipitate was collected, dried in air, dissolved in acetonitrile and left for crystallization with ether vapor diffusion. This formed yellow crystals of (*OC*-6-12)-[Ru(bpt)$_2$(CH_3CN)$_2$](PF_6)$_2$ (**12**) which were analyzed by XRD and ^{1}H NMR; see Figure 4.5.

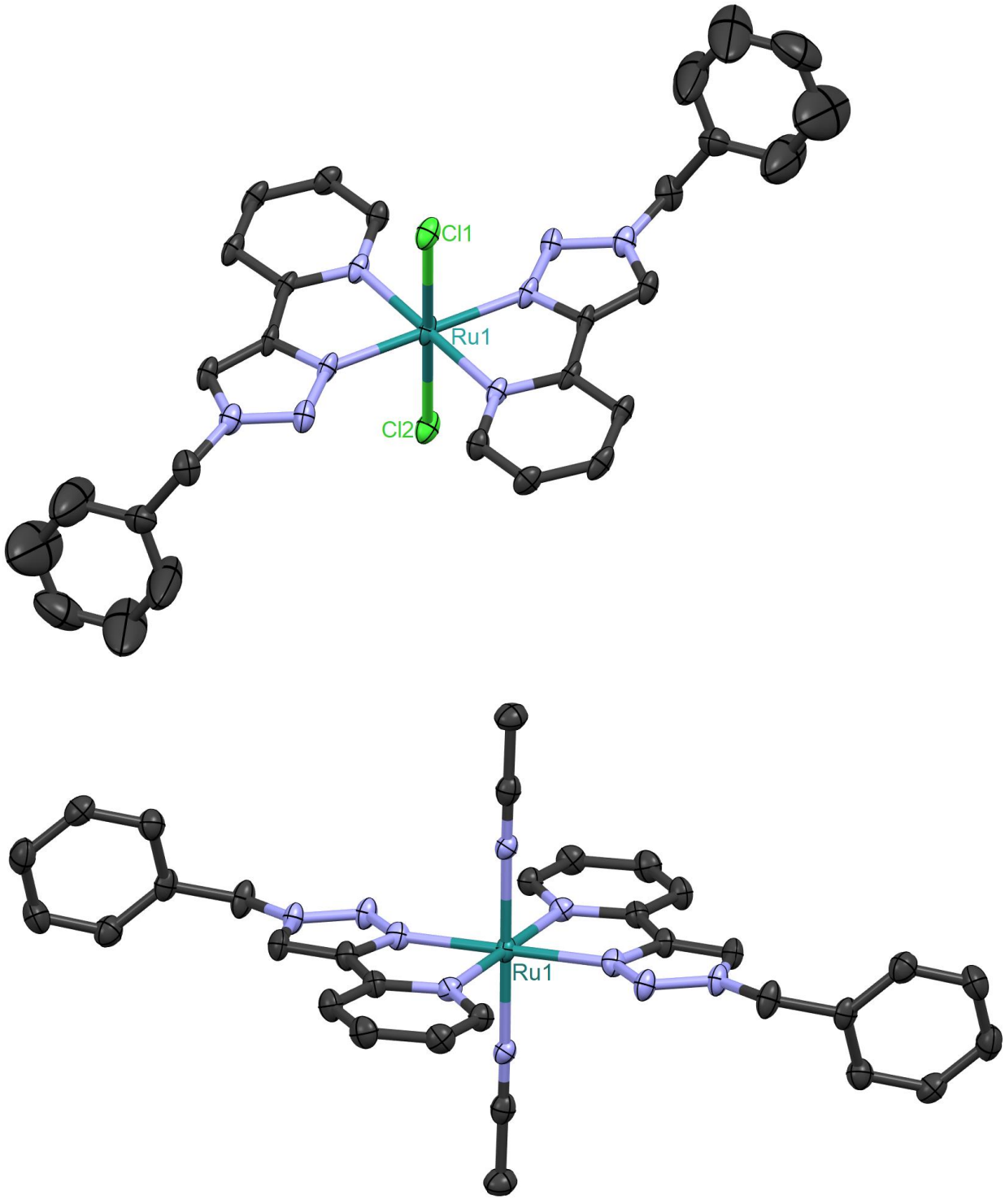

Figure 4.5. X-ray structure of (*OC*-6-12)-Ru(bpt)$_2$Cl$_2$ (**11**) (top) and (*OC*-6-12)-[Ru(bpt)$_2$(CH$_3$CN)$_2$](PF$_6$)$_2$ (**12**) (bottom). The thermal ellipsoids are at the 50% probability level. Hydrogen atoms and anions are removed for clarity.

Since we couldn't find a good approach for making a bis(bpt)-Ru complex in large scale for testing for water oxidation, we decided to make a different kind of ruthenium complex. $[Ru(tpy)(bpy)(H_2O)]^{2+}$ (**13**) with the meridional 2,2′:6,2″-terpyridine (tpy) ligand, is a well-known water oxidation catalyst with TOF of about 15 h^{-1}.[13] The complex was first introduced by Takeuchi et al., and details of its water oxidation activity and robustness were shown by Sakai et al. and then by Berlinguette's group.[14-16] Oxidation of the aqua complex **13** was carried out using $(NH_4)_2[Ce^{IV}(NO_3)_6]$, and it is a pH sensitive process; At pH < 1.5, it undergoes a single electron oxidation to $[Ru^{III}–OH_2]^{3+}$ followed by a one electron/two proton oxidation to $[Ru^{IV}=O]^{2+}$, while in the range 1.5 < pH < 10 it undergoes two one electron/one proton oxidations to form $[Ru^{IV}=O]^{2+}$.

A cyclic voltammogram of **13** at pH = 1 shows two oxidations at 1.04 and 1.23 V (vs. Ag/AgCl (in 3 M NaCl)), corresponding to the $[Ru^{III}–OH_2]^{2+}/[Ru^{III}–OH_2]^{3+}$ and $[Ru^{III}–OH_2]^{3+}/[Ru^{IV}=O]^{2+}$ couples, respectively. Further oxidation of $[Ru^{IV}=O]^{2+}$ to $[Ru^{V}=O]^{3+}$ occurs at 1.8 V, as measured by square wave voltammetry. Berlinguette et al. believe that water oxidation in this system follows the WNA mechanism shown in Figure 4.6, with O_2 evolution as the rate-determining step. Sakai et al. mentioned that after addition of Ce(IV) the absorption of $[Ru^{II}-OH_2]^{2+}$ disappears and doesn't regenerate even after water oxidation completes. However, addition of ascorbic acid regenerated the initial Ru(II) complex quantitatively indicating robustness of the catalyst.[15]

We were interested to test whether a pyridyltriazole analogue of **13**, such as $[Ru(tpy)(bpt)(H_2O)](PF_6)_2$ (**14**), can catalyze water oxidation. With this aim, $Ru(tpy)Cl_3$ was synthesized according to Meyer's procedure[17] and reduced to Ru(II) by ethanol and NEt_3 in the presence of bpt ligand. The synthetic pathway followed is outlined in Figure 4.7. Because of the

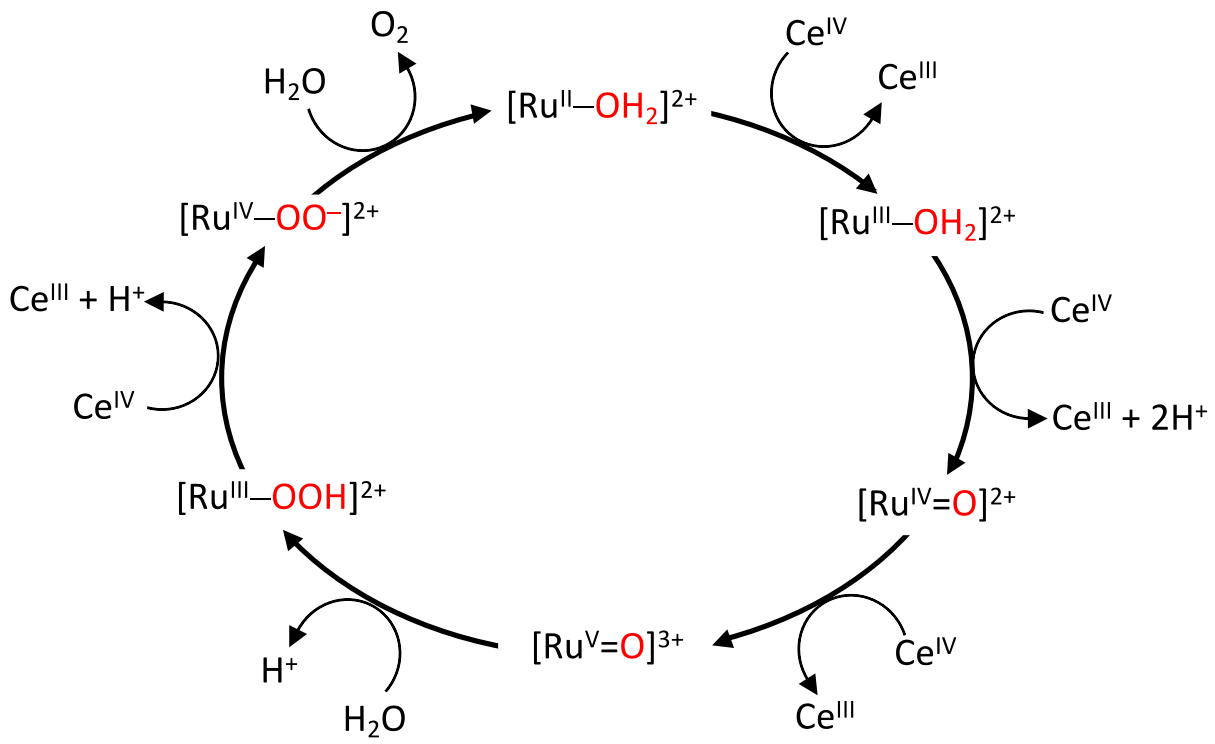

Figure 4.6. Schematic representation of one of the proposed H_2O oxidation pathways with $[Ru(tpy)(bpy)(H_2O)]^{2+}$ catalyst reported by Berlinguette et al.[16]

unsymmetrical structure of bpt, two isomers are possible, depending on whether the pyridine or triazole moiety of bpt is trans to the aqua (or chlorido) ligand. In Figure 4.7, these are called the trans-trz-**14a** and trans-py-**14b** isomers depending on triazole or pyridine is trans to the aqua ligand. In the initial synthesis, the two isomers of [Ru(tpy)(bpt)Cl]Cl (**15**) are formed in ca. 1:3 ratio. They do not elute from a silica gel column by use of common solvents in our lab; therefore, they converted to [Ru(tpy)(bpt)Cl](PF_6) by treatment with NH_4PF_6. Then, [Ru(tpy)(bpt)Cl](PF_6) (**16**) could be separated on silica gel by using a mixture of DCM-acetone as eluent. Most of the fractions collected were a mixture of two isomers; however, we could isolate pure isomers for characterization and further study. The faster-eluting component was identified as trans-trz-

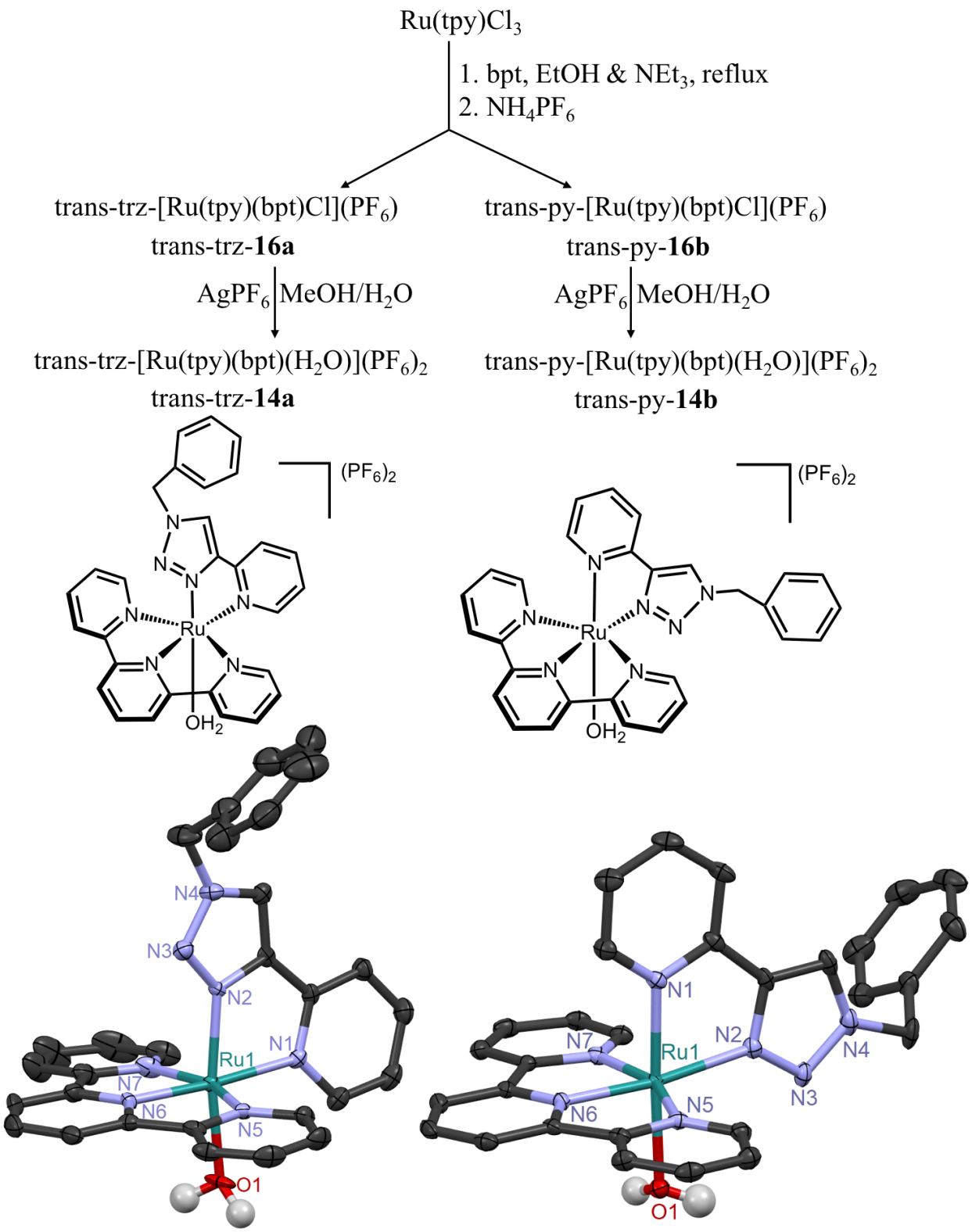

Figure 4.7. Outline of synthetic steps to make trans-trz-**14a** and trans-py-**14b**, and their X-ray structures. The thermal ellipsoids are at the 50% probability level. Hydrogen atoms (except those in OH_2) and anions are removed for clarity.

[Ru(tpy)(bpt)Cl](PF$_6$), trans-trz-**16a**, by X-ray analysis (see Figure 4.7; the structure of the trans-py-**16b** is also shown).

For conversion to the H_2O complexes trans-trz-**14a** and trans-py-**14b**, the two isomers of **16** were dissolved separately in a mixture of methanol and water and treated with $AgPF_6$. The desired aqua complexes [Ru(tpy)(bpt)(H_2O)](PF$_6$)$_2$, trans-trz-**14a** and trans-py-**14b** were isolated and characterized by XRD (see Figure 4.7) and ^{1}H NMR which showed the structure of isomers were remained stable during this reaction. UV/vis spectra of trans-trz-**14a**, trans-py-**14b**, and $Ru(bpy)_3Cl_2$ for comparison (in 0.1 M HNO_3) are shown in Figure 4.8. For the two isomers of **14**, the two peaks between 350 and 500 nm are assigned to MLCT transitions, and the shoulders above 500 nm probably belong to ruthenium d-d absorption. The absorption peaks for trans-trz-**14a** are slightly red-shifted relative to trans-py-**14b,** but the overall features are same in both isomers.

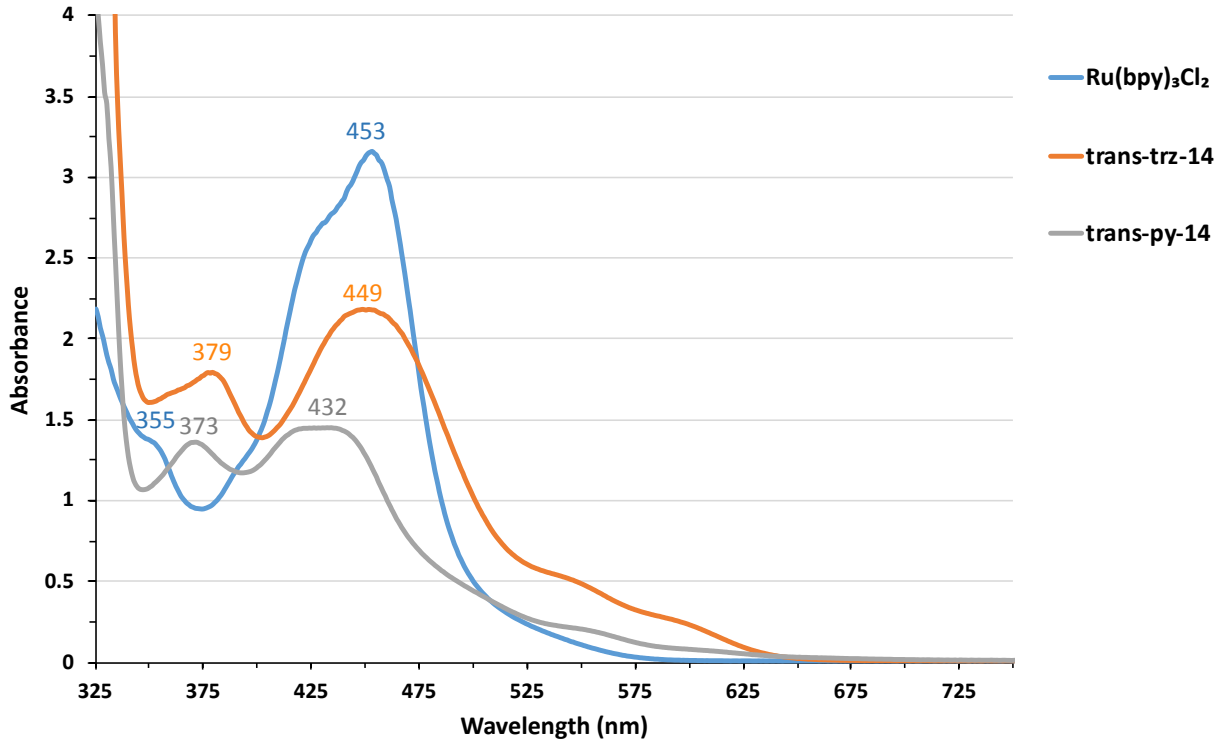

Figure 4.8. UV/vis absorption spectra of the two isomers of **14** (ca. 0.25 mM) and $Ru(bpy)_3Cl_2$ (ca. 0.30 mM) in 0.1 M HNO_3 (pH = 1).

Cyclic voltammetry (CV) in 0.1 M HNO_3 showed reversible peaks for trans-trz-**14a** and trans-py-**14b** at 0.858 V (ΔEp = 0.075 V) and 0.862 V (ΔEp = 0.063 V) vs Ag/AgCl at 500 mVs^{-1} scan rate, respectively; see Figure 4.9. These peaks are probably due to the $Ru^{II/III}$ couple, because of their similarity to many other Ru electrochemical systems. It would be helpful to check whether this is a one- or two-electron process by addition of a known amount of a standard such as $Ru(bpy)_3^{2+}$. When the scan rate decreased to 100 mVs^{-1} a shoulder close to the reduction peak was observed for both complexes; see Figure 4.9. We didn't observe any peaks at higher potentials that might be attributable to further oxidation of Ru(III). However, the current at 1.8 V is enhanced by 1.63 and 1.82 times in trans-trz-**14a** and trans-py-**14b** solutions, respectively, relative to the 0.1 M HNO_3 solution without the ruthenium complexes. This small current enhancement might be due to water oxidation, so we investigated these complexes further.

To test whether trans-py-**14b** can catalyze the oxidation of water to O_2, we mixed 0.0063 mmol (dissolved in 2 mL of 0.1 M HNO_3) of it with 0.18 mmol of ceric ammonium nitrate (CAN) in 2 mL of 0.1 M HNO_3. Gas bubbles were observed for about 5 min; the solution gradually became turbid during this period, and then the color of the solution changed to green after 30 min; see Figure 4.10. A similar experiment with trans-trz-**14a** showed it is less reactive. Formation of only a few gas bubbles was observed and the solution over 1 h became cloudy and after a day the color of solution changed to green; see Experimental Section. Formation of a precipitate and changes in the color of solution to green indicate that the complexes may be undergoing decomposition or side reactions. We will try to detect products by running a similar reaction on a larger scale and isolating and identifying the reaction products.

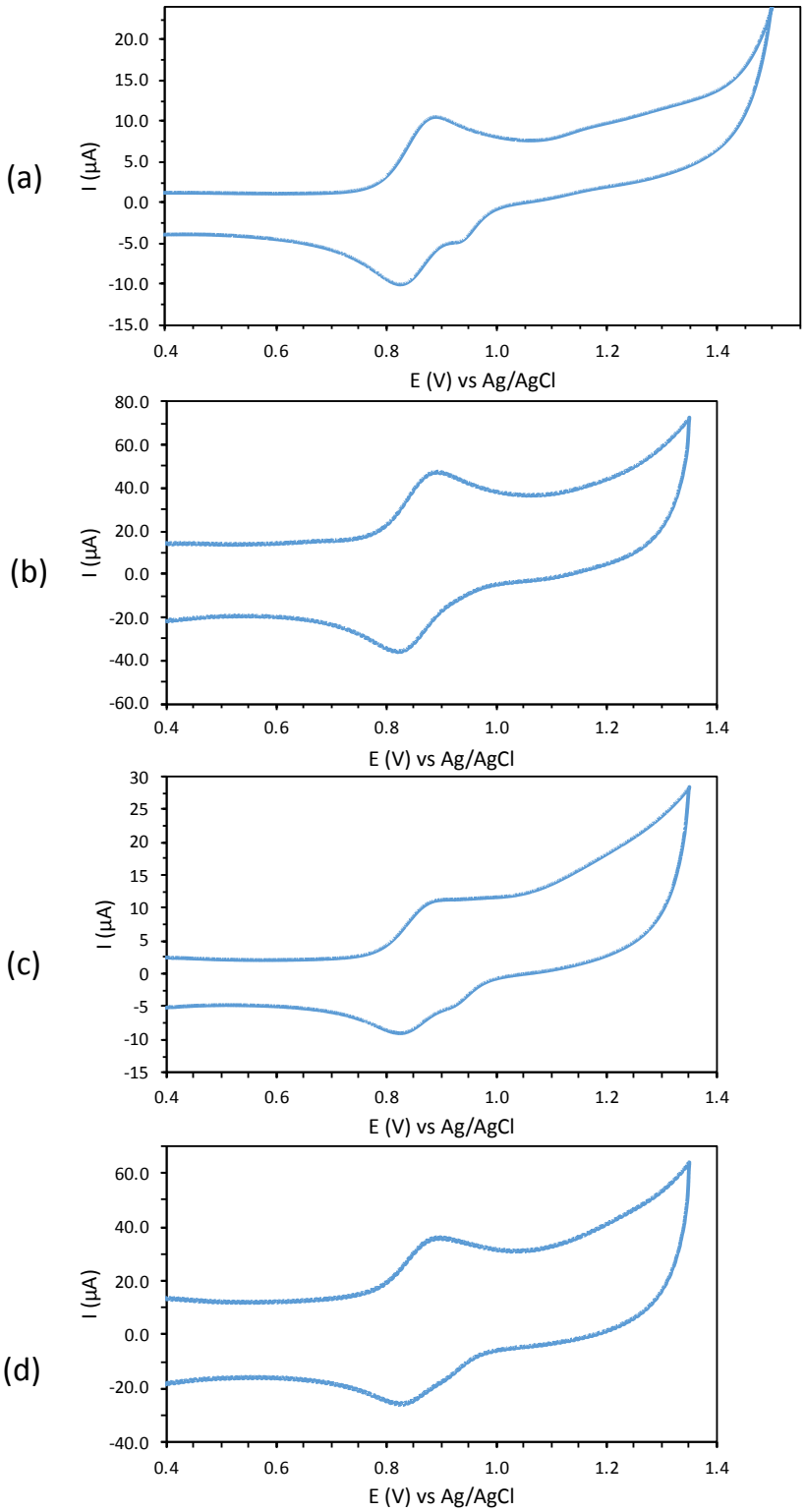

Figure 4.9. CV of trans-trz-**14a** at a scan rate of (a) 100 and (b) 500 mV s^{-1} and trans-py-**14b** at a scan rate of (c) 100 and (d) 500 mV s^{-1}. The solutions are in 0.1 M HNO_3 and voltammograms are recorded on a glassy carbon working electrode with a Pt wire auxiliary electrode and Ag/AgCl reference electrode at 25 °C.

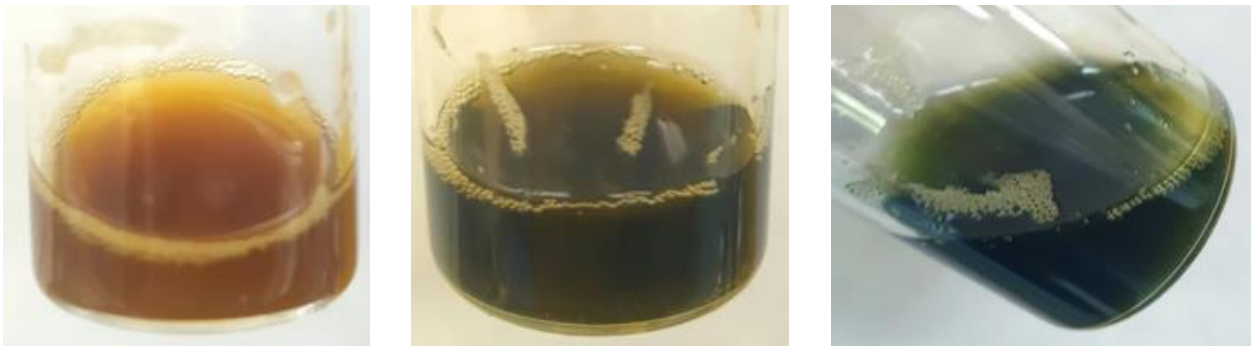

(a) (b) (c)

Figure 4.10. The color changes in a solution of CAN and trans-py-**14b** after (a) 5 min, (b) 15 min, (c) 30 min.

4.3. Experimental

General

fac-[$RuCl_2$(DMSO-*S*)$_3$(DMSO-*O*)]$RuCl_2$(DMSO)$_4$ was prepared following the literature procedure[6] and characterized by comparison with the ^{1}H NMR spectra of Bratsos & Alessio.[18] Elsewhere in this manuscript, it is referred to as $RuCl_2$(DMSO)$_4$ for simplicity. Ru(tpy)Cl_3,[17] bpt,[19] and xpt[20] were prepared according to literature procedures. Bpt was purified by trituration with ether. Tpy was purchased from Beantown Chemical. NMR spectra were recorded on Bruker 400 MHz (Avance 400) or 500 MHz (Avance 500) spectrometers. Electrospray ionization mass spectra were measured on an Agilent 6210 instrument. UV/vis spectra were recorded on an Aviv 14DS spectrometer (Aviv Biomedical). CV measurements were performed using an EC Epsilon EClipse potentiostat/galvanostat and recorded on a glassy carbon working electrode with a Pt wire auxiliary electrode and Ag/AgCl reference electrode at 25 °. Ellipsoids in the X-ray structures are shown at the 50% probability level, and hydrogen atoms and uncoordinated solvent molecules are omitted for clarity. For some X-ray structures uncoordinated counter anions are also omitted.

Synthesis of (*OC*-6-14)-Ru(bpt)(DMSO)$_2$Cl$_2$ (2).

$RuCl_2(DMSO)_4$ (101.5 mg, 0.2095 mmol) and bpt (98.3 mg, 0.416 mmol) were mixed with 20 mL acetone and the mixture refluxed for 12 h under nitrogen. The bright-yellow solution was allowed to cool to room temperature and the acetone evaporated *in vacuo*. Excess bpt was removed from the product as follows: The solid was sonicated with 5 mL of ether, the suspension centrifuged, and the solvent decanted. This process was repeated twice more. The resulting yellow solid was dried in air; yield 110 mg (93%). This material contains ca 95% (*OC*-6-14)-Ru(bpt)(DMSO)$_2$Cl$_2$ (**2**) and 5% (*OC*-6-32)-Ru(bpt)(DMSO)$_2$Cl$_2$ (**3**) by NMR. Yellow single crystals of **2** were obtained by vapor diffusion of ether into a solution of the complex in ethanol–chloroform (1:1 v/v). ^{1}H NMR (400 MHz, $CDCl_3$) δ 10.59 (d, J = 5.04, 1H, H1), 7.93 (s, 1H, H7), 7.81 (td, J_1 = 7.68 Hz, J_2 = 1.32 Hz, 1H, H3), 7.64 (d, J = 7.56, 1H, H4), 7.46–7.51 (m, 4H, H2, H11-13), 7.35–7.39 (m, 2H, H10, H14), 5.65 (s, 2H, H8), 3.60 (s, 6H, DMSO), 3.58 (s, 6H, DMSO). ^{13}C NMR (100 MHz, $CDCl_3$) δ 155.64 (C1), 148.92, 148.82 (C5, C6), 137.37(C3), 131. 94 (C9), 129.90, 129.70 (C11/C13, C12), 128.84 (C10/C14), 124.73 (C2), 122.39 (C7), 120.77 (C4), 56.20 (C8), 46.42 (DMSO), 44.53 (DMSO). ESI–MS: m/z [Ru(bpt)(DMSO)$_2$Cl$_2$+Na]$^+$ 580.9665 (calculated: 580.9686).

Synthesis of (*OC*-6-32)-Ru(bpt)(DMSO)$_2$Cl$_2$ (3).

$RuCl_2(DMSO)_4$ (513.5 mg, 1.059 mmol) and bpt (361.5 mg, 1.530 mmol) were mixed with 15 mL toluene and the mixture refluxed for 16 days under nitrogen, then cooled to room temperature. The resulting yellow suspension was filtered and the solid washed with fresh toluene and ether, then dried in air. Yield 590 mg (98%) of yellow solid **3**. For crystallization, a sample was mixed with acetonitrile, heated to boiling, allowed to cool, centrifuged, and the yellow decantate used for ether vapor diffusion. After a day, yellow cube-shaped crystals were obtained. ^{1}H NMR (400 MHz,

$CDCl_3$) 9.86 (d, J = 5.68, 1H, H1), 7.96 (s, 1H, H7), 7.87 (td, J_1 = 7.68 Hz, J_2 = 1.48 Hz, 1H, H3), 7.66 (d, J = 7.76 Hz, 1H, H4), 7.43–7.53 (m, 4H, H2, H11-13), 7.32–7.37 (m, 2H, H10, H14), 5.67 (m, 2H, H8), 3.69 (s, 3H, DMSO), 3.55 (s, 3H, DMSO), 3.12 (s, 3H, DMSO), 3.07 (s, 3H, DMSO). ^{13}C NMR (100MHz, DMSO-d^6) 152.02, 149.91, 149.52, 138.72, 135.27, 129.45, 129.20, 128.77, 125.69, 124.53, 121.39, 55.45, 46.55, 45.20, 44.70, 43.91. ESI–MS: m/z $[Ru(bpt)(DMSO)_2Cl_2+Na]^+$ 580.9670 (calculated: 580.9686).

Treatment of (*OC*-6-32)-Ru(bpt)(DMSO)$_2$Cl$_2$ (3) with bpt; formation of Ru(bpt)$_3$Cl$_2$.

Complex **3** (95.9 mg, 0.170 mmol), bpt (49.1 mg, 0.208 mmol) and 20 mL ethanol were placed in a reaction flask. The yellow suspension was refluxed for 18 h, then cooled to room temperature and centrifuged. The yellow solid was washed with ether and dried in air, then used for different types of crystallization. Ether vapor diffusion into an acetonitrile solution formed yellow crystals. These have a ^{1}H NMR spectrum matching that reported in the literature for *mer*-$Ru(bpt)_3(PF_6)_2$;[3] thus, they are probably *mer*-$Ru(bpt)_3Cl_2$.

^{1}H NMR (400 MHz, CD_3CN) δ 8.86 (s, 1H), 8.82 (s, 1H), 8.75 (s, 1H), 8.15 (d, J = 8.2 Hz, 1H), 7.91-8.08 (m, 5H), 7.77 (d, J = 5.2 Hz, 1H), 7.69 (m, 2H), 7.17-7.39 (m, 18H), 5.55-5.60 (m, 6H).

Formation of (*OC*-6-33)-[Ru(*m*-xpt)(CH$_3$CN)$_2$]$^{2+}$.

$RuCl_3 \cdot 3H_2O$ (113.0 mg 0.4322 mmol) was placed in a reaction flask and dissolved in 80 mL mixture of acetonitrile/ethanol (5:3). Then *m*-xpt (170.5 mg, 0.4322 mmol) was dissolved in ethanol and added dropwise. The resulting turbid dark brown mixture was refluxed for 16 h, then the solvents were evaporated. To the residue, 100 mL acetonitrile and $AgNO_3$ (220.2 mg, 1.296 mmol) were added; the mixture was refluxed for 12 h then centrifuged. The dark green supernatant was concentrated in *rota vap* and the solid was used for different types of crystallization. Ether vapor diffusion into an acetonitrile solution of the crude product formed yellow crystals which

were separated and dried in air. The crystals are believed to consist of [Ru(*m*-xpt)(CH_3CN)$_2$](NO_3)$_2$ (**[5](NO_3)$_2$**) because of the similarity of their ^{1}H NMR to that of [Ru(*m*-xpt)(CH_3CN)$_2$](BF_4)$_2$ (**6**), which we have characterized by XRD and ^{1}H NMR (see below).

The ^{1}H NMR spectrum of [Ru(*m*-xpt)(CH_3CN)$_2$](NO_3)$_2$ prepared in this way shows a small amount of an impurity in the 2-3 ppm range, which we attribute to [Ru(CH_3CN)$_5$Cl]$^+$. Ether vapor diffusion into acetonitrile solution of the crude mixture yielded yellow crystals of Ru(CH_3CN)$_5$Cl(NO_3)·Ag(CH_3CN)(NO_3) (**17**); see Figure 4.11.

From a similar reaction crystals of [Ru(*m*-xpt)(CH_3CN)$_2$][Ag(NO_3)$_3$] ([**5**][Ag(NO_3)$_3$]) were obtained. [Ru(*m*-xpt)(CH_3CN)$_2$](BF_4)$_2$ (**6**) was prepared according to the above procedure using $AgBF_4$ instead of $AgNO_3$; see Figure 4.12.

^{1}H NMR of (*OC*-6-33)-[Ru(*m*-xpt)(CH_3CN)$_2$](NO_3)$_2$ (400 MHz, CD_3CN) δ 9.22 (d, J = 5.56 Hz, 2H, H2), 8.58 (s, 2H, H8), 8.16-8.18 (m, 4H, H3 & H5), 7.66-7.70 (m, 2H, H4), 7.26-7.37 (m, 4H, H11 & H12 & H13), 5.51-5.62 (m, 4H, H9), 2.39 (s, 6H, H14).

^{1}H NMR of (*OC*-6-33)-[Ru(*m*-xpt)(CH_3CN)$_2$](BF_4)$_2$ (400 MHz, CD_3CN) δ 9.22 (d, J = 5.60 Hz, 2H, H2), 8.55 (s, 2H, H8), 8.09-8.18 (m, 4H, H3 & H5), 7.66-7.70 (m, 2H, H4), 7.26-7.37 (m, 4H, H11 & H12 & H13), 5.51-5.62 (m, 4H, H9), 2.39 (s, 6H, H14).

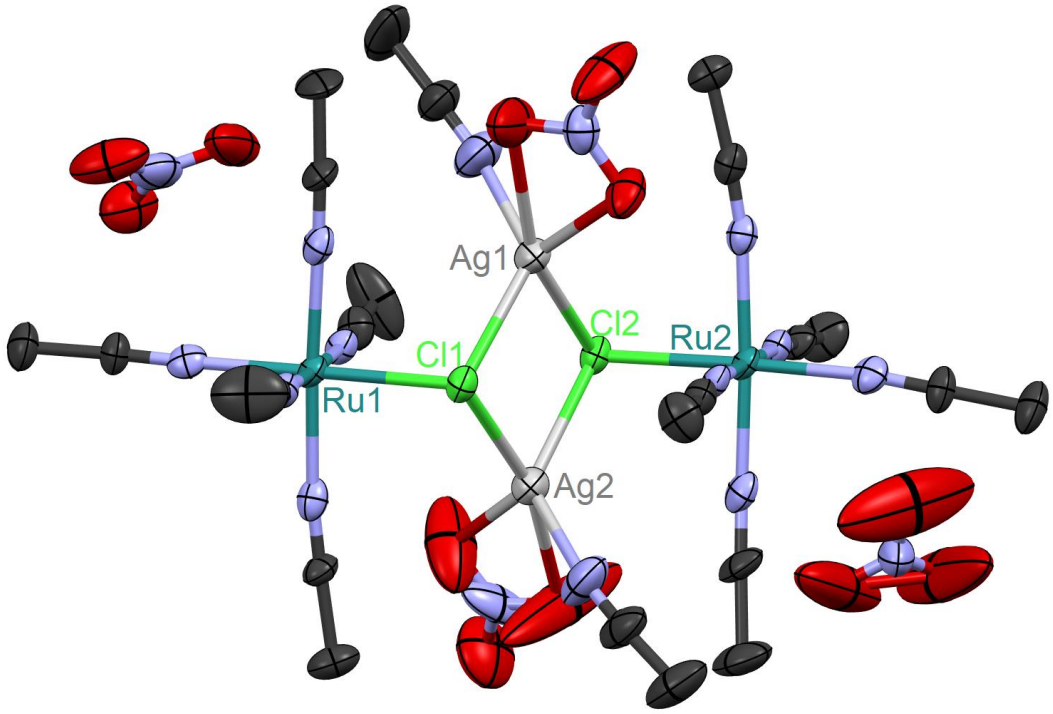

Figure 4.11. X-ray structure of $Ru(CH_3CN)_5Cl(NO_3)\cdot Ag(CH_3CN)(NO_3)$ (**17**). The thermal ellipsoids are at the 50% probability level. Hydrogen atoms are removed for clarity.

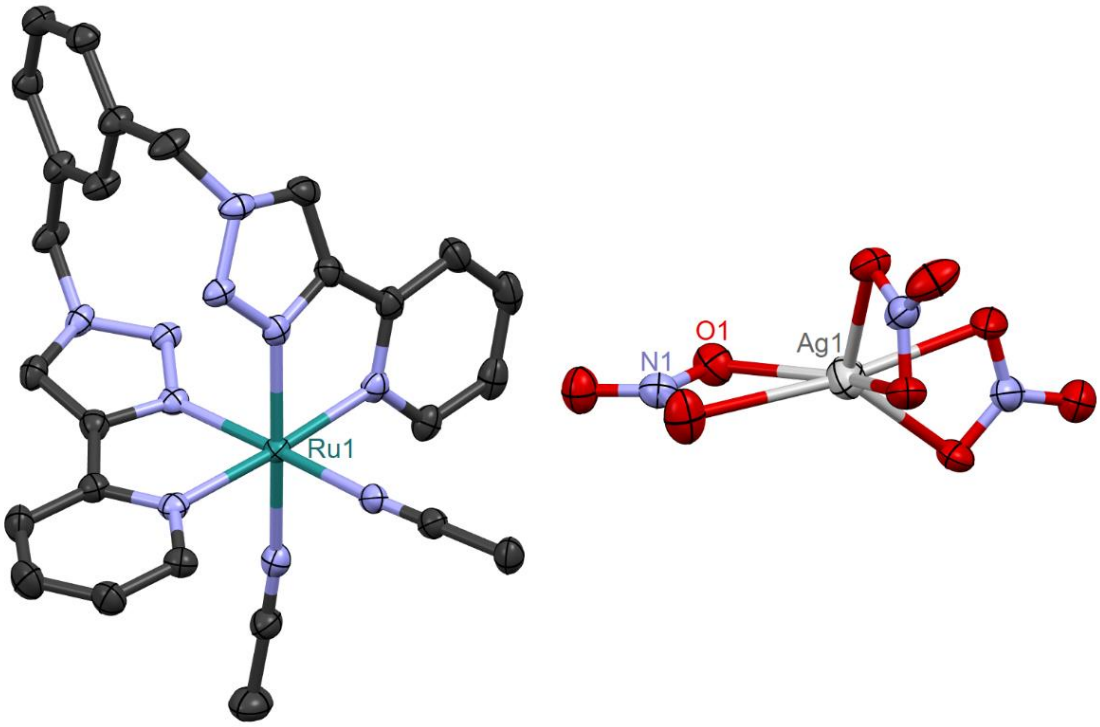

Figure 4.12. X-ray structure of (*OC*-6-33)-[Ru(*m*-xpt)$(CH_3CN)_2$][$Ag(NO_3)_3$] ([**5**][$Ag(NO_3)_3$]). The thermal ellipsoids are at the 50% probability level. Hydrogen atoms are removed for clarity.

Attempt at removing chlorides of 2 and further reaction with bpt in acetonitrile solution.

(*OC*-6-14)-Ru(bpt)$(DMSO)_2Cl_2$ (**2**) (205.4 mg, 0.3638 mmol), was dissolved in 20 mL of acetonitrile then 144 mg (0.740 mmol) $AgBF_4$ was added. The mixture was refluxed for 3.5 h under N_2 then cooled to room temperature and centrifuged. The supernatant was decanted and evaporated; ^{1}H NMR of the residue showed complete conversion of **2** to a new species which is tentatively assigned to [Ru(bpt)$(CH_3CN)_2(DMSO)_2](BF_4)_2$ (**7**). A bpt solution (86.3 mg, 0.365 mmol in 5 mL acetonitrile) was added to the crude mixture dropwise and the resulting solution was refluxed for 5 days under N_2. Even after that second treatment with bpt, peaks belonging to **7** could be detected in the ^{1}H NMR of the product mixture. Although some new peaks could also be observed, no new product could be isolated.

Synthesis of (*OC*-6-32)-[Ru(bpt)$_2$(dmso)$_2$](PF$_6$)(SiF$_6$)$_{0.5}$ (8) and (*OC*-6-32)-[Ru(bpt)$_2$(dmso)$_2$](OTf)$_2$ (9).

Complex **2** (194.0 mg, 0.3437 mmol), $AgPF_6$ (182.5 mg, 0.7218 mmol) and acetone (15 mL) were placed in a reaction flask and the mixture was refluxed for 22 h under N_2. ^{1}H NMR showed complete disappearance of **2**. The mixture was centrifuged and the supernatant was transferred to a new reaction flask. Bpt (163.7 mg, 0.6928 mmol) was dissolved in 1.5 mL of acetone and added to the above solution dropwise while stirring. The solution was refluxed for 7 h under N_2, then cooled to room temperature and the solvent was removed. Crystallization samples were set up with various solvent mixtures. Good quality crystals of **8** were obtained from ether vapor diffusion into an ethanol or DMF solution of the crude mixture, see Figure 4.3, which unexpectedly contained SiF_6^{2-} anion. We guess the batch of $AgPF_6$ used in this experiment was contaminated with Ag_2SiF_6.

Similar reaction but using complex **3** as starting material gave same product. Following the above procedure and using complex **2** (87.0 mg, 0.154 mmol), AgOTf (90.0 mg, 0.350 mmol) and bpt (40.9 mg, 0.173 mmol) formed **9**; see Figure 4.13.

^{1}H NMR of **8** (400 MHz, CD_3CN) δ 9.69 (d, J = 5.2 Hz, 1H), 8.89 (s, 1H), 8.67 (s, 1H), 8.28 (dt, J_1 = 8 Hz, J_2 = 1.6 Hz, 1H), 8.15 (d, J = 7.2 Hz, 1H), 7.97-8.04 (m, 2H), 7.81-7.85 (m, 1H), 7.42-7.52 (m, 6H), 7.26-7.40 (m, 4H), 7.04 (d, J = 7.2 Hz, 1H), 5.90 (d, J = 3.6 Hz, 2H), 5.41 (d, J = 4.0 Hz, 2H), 2.85 (s, 3H), 2.81 (s, 3H), 2.59 (s, 6H).

^{1}H NMR of **9** (400 MHz, CD_3CN) δ 9.69 (d, J = 6 Hz, 1H), 8.83 (s, 1H), 8.60 (s, 1H), 8.29 (t, J = 7.6 Hz, 1H), 8.13 (d, J = 8 Hz, 1H), 7.95-8.04 (m, 2H), 7.83 (t, J = 7.2 Hz, 1H), 7.42-7.50 (m, 6H), 7.27-7.40 (m, 4H), 7.03 (d, J = 7.6 Hz, 2H), 5.90 (d, J = 4.8, 2H), 5.41 (d, J = 4.8, 2H), 2.86 (s, 3H), 2.81 (s, 3H), 2.59 (s, 6H).

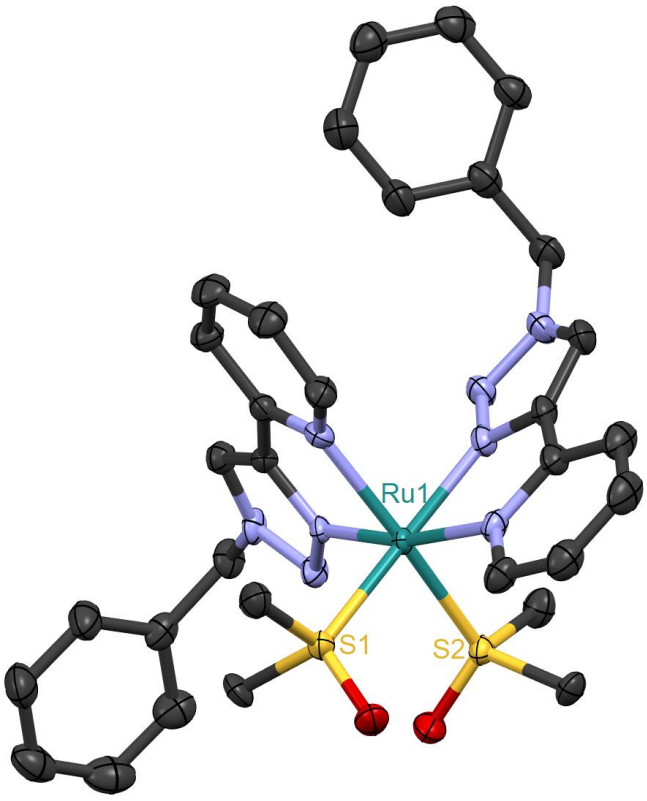

Figure 4.13. X-ray structure of (*OC*-6-32)-$[Ru(bpt)_2(dmso)_2](OTf)_2$ (**9**). The thermal ellipsoids are at the 50% probability level. Hydrogen atoms and anions are removed for clarity.

Synthesis of [Ru(bpt)(*p*-cymene)Cl]Cl (10) and (*OC*-6-12)-Ru(bpt)$_2$Cl$_2$ (11) using [Ru(p-cymene)Cl$_2$]$_2$ precursor.

[Ru(*p*-cymene)Cl$_2$]$_2$ (21.6 mg, 0.0353 mmol) and 8 mL chloroform were placed in a reaction flask. Bpt (17.1 mg, 0.0721 mmol) was dissolved in 5 mL of chloroform and added to the above solution dropwise. The solution was stirred at room temperature for 5 h under N_2 and complete conversion to **10** was observed by ^{1}H NMR. Then 17.0 mg (0.0716 mmol) bpt was added to the solution and stirred at room temperature for a day. No change in ^{1}H NMR of the crude mixture was observed, so the solution was refluxed for 4 days then the solvent was evaporated in *rota vap*. Complex **10** didn't react with bpt judged by ^{1}H NMR of crude mixture. However, when the crude mixture was used for different kinds of crystallization, diffusion of ether into a methanolic solution of the crude mixture formed crystals of **11** after a couple of months; see Figure 4.5.

^{1}H NMR of **10** (400 MHz, CD_3CN) δ 10.27 (s, 1H, H8), 9.28 (d, J = 5.6 Hz, 1H, H2), 8.52 (d, J = 8 Hz, 1H, H5), 7.93 (t, J = 7.6 Hz, 1H, H3), 7.37-7.56 (m, 6H, H2 & H11-13), 5.64-5.88 (m, 6H, H9 & H14 & H15), 2.69 (m, 1H, H17), 2.22 (s, 3H, H20), 1.12 (d, J = 6.8 Hz, 3H, H18 or H19), 1.02 (d, J = 6.8 Hz, 3H, H18 or H19).

A similar reaction was carried out by mixing [Ru(*p*-cymene)Cl$_2$]$_2$ and 4 equivalents of bpt in dichloroethane and refluxing the mixture for eight days under N_2. To analyze the product mixture, instead of growing crystal which takes a long time, after evaporation of the solvents a small amount of the solid was dissolved in acetonitrile and used for mass spectrometry. ESI-MS: m/z $[Ru(bpt)_3]^{2+}$ 402.11339 (calcd: 402.11309) $[Ru(bpt)(p\text{-cymene})Cl]^+$ 501.09038 (calcd: 501.09165), $[Ru(bpt)_2Cl]^+$ 603.08537 (calcd: 603.0883) $[Ru(bpt)_2(CH_3CN)Cl]^+$ 644.08861 (calcd: 644.11091).

Synthesis of (*OC*-6-12)-[Ru(bpt)$_2$(CH$_3$CN)$_2$](PF$_6$)$_2$ (12) using [Ru(*p*-cymene)Cl$_2$]$_2$ precursor.

[Ru(*p*-cymene)Cl$_2$]$_2$ (20.8 mg, 0.0339 mmol) and bpt (33.1 mg, 0.139 mmol) were placed in a reaction flask and kept under N_2. Anhydrous DMF (20 mL) was added to the solids, and the yellow/orange solution was refluxed for 16 h under N_2 in which the color of solution was turned to red then to brown. The solution was cooled to room temperature and centrifuged. The supernatant was dried under N_2 flow, then 10 mL water, 37 mL acetone and 34.4 mg (0.136 mmol) $AgPF_6$ was added, and the mixture was refluxed for 4 h then centrifuged. The volume of the supernatant was reduced to ca. 5 mL in *rota vap*. NH_4PF_6 (22.1 mg, 0.136 mmol) was added and the mixture was chilled in refrigerator overnight then centrifuged. The solid was dried under N_2 and used for different types of crystallization. Ether vapor diffusion into an acetonitrile solution of the crude mixture formed yellow crystals of **12** which were characterized by XRD; see Figure 4.5. ^{1}H NMR of **12** (400 MHz, CD_3CN) δ 10.04 (d, J = 5.6 Hz, 2H, H2), 8.74 (s, 2H, H8), 8.07-8.14 (m, 4H, H4 & H5), 7.65-7.69 (m, 2H, H3), 7.46-7.56 (m, 10H, H11-13), 5.90 (s, 4H, H9), 1.86 (s, 6H, H14).

Synthesis of trans-triazole and trans-pyridine isomers of [Ru(tpy)(bpt)Cl](PF$_6$) (16), trans-trz-16a and trans-py-16b.

Ru(tpy)Cl$_3$ (375.6 mg, 0.8523 mmol), 21 mL ethanol and 7 mL water were placed in a reaction flask. LiCl (108.4 mg, 2.557 mmol) and 0.3 mL NEt_3 were added to the mixture while stirring. The mixture was stirred under N_2 for 40 min then an ethanolic solution of bpt (201.4 mg, 0.8524 mmol in 10 mL ethanol) was added. The mixture was refluxed for 2 h under N_2 then cooled to room temperature and solvents were evaporated. ^{1}H NMR of the crude mixture showed formation of trans-trz- and trans-py-[Ru(tpy)(bpt)Cl]Cl (**15a** and **15b**) in 1 to 3 ratio with negligible by-products. The isomers were converted to the PF_6 salts and separated as follows: To the above crude mixture a few mL of a mixture of DCM-acetone (4:1) and 277.8 mg (1.704 mmol) NH_4PF_6 was

added and stirred for 15 min to form a mixture of isomers of [Ru(tpy)(bpt)Cl]PF_6 (**16**) then the mixture was purified by column chromatography using the same solvent system as eluent. Most of the fractions collected were a mixture of isomers, but each of the pure isomers of trans-trz-**16a** and trans-py-**16b** could be obtained in 16% yield.

^{1}H NMR of trans-trz-**16a** (400 MHz, $(CD_3)_2CO$) δ 10.19 (d, J = 4.96 Hz, 1H), 8.92 (s, 1H), 8.69 (d, J = 8.08 Hz, 2H), 8.62 (d, J = 8.04 Hz, 2H), 8.44 (d, J = 7.56 Hz, 1H), (dt, J_1 = 7.88 Hz, J_2 = 1.52 Hz, 1H), 8.18 (t, J = 8.12 Hz, 1H), 8.04 (dt, J_1 = 8.04 Hz, J_2 = 1.56 Hz, 2H), 7.92-9.98 (m, 3H), 7.42-7.46 (m, 2H), 7.22-7.30 (m, 3H), 6.96 (d, J = 7.36 Hz, 2H), 5.47 (s, 2H).

^{1}H NMR of trans-py-**16b** (500 MHz, $(CD_3)_2CO$) δ 9.36 (s, 1H), 8.71 (d, J = 8.08 Hz, 2H), 8.61 (d, J = 8.04 Hz, 2H), 8.14-8.19 (m, 2H), 7.95-8.00 (m, 4H), 7.68-7.73 (m, 3H), 7.50-7.55 (m, 3H), 7.38-7.41 (m, 3H), 6.96-6.99 (m, 1H), 6.15 (s, 2H).

Synthesis of trans-triazole and trans-pyridine isomers of [Ru(tpy)(bpt)(H_2O)](PF_6)$_2$ (14), trans-trz-14a and trans-py-14b.

To trans-trz-**16a** (90.9 mg, 0.121 mmol), 10 mL methanol, 10 mL distilled water and 34.0 mg (0.134 mmol) $AgPF_6$ was added, and the mixture was refluxed for 2 h under N_2. Then the mixture was centrifuged to remove AgCl and the supernatant was poured into a small beaker and kept in the hood for slow evaporation of solvents. After 2-3 days orange/brown crystals of trans-trz-**14a** were obtained and the solid was collected and dried in air (48%). The quality of the crystals was good for XRD. To obtain trans-py-**14b**, a similar procedure was followed using trans-py-**15b** (89.4 mg, 0.119 mmol) and $AgPF_6$ (31.0 mg, 0.123 mmol); yield 51%.

Trans-trz-**14a**: ^{1}H NMR (400 MHz, D_2O) δ 9.41 (d, J = 5.56 Hz, 1H), 8.61 (s, 1H), 8.44 (d, J = 8.16 Hz, 2H), 8.36 (d, J = 8.12 Hz, 2H), 8.22 (d, J = 3.96 Hz, 2H), 8.10 (t, J = 8.08 Hz, 1H), 7.83-7.97 (m, 5H), 7.16-7.32 (m, 5H), 6.82 (d, J = 7.6 Hz, 2H), 5.27 (s, 2H).

Trans-py-**14b**: ^{1}H NMR (400 MHz, D_2O) δ 9.11 (s, 1H), 8.54 (d, J = 8.12 Hz, 2H), 8.40 (d, J = 8.04 Hz, 2H), 8.18 (t, J = 8.2 Hz, 1H), 7.93 (t, J = 8.08 Hz, 2H), 7.86 (d, J = 7.72 Hz, 1H), 7.79 (d, J = 5.24 Hz, 2H), 7.68 (d, J = 6.96 Hz, 2H), 7.52-7.59 (m, 4H), 7.32 (t, J = 6.72 Hz, 2H), 7.17 (d, J = 5.8 Hz, 1H), 6.78 (t, J = 7.4 Hz, 1H), 6.04 (s, 2H).

Water oxidation test with trans-py-14b.

A 0.1 M HNO_3 solution was prepared by dissolving 1 mL of concentrated HNO_3 in deionized water and diluting to 158 mL. Ceric ammonium nitrate (CAN) (98.8 mg, 0.180 mmol) was dissolved in 2 mL of the HNO_3 solution in a vial. The Ru complex (5.5 mg, 0.0063 mmol) was almost dissolved in 2 mL of the HNO_3 solution by several heating and sonication cycles, then it was added to the CAN solution. Evolution of gas was observed and the solution became cloudy (turbid). The color of the solution became slightly greenish and when it was left on the benchtop for about an hour it became green; see Figure 4.10.

A similar test was carried out with trans-trz-**14a**. CAN (99.1 mg, 0.181 mmol) was dissolved in 2 mL of 0.1 M HNO_3. Then trans-trz-**14a** (6.0 mg, 0.0068 mmol) was almost dissolved in 3 mL of the acid by several sonicating and heating cycles, then it was added to the CAN solution. Formation of a very small amount of gas was observed. The solution was clear and yellow at first, became slightly cloudy after 1 h, and turned green after 24 h; see Figure 4.14.

Figure 4.14. A solution of CAN and trans-trz-**14a** (a) stayed clear and yellow and (b) after 1 h it became turbid (c) after 1 day left on benchtop it became green.

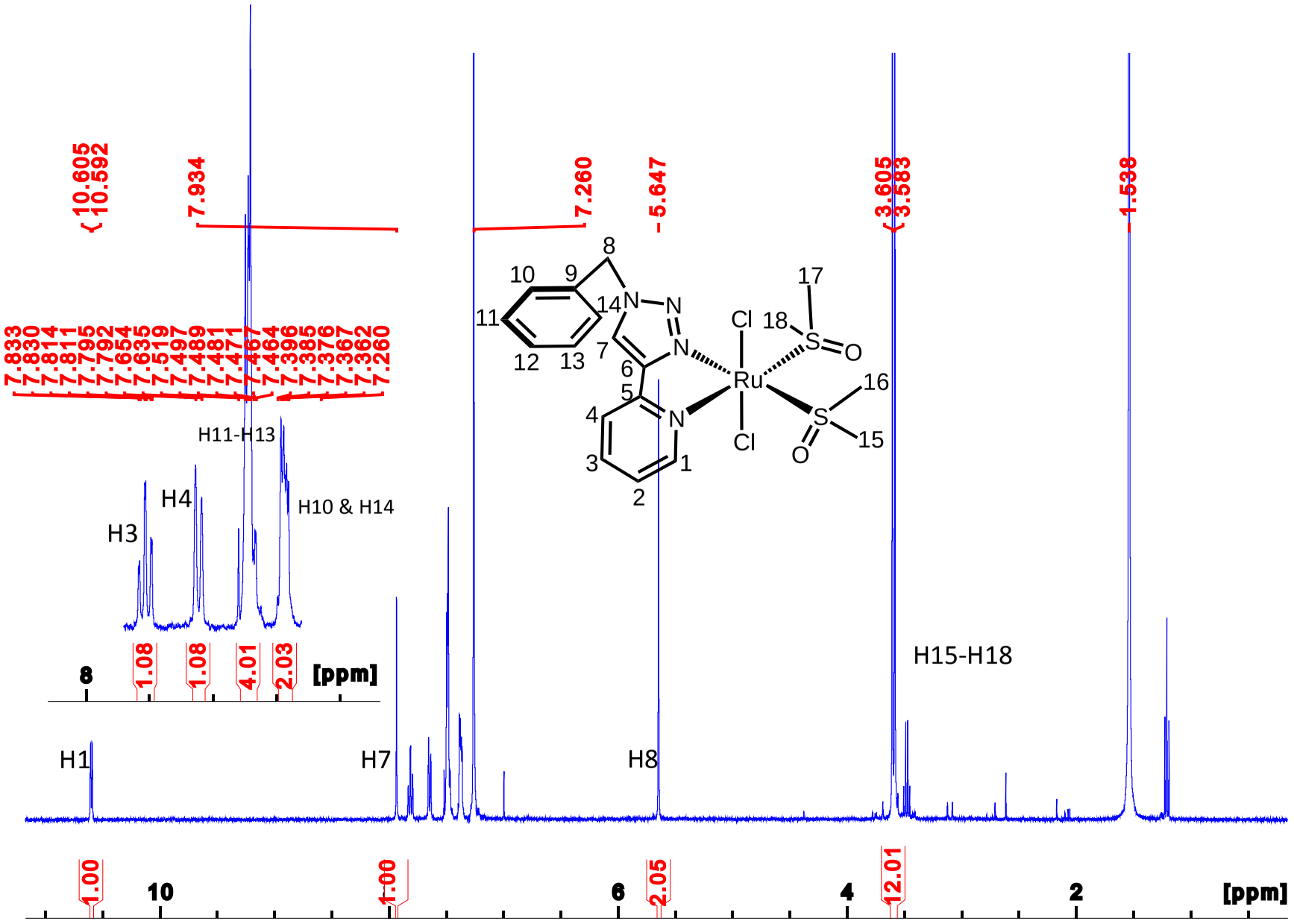

Figure 4.15. ^{1}H NMR of **2** in $CDCl_3$ at 400 MHz. The inset X axis marks are 0.2 ppm apart.

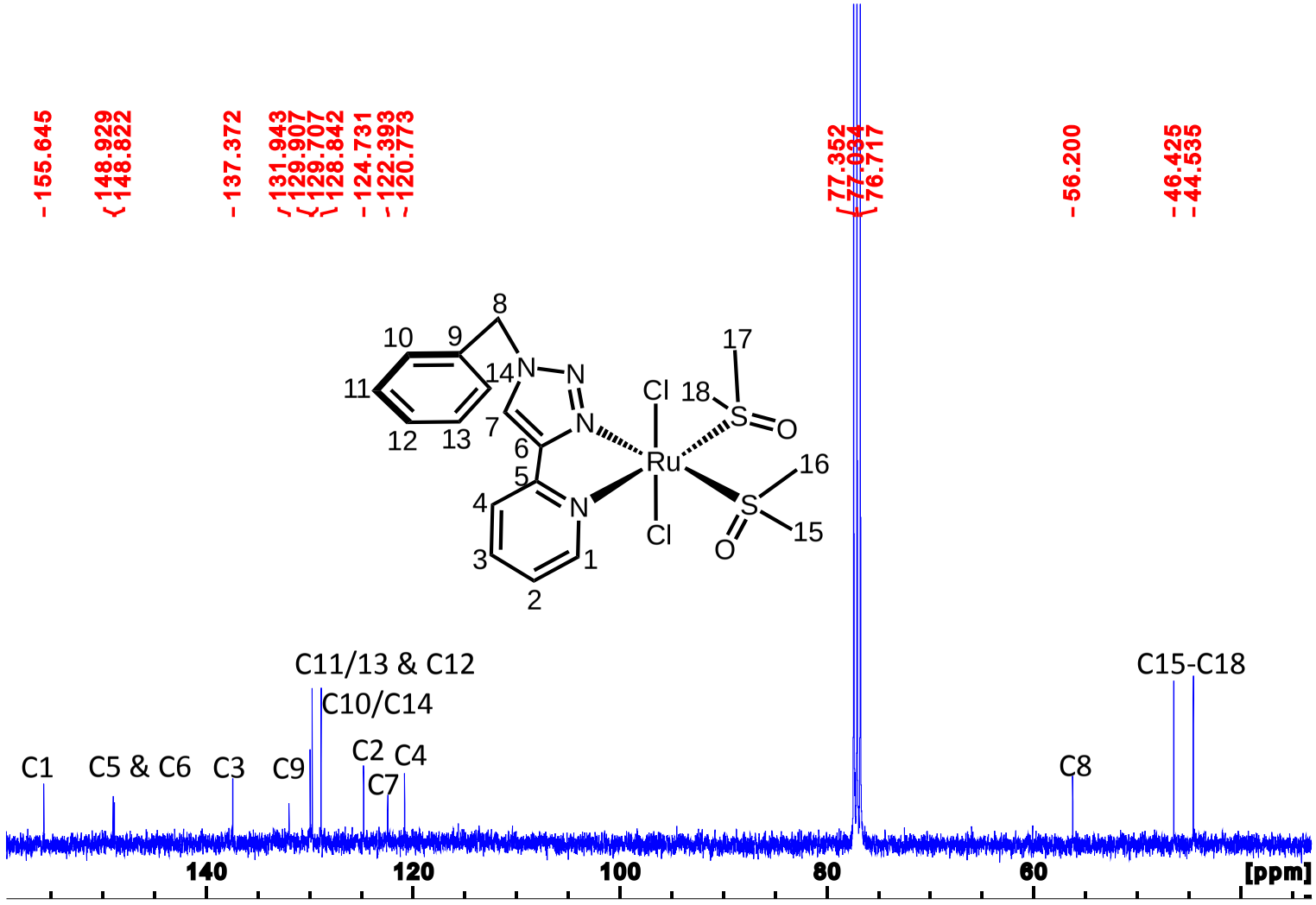

Figure 4.16. ^{1}H NMR of **2** in $CDCl_3$ at 400 MHz.

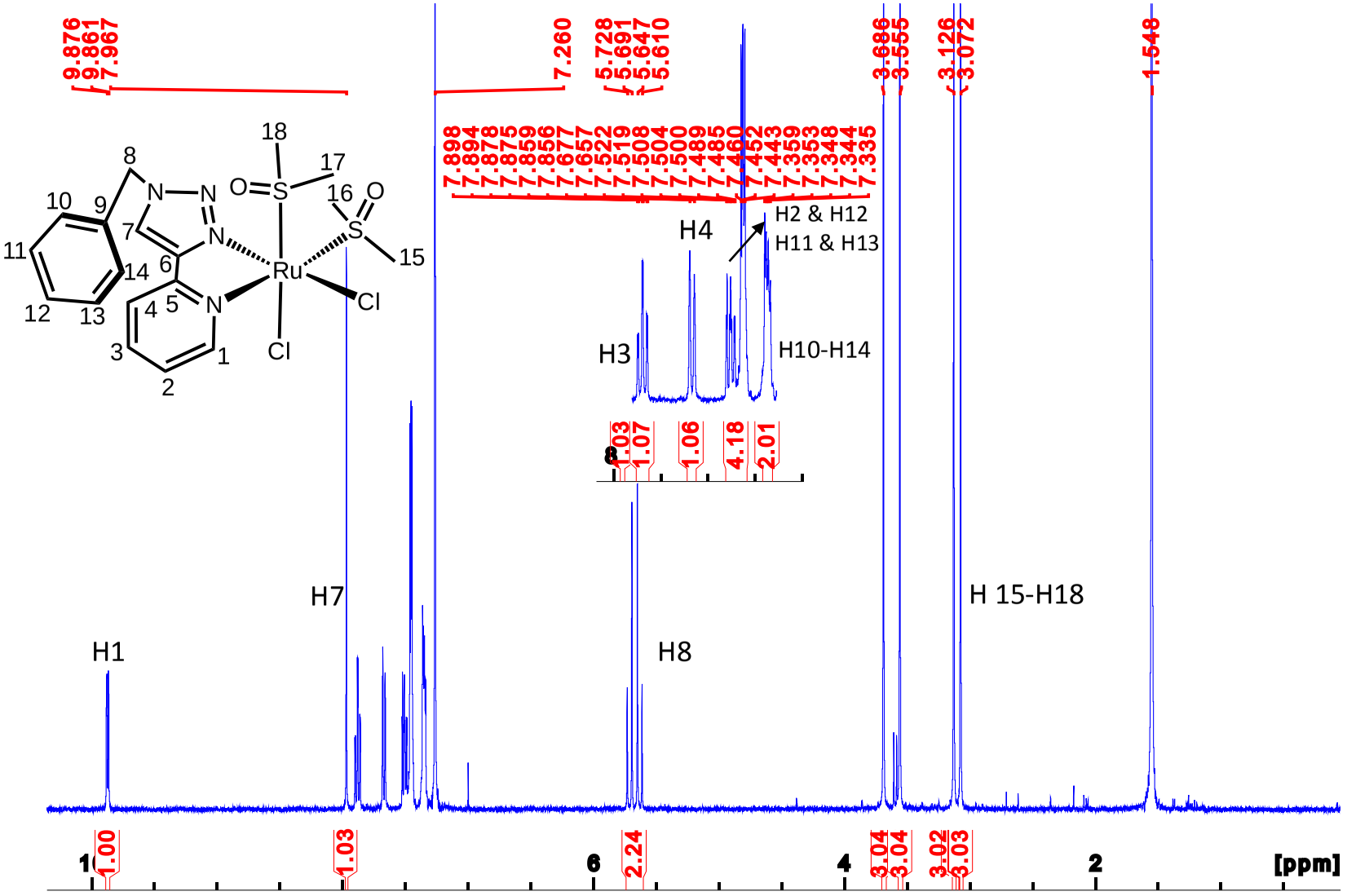

Figure 4.17. ^{1}H NMR of **3** in $CDCl_3$ at 400 MHz. The inset X axis marks are 0.2 ppm apart.

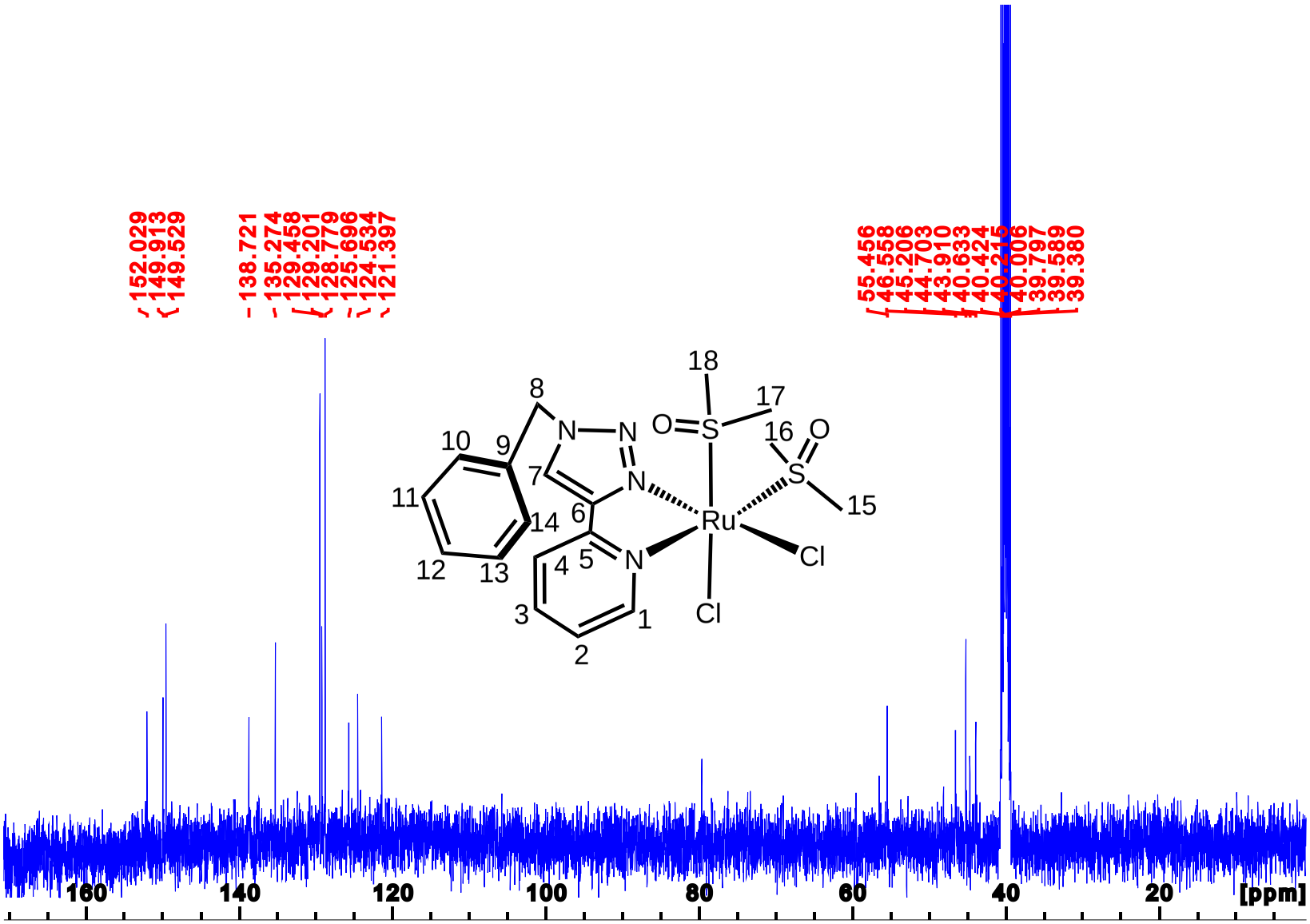

Figure 4.18. ^{1}H NMR of **3** in $(CD_3)_2SO$ at 400 MHz.

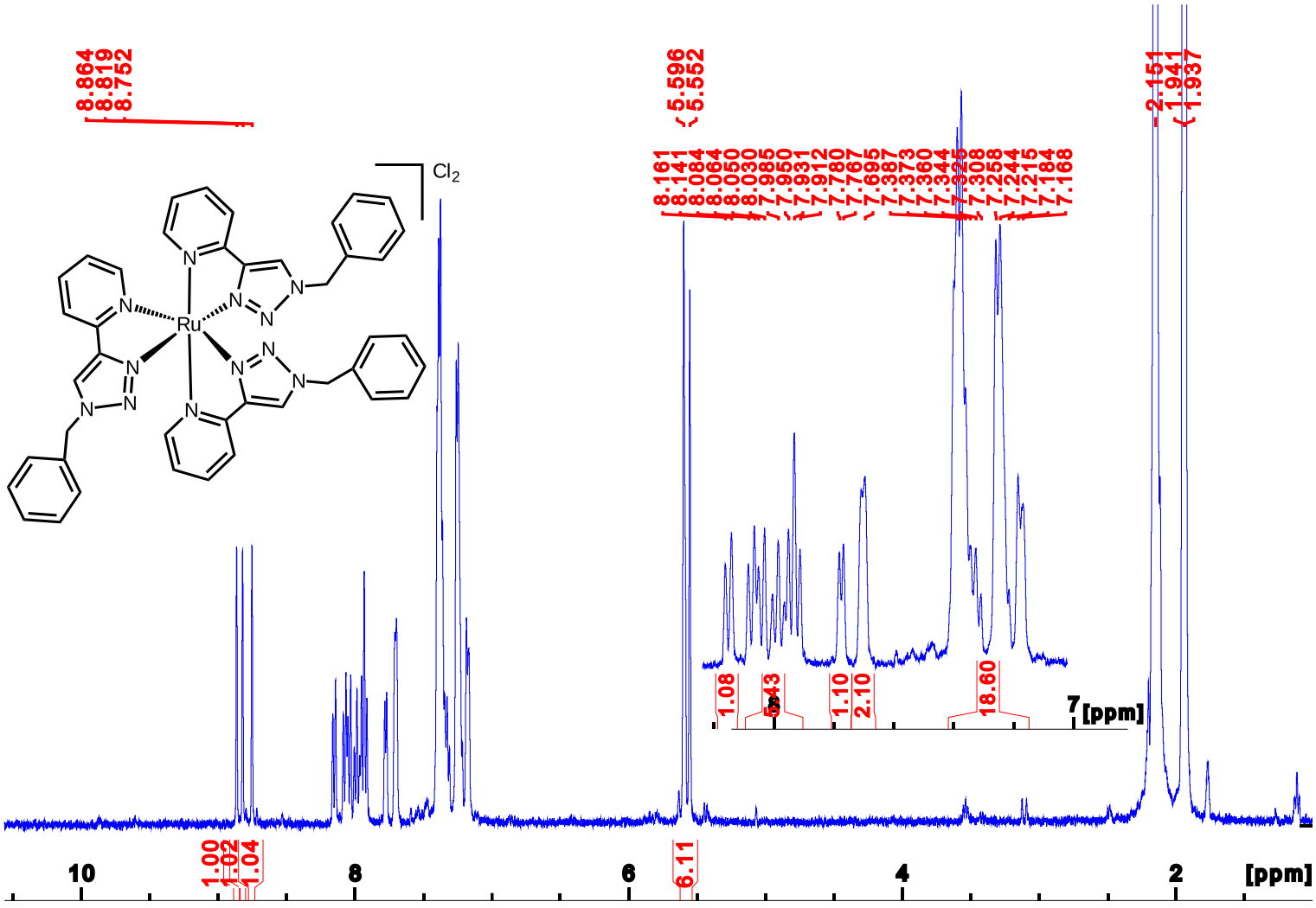

Figure 4.19. ^{1}H NMR of *mer*-Ru(bpt)$_3$Cl$_2$ in CD_3CN at 400 MHz.

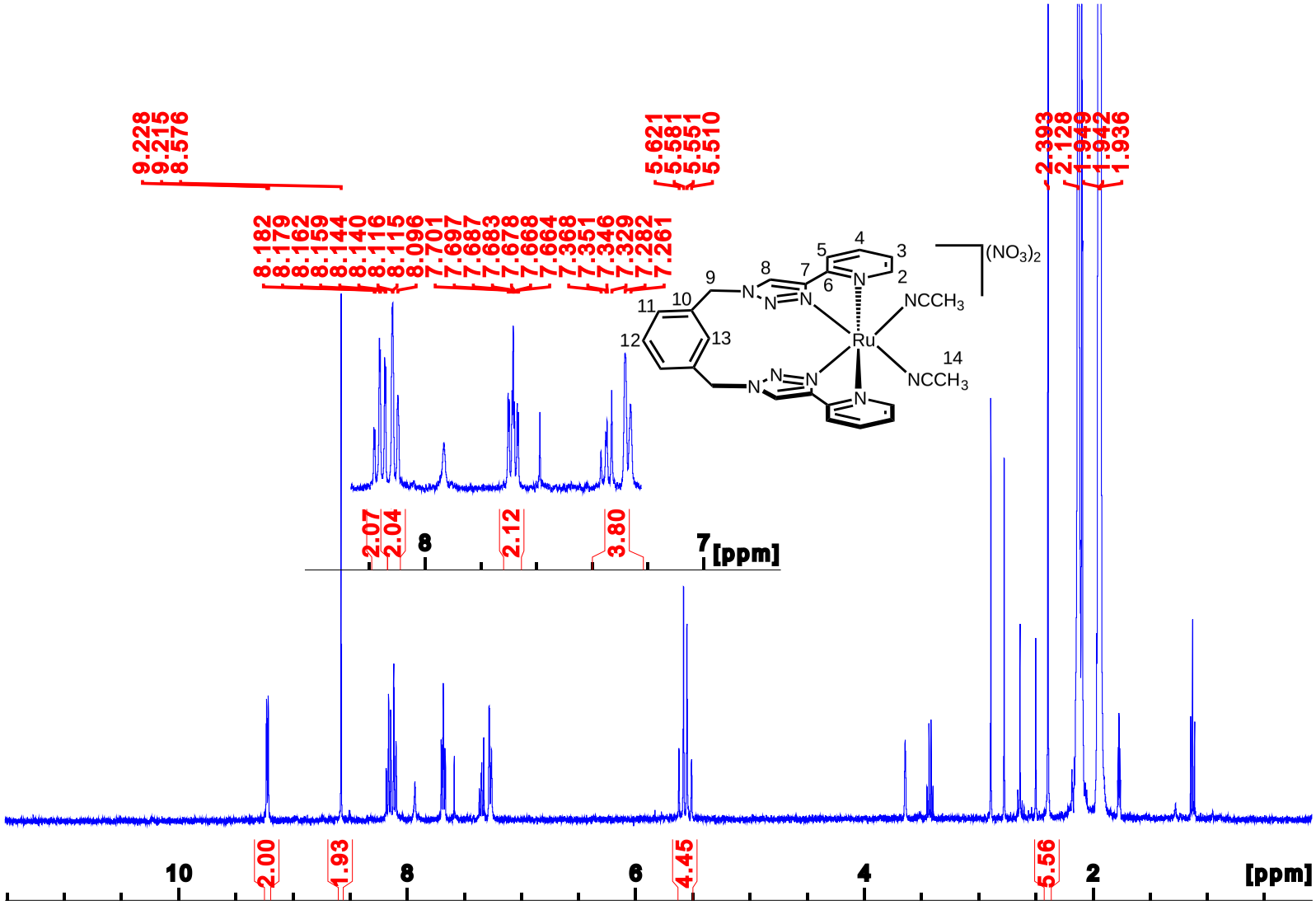

Figure 4.20. ^{1}H NMR of **5** in CD_3CN at 400 MHz.

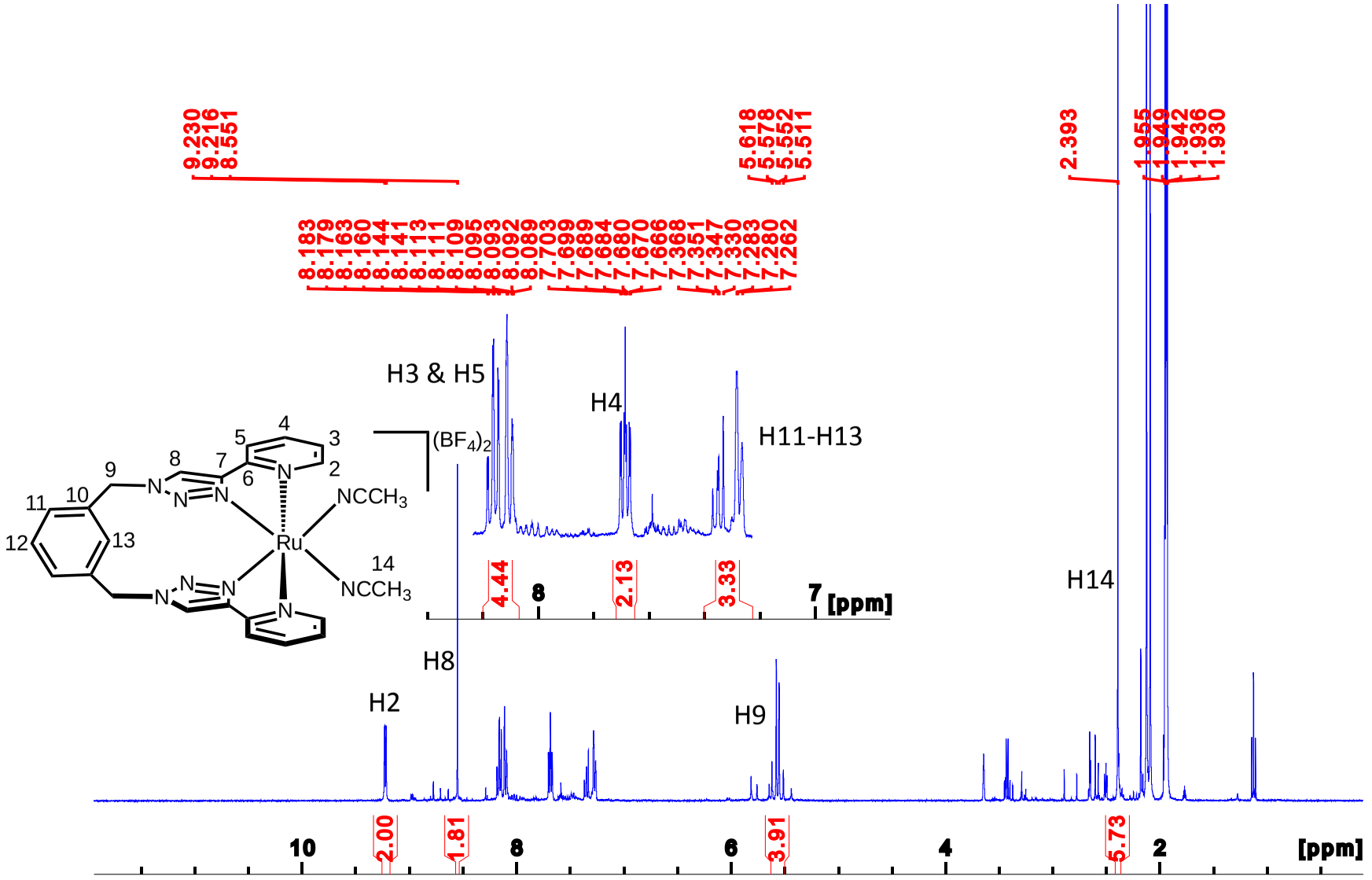

Figure 4.21. ^{1}H NMR of **6** in CD_3CN at 400 MHz.

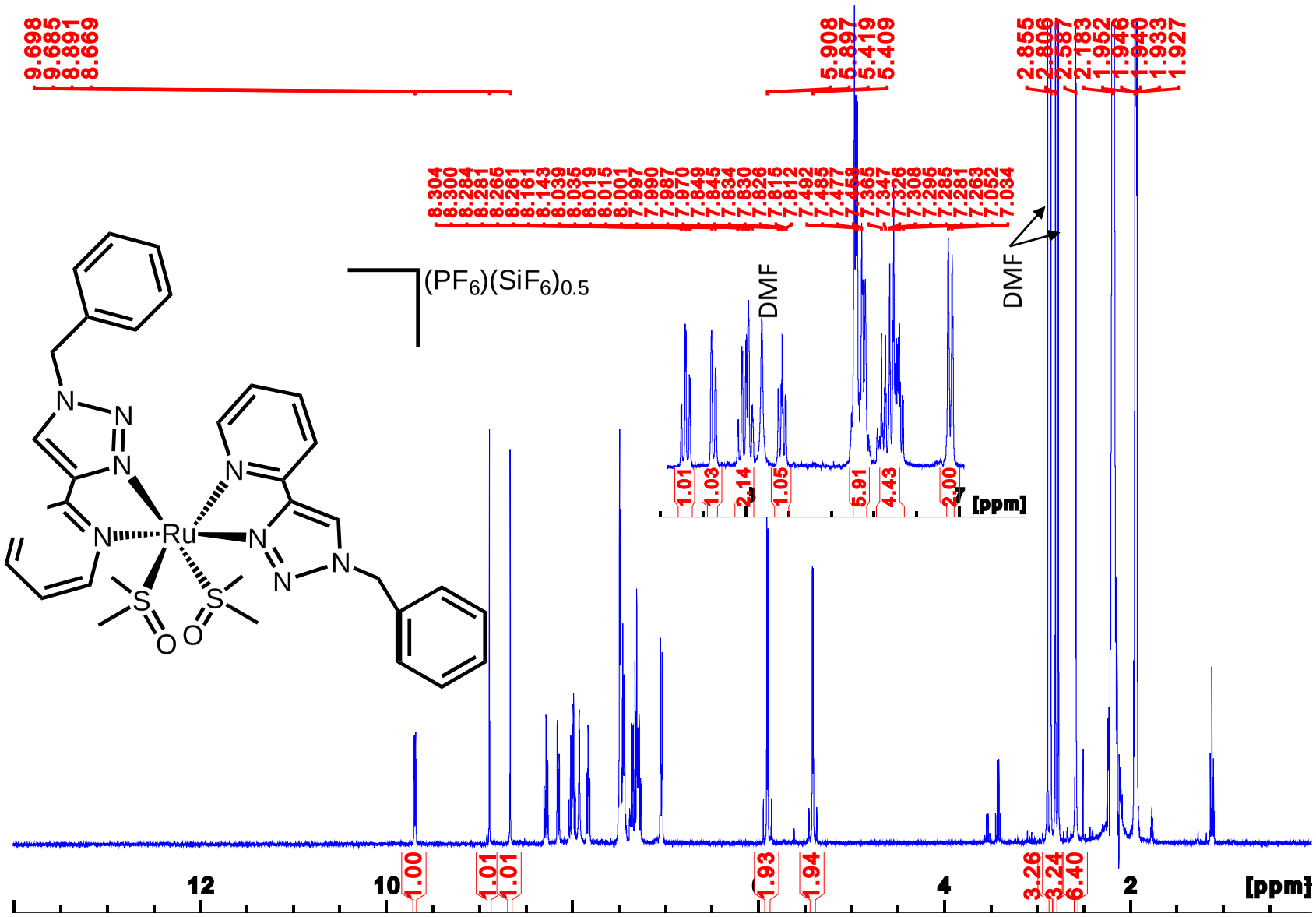

Figure 4.22. ^{1}H NMR of **8** in CD_3CN at 400 MHz.

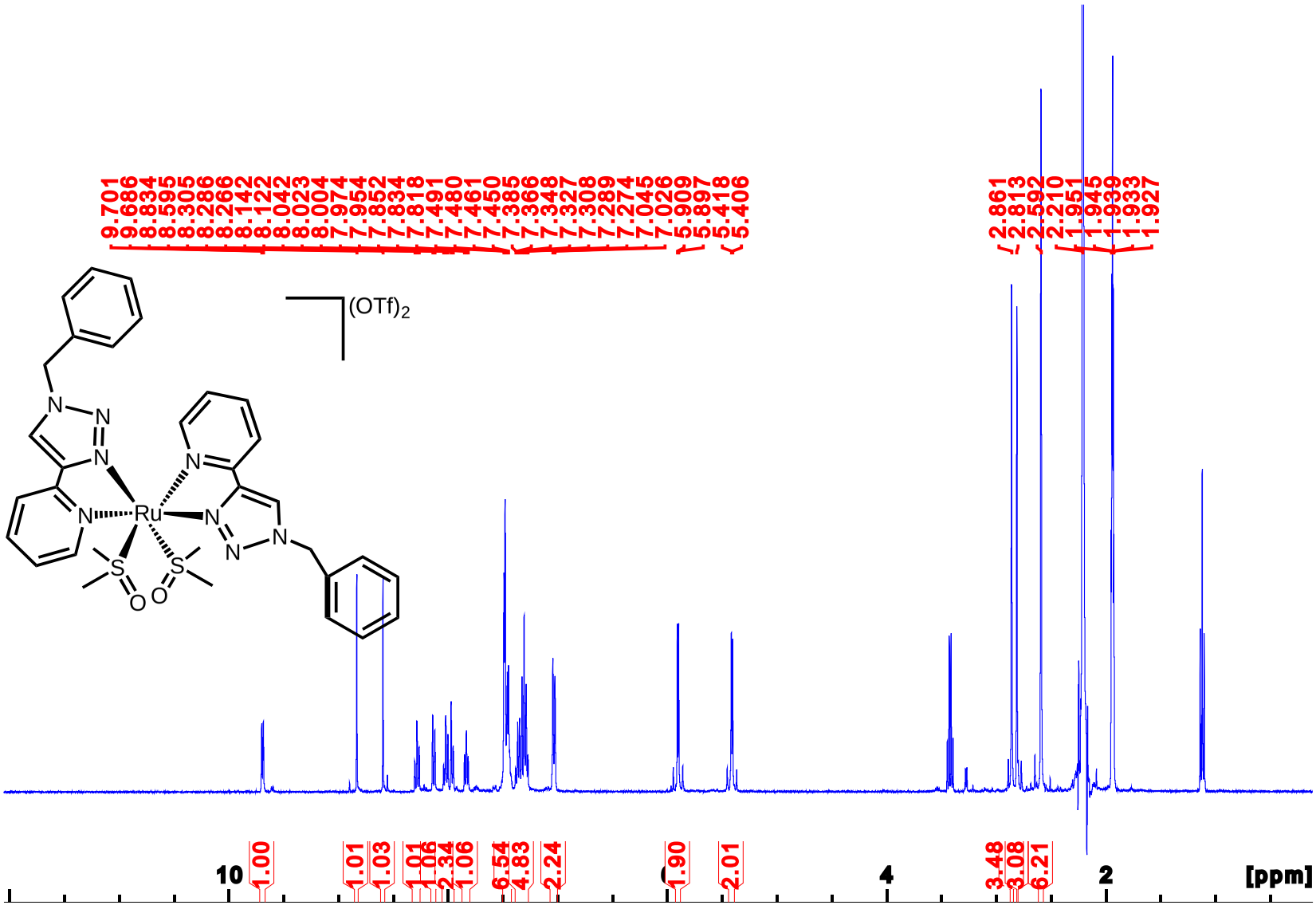

Figure 4.23. ^{1}H NMR of **9** in CD_3CN at 400 MHz.

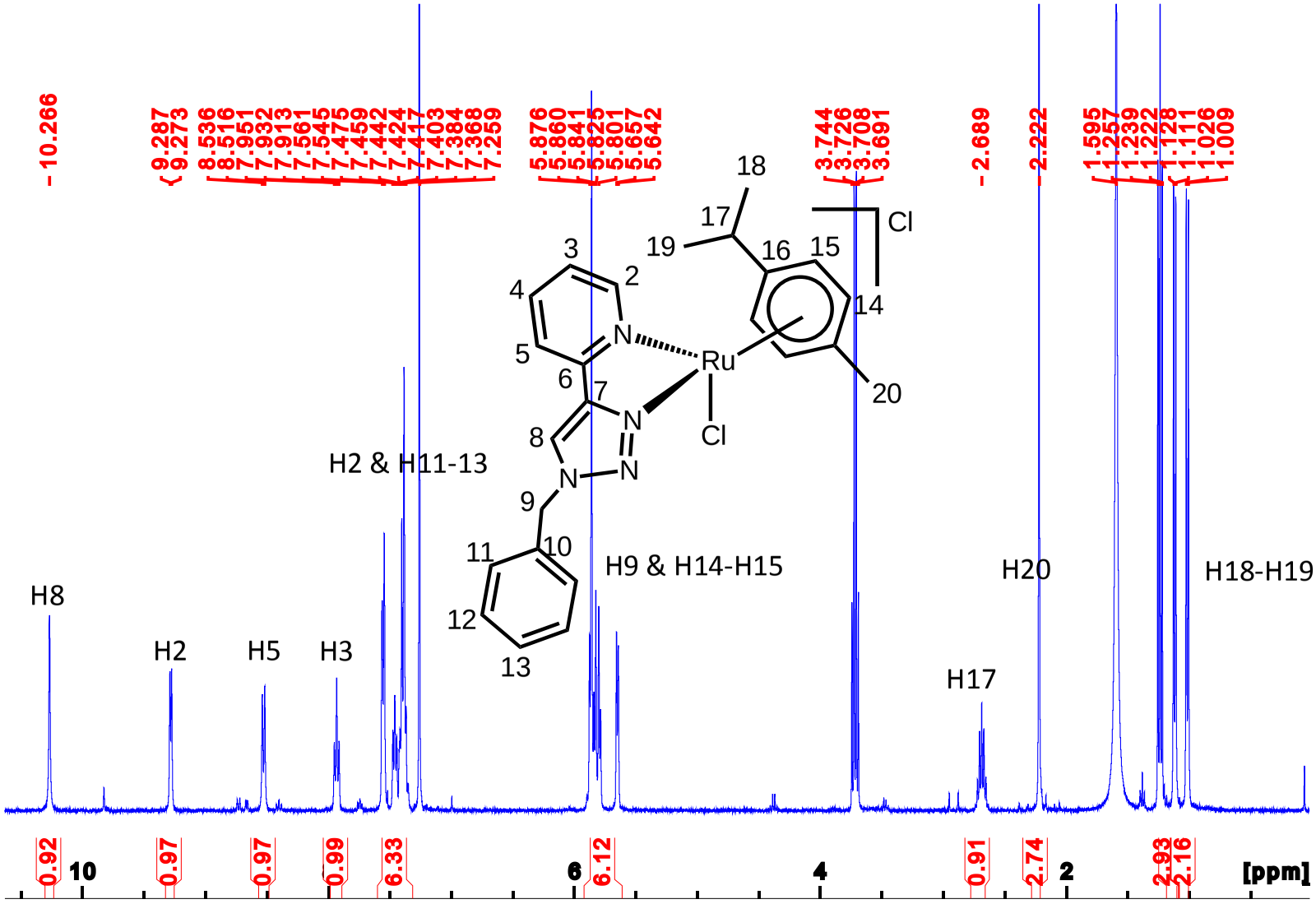

Figure 4.24. ^{1}H NMR of **10** in $CDCl_3$ at 400 MHz.

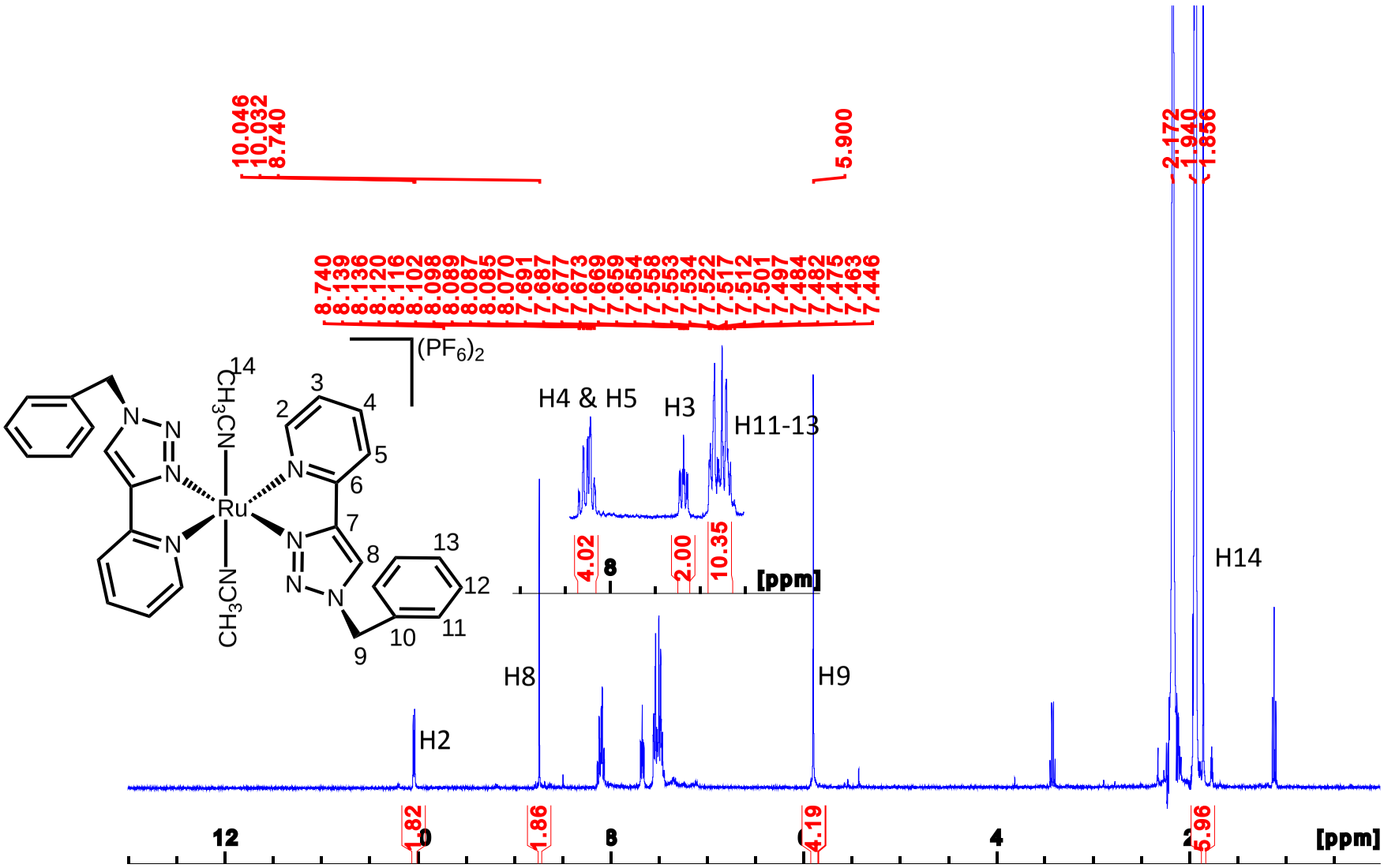

Figure 4.25. ^{1}H NMR of **12** in CD_3CN at 400 MHz. The inset X axis marks are 0.2 ppm apart.

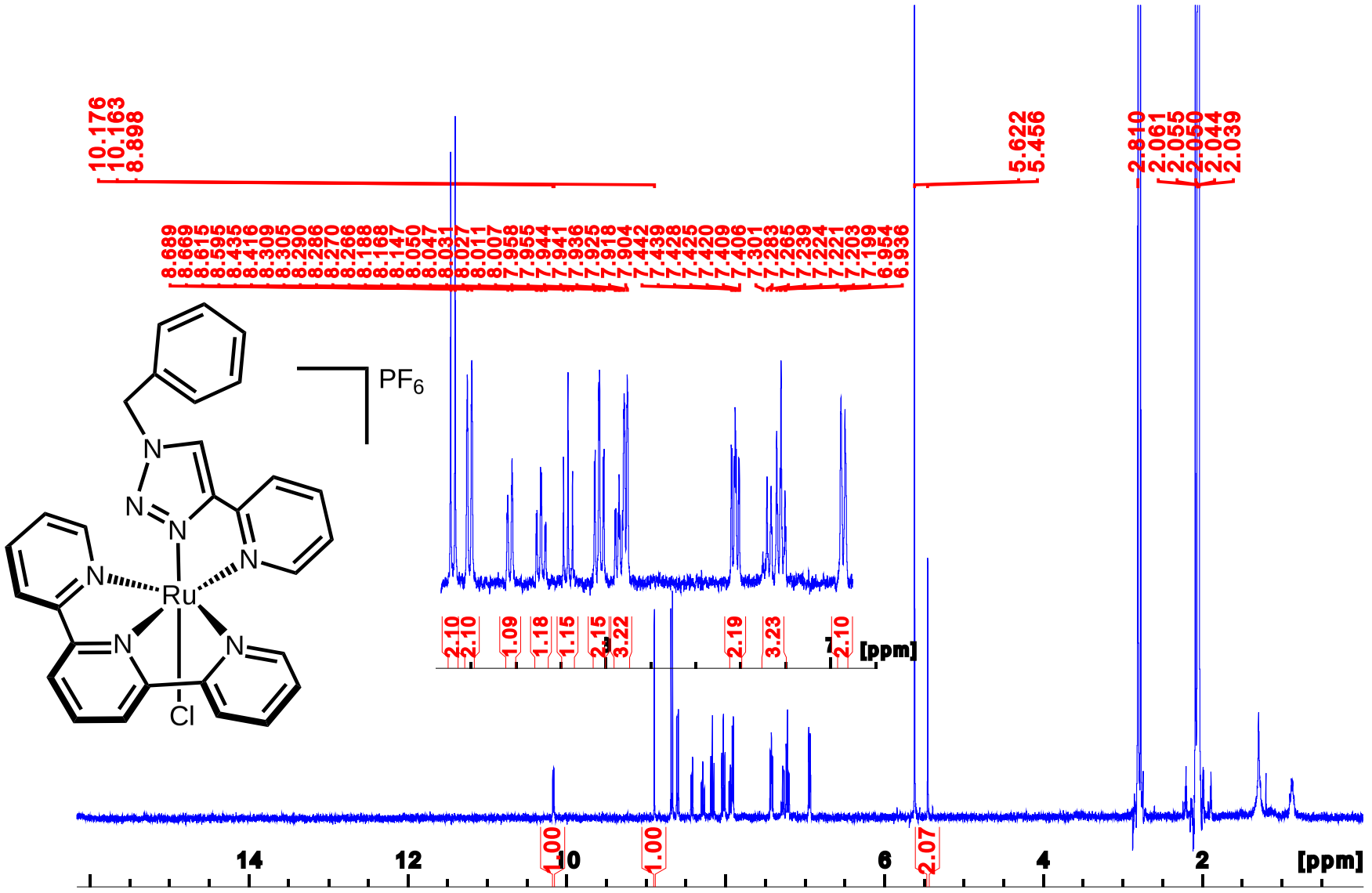

Figure 4.26. ^{1}H NMR of trans-trz-**16a** in $(CD_3)_2CO$ at 400 MHz.

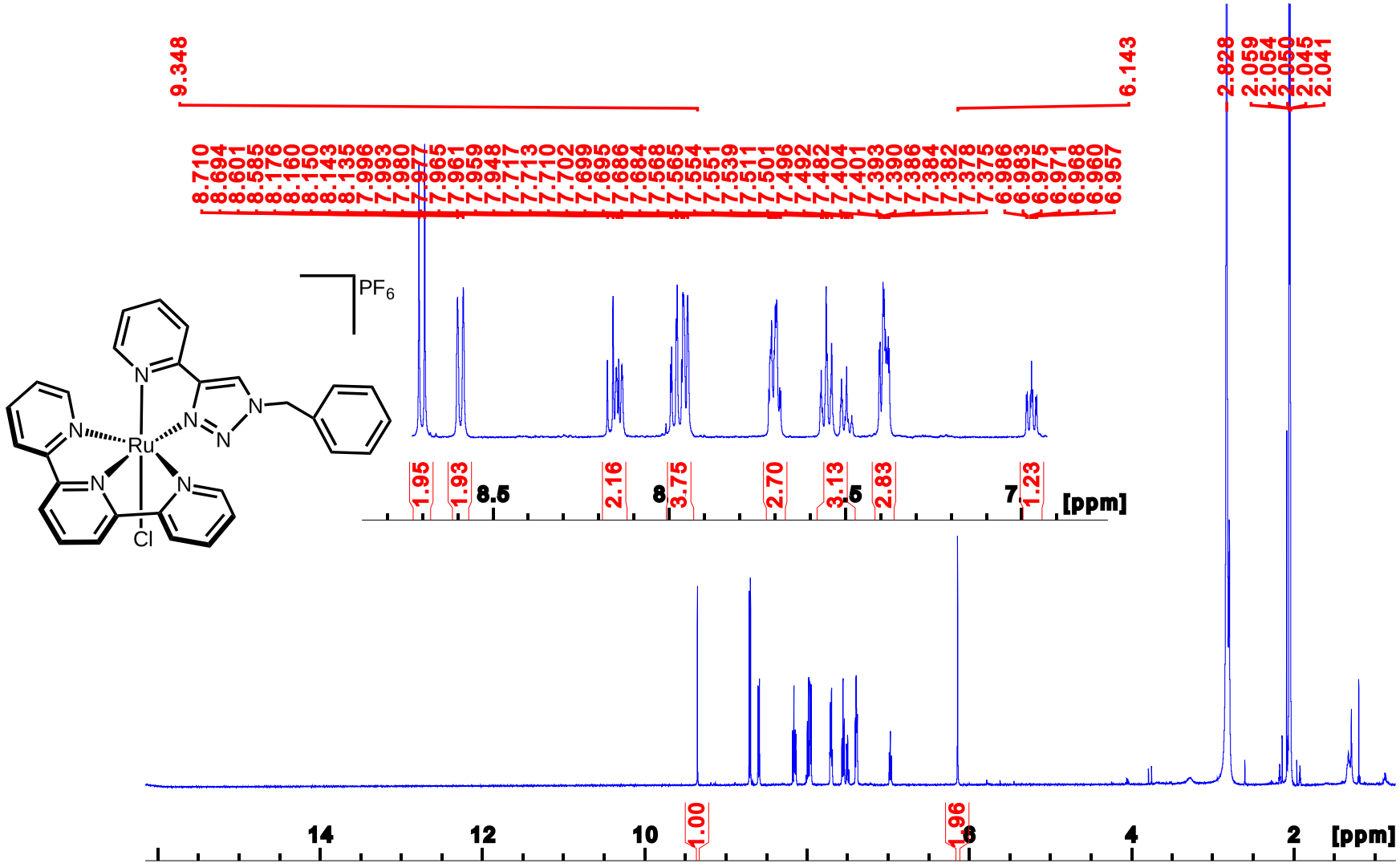

Figure 4.27. ^{1}H NMR of trans-py-**16b** in $(CD_3)_2CO$ at 500 MHz.

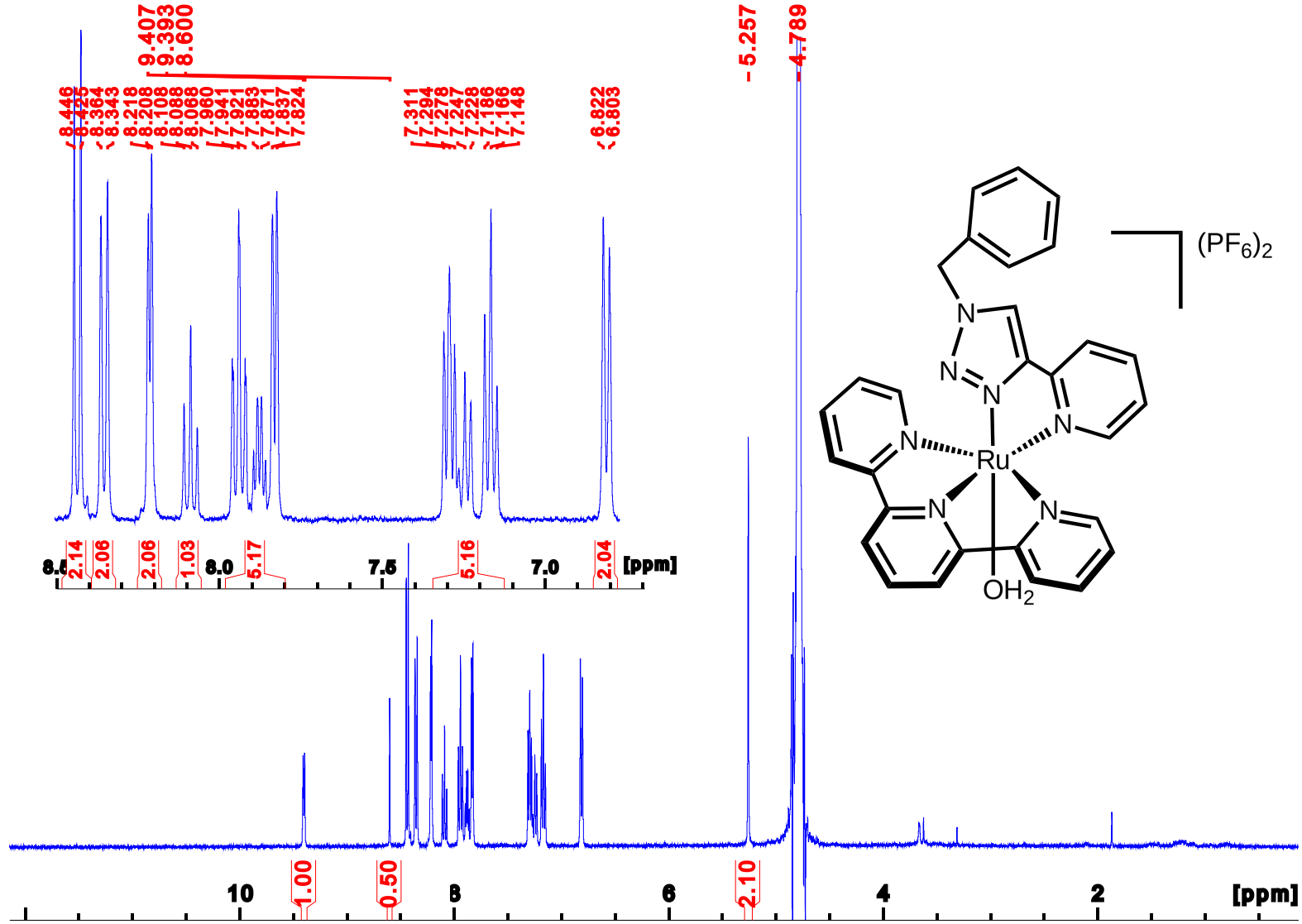

Figure 4.28. ^{1}H NMR of trans-trz-**14a** in D_2O at 400 MHz.

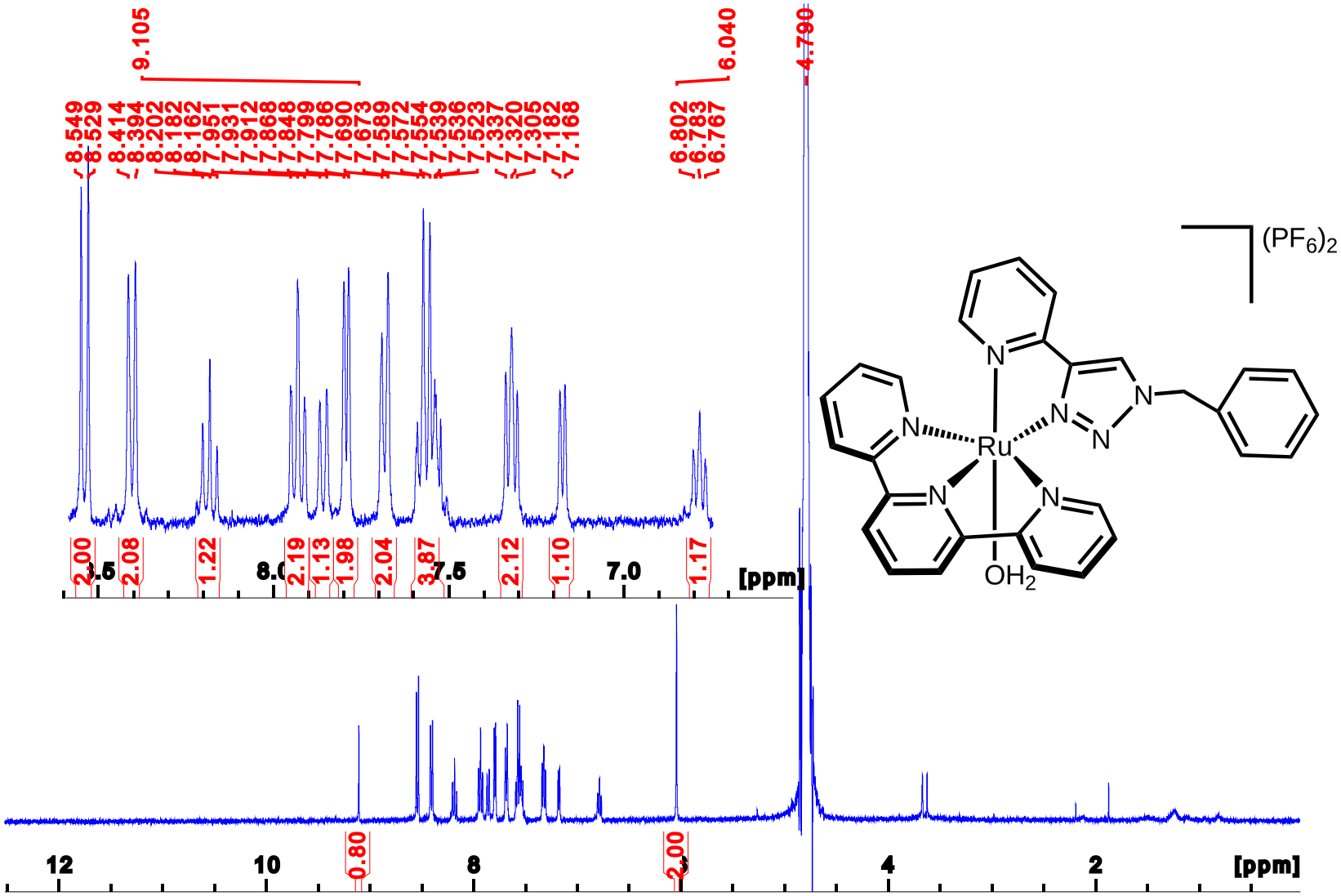

Figure 4.29. ^{1}H NMR of trans-trz-**14b** in D_2O at 400 MHz.

4.4. References

1. Vinyard, D. J.; Brudvig, G. W., Progress toward a molecular mechanism of water oxidation in photosystem II. *Annual Review of Physical Chemistry* **2017,** *68*, 101-116.

2. Fay, N.; Hultgren, V. M.; Wedd, A. G.; Keyes, T. E.; Forster, R. J.; Leane, D.; Bond, A. M., Sensitization of photo-reduction of the polyoxometalate anions $[S_2M_{18}O_{62}]^{4-}$ (M= Mo, W) in the visible spectral region by the $[Ru(bpy)_3]^{2+}$ cation. *Dalton Transactions* **2006,** (35), 4218-4227.

3. Kumar, S. V.; Scottwell, S. Ø.; Waugh, E.; McAdam, C. J.; Hanton, L. R.; Brooks, H. J.; Crowley, J. D., Antimicrobial properties of tris (homoleptic) ruthenium(II) 2-pyridyl-1,2,3-triazole "click" complexes against pathogenic bacteria, including Methicillin-Resistant Staphylococcus Aureus (MRSA). *Inorganic Chemistry* **2016,** *55* (19), 9767-9777.

4. Kumar, S. V.; Lo, W. K.; Brooks, H. J.; Crowley, J. D., Synthesis, structure, stability and antimicrobial activity of a ruthenium(II) helicate derived from a bis-bidentate "click" pyridyl-1,2,3-triazole ligand. *Inorganica Chimica Acta* **2015,** *425*, 1-6.

5. Sullivan, B.; Salmon, D.; Meyer, T., Mixed phosphine 2,2'-bipyridine complexes of ruthenium. *Inorganic chemistry* **1978,** *17* (12), 3334-3341.

6. Evans, I.; Spencer, A.; Wilkinson, G., Dichlorotetrakis(dimethyl sulphoxide)ruthenium(II) and its use as a source material for some new ruthenium(II) complexes. *Journal of the Chemical Society, Dalton Transactions* **1973,** (2), 204-209.

7. Damhus, T.; Hartshorn, R.; Hutton, A., Nomenclature of inorganic chemistry: IUPAC recommendations 2005. *CHEMISTRY International* **2005**.

8. Brown, M. F.; Cook, B. R.; Sloan, T. E., Stereochemical notation in coordination chemistry. Mononuclear complexes. *Inorganic Chemistry* **1975,** *14* (6), 1273-1278.

9. Khamespanah, F.; Maverick, A. W., Two isomers of [1-benzyl-4-(pyridin-2-yl-κ*N*)-1*H*-1,2,3-triazole-κN^3] dichloridobis (dimethyl sulfoxide-κ*S*)ruthenium(II). *Acta Crystallographica Section E: Crystallographic Communications* **2019,** *75* (8), 1108-1111.

10. Li, Y.; Flood, A. H., Pure C–H hydrogen bonding to chloride ions: A preorganized and rigid macrocyclic receptor. *Angewandte Chemie International Edition* **2008,** *47* (14), 2649-2652.

11. White, N. G.; Beer, P. D., A catenane host system containing integrated triazole C–H hydrogen bond donors for anion recognition. *Chemical Communications* **2012,** *48* (68), 8499-8501.

12. Yi, C. S.; Kwon, K.-H.; Lee, D. W., Aqueous phase C−H bond oxidation reaction of arylalkanes catalyzed by a water-soluble cationic Ru(III) complex $[(pymox\text{-}Me_2)_2RuCl_2]^+BF_4^-$. *Organic Letters* **2009,** *11* (7), 1567-1569.

13. Matheu, R.; Garrido-Barros, P.; Gil-Sepulcre, M.; Ertem, M. Z.; Sala, X.; Gimbert-Suriñach, C.; Llobet, A., The development of molecular water oxidation catalysts. *Nature Reviews Chemistry* **2019,** *3* (5), 331-341.

14. Takeuchi, K. J.; Thompson, M. S.; Pipes, D. W.; Meyer, T. J., Redox and spectral properties of monooxo polypyridyl complexes of ruthenium and osmium in aqueous media. *Inorganic Chemistry* **1984,** *23* (13), 1845-1851.

15. Masaoka, S.; Sakai, K., Clear evidence showing the robustness of a highly active oxygen-evolving mononuclear ruthenium complex with an aqua ligand. *Chemistry letters* **2009,** *38* (2), 182-183.

16. Wasylenko, D. J.; Ganesamoorthy, C.; Henderson, M. A.; Koivisto, B. D.; Osthoff, H. D.; Berlinguette, C. P., Electronic modification of the $[Ru^{II}(tpy)(bpy)(OH_2)]^{2+}$ scaffold: Effects on catalytic water oxidation. *Journal of the American Chemical Society* **2010,** *132* (45), 16094-16106.

17. Sullivan, B. P.; Calvert, J. M.; Meyer, T. J., Cis-trans isomerism in $(trpy)(PPh_3)RuC1_2$. Comparisons between the chemical and physical properties of a cis-trans isomeric pair. *Inorganic Chemistry* **1980,** *19* (5), 1404-1407.

18. Bratsos, I.; Alessio, E., Inorganic Syntheses, Vol. 35, edited by T. B. Rauchfuss. *Hoboken, New Jersey: Wiley* **2010**, 148-152.

19. Crowley, J. D.; Bandeen, P. H.; Hanton, L. R., A one pot multi-component CuAAC "click" approach to bidentate and tridentate pyridyl-1,2,3-triazole ligands: Synthesis, X-ray structures and copper(II) and silver(I) complexes. *Polyhedron* **2010,** *29* (1), 70-83.

20. Pokharel, U. R.; Fronczek, F. R.; Maverick, A. W., Cyclic pyridyltriazole–Cu(II) dimers as supramolecular hosts. *Dalton Transactions* **2013,** *42* (39), 14064-14067.

Chapter 5. Conclusions

This dissertation is focused on synthesis of new copper and ruthenium complexes with pyridyltriazole ligands and studies their reactivity with CO_2 and H_2O, which have attracted much attention as renewable sources of hydrogen, oxygen, and carbon fuels. Inspired by the process of photosynthesis in which light, H_2O and CO_2 as input, produces O_2 and carbohydrates, scientists are attempting to make artificial systems that oxidize water to O_2, and reduce carbon dioxide to fuels and other value-added chemicals. There are fewer than 50 examples in the literature of reductive coupling of CO_2 molecules to oxalate. Most of these claims are only based on isolation of crystals of an oxalate complex after exposing the reaction mixture to air or CO_2 atmosphere, without performing careful control experiments to evaluate the origin of the carbon atoms in oxalate. Oxalate could originate from oxidation of organic solvents such as acetonitrile, ligands, or other carbon containing compounds in the solution. Many novel systems capable of reduction of CO_2 molecules get published every day, and working on this cutting-edge science is in some cases accompanied by mistakes and misinterpretation of data. We hope this dissertation sheds light on one of the possible ways of production of oxalate besides CO_2 reduction, and demonstrates the importance of using isotope-labeling experiments to determine the origin of oxalate.

5.1. Cu complexes. (Note: compound numbers in this section are the same as those in chapters 2 and 3.) Our lab claimed reduction of CO_2 to oxalate mediated by *in situ* generated $[Cu^{I}_2(m\text{-xpt})_2](PF_6)_2$ (**7**) by ascorbate in a 2014 paper. The oxalate bridges between the copper centers and forms $[Cu_2(m\text{-xpt})_2(\mu_2\text{-}C_2O_4)_2](PF_6)_2$ complex (**6**). Based on this claim, in order to make a Cu(I) complex that reacts more quickly with CO_2, we prepared more electron-rich complexes by functionalization of pyridine of the *m*-xpt ligand with NH_2 and NMe_2 electron-donating groups. The new $[Cu_2(H_2N\text{-xpt})_2(NO_3)_2](PF_6)_2$ (**10**) and $[Cu_2(Me_2N\text{-xpt})_2(NO_3)_2](PF_6)_2$

(**25**) complexes were characterized by mass spectrometry. Then they were reduced to Cu(I) complexes by ascorbate or ascorbic acid. In contrast to **7**, exposure of the $[Cu^{I}_2L_2](PF_6)_2$ L = H_2N-xpt (**12**) or Me_2N-xpt (**26**) to air or a balloon of CO_2 resulted mostly in formation of carbonate trimers, $[Cu_3L_3(\mu_3\text{-}CO_3)](PF_6)_4$, L = H_2N-xpt (**14**) or Me_2N-xpt (**27**).

These results with substituted xpt ligands motivated us to reexamine the experiments of **7** with CO_2. We showed that **7** does not react with CO_2. Instead, under even pure oxygen atmosphere, the oxalate complex **6** forms. We made $[Cu^{I}_2(m\text{-xpt})_2](BF_4)_2$ (**7a**) in the absence of ascorbate and dehydroascorbic acid and exposure of this solution to air produced only $[Cu_3(m\text{-xpt})_3(\mu_3\text{-}CO_3)](BF_4)_4$ (**5a**). However, when we added dehydroascorbic acid to the same Cu(I) solution and stirred it in air for a few days, we could isolate crystals of $[Cu_2(m\text{-xpt})_2(\mu_2\text{-}C_2O_4)_2](BF_4)_2$ (**6a**). Therefore, we believe that the oxalate is formed by oxidation of dehydroascorbic acid. We showed that Cu(I) is not necessary for formation of oxalate and by stirring a solution of **4** and dehydroascorbic acid, crystals of **6** could be obtained. In order to fully confirm our claim, we made the genuine ^{13}C-labeled oxalate-bridged dimer, $[Cu_2(m\text{-xpt})_2(\mu_2\text{-}^{13}C_2O_4)_2](PF_6)_2$ (^{13}C-**6**) by treating **4** with $(Bu_4N)_2(^{13}C_2O_4)$, and recorded its FT-IR and MS data. Then, we exposed a solution of **7** to a $^{13}CO_2$–O_2 mixture (ca. 1:1 v/v), and the spectra of the oxalate dimer formed from this reaction were as expected for unlabeled **6**. This provides definitive evidence the oxalate does not come from CO_2. In the FT-IR spectrum, we assigned the peak at 1639 cm^{-1} to the oxalate CO stretching frequency, which shifted to 1600 cm^{-1} on ^{13}C substitution. This conclusion may explain the chemistry that we observed with **12** and **26**: When stoichiometric amounts of ascorbate were used, there is a minimum amount of DHA in the solution that could oxidize to oxalate, while the Cu centers in **12** and **26** could readily oxidize to Cu(II) and form the carbonate trimer **14** or **27** by

transformation of CO_2 to CO_3^{2-}. However, when excess ascorbate was used, formation of oxalate dimer was increased due to accessibility of ascorbate in the solution to oxidize to oxalate.

5.2. Ru complexes. (Note: compound numbers in this section are the same as those in chapter 4.) In order to expand the chemistry that I've been involved in, I attempted to synthesize a ruthenium dimer similar to $Cu_2(m\text{-xpt})_2^{4+}$. Ru(II) and Ru(III), with the d^6 and d^5 electronic configurations, are inert and usually need refluxing for ligand substitution reactions. With the *m*-xpt ligand, we could only obtain crystals of $Ru(m\text{-xpt})(CH_3CN)_2^{2+}$ (in **5** and **6**), with the *m*-xpt ligand in a surprising chelating arrangement. We also made $Ru(bpt)_2(DMSO)_2^{2+}$ (in **8** and **9**), and on the way of exploring how to make a bis(bpt)-Ru aqua complex we obtained (*OC*-6-14)- and (*OC*-6-32)-$Ru(bpt)(DMSO)_2Cl_2$ (**2** and **3**), $Ru(bpt)_2Cl_2$ (**11**), and $[Ru(bpt)_2(CH_3CN)_2](PF_6)_2$ (**12**). We also prepared two isomers of $[Ru(tpy)(bpt)(H_2O)]^{2+}$ (trans-trz-**14a** and trans-py-**14b**) in reasonable yield and tested their reactivity for water oxidation. The two isomers have almost the same Ru(III)/Ru(II) reduction potentials. In our qualitative experiment, when they were treated with excess Ce(IV) in 0.1 M HNO_3, the trans-py-**14b** formed more oxygen than the trans-trz-**14a** isomer. Both isomers turn green after longer treatment with Ce(IV), and as our future work we will try to isolate these green products.

Appendix A. X-ray Crystallography and Structure Refinement

Intensity data were collected at low temperature on a Bruker Kappa Apex-II DUO CCD diffractometer fitted with an Oxford Cryostream chiller. MoKα (λ = 0.71073 Å) radiation with a *TRIUMPH* curved graphite monochromator or CuKα (λ = 1.54184 Å) radiation from an I μS microfocus source with *QUAZAR* multilayer optics were used. Using *APEX3*[1] software, cell refinement was done by *SAINT*,[2] and data reduction included absorption corrections by the multiscan method, with *SADABS*,[3] or *TWINABS*.[4] The structures were determined by direct methods or intrinsic phasing and difference Fourier techniques and refined by full-matrix least squares, using *SHELXT2014* or *SHELXS97*[5] for solving the structures and *SHELXL2014, SHELXL2017* or *SHELXL2018*[6] for refinement. All H atoms were placed in idealized positions, except for water hydrogen atoms and ammonium N–H in FKhame14 and amino N–H in FKhame88 structures. U_{iso} (H) values were set to either 1.2 or 1.5 (CH_3) times U_{eq} of the attached atom. Restraints and constraints were employed when needed to obtain chemically reasonable refinement models. *PLATON SQUEEZE*[7] was used in some cases to remove disordered solvents. Crystal data and structure refinement parameters are presented in Table A-1.

Appendix A. References

1. Bruker, APEX3. Bruker AXS Inc., Madison, Wisconsin, USA, **2016**.
2. Bruker, SAINT. Bruker AXS Inc., Madison, Wisconsin, USA, **2012**.
3. Bruker, SADABS. Bruker AXS Inc., Madison, Wisconsin, USA, **2001**.
4. Bruker, TWINABS. Bruker AXS Inc., Madison, Wisconsin, USA, **2001**.
5. Sheldrick, G. M., *Acta Crystallographica Section A* **2015**, *71*, 3-8.
6. Sheldrick, G. M., *Acta Crystallographica Section C* **2015**, *71*, 3-8.
7. Spek, A. L., *Acta Crystallographica Section C* **2015**, *71*, 9-18.

Table A.1. Crystallographic Data and Structure Refinement Parameters

Compound	**27·DMF (Chapter 2)**	**28·2DMF (Chapter 2)**
LSU structure identifier	FKhame42	FKhame85
formula	$[Cu_3(Me_2N\text{-}xpt)_3(CO_3)](PF_6)_4\cdot DMF$ ($C_{82}H_{91}Cu_3F_{24}N_{31}O_4P_4$)	$[Cu_2(Me_2N\text{-}xpt)_2(C_2O_4)](PF_6)_2\cdot 2DMF$ ($C_{60}H_{70}Cu_2F_{12}N_{22}O_6P_2$)
M	2345.30	1612.36
crystal system	Triclinic	Triclinic
space group	$P\bar{1}$	$P\bar{1}$
a/Å	17.3319(7)	13.3095(4)
b/Å	18.2743(7)	13.3932(4)
c/Å	18.4856(7)	13.6082(4)
α/deg	103.445(2)	64.696(2)
β/deg	97.010(2)	86.261(2)
γ/deg	110.768(2)	61.037(2)
V/Å^3	5188.1(4)	1887.67(11)
Z	2	1
T/K	90(2)	90.0(5)
D_{calc}/g cm^{-3}	1.501	1.483
crystal dimensions/mm	0.225 x 0.055 x 0.020	0.080 x 0.060 x 0.050
Radiation	CuKα	CuKα
θ limits/deg	2.522 – 66.706	3.652 – 66.988
reflns, measd /unique/obsd	45661/17585/15035	70720/6682/4699
Data/params	17585/1359	6682/475
F(000)	2390	868
μ/mm^{-1}	2.232	1.933
R_{int}	0.0334	0.075
$R[I>2\sigma(I)]$	0.0656	0.0904
R_w (all data)	0.2024	0.2377
GOF	1.025	1.057

Compound	**14·3DMF (Chapter 2)**	**13·5DMF·4H_2O (Chapter 2)**
LSU structure identifier	FKhame6	FKhame88
formula	[Cu_3(H_2N-xpt)$_3$(CO_3)](PF_6)$_4$·3DMF ($C_{76}H_{81}Cu_3F_{24}N_{33}O_6P_4$)	[Cu_3(H_2N-xpt)$_3$(CO_3)](NO_3)$_4$·5DMF.4H_2O ($C_{82}H_{103}Cu_3N_{39}O_{24}$)
M	2323.17	2209.58
crystal system	Triclinic	Monoclinic
space group	$P\bar{1}$	$P2_1/n$
a/Å	16.4837(8)	18.947(7)
b/Å	27.8837(14)	22.226(9)
c/Å	28.3839(13)	23.740(9)
α/deg	75.489(4)	90
β/deg	89.512(3)	93.799(5)
γ/deg	76.586(3)	90
V/Å^3	12268.2(11)	9975(7)
Z	4	4
T/K	90.0(5)	90.0(5)
D_{calc}/g cm^{-3}	1.277	1.471
crystal dimensions/mm	0.420 x 0.35 x 0.10	0.44 x 0.23 x 0.05
Radiation	CuKα	MoKα
θ limits/deg	2.872 – 64.186	1.414 – 33.188
reflns, measd /unique/obsd	77629/39058/19509	249464/37979/27254
Data/params	39058/2662	37979/1403
F(000)	4794	4588
μ/mm^{-1}	1.913	0.725
R_{int}	0.0897	0.0515
R[I>2σ(I)]	0.1339	0.0469
R_w (all data)	0.4173	0.1200
GOF	1.280	1.054

Compound	**6a·2DMF (Chapter 3)**	**5a·2.5DMF (Chapter 3)**
LSU structure identifier	Crochet4	FKhame4
formula	$[Cu_3(m\text{-xpt})_3(\mu\text{-}C_2O_4)](BF_4)_2\cdot 2DMF$ ($C_{52}H_{50}B_2Cu_2F_8N_{18}O_6$)	$[Cu_3(m\text{-xpt})_3(\mu_3\text{-}CO_3)](BF_4)_4\cdot 2.5DMF$ ($C_{74.5}H_{71.5}B_4Cu_3F_{16}N_{26.5}O_{5.5}$)
M	1323.77	1963.94
crystal system	Monoclinic	Monoclinic
space group	$P2_1/c$	$I2/a$
a/Å	10.3437(4)	29.1381(9)
b/Å	24.0279(10)	17.6927(5)
c/Å	12.7325(5)	33.1192(14)
α/deg	90	90
β/deg	111.179(3)	99.0670(10)
γ/deg	90	90
V/Å^3	2950.8(2)	16860.6(10)
Z	2	8
T/K	90.0(5)	100.0(5)
D_{calc}/g cm^{-3}	1.490	1.547
crystal dimensions/mm	0.100 x 0.04 x 0.02	0.51 x 0.36 x 0.22
Radiation	CuKα	MoKα
θ limits/deg	3.679 – 61.213	1.732 – 34.459
reflns, measd /unique/obsd	17493/4481/3241	198022/35460/23758
Data/params	4481/399	35460/1213
F(000)	1352	7992
μ/mm^{-1}	1.671	0.854
R_{int}	0.0677	0.0524
$R[I>2\sigma(I)]$	0.0419	0.0626
R_w (all data)	0.0937	0.1767
GOF	1.012	1.038

Compound	**14b·H_2O (Chapter 4)**	**14a (Chapter 4)**
LSU structure identifier	FKhame83	FKhame68
formula	trans-py-[Ru(tpy)(bpt)(OH_2)](PF_6)$_2$·H_2O ($C_{29}H_{27}F_{12}N_7O_2P_2Ru$)	trans-trz-[Ru(tpy)(bpt)(OH_2)](PF_6)$_2$ ($C_{29}H_{25}F_{12}N_7OP_2Ru$)
M	896.56	878.55
crystal system	Monoclinic	Triclinic
space group	$P2_1/c$	$P\bar{1}$
a/Å	19.3056(11)	11.7492(8)
b/Å	9.8599(7)	12.0542(8)
c/Å	18.3968(11)	13.9800(9)
α/deg	90	67.705(2)
β/deg	104.174(4)	83.249(2)
γ/deg	90	64.265(2)
V/Å^3	3395.2(4)	1647.58(19)
Z	4	2
T/K	90(2)	90.0(2)
D_{calc}/g cm^{-3}	1.754	1.771
crystal dimensions/mm	0.070 x 0.051x 0.021	1.083 x 0.075 x 0.055
Radiation	MoKα	CuKα
θ limits/deg	2.176 – 30.085	8.617 – 66.723
reflns, measd /unique/obsd	93062/9956/7020	10675/5557/5383
Data/params	9956/531	5557/ 479
F(000)	1792	876
μ/mm^{-1}	0.663	5.751
R_{int}	0.0942	0.0414
$R[I>2\sigma(I)]$	0.0426	0.0765
R_w (all data)	0.1214	0.2136
GOF	0.796	1.054

Compound	**2 (Chapter 4)**	**3 (Chapter 4)**
LSU structure identifier	FKhame21	FKhame23
formula	(*OC*-6-14)-Ru(bpt)(DMSO)$_2$Cl$_2$ ($C_{18}H_{24}Cl_2N_4O_2RuS_2$)	(*OC*-6-32)-Ru(bpt)(DMSO)$_2$Cl$_2$ ($C_{18}H_{24}Cl_2N_4O_2RuS_2$)
M	564.51	564.51
crystal system	Orthorhombic	Triclinic
space group	*Pbca*	$P\bar{1}$
a/Å	21.3094(11)	9.3535(14)
b/Å	9.4213(5)	9.4900(15)
c/Å	22.5267(12)	13.904(2)
α/deg	90	98.893(5)
β/deg	90	106.772(5)
γ/deg	90	106.276(5)
V/Å^3	4522.5(4)	1096.4(3)
Z	8	2
T/K	90	90
D_{calc}/g cm^{-3}	1.658	1.710
crystal dimensions/mm	0.714 x 0.159 x 0.037	0.670 x 0.625 x 0.450
Radiation	CuKα	CuKα
θ limits/deg	3.925 – 66.688	3.435 – 66.869
reflns, measd /unique/obsd	34572/3970/3628	9693/3704/3657
Data/params	3970/266	3704/266
F(000)	2288	572
μ/mm^{-1}	9.703	10.006
R_{int}	0.0431	0.026
$R[I>2\sigma(I)]$	0.0251	0.0371
R_w (all data)	0.0668	0.1027
GOF	1.039	1.155

Compound	**17 (Chapter 4)**	**6 (Chapter 4)**
LSU structure identifier	FKhame30	FKhame31
formula	$Ru(CH_3CN)_5Cl(NO_3)\cdot Ag(CH_3CN)(NO_3)$ ($C_{12}H_{18}AgClN_8O_6Ru$)	$[Ru(m\text{-xpt})(CH_3CN)_2](BF_4)_2$ ($C_{26}H_{24}B_2F_8N_{10}Ru$)
M	614.71	751.21
crystal system	Triclinic	Monoclinic
space group	$P\bar{1}$	$P2_1/c$
a/Å	10.0120(7)	14.354(4)
b/Å	14.2316(10)	11.439(3)
c/Å	16.7961(14)	18.666(5)
α/deg	82.675(4)	90
β/deg	76.051(4)	104.089(15)
γ/deg	73.309(3)	90
V/Å^3	2220.4(3)	2972.7(14)
Z	2	4
T/K	90(2)	90(2)
D_{calc}/g cm^{-3}	1.839	1.679
crystal dimensions/mm	0.66 x 0.46 x 0.33	0.382 x 0.107 x 0.095
Radiation	CuKα	MoKα
θ limits/deg	2.716 – 66.765	1.463 – 30.054
reflns, measd /unique/obsd	19240/7464/6351	113534/8649/ 7406
Data/params	7464/535	8649/426
F(000)	1208	1504
μ/mm^{-1}	14.094	0.616
R_{int}	0.0578	0.0355
$R[I>2\sigma(I)]$	0.0735	0.0294
R_w (all data)	0.2105	0.0764
GOF	1.043	1.042

Compound	**9 (Chapter 4)**	**8·CH_3OH (Chapter 4)**
LSU structure identifier	FKhame43	FKhame39
formula	$[Ru(bpt)_2(DMSO)_2](OTf)_2$ ($C_{34}H_{36}F_6N_8O_{10}RuS_4$)	$[Ru(bpt)_2(DMSO)_2](PF_6)0.5(SiF_6)\cdot CH_3OH$ ($C_{33}H_{40}F_9N_8O_3PRuS_2Si_{0.5}$)
M	1028.01	977.92
crystal system	Triclinic	Triclinic
space group	$P\bar{1}$	$P\bar{1}$
a/Å	9.7370(8)	9.8532(6)
b/Å	12.7715(10)	12.7266(6)
c/Å	18.4204(14)	18.1087(9)
α/deg	109.742(2)	100.346(2)
β/deg	101.554(2)	104.143(2)
γ/deg	92.679(2)	106.843(2)
V/Å^3	2096.0(3)	2029.35(19)
Z	2	2
T/K	90(2)	90(2)
D_{calc}/g cm^{-3}	1.629	1.600
crystal dimensions/mm	0.383 x 0.180 x 0.104	0.304 x 0.122 x 0.085
Radiation	CuKα	CuKα
θ limits/deg	3.702 – 66.589	3.768 – 66.680
reflns, measd /unique/obsd	16578/7066/6805	23683/6975/6522
Data/params	7066/554	6975/554
F(000)	1044	993
μ/mm^{-1}	5.655	5.379
R_{int}	0.0276	0.0333
$R[I>2\sigma(I)]$	0.0459	0.0519
R_w (all data)	0.1899	0.1371
GOF	1.252	1.071

Compound	**11 (Chapter 4)**	**12 (Chapter 4)**
LSU structure identifier	FKhame56	FKhame60
formula	$Ru(bpt)_2Cl_2$ ($C_{28}H_{24}Cl_2N_8Ru$)	$[Ru(bpt)_2(CH_3CN)_2](PF_6)_2$ ($C_{32}H_{30}F_{12}N_{10}P_2Ru$)
M	644.52	945.64
crystal system	Monoclinic	Monoclinic
space group	$P2_1/c$	$P2_1/c$
a/Å	11.632(5)	8.7636(4)
b/Å	12.887(5)	21.2085(10)
c/Å	9.230(4)	10.3066(4)
α/deg	90	90
β/deg	99.46(3)	108.536(16)
γ/deg	90	90
V/Å^3	1364.7(10)	1816.2(2)
Z	2	2
T/K	120(2)	90(2)
D_{calc}/g cm^{-3}	1.320	1.729
crystal dimensions/mm	0.219 x 0.200 x 0.081	0.523 x 0.105 x 0.097
Radiation	MoKα	CuKα
θ limits/deg	1.775 – 30.150	4.169 – 67.067
reflns, measd /unique/obsd	25223/3880/2843	10548/3221/3073
Data/params	3880/178	3221/260
F(000)	552	948
μ/mm^{-1}	0.786	5.271
R_{int}	0.0850	0.0347
$R[I>2\sigma(I)]$	0.0591	0.0398
R_w (all data)	0.2026	0.1084
GOF	1.401	1.098

Compound	**5·$(AgNO_3)_3$ (Chapter 4)**
LSU structure identifier	FKhame27
formula	$[Ru(m\text{-xpt})(CH_3CN)_2]\cdot Ag(NO_3)_3$ ($C_{28}H_{27}AgN_{14}O_9Ru$)
M	912.54
crystal system	Monoclinic
space group	$P2_1/n$
a/Å	8.3480(5)
b/Å	20.9208(11)
c/Å	20.0033(11)
α/deg	90
β/deg	101.262(3)
γ/deg	90
V/Å^3	3426.2(3)
Z	4
T/K	90(2)
D_{calc}/g cm^{-3}	1.769
crystal dimensions/mm	? x ? x ?
Radiation	CuKα
θ limits/deg	4.226 – 66.616
reflns, measd /unique/obsd	30206/5904/5412
Data/params	5904/481
F(000)	1824
μ/mm^{-1}	8.802
R_{int}	0.0430
$R[I>2\sigma(I)]$	0.0372
R_w (all data)	0.1053
GOF	1.028

The remaining structures were not mentioned in the chapters:

LSU structure identifier	FKhame79	FKhame75
formula	Ru(tpy)(bpt)(EtOH)](PF$_6$)$_2$·dioxane ($C_{35}H_{36}F_{12}N_7O_3P_2Ru$)	1,3,5-tris(pyridyl-triazolylmethyl)benzene ($C_{30}H_{24}N_{12}$)
M	993.70	552.59
crystal system	Monoclinic	Triclinic
space group	$P2_1/c$	$P\bar{1}$
a/Å	11.0484(6)	9.0788(5)
b/Å	22.0339(12)	10.4573(6)
c/Å	16.2346(9)	14.4276(8)
α/deg	90	74.039(4)
β/deg	97.090(3)	81.515(4)
γ/deg	90	86.138(4)
V/Å^3	3921.9(4)	1302.02(13)
Z	4	2
T/K	90(2)	90(2)
D_{calc}/g cm^{-3}	1.683	1.410
crystal dimensions/mm	0.510 x 0.185 x 0.034	? x ? x ?
Radiation	MoKα	MoKα
θ limits/deg	1.566 – 33.050	2.026 – 30.127
reflns, measd /unique/obsd	60821/14795/10317	26256/7592/4057
Data/params	14795/547	7592/4057
F(000)	2004	576
μ/mm^{-1}	0.585	0.091
R_{int}	0.0616	0.0684
$R[I>2\sigma(I)]$	0.0598	0.0607
R_w (all data)	0.1433	0.1827
GOF	1.017	0.950

LSU structure identifier	FKhame73	FKhame69
formula	trans-trz-[Ru(tpy)(bpt)Cl]PF_6·CH_2Cl_2 ($C_{30}H_{25}Cl_3F_6N_7PRu$)	trans-py-[Ru(tpy)(bpt)(CH_3CN)](PF_6)$_2$ ($C_{31}H_{26}F_{12}N_8P_2Ru$)
M	835.96	901.59
crystal system	Monoclinic	Monoclinic
space group	$P2_1/c$	$P2_1/c$
a/Å	18.0058(11)	10.7265(4)
b/Å	11.0111(7)	26.8727(10)
c/Å	16.4634(10)	12.7006(5)
α/deg	90	90
β/deg	94.897(3)	109.619(2)
γ/deg	90	90
V/Å^3	3252.2(3)	3448.4(2)
Z	4	4
T/K	90(2)	90(2)
D_{calc}/g cm^{-3}	1.707	1.737
crystal dimensions/mm	1.220 x 0.140 x 0.070	0.164 x 0.035 x 0.027
Radiation	MoKα	CuKα
θ limits/deg	2.170 – 30.176	3.289 – 66.693
reflns, measd /unique/obsd	147151/9543/ 8687	25604/6055/5487
Data/params	9543/433	6055 / 488
F(000)	1672	1800
μ/mm^{-1}	0.848	5.501
R_{int}	0.0332	0.0725
$R[I>2\sigma(I)]$	0.0320	0.0423
R_w (all data)	0.0877	0.1052
GOF	1.040	1.079

LSU structure identifier	FKhame47	FKhame14
formula	$[Cu(\mu\text{-}p\text{-xpt})(\mu\text{-OTf})]_n(OTf)_n$ $(C_{24}H_{18}CuF_6N_8O_6S_2)n$	2,3-diaminophenazine·HCl·$3H_2O$ $(C_{12}H_{17}ClN_4O_3)$
M	756.12	300.74
crystal system	Triclinic	Triclinic
space group	$P2_1/c$	$P\bar{1}$
a/Å	7.5250(12)	6.7253(4)
b/Å	13.449(2)	9.8257(5)
c/Å	16.916(2)	11.2574(6)
α/deg	76.692(9)	74.870(3)
β/deg	78.930(9)	76.375(3)
γ/deg	82.325(10)	82.134(3)
V/$Å^3$	1627.8(4)	695.65(7)
Z	2	2
T/K	90(2)	90(2)
D_{calc}/g cm^{-3}	1.543	1.436
crystal dimensions/mm	0.100 x 0.080 x 0.030	? x ? x ?
Radiation	CuKα	MoKα
θ limits/deg	3.392 – 66.599	1.916 – 30.457
reflns, measd /unique/obsd	14786/5466/3084	24628/4156/ 2787
Data/params	5466/427	4156/ 215
F(000)	762	316
μ/mm^{-1}	2.921	0.288
R_{int}	0.0990	0.0734
$R[I>2\sigma(I)]$	0.1430	0.0447
R_w (all data)	0.4377	0.1177
GOF	1.537	0.980

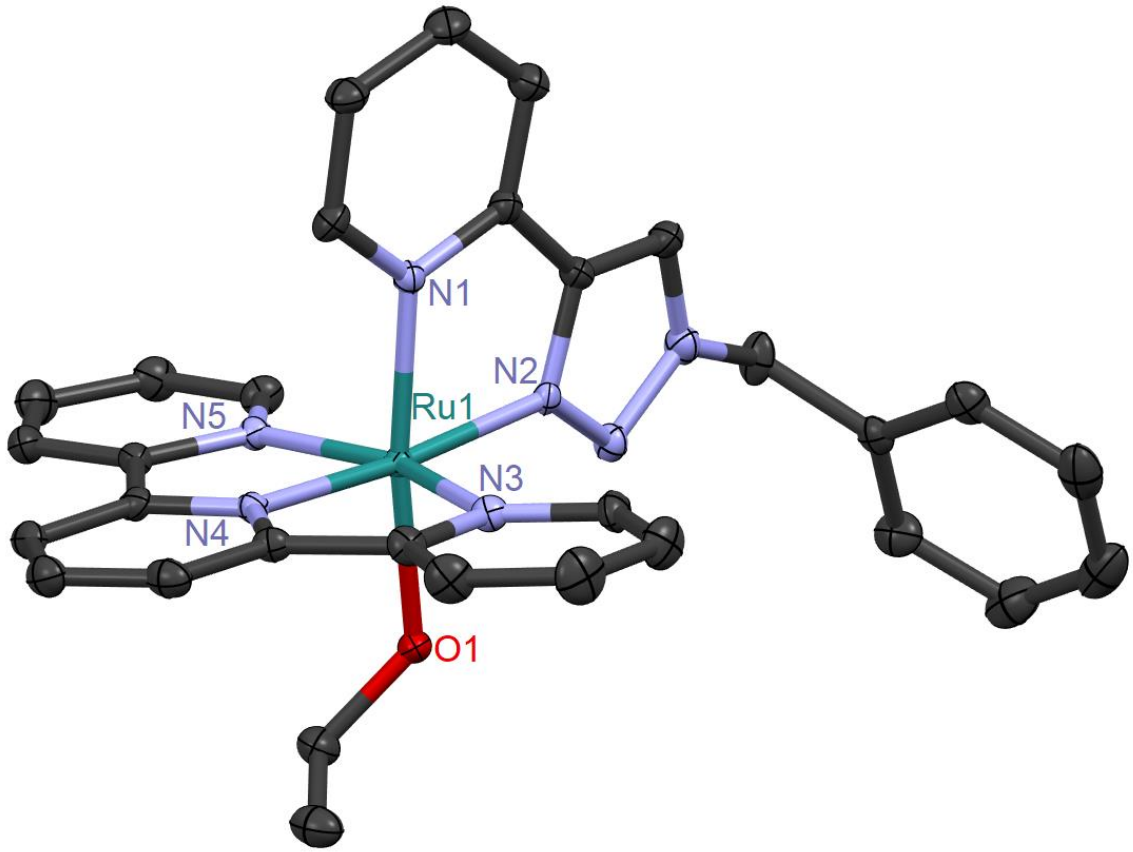

Figure A.1. X-ray structure of trans-py-[Ru(tpy)(bpt)(EtOH)]$(PF_6)_2$·dioxane; see FKhame79 in Table A.1.

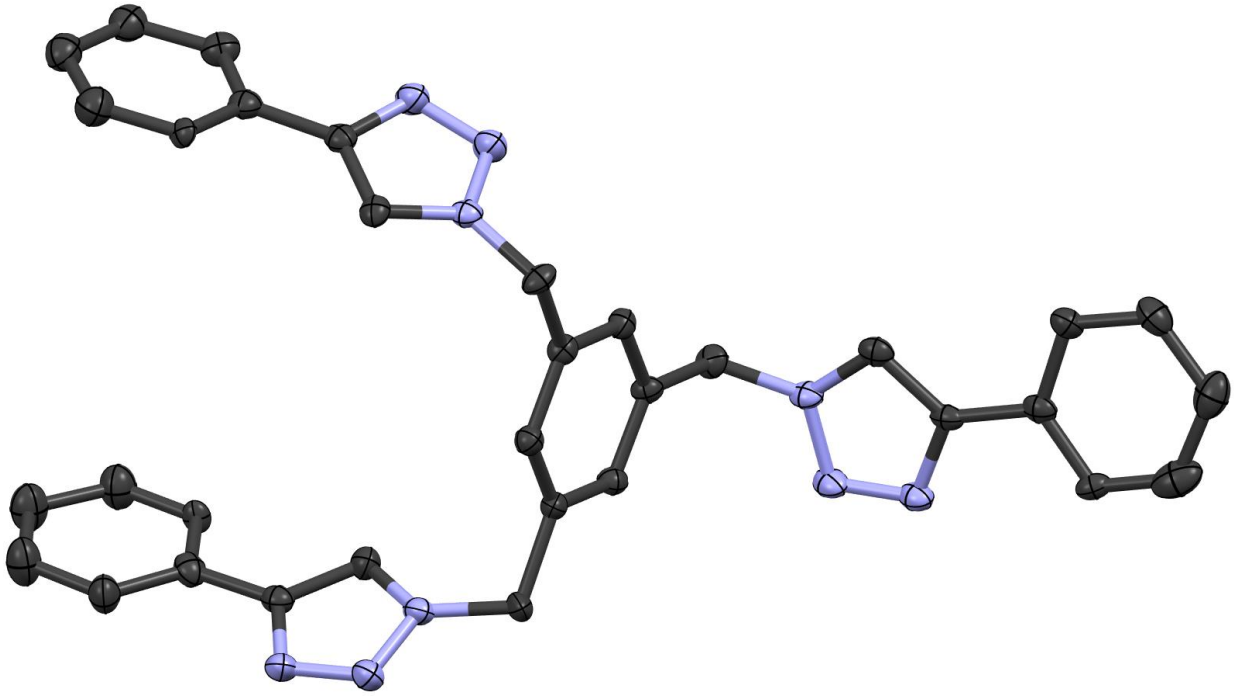

Figure A.2. X-ray structure of 1,3,5-tris(pyridyltriazolylmethyl)benzene; see FKhame75 in Table A.1.

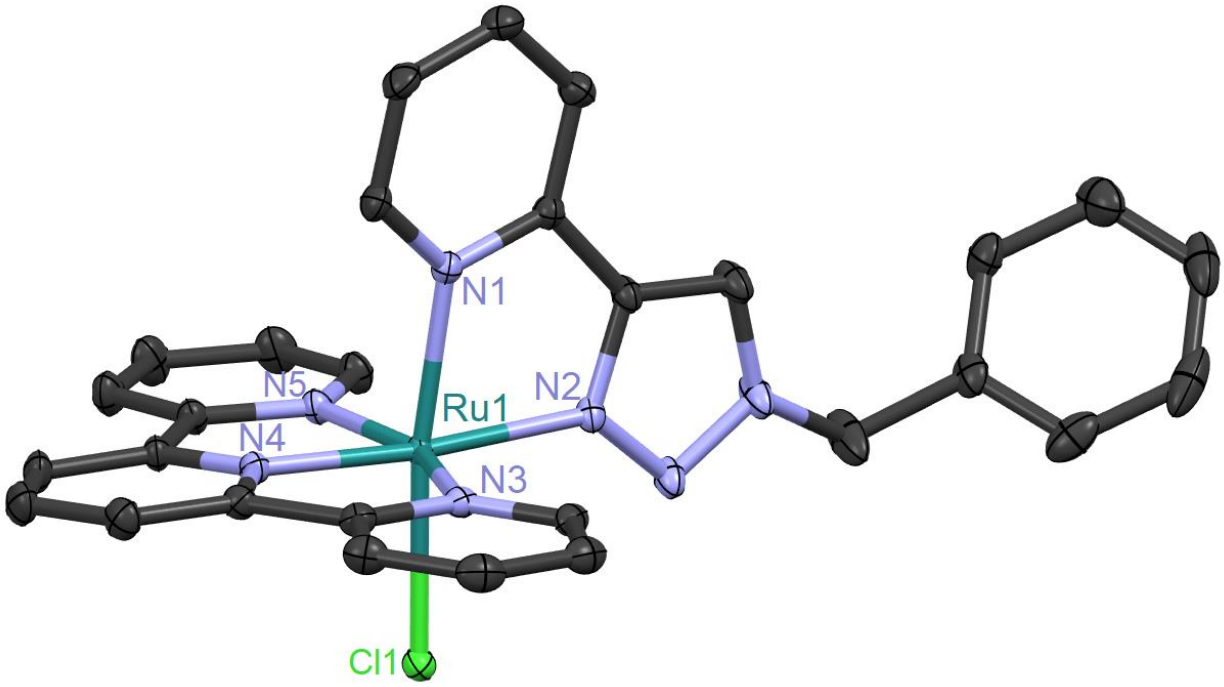

Figure A.3. X-ray structure of trans-py-[Ru(tpy)(bpt)Cl]$PF_6 \cdot CH_2Cl_2$; see FKhame73 in Table A.1.

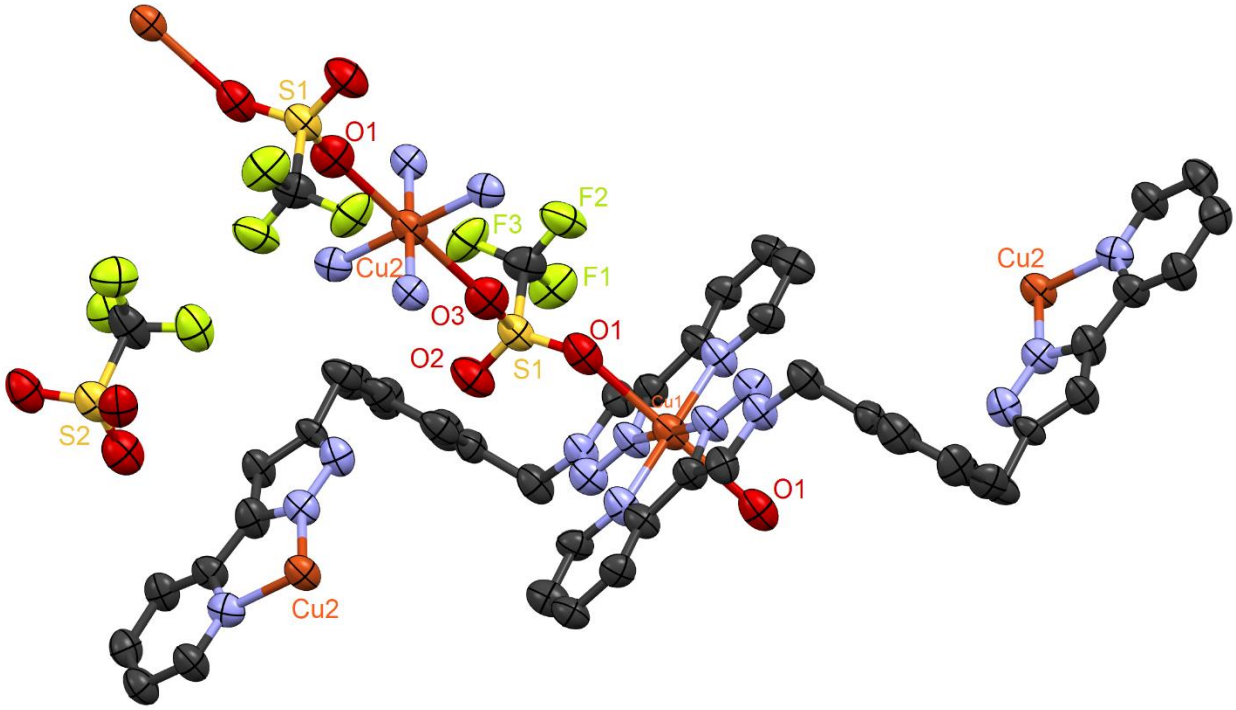

Figure A.4. X-ray structure of $[Cu(\mu\text{-}p\text{-xpt})(\mu\text{-OTf})]_n(OTf)_n$; see FKhame69 in Table A.1.

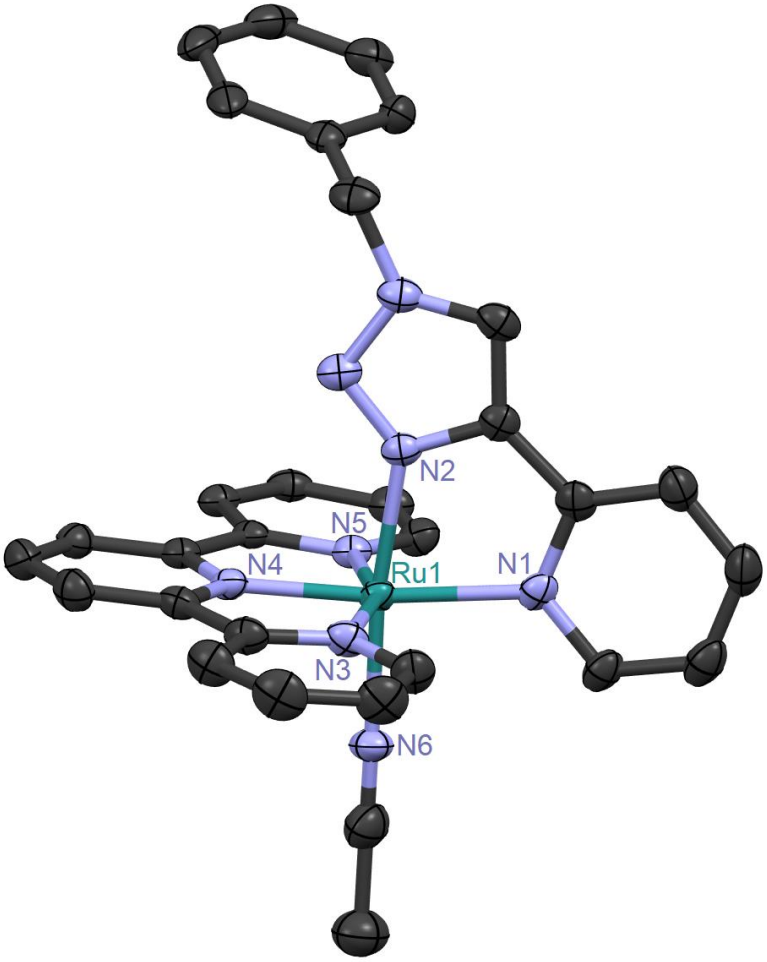

Figure A.5. X-ray structure of trans-trz-[Ru(tpy)(bpt)(CH_3CN)](PF_6)$_2$; see FKhame47 in Table A.1.

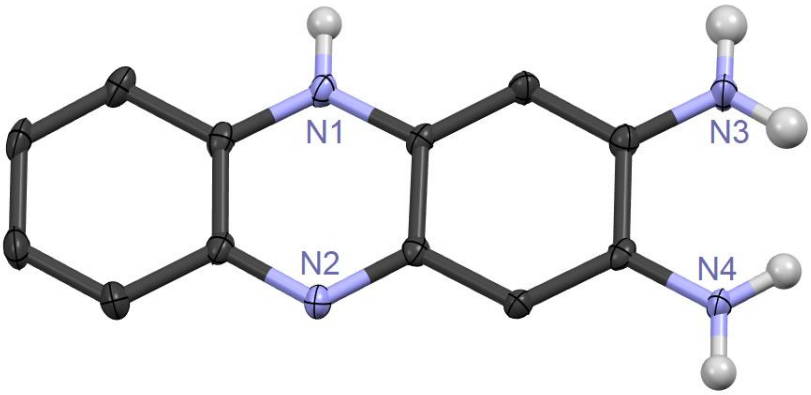

Figure A.6. X-ray structure of 2,3-diaminophenazine·HCl·3H_2O; see FKhame14 in Table A.1.

Appendix B. Permissions

Permission for Figures 1.1 and 1.8 printed from *Accounts of Chemical Research* 2012, *45* (5), 767-776

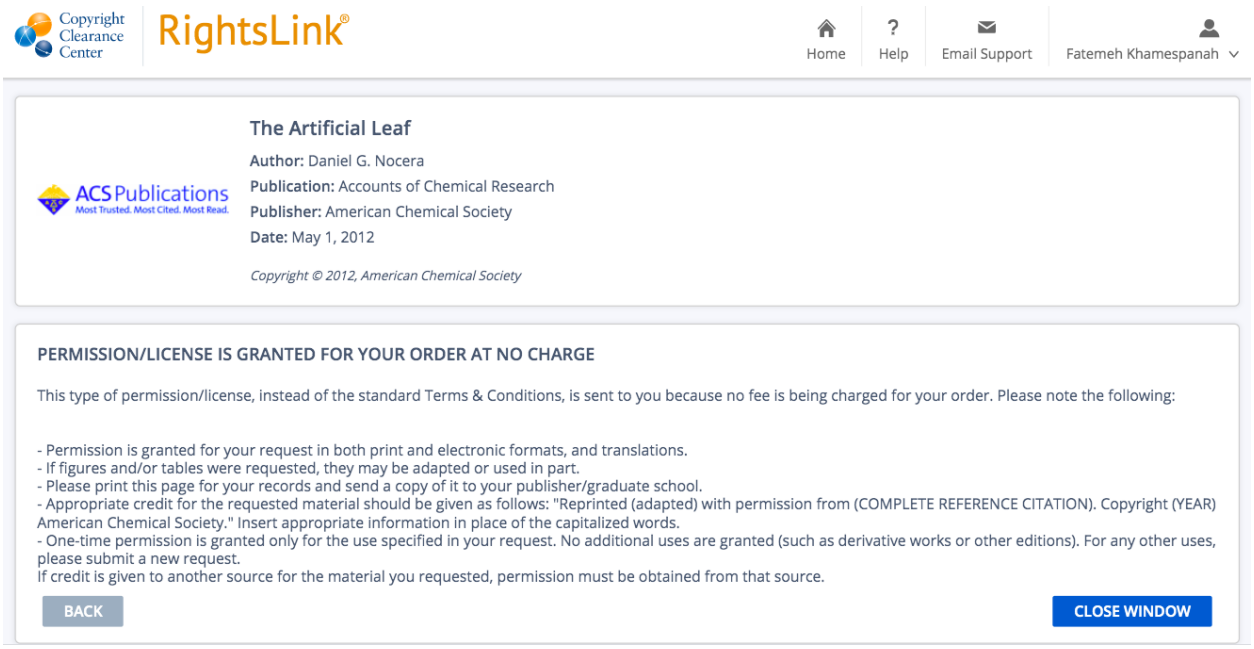

Permission for Figure 1.2 printed from *Energy & Environmental Science* 2012, *5* (7), 7923-7926

Copyright Clearance Center Marketplace™

Royal Society of Chemistry - License Terms and Conditions

This is a License Agreement between Fatemeh Khamespanah ("You") and Royal Society of Chemistry ("Publisher") provided by Copyright Clearance Center ("CCC"). The license consists of your order details, the terms and conditions provided by Royal Society of Chemistry, and the CCC terms and conditions.

All payments must be made in full to CCC.

Order Date	19-May-2020	**Type of Use**	Republish in a thesis/dissertation
Order license ID	1035982-1		
ISSN	1754-5706	**Publisher**	RSC Publishing
		Portion	Image/photo/illustration

LICENSED CONTENT

Publication Title	Energy & environmental science	**Country**	United Kingdom of Great Britain and Northern Ireland
Author/Editor	Royal Society of Chemistry (Great Britain)	**Rightsholder**	Royal Society of Chemistry
Date	01/01/2008	**Publication Type**	e-Journal
Language	English	**URL**	http://www.rsc.org/Publishing/Journals/EE/Index.asp

REQUEST DETAILS

Portion Type	Image/photo/illustration	**Distribution**	Worldwide
Number of images / photos / illustrations	1	**Translation**	Original language of publication
Format (select all that apply)	Electronic	**Copies for the disabled?**	No
		Minor editing privileges?	No
Who will republish the content?	Not-for-profit entity	**Incidental promotional use?**	No
Duration of Use	Life of current edition	**Currency**	USD
Lifetime Unit Quantity	Up to 499		
Rights Requested	Main product		

NEW WORK DETAILS

Title	Figure 1.2 of dissertation	**Institution name**	Louisiana State University
Instructor name	Fatemeh Khamespanah	**Expected presentation date**	2020-05-25

ADDITIONAL DETAILS

Order reference number	N/A	**The requesting person / organization to appear on the license**	Fatemeh Khamespanah

Continued. Permission for Figure 1.2 printed from *Energy & Environmental Science* 2012, *5* (7), 7923-7926

REUSE CONTENT DETAILS

Title, description or numeric reference of the portion(s)	Proposed mechanism for the hydrogenation of CO2 by complex 3a.	Title of the article/chapter the portion is from	Second-coordination-sphere and electronic effects enhance iridium(III)-catalyzed homogeneous hydrogenation of carbon dioxide in water near ambient temperature and pressure.
Editor of portion(s)	N/A	Author of portion(s)	Royal Society of Chemistry (Great Britain)
Volume of serial or monograph	N/A	Issue, if republishing an article from a serial	N/A
Page or page range of portion	7925	Publication date of portion	2012-05-14

Permission for Figure 2.1 adapted from *Inorganic Chemistry* 2011, *50* (7), 2748–2753

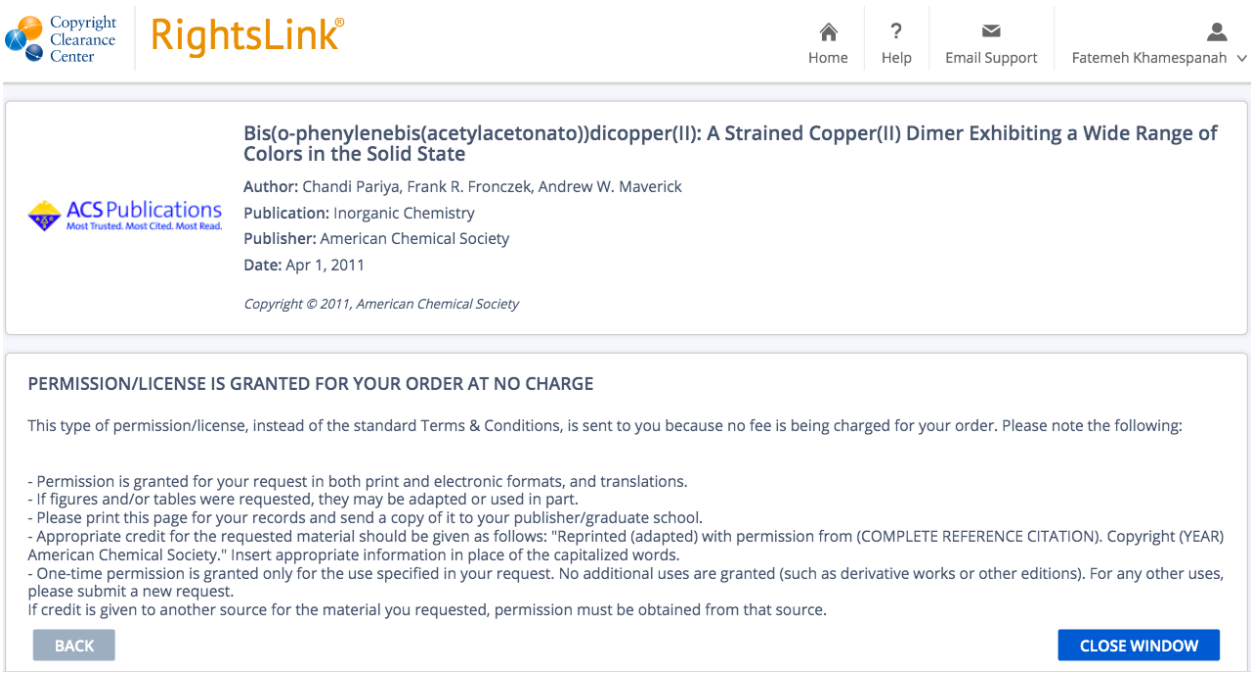

Permission for Figure 3.5 adapted from *Chemical Reviews* 2018, *118* (22), 10840-11022

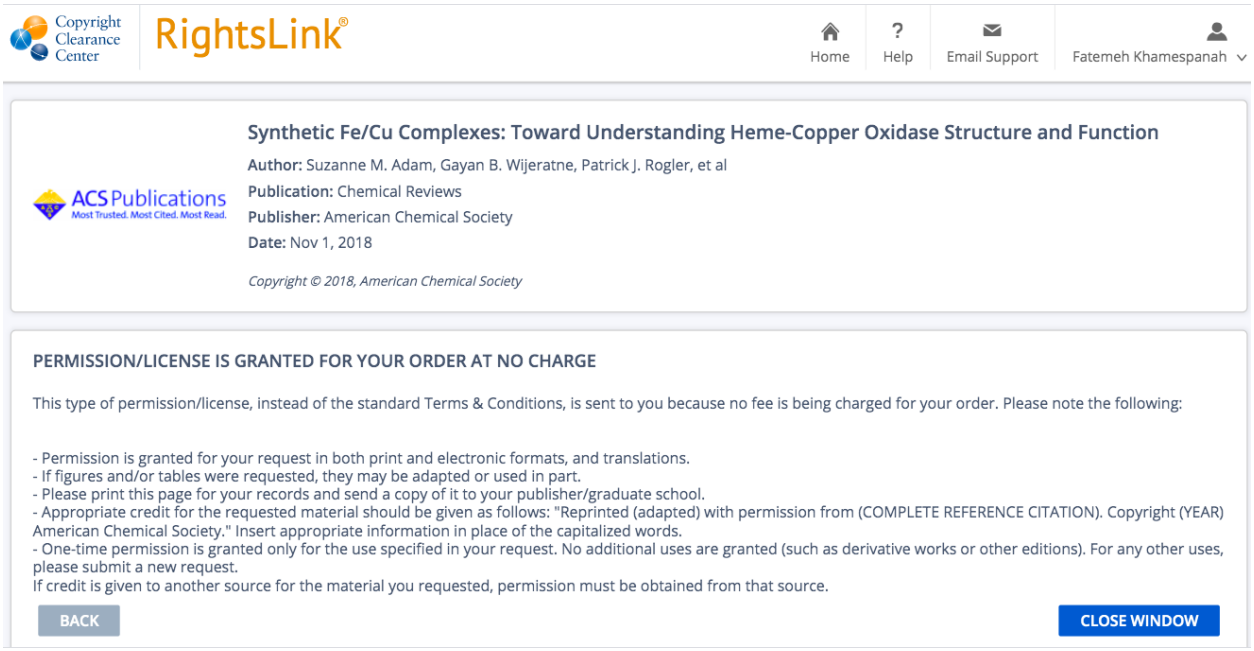

List of References

Adam, S. M.; Wijeratne, G. B.; Rogler, P. J.; Diaz, D. E.; Quist, D. A.; Liu, J. J.; Karlin, K. D., Synthetic Fe/Cu complexes: toward understanding heme-copper oxidase structure and function. *Chemical Reviews* **2018,** *118* (22), 10840-11022.

Angamuthu, R.; Byers, P.; Lutz, M.; Spek, A. L.; Bouwman, E., Electrocatalytic CO_2 conversion to oxalate by a copper complex. *Science* **2010,** *327* (5963), 313-315.

Arendse, M. J.; Anderson, G. K.; Rath, N. P., Oxidative degradation of the ascorbate anion in the presence of platinum and palladium. Formation and structures of platinum and palladium oxalate complexes. *Polyhedron* **2001,** *20* (19), 2495-2503.

Becker, J. Y.; Vainas, B.; Eger, R.; Kaufman, L., Electrocatalytic reduction of CO_2 to oxalate by Ag^{II} and Pd^{II} porphyrins. *Journal of the Chemical Society, Chemical Communications* **1985,** (21), 1471-1472.

Benson, E. E.; Kubiak, C. P.; Sathrum, A. J.; Smieja, J. M., Electrocatalytic and homogeneous approaches to conversion of CO_2 to liquid fuels. *Chemical Society Reviews* **2009,** *38* (1), 89-99.

Bratsch, S. G., Standard electrode potentials and temperature coefficients in water at 298.15 K. *Journal of Physical and Chemical Reference Data* **1989,** *18* (1), 1-21.

Bratsos, I.; Alessio, E., Inorganic Syntheses, Vol. 35, edited by T. B. Rauchfuss. *Hoboken, New Jersey: Wiley* **2010**, 148-152.

Brown, M. F.; Cook, B. R.; Sloan, T. E., Stereochemical notation in coordination chemistry. Mononuclear complexes. *Inorganic Chemistry* **1975,** *14* (6), 1273-1278.

Bruker, APEX3. Bruker AXS Inc., Madison, Wisconsin, USA, **2016**.

Bruker, SADABS. Bruker AXS Inc., Madison, Wisconsin, USA, **2001**.

Bruker, SAINT. Bruker AXS Inc., Madison, Wisconsin, USA, **2012**.

Bruker, TWINABS. Bruker AXS Inc., Madison, Wisconsin, USA, **2001**.

Burnap, R. L., D1 protein processing and Mn cluster assembly in light of the emerging photosystem II structure. *Physical Chemistry Chemical Physics* **2004,** *6* (20), 4803-4809.

Carlsson, A.-C. C.; Mehmeti, K.; Uhrbom, M.; Karim, A.; Bedin, M.; Puttreddy, R.; Kleinmaier, R.; Neverov, A. A.; Nekoueishahraki, B.; Gräfenstein, J.; Rissanen, K.; Erdeĺyi, M., Substituent effects on the $[N–I–N]^+$ halogen bond. *Journal of the American Chemical Society* **2016,** *138* (31), 9853-9863.

Concepcion, J. J.; Jurss, J. W.; Templeton, J. L.; Meyer, T. J., One site is enough. Catalytic water oxidation by $[Ru(tpy)(bpm)(OH_2)]^{2+}$ and $[Ru(tpy)(bpz)(OH_2)]^{2+}$. *Journal of the American Chemical Society* **2008,** *130* (49), 16462-16463.

Cook, B. J.; Di Francesco, G. N.; Abboud, K. A.; Murray, L. J., Countercations and solvent influence CO_2 reduction to oxalate by chalcogen-bridged tricopper cyclophanates. *Journal of the American Chemical Society* **2018,** *140* (17), 5696-5700.

Creutz, C., The complexities of ascorbate as a reducing agent. *Inorganic Chemistry* **1981,** *20* (12), 4452-4453.

Crowley, J. D.; Bandeen, P. H.; Hanton, L. R., A one pot multi-component CuAAC "click" approach to bidentate and tridentate pyridyl-1,2,3-triazole ligands: Synthesis, X-ray structures and copper(II) and silver(I) complexes. *Polyhedron* **2010,** *29* (1), 70-83.

Csonka, R.; Kaizer, J.; Giorgi, M.; Reglier, M.; Hajba, L.; Mink, J.; Speier, G., Oxidative C-H and C-C bond cleavage by a (2,2'-bipyridine)copper(I) chloride complex. *Inorganic Chemistry* **2008,** *47* (14), 6121-6123.

Cuperly, D.; Gros, P.; Fort, Y., First direct C-2-lithiation of 4-DMAP. Convenient access to reactive functional derivatives and ligands. *The Journal of Organic Chemistry* **2002,** *67* (1), 238-241.

Damhus, T.; Hartshorn, R.; Hutton, A., Nomenclature of inorganic chemistry: IUPAC recommendations 2005. *CHEMISTRY International* **2005**.

de Ruiter, G.; Costa, J. S.; Lappalainen, K.; Roubeau, O.; Gamez, P.; Reedijk, J., The system iron(II)/mpzbpy mediates the H_2O_2 oxidation of cyclohexane and cyclooctene and the aerobic oxidative cleavage of ascorbic acid to oxalate. *Inorganic Chemistry Communications* **2008,** *11* (7), 787-790.

Dewhirst, R. A.; Fry, S. C., The oxidation of dehydroascorbic acid and 2,3-diketogulonate by distinct reactive oxygen species. *Biochemical Journal* **2018,** *475* (21), 3451-3470.

Dogutan, D. K.; Nocera, D. G., Artificial photosynthesis at efficiencies greatly exceeding that of natural photosynthesis. *Accounts of Chemical Research* **2019,** *52* (11), 3143-3148.

Duan, L.; Bozoglian, F.; Mandal, S.; Stewart, B.; Privalov, T.; Llobet, A.; Sun, L., A molecular ruthenium catalyst with water-oxidation activity comparable to that of photosystem II. *Nature Chemistry* **2012,** *4* (5), 418-423.

Duan, L.; Fischer, A.; Xu, Y.; Sun, L., Isolated seven-coordinate Ru(IV) dimer complex with $[HOHOH]^-$ bridging ligand as an intermediate for catalytic water oxidation. *Journal of the American Chemical Society* **2009,** *131* (30), 10397-10399.

Essential of heterocyclic chemistry-I. https://www.scripps.edu/baran/heterocycles (accessed Mar 24, 2020).

Evans, I.; Spencer, A.; Wilkinson, G., Dichlorotetrakis(dimethyl sulphoxide)ruthenium(II) and its use as a source material for some new ruthenium(II) complexes. *Journal of the Chemical Society, Dalton Transactions* **1973,** (2), 204-209.

Evans, W. J.; Seibel, C. A.; Ziller, J. W., Organosamarium-mediated transformations of CO_2 and COS: Monoinsertion and disproportionation reactions and the reductive coupling of CO_2 to $[O_2CCO_2]_2$. *Inorganic Chemistry* **1998,** *37* (4), 770-776.

Farrugia, L. J.; Lopinski, S.; Lovatt, P. A.; Peacock, R. D., Fixing carbon dioxide with copper: crystal structure of $[LCu(mu\text{-}C_2O_4)CuL][Ph_4B]_2$ (L = N,N',N''-triallyl-1,4,7-triazacyclo-nonane). *Inorganic Chemistry* **2001,** *40* (3), 558-559.

Fay, N.; Hultgren, V. M.; Wedd, A. G.; Keyes, T. E.; Forster, R. J.; Leane, D.; Bond, A. M., Sensitization of photo-reduction of the polyoxometalate anions $[S_2M_{18}O_{62}]^{4-}$ (M= Mo, W) in the visible spectral region by the $[Ru(bpy)_3]^{2+}$ cation. *Dalton Transactions* **2006,** (35), 4218-4227.

Garcia-Bosch, I.; Cowley, R. E.; Díaz, D. E.; Siegler, M. A.; Nam, W.; Solomon, E. I.; Karlin, K. D., Dioxygen activation by a macrocyclic copper complex leads to a Cu_2O_2 core with unexpected structure and reactivity. *Chemistry–A European Journal* **2016,** *22* (15), 5133-5137.

Garrido-Barros, P.; Funes-Ardoiz, I.; Drouet, S.; Benet-Buchholz, J.; Maseras, F.; Llobet, A., Redox non-innocent ligand controls water oxidation overpotential in a new family of mononuclear Cu-based efficient catalysts. *Journal of the American Chemical Society* **2015,** *137* (21), 6758-6761.

Gennaro, A.; Isse, A. A.; Saveant, J.-M.; Severin, M.-G.; Vianello, E., Homogeneous electron transfer catalysis of the electrochemical reduction of carbon dioxide. Do aromatic anion radicals react in an outer-sphere manner? *Journal of the American Chemical Society* **1996,** *118* (30), 7190-7196.

Gennaro, A.; Isse, A. A.; Severin, M.-G.; Vianello, E.; Bhugun, I.; Savéant, J.-M., Mechanism of the electrochemical reduction of carbon dioxide at inert electrodes in media of low proton availability. *Journal of the Chemical Society, Faraday Transactions* **1996,** *92* (20), 3963-3968.

Harkrader, R. J.; Plunkett, L. M.; Tolbert, B. M., Periodate degradation of labeled ascorbic acid. *Analytical Biochemistry* **1976,** *72* (1-2), 310-314.

Herbert, R. W.; Hirst, E. L.; Percival, E. G. V.; Reynolds, R. J. W.; Smith, F., The constitution of ascorbic acid. *Journal of the Chemical Society* **1933**, 1270-1290.

Horn, B.; Limberg, C.; Herwig, C.; Braun, B., Nickel(I)-mediated transformations of carbon dioxide in closed synthetic cycles: reductive cleavage and coupling of CO_2 generating $Ni^{I}CO$, $Ni^{II}CO_3$ and $Ni^{II}C_2O_4Ni^{II}$ entities. *Chemical Communications* **2013,** *49* (93), 10923-10925.

Janzen, E. G.; Julia, I.; Liu, P., Radical addition reactions of 5,5-dimethyl-1-pyrroline-1-oxide. ESR spin trapping with a cyclic nitrone. *Journal of Magnetic Resonance* **1973,** *9* (3), 510-512.

Karkas, M. D.; Verho, O.; Johnston, E. V.; Åkermark, B., Artificial photosynthesis: molecular systems for catalytic water oxidation. *Chemical Reviews* **2014,** *114* (24), 11863-12001.

Kawamata, Y.; Yan, M.; Liu, Z.; Bao, D.; Chen, J.; Starr, J. T.; Baran, P. S., Scalable, electrochemical oxidation of unactivated C–H bonds. *Journal of the American Chemical Society* **2017,** *139* (22), 7448-7451.

Khamespanah, F.; Maverick, A. W., Two isomers of [1-benzyl-4-(pyridin-2-yl-κ*N*)-1*H*-1,2,3-triazole-κN^3] dichloridobis (dimethyl sulfoxide-κ*S*)ruthenium(II). *Acta Crystallographica Section E: Crystallographic Communications* **2019,** *75* (8), 1108-1111.

Knope, K. E.; Kimura, H.; Yasaka, Y.; Nakahara, M.; Andrews, M. B.; Cahill, C. L., Investigation of in situ oxalate formation from 2,3-pyrazinedicarboxylate under hydrothermal conditions using nuclear magnetic resonance spectroscopy. *Inorganic Chemistry* **2012,** *51* (6), 3883-3890.

Kumar, S. V.; Lo, W. K.; Brooks, H. J.; Crowley, J. D., Synthesis, structure, stability and antimicrobial activity of a ruthenium(II) helicate derived from a bis-bidentate "click" pyridyl-1,2,3-triazole ligand. *Inorganica Chimica Acta* **2015,** *425*, 1-6.

Kumar, S. V.; Scottwell, S. Ø.; Waugh, E.; McAdam, C. J.; Hanton, L. R.; Brooks, H. J.; Crowley, J. D., Antimicrobial properties of tris (homoleptic) ruthenium(II) 2-pyridyl-1,2,3-triazole "click" complexes against pathogenic bacteria, including Methicillin-Resistant Staphylococcus Aureus (MRSA). *Inorganic Chemistry* **2016,** *55* (19), 9767-9777.

Kurata, T.; Miyake, N.; Otsuka, Y., Formation of L-threonolactone and oxalic acid in the autoxidation reaction of L-ascorbic acid: possible involvement of singlet oxygen. *Bioscience, Biotechnology, and Biochemistry* **1996,** *60* (7), 1212-1214.

Kuroda, D. G.; Hochstrasser, R. M., Two-dimensional infrared spectral signature and hydration of the oxalate dianion. *The Journal of Chemical Physics* **2011,** *135* (20), 204502.

Kushi, Y.; Nagao, H.; Nishioka, T.; Isobe, K.; Tanaka, K., Oxalate formation in electrochemical CO_2 reduction catalyzed by Rhodium-Sulfur cluster. *Chemistry Letters* **1994,** *23* (11), 2175-2178.

Kushi, Y.; Nagao, H.; Nishioka, T.; Isobe, K.; Tanaka, K., Remarkable decrease in overpotential of oxalate formation in electrochemical CO_2 reduction by a metal–sulfide cluster. *Journal of the Chemical Society, Chemical Communications* **1995,** (12), 1223-1224.

Lam, B. M.; Halfen, J. A.; Young, V. G.; Hagadorn, J. R.; Holland, P. L.; Lledós, A.; Cucurull-Sánchez, L.; Novoa, J. J.; Alvarez, S.; Tolman, W. B., Ligand macrocycle structural effects on copper−dioxygen reactivity. *Inorganic Chemistry* **2000,** *39* (18), 4059-4072.

Lamy, E.; Nadjo, L.; Saveant, J. M., Standard potential and kinetic parameters of the electrochemical reduction of carbon dioxide in dimethylformamide. *Journal of Electroanalytical Chemistry* **1977,** *78* (2), 403-407.

Lewis, E. A.; Tolman, W. B., Reactivity of dioxygen−copper systems. *Chemical Reviews* **2004,** *104* (2), 1047-1076.

Li, Y.; Flood, A. H., Pure C–H hydrogen bonding to chloride ions: A preorganized and rigid macrocyclic receptor. *Angewandte Chemie International Edition* **2008,** *47* (14), 2649-2652.

Llobet, A., Synthesis, spectral and redox properties of a new series of aqua complexes of ruthenium(II). *Inorganica Chimica Acta* **1994,** *221* (1-2), 125-131.

Lu, C. C.; Saouma, C. T.; Day, M. W.; Peters, J. C., Fe(I)-mediated reductive cleavage and coupling of CO_2: An $Fe^{II}(\mu\text{-}O, \mu\text{-}CO)Fe^{II}$ core. *Journal of the American Chemical Society* **2007,** *129* (1), 4-5.

Magda, D.; Gerasimchuk, N.; Lecane, P.; Miller, R. A.; Biaglow, J. E.; Sessler, J. L., Motexafin gadolinium reacts with ascorbate to produce reactive oxygen species. *Chemical Communications* **2002,** (22), 2730-2731.

Masaoka, S.; Sakai, K., Clear evidence showing the robustness of a highly active oxygen-evolving mononuclear ruthenium complex with an aqua ligand. *Chemistry letters* **2009,** *38* (2), 182-183.

Matheu, R.; Ertem, M. Z.; Benet-Buchholz, J.; Coronado, E.; Batista, V. S.; Sala, X.; Llobet, A., Intramolecular proton transfer boosts water oxidation catalyzed by a Ru complex. *Journal of the American Chemical Society* **2015,** *137* (33), 10786-10795.

Matheu, R.; Garrido-Barros, P.; Gil-Sepulcre, M.; Ertem, M. Z.; Sala, X.; Gimbert-Suriñach, C.; Llobet, A., The development of molecular water oxidation catalysts. *Nature Reviews Chemistry* **2019,** *3* (5), 331-341.

Nelson, I.; Larson, R.; Iwamoto, R., Polarographic evidence for the stability of copper(I) ion in some non-complexing nonaqueous solvents. *Journal of Inorganic and Nuclear Chemistry* **1961,** *22* (3-4), 279-284.

Nocera, D. G., The artificial leaf. *Accounts of Chemical Research* **2012,** *45* (5), 767-776.

Orioli, P.; Bruni, B.; Di Vaira, M.; Messori, L.; Piccioli, F., Decomposition of ascorbic acid in the presence of cadmium ions leads to formation of a polymeric cadmium oxalate species with peculiar structural features. *Inorganic Chemistry* **2002,** *41* (17), 4312-4314.

Osredkar, J.; Sustar, N., Copper and zinc, biological role and significance of copper/zinc imbalance. *Journal of Clinical Toxicology* **2011,** *3* (2161), 0495.

Pariya, C.; Fronczek, F. R.; Maverick, A. W., Bis(o-phenylenebis (acetylacetonato)) dicopper(II): A strained copper(II) dimer exhibiting a wide range of colors in the solid state. *Inorganic Chemistry* **2011,** *50* (7), 2748-2753.

Park, G. Y.; Qayyum, M. F.; Woertink, J.; Hodgson, K. O.; Hedman, B.; Narducci Sarjeant, A. A.; Solomon, E. I.; Karlin, K. D., Geometric and electronic structure of $[\{Cu(MeAN)\}_2(\mu\text{-}\eta^2\text{:}\eta^2(O_2^{2-}))]^{2+}$ with an unusually long O–O bond: O–O bond weakening vs activation for reductive cleavage. *Journal of the American Chemical Society* **2012,** *134* (20), 8513-8524.

Pavlishchuk, V. V.; Addison, A. W., Conversion constants for redox potentials measured versus different reference electrodes in acetonitrile solutions at 25 C. *Inorganica Chimica Acta* **2000,** *298* (1), 97-102.

Pegis, M. L.; Roberts, J. A.; Wasylenko, D. J.; Mader, E. A.; Appel, A. M.; Mayer, J. M., Standard reduction potentials for oxygen and carbon dioxide couples in acetonitrile and N,N-dimethylformamide. *Inorganic Chemistry* **2015,** *54* (24), 11883-11888.

Pokharel, U. R.; Fronczek, F. R.; Maverick, A. W., Cyclic pyridyltriazole–Cu(II) dimers as supramolecular hosts. *Dalton Transactions* **2013,** *42* (39), 14064-14067.

Pokharel, U. R.; Fronczek, F. R.; Maverick, A. W., Reduction of carbon dioxide to oxalate by a binuclear copper complex. *Nature Communications* **2014,** *5*, 5883.

Rauch, M.; Parkin, G., Zinc and magnesium catalysts for the hydrosilylation of carbon dioxide. *Journal of the American Chemical Society* **2017,** *139* (50), 18162-18165.

Reece, S. Y.; Hamel, J. A.; Sung, K.; Jarvi, T. D.; Esswein, A. J.; Pijpers, J. J.; Nocera, D. G., Wireless solar water splitting using silicon-based semiconductors and earth-abundant catalysts. *Science* **2011,** *334* (6056), 645-648.

Renger, G.; Renger, T., Photosystem II: the machinery of photosynthetic water splitting. *Photosynthesis Research* **2008,** *98* (1-3), 53-80.

Rudolph, M.; Dautz, S.; Jäger, E.-G., Macrocyclic $[N_4^{2-}]$ coordinated nickel complexes as catalysts for the formation of oxalate by electrochemical reduction of carbon dioxide. *Journal of the American Chemical Society* **2000,** *122* (44), 10821-10830.

Sadique, A. R.; Brennessel, W. W.; Holland, P. L., Reduction of CO_2 to CO using low-coordinate iron: formation of a four-coordinate iron dicarbonyl complex and a bridging carbonate complex. *Inorganic Chemistry* **2008,** *47* (3), 784-786.

Saha, M. S.; Ohsaka, T., Electrode kinetics of the O_2/O_2^- redox couple at Hg electrode in the presence of PVC in aprotic media. *Electrochimica Acta* **2005,** *50* (24), 4746-4751.

Saouma, C. T.; Lu, C. C.; Day, M. W.; Peters, J. C., CO_2 reduction by Fe(I): solvent control of C–O cleavage versus C–C coupling. *Chemical Science* **2013,** *4* (10), 4042-4051.

Sato, T.; Hamada, Y.; Sumikawa, M.; Araki, S.; Yamamoto, H., Solubility of oxygen in organic solvents and calculation of the Hansen solubility parameters of oxygen. *Industrial & Engineering Chemistry Research* **2014,** *53* (49), 19331-19337.

Sens, C.; Romero, I.; Rodríguez, M.; Llobet, A.; Parella, T.; Benet-Buchholz, J., A new Ru complex capable of catalytically oxidizing water to molecular dioxygen. *Journal of the American Chemical Society* **2004,** *126* (25), 7798-7799.

Sheldrick, G. M., *Acta Crystallographica Section A* **2015**, *71*, 3-8.

Sheldrick, G. M., *Acta Crystallographica Section C* **2015**, *71*, 3-8.

Shin, D. B.; Feather, M. S., The degradation of L-ascorbic acid in neutral solutions containing oxygen. *Journal of Carbohydrate Chemistry* **1990,** *9* (4), 461-469.

Smieja, J. M.; Kubiak, C. P., $Re(bipy\text{-}tBu)(CO)_3Cl^-$ improved catalytic activity for reduction of carbon dioxide: IR-spectroelectrochemical and mechanistic studies. *Inorganic Chemistry* **2010,** *49* (20), 9283-9289.

Soares-Santos, P. C. R.; Cunha-Silva, L.; Paz, F. A. A.; Ferreira, R. A. S.; Rocha, J.; Carlos, L. D.; Nogueira, H. I. S., Photoluminescent lanthanide-organic bilayer networks with 2, 3-pyrazinedicarboxylate and oxalate. *Inorganic Chemistry* **2010,** *49* (7), 3428-3440.

Spek, A. L., *Acta Crystallographica Section C* **2015**, *71*, 9-18.

Stibrany, R. T.; Schugar, H. J.; Potenza, J. A., A copper(II)–oxalate compound resulting from the fixation of carbon dioxide: μ-oxalato-bis[bis(1-benzyl-1H-pyrazole)(trifluoromethane-sulfonato)copper(II)]. *Acta Crystallographica Section E Structure Reports Online* **2005,** *61* (10), m1904-m1906.

Suga, M.; Akita, F.; Hirata, K.; Ueno, G.; Murakami, H.; Nakajima, Y.; Shimizu, T.; Yamashita, K.; Yamamoto, M.; Ago, H., Native structure of photosystem II at 1.95 Å resolution viewed by femtosecond X-ray pulses. *Nature* **2015,** *517* (7532), 99-103

Sullivan, B. P.; Calvert, J. M.; Meyer, T. J., Cis-trans isomerism in $(trpy)(PPh_3)\ RuC1_2$. Comparisons between the chemical and physical properties of a cis-trans isomeric pair. *Inorganic Chemistry* **1980,** *19* (5), 1404-1407.

Sullivan, B.; Salmon, D.; Meyer, T., Mixed phosphine 2,2'-bipyridine complexes of ruthenium. *Inorganic chemistry* **1978,** *17* (12), 3334-3341.

Surendranath, Y.; Kanan, M. W.; Nocera, D. G., Mechanistic studies of the oxygen evolution reaction by a cobalt-phosphate catalyst at neutral pH. *Journal of the American Chemical Society* **2010,** *132* (46), 16501-16509.

Takeuchi, K. J.; Thompson, M. S.; Pipes, D. W.; Meyer, T. J., Redox and spectral properties of monooxo polypyridyl complexes of ruthenium and osmium in aqueous media. *Inorganic Chemistry* **1984,** *23* (13), 1845-1851.

Thomas, A. M.; Lin, B.-L.; Wasinger, E. C.; Stack, T. D. P., Ligand noninnocence of thiolate/disulfide in dinuclear copper complexes: solvent-dependent redox isomerization and proton-coupled electron transfer. *Journal of the American Chemical Society* **2013,** *135* (50), 18912-18919.

Thomas, A. M.; Mandal, G. C.; Tiwary, S. K.; Rath, R. K.; Chakravarty, A. R., Ascorbate oxidation leading to the formation of a catalytically active oxalato bridged dicopper(II) complex as a model for dopamine β-hydroxylase. *Journal of the Chemical Society, Dalton Transactions* **2000**, 1395-1396.

Ünaleroğlu, C.; Zümreoğlu-Karan, B.; Zencir, Y.; Hökelek, T., pH-independent decomposition reactions of L-ascorbic acid in aqueous metal solutions—I. Formation and structures of Co^{II} and Gd^{III} oxalates. *Polyhedron* **1997,** *16* (13), 2155-2161.

Vinyard, D. J.; Brudvig, G. W., Progress toward a molecular mechanism of water oxidation in photosystem II. *Annual Review of Physical Chemistry* **2017,** *68*, 101-116.

Wang, J.-W.; Zhong, D.-C.; Lu, T.-B., Artificial photosynthesis: Catalytic water oxidation and CO_2 reduction by dinuclear non-noble-metal molecular catalysts. *Coordination Chemistry Reviews* **2018,** *377*, 225-236.

Wang, W.-H.; Himeda, Y.; Muckerman, J. T.; Manbeck, G. F.; Fujita, E., CO_2 hydrogenation to formate and methanol as an alternative to photo-and electrochemical CO_2 reduction. *Chemical Reviews* **2015,** *115* (23), 12936-12973.

Wang, W.-H.; Hull, J. F.; Muckerman, J. T.; Fujita, E.; Himeda, Y., Second-coordination-sphere and electronic effects enhance iridium(III)-catalyzed homogeneous hydrogenation of carbon dioxide in water near ambient temperature and pressure. *Energy & Environmental Science* **2012,** *5* (7), 7923-7926.

Warren, J. J.; Mayer, J. M., Surprisingly long-lived ascorbyl radicals in acetonitrile: concerted proton-electron transfer reactions and thermochemistry. *Journal of the American Chemical Society* **2008,** *130* (24), 7546-7547.

Wasylenko, D. J.; Ganesamoorthy, C.; Henderson, M. A.; Koivisto, B. D.; Osthoff, H. D.; Berlinguette, C. P., Electronic modification of the $[Ru^{II}(tpy)(bpy)(OH_2)]^{2+}$ scaffold: Effects on catalytic water oxidation. *Journal of the American Chemical Society* **2010,** *132* (45), 16094-16106.

Wasylenko, D. J.; Ganesamoorthy, C.; Koivisto, B. D.; Henderson, M. A.; Berlinguette, C. P., Insight into water oxidation by mononuclear polypyridyl Ru catalysts. *Inorganic Chemistry* **2010,** *49* (5), 2202-2209.

White, N. G.; Beer, P. D., A catenane host system containing integrated triazole C–H hydrogen bond donors for anion recognition. *Chemical Communications* **2012,** *48* (68), 8499-8501.

Wikipedia. https://en.wikipedia.org/wiki/Sunlight (accessed Apr 20, 2020).

Yang, C. T.; Fu, Y.; Huang, Y. B.; Yi, J.; Guo, Q. X.; Liu, L., Room-temperature copper-catalyzed carbon–nitrogen coupling of aryl iodides and bromides promoted by organic ionic bases. *Angewandte Chemie International Edition* **2009,** *48* (40), 7398-7401.

Yi, C. S.; Kwon, K.-H.; Lee, D. W., Aqueous phase C−H bond oxidation reaction of arylalkanes catalyzed by a water-soluble cationic Ru(III) complex $[(\text{pymox-Me}_2)_2\text{RuCl}_2]^+\text{BF}_4^-$. *Organic Letters* **2009,** *11* (7), 1567-1569.

Zhou, P.; Zhang, J.; Zhang, Y.; Liu, Y.; Liang, J.; Liu, B.; Zhang, W., Generation of hydrogen peroxide and hydroxyl radical resulting from oxygen-dependent oxidation of L-ascorbic acid via copper redox-catalyzed reactions. *RSC Advances* **2016,** *6* (45), 38541-38547.

Ziegelgruber, K. L.; Knope, K. E.; Frisch, M.; Cahill, C. L., Hydrothermal chemistry of Th(IV) with aromatic dicarboxylates: New framework compounds and in situ ligand syntheses. *Journal of Solid State Chemistry* **2008,** *181* (2), 373-381.

Zong, R.; Thummel, R. P., A new family of Ru complexes for water oxidation. *Journal of the American Chemical Society* **2005,** *127* (37), 12802-12803.

Vita

Fatemeh Khamespanah was born in Birjand, Iran. She received her Bachelor of Science degree in Chemistry from Sharif University of Technology in 2014. She is currently a candidate for the Doctor of Philosophy degree in the Department of Chemistry at Louisiana State University and Agricultural and Mechanical College with Dr. Andrew W. Maverick as her advisor.